Provided by the author(s) and University of Galway in accordance with publisher policies. Please cite the published version when available.

Title	Experimental and finite element investigations of the serviceability behaviour of CLT floors
Author(s)	Uí Chúláin, Caitríona
Publication Date	2020-02-06
Publisher	NUI Galway
Item record	http://hdl.handle.net/10379/15763

Downloaded 2024-05-24T03:33:22Z

Some rights reserved. For more information, please see the item record link above.

Experimental and Finite Element Investigations of the Serviceability Behaviour of CLT Floors

A thesis submitted to the National University of Ireland as fulfilment of the requirements for the Degree of Doctor of Philosophy

Caitríona Uí Chúláin BE (2014)

Supervisor: ***Prof. Annette Harte***

Civil Engineering, National University of Ireland Galway
2019

ACKNOWLEDGEMENTS

Primarily, I would like to thank my supervisor Prof. Annette Harte for her invitation to undertake this research and for her continued guidance and support during the course of the study.

I wish to express my appreciation to the College of Engineering and Informatics, National University of Ireland Galway (NUI Galway), for funding this research and I also thank The Wood Marketing Federation of Ireland and Enterprise Ireland for their supplementary financial support. Kind thanks to Kay Hartmann and KLH UK of KLH Massivholz GmbH, Rothoblaas srl, in particular Miklos Erszegi, and Richard Mc Donagh of SDR Group, for their backing.

I wish to thank the staff and students of NUI Galway, in particular the members of the Timber Engineering Research Group (TERG) for all their help and support, and most especially Karlo Simič who accompanied me to the UK for the experimental field work. A great companion for the trip. Thank you to Prof. Padraic O’Donoghue and Brid Flaherty. From the technical staff, kind thanks to Peter Fahy for all his work in the laboratory, and to Martin Burke for his guidance on electronics generally. I would also like to mention Gerry Hynes, Dermot Mc Dermott, and William Kelly.

Finally, I am most grateful to Iseult, Ruadhán, Hazel, Marcus, and Marion for their exceptional support over the duration of this research and always.

ABSTRACT

Global environmental concerns with regard to sustaining our growing population is prompting the building community worldwide to increase urban density, while using optimised and sustainable resources. The traditional materials used for high density and high rise development are carbon intensive, in contrast timber construction sequesters carbon and is renewable. Therefore, there is a concerted effort in timber engineering research to offer credible solutions with respect to sustainable construction in contemporary design. There are numerous prefabricated timber engineered building elements that are suitable for modern buildings. A product which is emerging as the most viable alternative to concrete or steel construction for multi-storey development is cross laminated timber (CLT).

This study aims to characterise the serviceability performance of CLT floor systems used in mid-rise buildings, focusing on floor deflection and excitation due to human activity within the range of people's perception.

The research includes experimental investigations exploring the serviceability performance of floors using particular connection details in keeping with the prevailing CLT floor-to-wall junctions that are suitable for mid-rise construction of residential, office, and educational buildings. The influence of non-structural elastomeric interlayers and the effect of non-structural added mass is also explored. The effect of CLT panels connected in parallel and the influence of the integration of the floor in the building are examined in field studies. The dynamic influence of floor voids to accommodate vertical circulation and building services are examined using a numerical modelling approach. This approach was also used to characterise the effect of non-structural intermediate supports and irregular mass distributions, representative of typical floor loadings.

The floor assemblies tested were all substantially compliant with current European timber design frequency criteria. However, the field tests on multi-panel floors indicated a marked reduction in the natural mode separation. This is attributed to the floor widths and the number of panels connected in parallel. The mode separation and

the number of first order modes below a defined range can prove significant with regard to compliance with velocity impulse criteria.

The experimental testing showed that alternative assembly configurations did not substantially influence the rotational stiffness of the floor support. All tested floor experimental results indicate that the responses to pedestrian traffic will be transient. The results suggest that optimum CLT floor design, in non-industrial buildings, with respect to serviceability performance will more significantly rely on the floor's mass and flexural stiffness, which are dictated by the floor panel geometry and intermediate supports. The numerical models showed that the natural mode shapes of the floor are significantly influenced by floor void positions and that the natural frequency and mode shape values are strongly effected by intermediate supports. All investigations showed that a CLT floor's dynamic performance is substantially affected by added mass and the distribution of the mass over the floor area.

Conclusions from this research will serve to advise building designers with respect to floor-to-wall connection assembly, floor geometry, floor voids, and void support locations, and the positioning of intermediate supports with respect to mitigating disturbing structural vibration in CLT floors due to pedestrian traffic and other human induced floor excitation.

NOMENCLATURE

A	Cross-sectional area
a	Acceleration
a_{rms}	RMS acceleration
$a_{w,rms}$	Weighted RMS acceleration
b	Parameter directly related to deflection limit in EC-5
c	Damping coefficient
$^{c}/_{c}$	Distance between centres (spacing)
d	Static point load deflection
$E_{0,CLT,mean}$	Characteristic modulus of elasticity parallel to grain of CLT
F	Force
f	Frequency, in Hz
f_1	Fundamental frequency, in Hz
f_n	Natural frequency, in Hz
f_w	Walking frequency, in Hz
$f_{m,CLT,k}$	Characteristic bending strength of CLT
$f_{t,0,CLT,net,k}$	Characteristic tensile strength of CLT
$f_{c,0,CLT,net,k}$	Characteristic compressive strength of CLT
$f_{v,CLT,IP,k}$	Characteristic shear strength in-plane of CLT
$f_{v,CLT,OP,k}$	Characteristic shear strength out-of-plane of CLT
$G_{CLT,mean}$	Characteristic shear modulus of CLT
$G_{r,CLT,mean}$	Characteristic rolling shear modulus of CLT

h	Lamina thickness of CLT
I	Second moment of area
I_{eff}	Effective impulse value
k	Spring stiffness
L	Span
m	Mass
$\hat{m}$	Modal mass
mV/g	Millivolts per gravity acceleration
n_{40}	Number of first-order modes below 40 Hz
P	1 kN point load
R	Response factor
RMS	Root mean square
s	Spacing
t	Time, in seconds
u	Linear displacement
v	Unit impulse velocity response
v_{rms}	RMS velocity of a single impulse
$\hat{v}$	Peak velocity of a single impulse
w	Vertical displacement
W	Width
W/mK	Watts per meter-Kelvin
x	Linear displacement
$\dot{x}$	Velocity

$\ddot{x}$	Acceleration
β	Forcing frequency to natural frequency ratio
ζ	Damping ratio
θ	Phase angle
ρ	Density
$\rho_{CLT,k}$	Characteristic density of CLT
$\rho_{CLT,mean}$	Mean density of CLT
ω	Angular frequency, in radians per second

ACRONYMS

2D	Two-dimensional
3D	Three-dimensional
ACRF	Advanced Characteristic Response Function
CLT	Cross laminated timber
DFT	Discrete Fourier transform
DLT	Dowel laminated timber
EC-5	European Timber Design Standard EN 1995-1-1
ETA	European Technical Approval
EU	European Union
FD30	Half-hour rated fire door
FD120	Two-hour rated fire door
FE	Finite element
FEM	Finite element model
FFT	Fast Fourier Transform
FINA	International Swimming Federation (Fédération Internationale de Natation)
FRF	Frequency response function
GLT	Glued laminated timber
IEPE	Integrated Electronics Piezo-Electric
LIVM	Low Impedance Voltage Mode
LVDT	Linear Variable Differential Transformer
LVL	Laminated veneer lumber
MDOF	Multiple degrees of freedom

MIMO	Multiple Input-Multiple Output
MPC	Multi-point constraints
MUF	Melamine Urea Formaldehyde
NA	National Annex
NLT	Nailed laminated timber
OSB	Orientated strandboard
PUR	One-component Polyurethane
RIBA	Royal Institute of British Architects
SDOF	Single degree of freedom
SIMO	Single Input-Multiple Output
SISO	Single Input-Single Output
TCC	Timber-concrete composite
VDV	Vibration dose value

TABLE OF CONTENTS

Abstract i

Nomenclature iii

Acronyms vii

Table of Contents ix

List of Figures xv

List of Tables xxv

1 Introduction 1

- 1.1 Modern timber construction 1
  - 1.1.1 Mass-timber and CLT 2
  - 1.1.2 Building with timber 3
  - 1.1.3 Timber floors 5
- 1.2 Research aims and objectives 7
- 1.3 Structure of the thesis 8

2 Cross laminated timber 11

- 2.1 Introduction 11
  - 2.1.1 CLT buildings 11
  - 2.1.2 Hybrid CLT buildings 14
  - 2.1.3 CLT buildings in Ireland 14
- 2.2 CLT design 16
  - 2.2.1 CLT design standards 18
  - 2.2.2 Commercial CLT panel mechanical characteristics 19
  - 2.2.3 CLT connection design and fastener selection 22
  - 2.2.4 Revisions to EN 1995-1-1 (EC-5) 25
- 2.3 Conclusions 26

3 Vibration 27

3.1 Introduction 27
3.2 Vibration theory 27
  3.2.1 Free vibration without damping 28
  3.2.2 Damping 30
  3.2.3 Free vibration with viscous damping: SDOF system 31
  3.2.4 Forced vibration with viscous damping: SDOF system 34
  3.2.5 Vibrations of real systems: MDOF 37
3.3 Floor vibration design criteria 39
  3.3.1 Human tolerance to floor vibration 40
3.4 European floor vibration design criteria EN 1995-1-1 (EC-5) 41
  3.4.1 Fundamental frequency limit 42
  3.4.2 Static unit point load deflection limit 42
  3.4.3 Unit impulse velocity response limit 43
  3.4.4 Irish national annex to EC-5 44
  3.4.5 Other EC-5 national annexes 45
3.5 International vibration design criteria 46
  3.5.1 Common forcing frequencies 46
  3.5.2 Damping ratios 47
  3.5.3 Acceptance criteria 47
  3.5.4 Vibration perception 47
  3.5.5 Continuous, intermittent, and occasional vibration 50
  3.5.6 Tolerance of vibration 51
  3.5.7 Low and high frequency floors 52
  3.5.8 Dynamic actions of groups of people 53
  3.5.9 Concrete and steel floor vibration design criteria 53
  3.5.10 Vibration dose values 56

3.6 US and Canadian CLT floor vibration design criteria 57
3.7 Conclusions 59
4 Literature Review 61
4.1 Introduction 61
4.2 Static and vibration measurement 61
4.2.1 Static deflection measurement 61
4.2.2 Dynamic measurement 62
4.2.3 Operating data 62
4.2.4 Modal data 65
4.2.5 SISO, SIMO, and MIMO vibration measurement 66
4.3 Provisional EU testing standard for timber floors prEN 16929 69
4.4 Laboratory and field floor vibration studies 71
4.4.1 Traditional timber floor serviceability studies 71
4.4.2 CLT and composite floor serviceability studies 75
4.5 Finite element modelling approaches to timber 79
4.6 Conclusions 81
5 Experimental methods 89
5.1 Introduction 89
5.2 Overview of experimental testing programme 89
5.3 Laboratory CLT test assembly 91
5.3.1 CLT floor and wall panels 91
5.3.2 Floor orientations 92
5.3.3 Laboratory test assembly 95
5.3.4 Bracket and screw schedule 95
5.3.5 CLT support walls to concrete floor 96
5.3.6 CLT floor to CLT wall assembly 98

5.4 Laboratory testing programme 106
5.4.1 Environmental conditions 106
5.4.2 Overview of testing 106
5.4.3 Apparatus 108
5.4.4 Deflection measurement 109
5.4.5 Initial frequency analysis and impulse measurement 110
5.4.6 Modal measurement 113
5.4.7 Acceleration amplification measurement 115
5.4.8 Footfall acceleration measurement 116
5.4.9 Damping ratio measurement 117
5.5 Field testing programme 118
5.5.1 Room geometries and floor supports 119
5.5.2 Test scope 120
5.5.3 Environmental conditions 121
5.5.4 Apparatus 121
5.5.5 Initial static and modal analysis 121
5.5.6 Deflection measurement 122
5.5.7 Frequency measurement 122
5.6 Conclusions 124
6 Experimental results 125
6.1 Introduction 125
6.2 Laboratory test results 125
6.2.1 Floor geometry, moisture content, mass and room environment 126
6.2.2 Static point load deflection results 126
6.2.3 Initial theoretical and impulse frequency results 132
6.2.4 Modal frequency analysis results 134

6.2.5 Acceleration amplification results 146

6.2.6 Footfall acceleration results 156

6.2.7 Damping ratio results 160

6.3 Field CLT test results 167

6.3.1 Room environment 168

6.3.2 Initial theoretical frequency results 168

6.3.3 Static point load deflection results 169

6.3.4 Impulse frequency results 170

6.4 Conclusions 173

7 FE Analysis of CLT floor systems 177

7.1 Introduction 177

7.2 Overview of numerical analysis 178

7.2.1 Numerical background of Abaqus dynamic analysis 181

7.3 FE modelling of laboratory tested floor 182

7.4 FE modelling of field tested floors 188

7.5 Generic FE room design 189

7.5.1 Floor voids 190

7.5.2 Internal partition walls 192

7.6 Specific standard room design 193

7.6.1 Residential: Twin hotel room model 193

7.6.2 Standard schoolroom design 198

7.7 Conclusions 202

8 FE CLT floor results 205

8.1 Introduction 205

8.2 FE model of laboratory tested floor 205

8.2.1 Static point load FE deflection results 205

8.2.2 Modal frequency FE results 208

8.3 FE models of the field tested floors 221

8.4 Parametric study of a multi-panel CLT floor 225

8.5 Specific standard room design 238

8.5.1 Residential: Twin hotel room model 238

8.5.2 Standard schoolroom design 244

8.6 Conclusions 248

9 Conclusions 251

9.1 Conclusions 251

9.2 Contribution to knowledge 257

9.3 Future work 259

References 261

LIST OF FIGURES

Figure 1.1 *Glulam roof structure: Ballinasloe swimming pool [5]* 2

Figure 1.2 *CLT panel* 3

Figure 1.3 *CLT construction* 3

Figure 1.4 *Grandview heights aquatic centre, under construction [Image by Seagate Mass Timber [8]]* 4

Figure 2.1 *Proposed 80-storey Oakwood timber tower for London [Image by PLP Architecture [30]]* 12

Figure 2.2 *Murray Grove, a nine-storey residential building in Hackney, London, 2009* 12

Figure 2.3 *dRMM's Maggie's Oldham building [Image by Alex de Rijke [36]]* 13

Figure 2.4 *Dalston Lane adjacent a high-speed railway line [Image by Daniel Shearing [38]]* 13

Figure 2.5 *Ballyogan Environmental Centre [Image by Michael Moran courtesy of Bucholz McEvoy]* 14

Figure 2.6 *Ballyogan Environmental Centre* 15

Figure 2.7 *Samuel Beckett Civic Campus* 15

Figure 2.8 *Private house in Co. Down [Images courtesy of G-Frame Structures]* .. 15

Figure 2.9 *CLT balloon construction [Image by GB-Legname [51]]* 17

Figure 2.10 *CLT platform construction* 17

Figure 2.11 *CLT platform construction* 17

Figure 2.12 *Proprietary multi-point CLT connection system [Image by Rothoblaas [52]]* 17

Figure 2.13 *Cross section of a five-layer CLT element loaded out-of-plane showing normal and shear stress distributions [67].* 20

Figure 2.14 *Standard wall to upper floor to wall detail* 23

Figure 2.15 *Typical CLT floor-to-floor panel junctions* 24

Figure 2.16 *Alternative CLT floor-to-floor panel junction assemblies* 24

Figure 3.1 *Linear spring [96]* 28

Figure 3.2 *Rigid mass* 28

Figure 3.3 *Undamped single degree-of-freedom system* 29

Figure 3.4 *Variation with time, displacement, velocity, and acceleration* [97] 30

Figure 3.5 *Viscous damper* 31
Figure 3.6 *Damped single degree-of-freedom system* 31
Figure 3.7 *Sample FRF free decaying damped oscillation (Assembly P)* 34
Figure 3.8 *Forced vibration applied to a damped single degree-of-freedom system* 34
Figure 3.9 *Amplification ratio (a) and phase angle (b), plotted against the frequency ratio [99]* 36
Figure 3.10 *First bending mode of a homogeneous plate* 39
Figure 3.11 *Second mode of a homogeneous plate, torsional* 39
Figure 3.12 *Limits and relationships between parameters a and b, [EC-5_7.3.3 [22]]* 43
Figure 3.13 *Basicentric axes (x, y, and z) for vibration defined in ISO 2631-1. Image [19]* 48
Figure 3.14 *Building vibration z-axis base curve for acceleration (foot-to-head) ISO 10137 [115]* 49
Figure 3.15 *Building vibration x- and y-axis base curve for acceleration (side-to-side and back-to-chest) ISO 10137 [115]* 49
Figure 3.16 *Building vibration x-, y-, and z-axis base curve for acceleration, ISO 10137 [115]* 50
Figure 3.17 *Recommended peak acceleration for human comfort for vibrations due to human activity. Steel Design Guide Series 11: Floor Vibrations due to Human Activity [21]* 56
Figure 4.1 *Impulse provided by a heel drop [137]* 63
Figure 4.2 *Impulse provided by a heavy rubber ball* 63
Figure 4.3 *Walking and impulse hammer field tests on timber floors [132]* 64
Figure 4.4 *Traditional measurement-system model, where noise is present in the system, basic SISO model [98][95]* 68
Figure 5.1 *Assembly of the two-way span platform construction @ NUI Galway* 92
Figure 5.2 *One-way long span platform construction (3812 mm span)* 93
Figure 5.3 *One-way long span balloon construction (4000 mm span)* 93
Figure 5.4 *One-way short span platform construction (2212 mm span)* 94
Figure 5.5 *Two-way spanning platform construction (3812, 2212 mm span)* 94
Figure 5.6 *Erection of one-way span balloon construction @ NUI, Galway* 95

Figure 5.7 *Hold-down brackets in-situ, Bishop’s Stortford, UK. A 10 mm gap is maintained between concrete ground floor and vertical timber wall panel.* 96
Figure 5.8 *Hold-down brackets fixed to concrete laboratory floor @ 500 mm c/c with epoxy chemical anchor, min. 100 mm embedment in the structural floor slab.* 97
Figure 5.9 *Platform construction partially threaded vertical screws @ 150 mm c/c*99
Figure 5.10 *Platform construction partially threaded vertical screws @ 300 mm c/c* 99
Figure 5.11 *Platform construction fully threaded inclined screws, 250 mm c/c* 99
Figure 5.12 *Platform construction with partially threaded vertical screws @ 300 mm c/c with shear-stress brackets* 100
Figure 5.13 *Platform construction with partially threaded vertical screws @ 300 mm c/c with reinforced angle brackets* 100
Figure 5.14 *Balloon construction with reinforced angle brackets @ 250 mm c/c* . 100
Figure 5.15 *Balloon construction with inclined screws, 250 mm c/c*...................... 101
Figure 5.16 *Platform construction partially threaded vertical screws @ 600 mm c/c* 101
Figure 5.17 *Platform construction partially threaded vertical screws @ 600 mm c/c and shear-stress brackets* 101
Figure 5.18 *XYLOFON 35* 104
Figure 5.19 *Assembly C during construction* 104
Figure 5.20 *Applied mass on a 500 mm x 300 mm grid* 105
Figure 5.21 *Long span platform construction dynamic testing with evenly distributed added mass, Assembly D* 105
Figure 5.22 *Impulse and modal testing equipment* 109
Figure 5.23 *Static point load deflection measurement, one-way long span platform construction @ NUI Galway* 110
Figure 5.24 *Diagnostic impulse impact and response locations on a one-way long span balloon construction, Assembly I* 112
Figure 5.25 *Independent scaffold erected for diagnostic impulse tests @ NUI Galway* 112
Figure 5.26 *Fixing of shaker to the floor* 113

Figure 5.27 *Transducer locations: 500 x 300 mm grid of 64 measurement points. Two alternative shaker locations, midspan and quarter-span* 113
Figure 5.28 *Modal testing in the laboratory with mass added to the floor panel (Assembly D)* 114
Figure 5.29 *Accelerometer fixing to floor: Threaded (a), and wax (b)* 115
Figure 5.30 *Electromagnetic shaker fixed to floor midspan, with cooling blower supported separately from the CLT test floor* 116
Figure 5.31 *Sample damping measurement. Control measurement in red.* 117
Figure 5.32 *CLT construction in Bishop's Stortford, UK: Test building* 118
Figure 5.33 *CLT construction in Bishop's Stortford, UK* 119
Figure 5.34 *CLT building in Bishop's Stortford, UK [Image courtesy of KLH UK]* 119
Figure 5.35 *Static point load deflection testing* 123
Figure 5.36 *Static point load applied midspan* 123
Figure 5.37 *Impulse testing using a 2 kg ball* 123
Figure 6.1 *Static 1kN point load applied midspan deflection results, Assemblies A to P* 127
Figure 6.2 *Deflection results for Assemblies A to H, One-way long span platform construction* 128
Figure 6.3 *Deflection results for Assemblies I to K, One-way long span balloon construction* 129
Figure 6.4 *Deflection results for Assemblies L to P, one-way short span and two-way spanning platform construction* 130
Figure 6.5 *Initial theoretical frequency estimates for Assembly I: Modes 0 to 80 Hz* 133
Figure 6.6 *Impulse test results for natural frequencies 0 to 80 Hz, Assembly I. A dotted line indicates the FEM simply-supported frequency values* 134
Figure 6.7 *Impulse and modal test results for natural frequencies 0 to 80 Hz, Assembly I* 135
Figure 6.8 *Typical mode shapes for assemblies A to K* 136
Figure 6.9 *Typical mode shapes for assemblies L to O* 137
Figure 6.10 *Assembly P mode shape* 137

Figure 6.11 *Natural frequency results ranging between 0 and 80 Hz, Assemblies A to P* 139

Figure 6.12 *Natural frequency results for the alternative bracket and screw configurations for one-way long span platform construction, without resilient interlayer or added load, Assemblies A, B, E, F, G, and H* 140

Figure 6.13 *Modes 1 and 2, Assemblies A, B, E, F, G, and H* 140

Figure 6.14 *Modes 3 and 4, Assemblies A, B, E, F, G, and H* 141

Figure 6.15 *Natural frequency results for the one-way long span platform construction, using partially threaded vertical screws @ 300 mm c/c (Assembly B), with resilient layer (Assembly C), and with added non-structural load (Assembly D)* 142

Figure 6.16 *Natural frequency results for the one-way long span balloon construction, using brackets and inclined fully threaded screws (Assembly J), and with added non-structural load (Assembly K)* 143

Figure 6.17 *Natural frequency results for the alternative bracket and screw configurations for one-way short span platform construction, and with added non-structural load (Assembly O)* 144

Figure 6.18 *Natural frequency results for the one-way short span and two-way span platform construction (Assemblies L and P)* 145

Figure 6.19 *Accelerance results for floor to wall assemblies A to P* 147

Figure 6.20 *Accelerations results for one-way long span platform construction, without resilient interlayer or added load, Assemblies A, B, E, F, G, and H* 148

Figure 6.21 *Accelerations results of Assemblies A, B, E, F, G, and H Modes 1, 2, and 3* 148

Figure 6.22 *Acceleration results of long span platform construction with vertical screws @ 300 mm c/c, with resilient layer (Assembly C), with added non-structural load (Assembly D)* 150

Figure 6.23 *Acceleration results for the balloon construction (Assemblies I, J, and K)* 150

Figure 6.24 *Accelerance results for the alternative bracket and screw configurations for one-way short span platform construction (Assemblies L to N), and with added non-structural load (Assembly O)* 151

Figure 6.25 *Acceleration results of one- and two-way spanning platform construction acceleration values (Assemblies L and P, respectively)*..152

Figure 6.26 *Frequency dependant accelerance measured, with permitted residential daytime acceleration limit values*..155

Figure 6.27 *Frequency dependant accelerance measured, with permitted residential daytime acceleration limit values (Assemblies B and D)*......................................156

Figure 6.28 *Frequency dependant accelerance measured, with permitted residential daytime acceleration limit values (Assemblies N and O)*......................................156

Figure 6.29 *Sample response measurement of one person walking (Assembly A)* .158

Figure 6.30 *Sample measurement of three adults walking (Assembly A)* 158

Figure 6.31 *Sample measurement of one person walking with a cane (Assembly A)* 158

Figure 6.32 *Sample FRF accelerance fundamental frequency measurements (Assembly A)*...159

Figure 6.33 *Damping ratios results for floor to wall Assemblies A to P* 161

Figure 6.34 *Damping ratios results for one-way long span platform construction, without resilient interlayer or added load, Assemblies A, B, E, F, G, and H* 162

Figure 6.35 *Damping ratios results Assemblies A, B, E, F, G, and H: Modes 1, 2, and 3*...162

Figure 6.36 *Damping ratios results for one-way long span platform constructions (Assembly B), with a resilient layer (Assembly C), and with added mass (Assembly D)* 164

Figure 6.37 *Damping ratios results for the balloon construction (Assemblies I, J, and K)*...164

Figure 6.38 *Damping ratios results for the alternative bracket and screw configurations for one-way short span platform construction (Assemblies L to N), with added non-structural load (Assembly O), and the two-way spanning floor (Assembly P)* 165

Figure 6.39 *Wall-to-floor assembly at an external wall in Bishop's Stortford, UK*168

Figure 6.40 *Static point in-situ deflection results, Rooms 1, 2, and 3*.....................170

Figure 6.41 *Sample in-situ impulse measurement (time domain): Room 1*............171

Figure 6.42 *FFT of the Room 1 impulse measurement (frequency domain): 0 to 80 Hz* 171
Figure 6.43 *Impulse test results for natural frequencies 0 to 80 Hz, Rooms 1 and 3* 172
Figure 7.1 *Numerical analysis of laboratory tested floor* 178
Figure 7.2 *Numerical analysis of field tested CLT floors* 179
Figure 7.3 *Numerical analysis of generic floor layout* 179
Figure 7.4 *Numerical analysis of twin hotel room floor layout* 180
Figure 7.5 *Numerical analysis of primary classroom floor layout* 180
Figure 7.6 *One-way long span platform construction with the shaker locations (Assemblies B, H, and D)* 182
Figure 7.7 *One-way long span balloon construction (Assemblies J and K)* 183
Figure 7.8 *One-way short span platform construction (Assemblies L and O)* 183
Figure 7.9 *Two-way spanning platform construction (Assembly P)* 184
Figure 7.10 *Single-panel CLT floor panel mesh, generally 25 mm element size* 185
Figure 7.11 *Distribution of added mass on a 500 mm x 300 mm grid (Assembly D)* 187
Figure 7.12 *2700 x 1800 mm rectangular stairwell midspan* 191
Figure 7.13 *2700 x 1800 mm rectangular stairwell midspan adjacent a support* .. 191
Figure 7.14 *2700 x 1800 mm rectangular stairwell adjacent two supporting walls* 191
Figure 7.15 *2700 x 1800 mm rectangular stairwell straddling two panels* 191
Figure 7.16 *Ø 1800 mm stairwell between two panels* 191
Figure 7.17 *Ø 100 mm service penetrations adjacent the floor support* 191
Figure 7.18 *Quarter-span support* 192
Figure 7.19 *Cross midspan support* 192
Figure 7.20 *Cross diagonal supports* 192
Figure 7.21 *Standard modern twin-bed hotel room with en-suite and furniture fit-out [195]* 194
Figure 7.22 *Standard modern twin-bedded hotel room without internal walls or furniture* 195

Figure 7.23 *Standard modern twin-bedded hotel room with non-load bearing internal walls*.......... 196
Figure 7.24 *Irish Department of Education and Sciences generic classroom design for primary schools [196].*.......... 199
Figure 7.25 *Classroom CLT panel layout*.......... 200
Figure 8.1 *Static deflection results, Assemblies B, H, and D; J and K; L and O; and P with EC-5 [22] minimum deflection limits 0.5 mm/kN*.......... 206
Figure 8.2 *Static deflection results, Assemblies B, H, and D; J and K; L and O; and P with EC-5 [22] 0.5 to 4.0 mm/kN limits and Irish NA: 1.8 mm/kN for spans ≤ 4000 mm [111].*.......... 207
Figure 8.3 *FE and experimental frequency results for platform Assemblies B and H*.......... 212
Figure 8.4 *FE and experimental frequency results for platform Assembly D*.......... 213
Figure 8.5 *FE and experimental frequency results for balloon Assemblies I and J* 214
Figure 8.6 *FE and experimental frequency results for balloon Assembly K*.......... 215
Figure 8.7 *FE and experimental frequency results for platform Assembly L*.......... 217
Figure 8.8 *FE and experimental frequency results for platform Assembly O*.......... 218
Figure 8.9 *FE and experimental frequency results for platform Assembly P*.......... 220
Figure 8.10 *Experimental Impulse and FE results compared for Room 1: Modes 1 to 10*.......... 223
Figure 8.11 *Experimental Impulse and FE results compared for Room 3. Modes 1 to 7*.......... 223
Figure 8.12 *FE frequency results of one CLT panel spanning 7000 mm (SP), a 7000 mm x 7000 mm three-panel floor spanning one direction (MP), and spanning in two directions (MP-TS). Modes 1 to 10*.......... 226
Figure 8.13 *FE frequency results of a three-panel floor spanning in two directions with a 1800 mm x 2700 mm void, unsupported (A), supported along two parallel sides (B), and along two adjacent sides (C), with (MP-TS) is represented by a broken line. Modes 1 to 10*.......... 229
Figure 8.14 *FE frequency results of the 1800 mm x 2700 mm void unsupported adjacent the main floor support (D), adjacent the corner of the floor (E), and midspan*

over two panels (F). Modes 1 to 10. (MP-TS) is represented by a broken grey line, the void unsupported mid-floor is shown in red (A). 231

Figure 8.15 *FE frequency results of the 1800 mm x 2700 mm void simply-supported adjacent the main floor support (D'), adjacent the corner of the floor (E'), and midspan over two panels (F'). Modes 1 to 10. (MP-TS) is represented by a broken grey line*.. 233

Figure 8.16 *FE frequency results due to an Ø 1800 mm void unsupported (G), supported (G'), and small service penetrations (H). Modes 1 to 10. (MP-TS) is represented by a broken grey line.*... 235

Figure 8.17 *FE frequency results of the three-panel floor spanning in two directions with an intermediate support at quarter-span (I), cross intermediate supports midspan (J), and diagonal cross support (K). Modes 1 to 10. (MP-TS) is represented by a broken grey line.*... 237

Figure 8.18 *FE frequency results of the two- and four- standard twin hotel room unfurnished (UF). Modes 1 to 10*.. 240

Figure 8.19 *FE results for a typical hotel bedroom layout, comparing the unloaded floor (UF), the effect of internal non-load bearing partitions (PW), including the bathroom fittings (BF), fully furnished (FF), and the equivalent loading evenly distributed across the floor (UDL). The rooms with an evenly distributed load without internal en-suite walls is also charted (UDL-W). Natural frequencies modes ranging 0 to 80 Hz* 243

Figure 8.20 *FE frequency results for a standard Classroom layout, with the room unfurnished (UF), fully furnished (FF), and fully occupied (FO). Modes 1 to 10* . 246

LIST OF TABLES

Table 2.1 *Proposed characteristic properties for homogeneous CLT, base material strength class T14, CV[$f_{t,0,l}$] 25 ± 5% Schickhofer et al. [77].* 20

Table 3.1 *Multiplying factors from Table C.1 ISO 10137: 2007 [115]* 51

Table 3.2 *Vibration dose values (m/s$^{1.75}$) [115][117]* 57

Table 5.1 *One-way long span platform construction: Assemblies A-H* 102

Table 5.2 *One-way long span balloon construction: Assemblies I-K* 103

Table 5.3 *One-way short span platform construction: Assemblies L-O* 103

Table 5.4 *Two-way platform construction: Assembly P* 104

Table 5.5 *Laboratory testing schedule* 107

Table 6.1 *Static 1kN point load applied midspan deflection results, Assemblies A to P* 127

Table 6.2 *Initial theoretical frequency estimates for Assembly I: Modes 0 to 80 Hz* 132

Table 6.3 *Impulse test results for natural frequencies 0 to 80 Hz, Assembly I* 133

Table 6.4 *Impulse and modal test results for natural frequencies 0 to 80 Hz, Assembly I* 134

Table 6.5 *Natural frequencies 0 to 80 Hz range for floor to wall, Assemblies A to P* 138

Table 6.6 *Accelerance for floor to wall, Assemblies A to P* 147

Table 6.7 *Frequency dependant measured and permitted accelerations. Unit force measured values and residential daytime limits* 154

Table 6.8 *Frequency dependant measured and permitted accelerations. Unit force measured values and residential daytime limits (Platform assemblies)* 155

Table 6.9 *Damping ratios for floor to wall, Assemblies A to P* 161

Table 6.10 *Initial floor fundamental frequency estimates* 169

Table 6.11 *In-situ static point load deflection results* 169

Table 6.12 *Impulse test results for natural frequencies 0 to 80 Hz, Rooms 1 and 3* 172

Table 7.1 *Material properties for CLT finite element model of laboratory 162 mm five-ply floor* 186

Table 7.2 *Standard hotel furniture* 197

Table 7.3 *Standard classroom furniture masses* 202

Table 8.1 *FE displacement analysis due to a 1kN load applied midspan, with experimental results for Assemblies B, H, D, J, K, L, O, and P* 206

Table 8.2 *Initial FE frequency mode shape estimates for Assembly I: 0 to 80 Hz*.. 209

Table 8.3 *FE frequency results compared for platform Assemblies B, H, and D* ... 210

Table 8.4 *FE modal results 0 to 80 Hz, for Assemblies B and H* 211

Table 8.5 *FE frequency results compared for platform Assemblies J and K* 214

Table 8.6 *FE modal results 0 to 80 Hz, for Assembly L* 216

Table 8.7 *FE frequency results compared for platform Assemblies L and O* 217

Table 8.8 *FE modal results 0 to 80 Hz, for Assembly P* 219

Table 8.9 *FE frequency results compared for platform Assembly P* 219

Table 8.10 *FE mode shape results for Room 1 and 3: Modes 1 to 3* 222

Table 8.11 *Experimental Impulse and FE results compared for Room 1: Modes 1 to 10* 222

Table 8.12 *Experimental Impulse and FE results compared for Room 3. Modes 1 to 7* 223

Table 8.13 *FE mode shape results of one CLT panel spanning 7000 mm (SP), a 7000 mm x 7000 mm three-panel floor spanning one direction (MP), and spanning in two directions (MP-TS). Modes 1 to 3* 225

Table 8.14 *FE frequency results of one CLT panel spanning 7000 mm (SP), a 7000 mm x 7000 mm three-panel floor spanning one direction (MP), and spanning in two directions (MP-TS). Modes 1 to 10* 226

8.15 *FE mode shape results of a three-panel floor spanning in two directions with a 1800 mm x 2700 mm void, unsupported (A), supported along two parallel sides (B), and along two adjacent sides (C). Modes 1 to 3* 228

Table 8.16 *FE frequency results of a three-panel floor spanning in two directions with a 1800 mm x 2700 mm void, unsupported (A), supported along two parallel sides (B), and along two adjacent sides (C). Modes 1 to 10* 228

Table 8.17 *FE mode shape results of the 1800 mm x 2700 mm void unsupported adjacent the main floor support (D), adjacent the corner of the floor (E), and midspan over two panels (F). Modes 1 to 3.* 230

Table 8.18 *FE frequency results of 1800 mm x 2700 mm void unsupported adjacent the main floor support (D), adjacent the corner of the floor (E), and midspan over two panels (F). Modes 1 to 10.* 230

Table 8.19 *FE mode shape results of the 1800 mm x 2700 mm void simply-supported adjacent the main floor support (D'), adjacent the corner of the floor (E'), and midspan over two panels (F'). Modes 1 to 3.* 232

Table 8.20 *FE frequency results of the 1800 mm x 2700 mm void simply-supported adjacent the main floor support (D'), adjacent the corner of the floor (E'), and midspan over two panels (F'). Modes 1 to 10* 232

Table 8.21 *FE mode shape results due to an Ø 1800 mm void unsupported (G), supported (G'), and small service penetrations (H). Modes 1 to 3.* 234

Table 8.22 *FE frequency results due to an Ø 1800 mm void unsupported (G), supported (G'), and small service penetrations (H). Modes 1 to 10* 234

Table 8.23 *FE mode shape results of the three-panel floor spanning in two directions with an intermediate support at quarter-span (I), cross intermediate supports midspan (J), and diagonal cross support (K). Modes 1 to 3* 236

Table 8.24 *FE frequency results of the three-panel floor spanning in two directions with an intermediate support at quarter-span (I), cross intermediate supports midspan (J), and diagonal cross support (K). Modes 1 to 10* 237

Table 8.25 *FE mode shape results of two, and four standard twin hotel rooms unfurnished (UF). Modes 1 to 3* 239

Table 8.26 *FE frequency results of the two- and four- standard twin hotel room unfurnished (UF). Modes 1 to 10* 239

Table 8.27 *FE mode shape results of the four standard twin hotel rooms with the addition of en-suite partitions (PW), and the bathroom fittings (BF). Modes 1 to 3.* 241

Table 8.28 *FE mode shape results of the four standard twin hotel rooms with the addition of the discrete loading of the rooms fully furnished (FF), and the equivalent mass evenly distributed (UDL) Modes 1 to 3.* 242

Table 8.29 *FE results for a typical hotel four bedroom layout, comparing the unloaded floor (UF), the effect of internal non-load bearing partitions (PW), with bathroom fittings (BF), fully furnished (FF), and the equivalent loading evenly distributed*

across the floor (UDL). The rooms with an evenly distributed load without internal en-suite walls is also charted (UDL-W) The natural frequencies modes ranging 0 to 80 Hz are presented...242
Table 8.30 *FE modal results for a standard Classroom layout, with the room unfurnished (UF), fully furnished (FF), and fully occupied (FO). Modes 1 to 3*....245
Table 8.31 *FE frequency results for a standard Classroom layout, with the room unfurnished (UF), fully furnished (FF), and fully occupied (FO). Modes 1 to 10*..245

1 INTRODUCTION

1.1 Modern timber construction

The built environment is ever evolving, and our cities, along with the world's population, are growing at an exponential rate [1][2]. In addition to traditional economic or cultural migration from rural to urban areas, more frequent and severe occurrences of drought, floods, and famine has forced many rural communities across the globe to relocate for survival. This in tandem with the cyclical flow of refugees from conflict zones is causing a significant strain on the capacity of modern cities especially. Ironically this increased urbanisation with the inevitable degree of consumerism, in comparison with the self-sufficiency associated with rural living, feeds the problem. It is reasonable to assume also that the trend towards more densely populated living will not be reversed in the foreseeable future. Aside from an augmented population size and the amalgamation of lands in an effort to intensify crop yields, the necessary rural skillsets will be lost or forgotten to urban dwellers along with an inevitable shift in people's lifestyle expectations. If urban sprawl is to be restricted at all, there is a need to increase density and build taller. However the materials currently preferred for use in high density and high rise development are carbon intensive. Their sourcing, manufacturing, transport, and ultimately their disposal, can only exacerbate the challenging environmental concerns. In contrast, timber construction is carbon neutral, sustainable, and renewable. As a natural composite, timber is lightweight and strong. It is not a new building material, with a wealth of knowledge, skill, and craftsmanship inherited and ever enriched since B.C. Its use in construction has the potential to reduce global fossil fuel use by up to 15%, resulting in a possible 31% reduction in CO_2 emissions [3]. Recent research on sustainable forestry has found that appropriate forest management has the potential to reduce the EU's CO_2 emissions by up to 20% by 2050 [4].

The tendency in modern architecture is towards modular, pre-manufactured, and engineered components. Materials and resources are optimised into component parts that can be assembled quickly and simply. Research and development in timber engineering endeavours to capitalise on timber's known strengths, to create prefabricated building elements suitable for the current construction preferences while maintaining its environmental benefits, thereby meeting the demands of modern construction now and in times to come.

1.1.1 Mass-timber and CLT

There are numerous prefabricated timber engineered building elements that are suitable for modern buildings. The elements defined as mass-timber products include glued laminated timber (glulam or GLT), cross laminated timber (CLT), nail laminated timber (NLT), and dowel laminated timber (DLT) or Brettstapel. Glulam, usually associated with long-spanning roof structures or bridge constructs, are timber beams manufactured with timber boards laminated parallel to the main axis. Due to their composite make-up there is a wide scope in their size, shape, and therefore application. Figure 1.1 shows a 25 meter swimming pool in Galway where curved glulam beams provide the roof support.

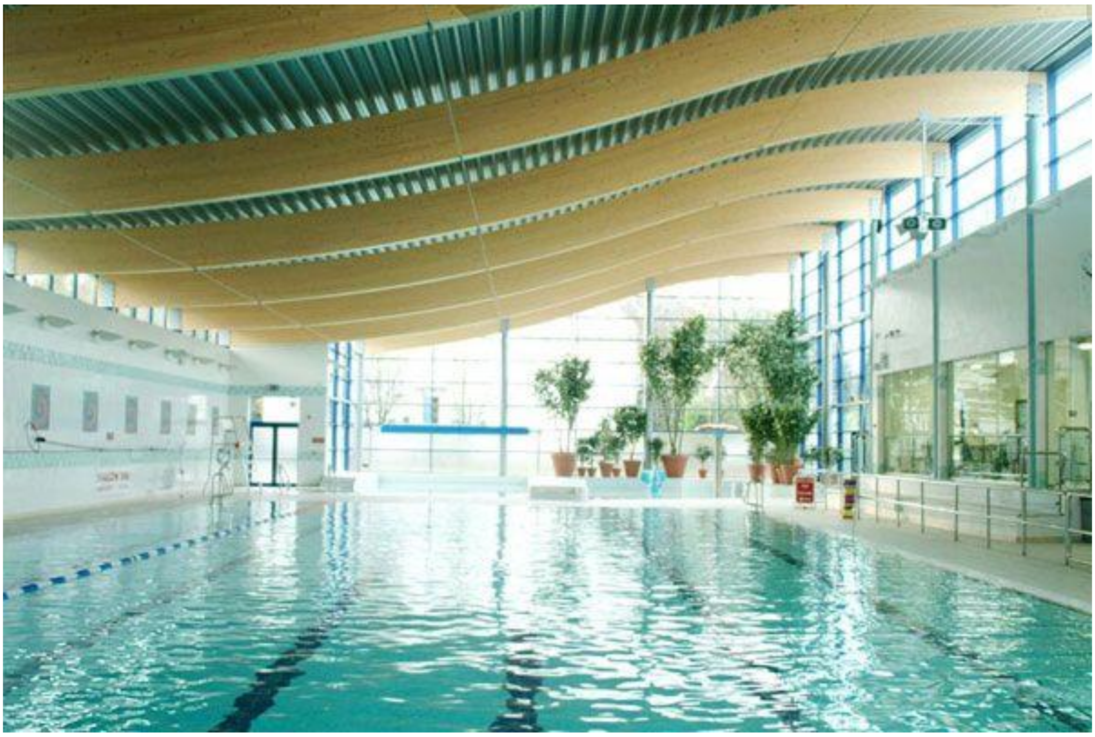

Figure 1.1 *Glulam roof structure: Ballinasloe swimming pool [5]*

CLT (Brettlagenholz or BSP in Germany, or X-lam in Australia/New Zealand) is manufactured in much the same way. It comprises timber boards aligned in laminae, which are stacked with alternate laminae at right angles and then glued under high pressure into large solid panels. The panels can bear loads in- and out-of-plane, and are therefore suitable for roof, wall, floor, and stair construction. The panels are manufactured offsite and transported in sequence for assembly in-situ. Figures 1.2 and 1.3 show, respectively, a typical 5-ply CLT panel and a three-storey building during construction where CLT forms the structure for the upper floors, walls, and roof. Alternatively, panels may be manufactured using nails (NLT), or timber dowels in place of glue (DLT and Brettstapel). CLT for now is the most viable timber alternative to concrete or steel construction for multi-storey development. This study concentrates on CLT floor construction, specifically with respect to its serviceability response.

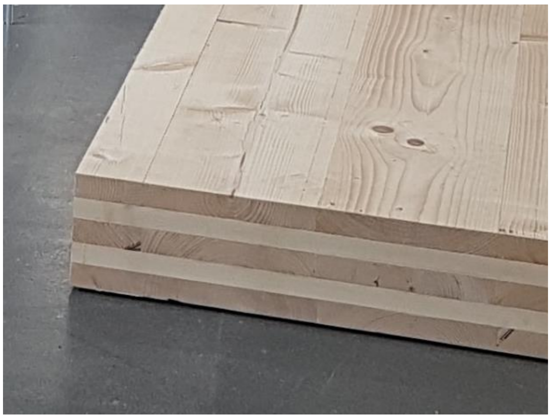

Figure 1.2 *CLT panel*

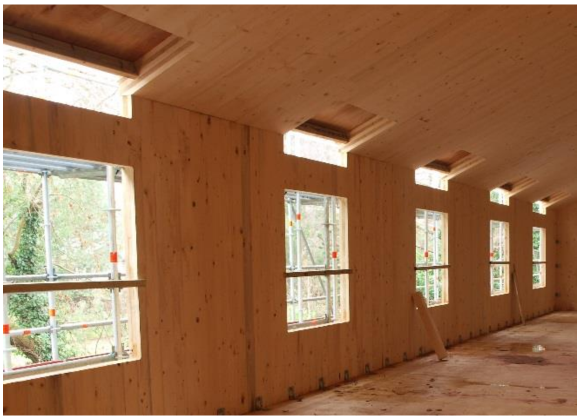

Figure 1.3 *CLT construction*

1.1.2 Building with timber

Although timber is an age old construction material, there is a perception sometimes that it may not be as robust as other alternatives. However in some cases, timber's material characteristics make it a more appropriate choice. Wood performs significantly better compared with steel or concrete with regard to thermal efficiency. Its thermal conductivity is 0.13 W/mK, compared with 2.50 W/mK for reinforced concrete, or 50.00 W/mK for steel [6]. A timber building will meet the required U-value standards using less insulation or alternatively, the overall energy loss may be reduced by using the standard thickness of insulation. The carbon footprint of the building is reduced in either instance.

Susceptibility to fire or corrosion is at times cited as a deterrent in selecting timber structurally. However, both concerns apply to steel also and are overcome with chemical treatment or careful detailing. In the case of fire protection, gypsum cladding or an intumescent paint is applied to prevent heat damage or surface flame for steel or timber construction. Although steel is not flammable, it can distort and buckle in a fire. Timber chars uniformly at a predictable rate, providing insulation to the remaining wood core, hence maintaining its integrity for a known timeframe. Safe, timely evacuation is the cornerstone of building fire safety. A structure is compartmentalised to contain a fire, allowing adequate time for egress or rescue in alternative opposite directions. The certified FD30 to FD120 fire doors through the compartments have precise details and specific test criteria [7]. Their location along an escape route, glazing, closing mechanism, and smoke and fire resistance are strictly regulated to ensure safe passage away from danger. These doors and frames are predominantly made with timber, softwood, or hardwood, depending on the fire rating required.

In the case of an especially corrosive environment, such as a swimming pool treated with chlorine, timber glulam beams are frequently selected as the main roof support. When determining the design approach for a new 50 m FINA Olympic pool, in Surrey, Canada, it was decided in order to satisfy a design aesthetic to span the roof along the pool length. A glulam catenary roof spanning up to 55 m was proposed. Figure 1.4 shows the timber roof structure during construction.

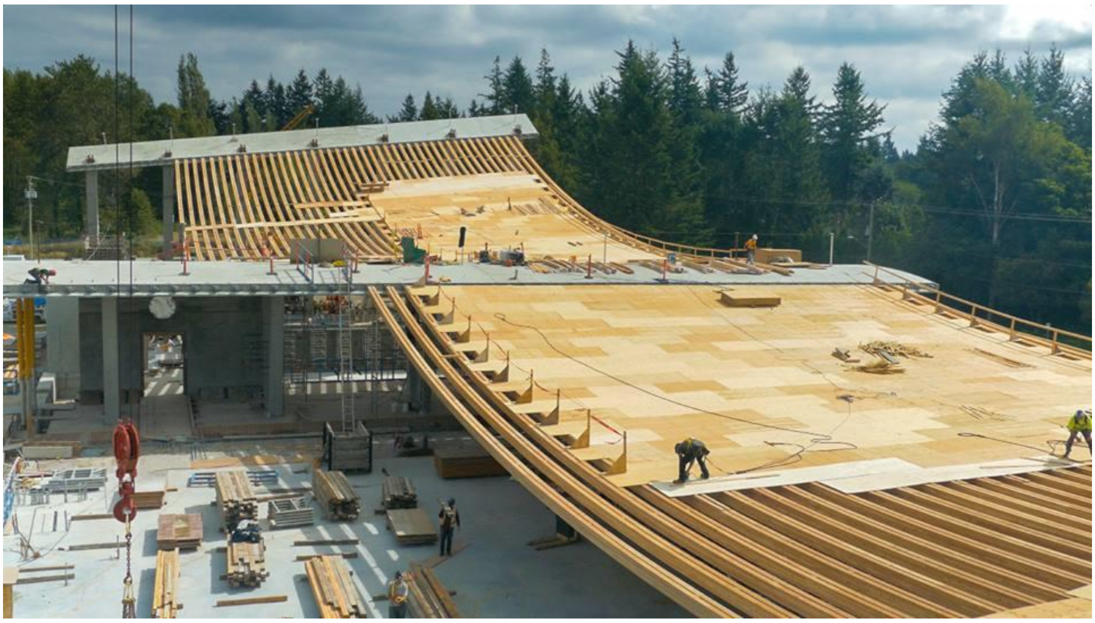

Figure 1.4 *Grandview heights aquatic centre, under construction [Image by Seagate Mass Timber [8]]*

An alternative steel cable roof with timber infills was deemed to be more connection intensive and more susceptible to corrosion [9]. The glulam cables measured 130 mm x 266 mm at 800 mm centres. Using timber in this way, in tension, resulted in a 300 mm structural roof depth, compared with an estimated 3000 mm for a conventional steel truss design of the same span [10]. Timber had the advantage over steel, because it was more resistant to corrosion. It was preferable to concrete as the design required strength in tension. The timber structure could be left exposed internally as a cladding or suspended ceiling was not required. The ribbed profile of the beamed ceiling had an additional acoustic benefit, very welcome in a building with high noise levels and mostly hard reflective surfaces. Two Irish examples of swimming pool buildings with exposed glulam roof supports are in Ballinasloe, Co. Galway, shown in Figure 1.1, and Longford Town leisure centre.

Timber construction is up to a quarter the weight of concrete construction. When looking for a building system suitable for relatively poor soil conditions in the Docklands region of Melbourne, Australia, due diligence prompted the selection of CLT construction for the ten storey high residential Forte building [11]. The building was completed in 2013. The panels were shipped from Europe in this case, but Australia has now its own CLT manufacturing facility [12].

1.1.3 Timber floors

Traditional timber-joist flooring

Timber is generally considered to be a cylindrically orthotropic material, and is significantly stiffer along the grain direction. Traditional carpentry, including timber-joist and engineered-joist floor construction, naturally exploits this quality with members spanning parallel to the grain. Joists usually span up to 6000 mm at between 300 mm to 600 mm centres with cross bracing providing lateral stiffness at spacing ranging between 600 mm and 1200 mm. The floor deck, measuring less than 25 mm in thickness, may comprise oriented strandboard (OSB), plywood, or tongued and grooved softwood or hardwood boards. The deck is fixed to the joists. A ceiling below, usually constructed with gypsum board or timber boards, is not always required. Additional thermal or acoustic insulation may be incorporated into the floor build-up. As all components are assembled on site, the quality of the workmanship at the supports and the fit and accuracy of the bracing members all influence the floor’s stiffness. The possibility of distortion of members due to poor storage conditions and exposure to moisture, heat, or lack of ventilation before and after assembly can also impact on a traditional timber floor's rigidity.

Essentially traditional timber floors are strongly orthotropic, with their stiffness considerably lower in the direction perpendicular to the beams [13]. Although, the floor deck and ceiling have been found to have some influence on the floor's shear strength, its rigidity will be influenced in the main by the choice and spacing of the joists along the direction of the joist span. Any lateral stiffness is predominantly influenced by the quality of cross strutting or bracing.

CLT floors

A CLT floor behaves more like a plate structure. It has a greater mass, higher shear strength, and multi-directional floor support is possible with CLT construction. These reasons distinguish it from traditional timber floors with regard to its vibration response [14].

CLT floor panels are normally five-ply, measuring over 160 mm thick, over 2000 mm wide, and up to 16500 mm in length. The panels commonly span multiple rooms, often measuring in excess of 6000 mm between supports.

While a traditional timber floor comprises a floor deck spanning between joists, a CLT floor is a solid panel with a uniform thickness through-out and so may be supported in any direction. A small degree of lateral and longitudinal expansion or shrinkage is expected in CLT construction, however, the sequenced delivery and quick assembly of CLT floors, in tandem with their mass and stiffness, make CLT floors less susceptible to cupping, twisting, or bowing from changing environmental conditions. Any movement in CLT construction will most likely to occur at the connections [15][16].

Vibration in timber floors

All buildings must be designed and constructed to a standard of stability and robustness appropriate to their use and location. An anticipation of a level of privacy between separate inhabitants is reasonable, especially in the case of multi-family occupancy, hotel accommodation, or where the occupant's work necessitates a degree of quiet.

Floor serviceability has been a significant design concern in modern buildings, particularly for steel-deck or long spanning and slender concrete floor design [17][18], with many studies aimed at quantifying and improving vibration performance in both cases [19][20][21].

An obstacle for designers when selecting timber for floors may be the reputation earned by light-weight timber frame structures, particularly timber-joisted floors with regard to human-induced deflection and vibration. The serviceability criteria is generally the limiting factors of traditional timber floor design, and its correlation with human comfort has been extensively examined. However, the existing European timber design standard EN 1995-1-1 (EC-5) [22] relates to traditional timber-joist floor construction and it does not provide specific guidance on CLT structural design [23]. The serviceability performance of CLT floors is not fully established. Essential for designers is the need to establish the effects of the floor support, fixing design, the floor geometry, the mass, and the dynamic loading distribution on the serviceability performance of the floor.

1.2 Research aims and objectives

The primary aim of this research is to characterise the serviceability performance of CLT floor systems used in mid-rise buildings. The research is focused on the excitation of the floor systems due to human activity within the structural vibration frequency range of people’s perception.

In order to achieve this aim, seven key objectives are defined.

The first objective is to specifically quantify the performance of a particular connection detail, fixing type, or connection positioning with respect to the serviceability of the floor. The research will focus on the prevailing CLT floor-to-wall junctions that are suitable for mid-rise construction of residential, office, and school buildings. The influence of spanning in one and two directions on the deflection and vibration response will be also explored. This part of the study will be carried out using floor-wall systems in the laboratory.

The second objective is to establish the influence on the vibration performance of the provision of non-structural elastomeric interlayers, which are used in typical timber floor junctions to reduce sound transmission. This will be investigated on the laboratory CLT floor-wall systems.

Thirdly, the study proposes to establish the effect of an added mass evenly distributed on the laboratory floor. The mass will be equivalent to that of a non-structural floor screed.

Fourthly, the influence of the floor integration into a building will be measured by conducting in-situ measurements on a residential building. The influence on the static and dynamic performance of the number of CLT panels connected in parallel will be determined.

The fifth objective is to determine the influence of floor voids, the void position, and support, and the effect of non-structural intermediate supports on floor serviceability. The support position and angle relative to the main floor span will be examined. This parameter study will be undertaken using a numerical modelling approach.

The sixth objective is to explore the dynamic influence of irregular mass distributions on a floor. The mass sizes and their distributions will be representative of typical objects or loading on specific standard room layouts.

Finally, an efficient numerical modelling approach will be developed that can be used to identify the optimum CLT floor design choice with respect to support choices, geometry, and mass or loading distribution that best serve to mitigate unacceptable or uncomfortable static or dynamic performance in CLT floors.

1.3 Structure of the thesis

Chapter 1 is an introduction to the thesis, giving the background to the research, and outlining the research goals and objectives.

Chapter 2 provides a brief state-of-the-art review of CLT construction. Examples of noteworthy CLT design are given. An overview of the current CLT design standards, commercial CLT material characteristics, and contemporary assembly practices are presented.

Chapter 3 gives an overview of classic vibration theory to provide a basis of understanding of the dynamic behaviour of structures. A review of the current serviceability limit design criteria for timber floor design is presented. The study focuses particularly on European timber floor serviceability design standards, the Canadian and US CLT floor serviceability criteria, and international design criteria on human tolerance to vibration with respect to building design.

Chapter 4 précises the non-destructive measurement and analysis techniques that are applied in determining a floor's dynamic behaviour. A literature review of field and laboratory studies made on timber floors with respect to serviceability is presented. Finite element (FE) approaches to modelling timber and CLT are also reviewed.

Chapter 5 presents the experimental testing programme, which was designed to address the first four research objectives. This includes tests on sixteen variations of contemporary CLT floor to CLT wall fixing assemblies in the laboratory. Also described are static and dynamic tests of multiple panel CLT floors carried out in-situ on a residential building. Details of the static and dynamic testing methods applied are outlined.

Chapter 6 presents the results of the experimental laboratory and field testing, comprising static and dynamic measurements. The laboratory dynamic testing included impulse, mechanical, and footfall excitation. The modal frequencies, accelerance, and damping characteristics of each alternative floor assembly was recorded. An impulse excitation was recorded and analysed for the floors tested in the field. Flexural stiffness was measured with static tests in each case.

Chapter 7 outlines the FE analysis programme, which was designed to address objectives 5 to 8. This includes FE models that were developed based on the tested laboratory and in-situ CLT floors and parametric studies of generic multi-panel CLT floors. Additionally, an FE study that examines the correlation between design standard criteria and the likely performance of in-situ floors that are furnished and occupied is outlined.

Chapter 8 presents the results of the FE studies. Experimental and FE results are compared and the suitability of the FE approach is appraised. The results of the FE parametric studies and specific room designs are also outlined.

Chapter 9 summaries the conclusions of the research and gives recommendations for further research.

2 CROSS LAMINATED TIMBER

2.1 Introduction

When CLT was introduced to the UK in 2000, it was deemed a niche product. It is now considered a viable alternative to steel and concrete construction, with more than 500 buildings in the UK constructed using CLT. Reasons given by designers for choosing CLT include its relative speed of assembly, versatility where space is restricted, and lower dead weight in comparison to concrete [24]. This chapter outlines some noteworthy examples of architecture using CLT, the current design standards regarding its manufacture and assembly, along with contemporary design practices for mid-rise CLT construction.

2.1.1 CLT buildings

Since it was developed in the 1980s, the majority of CLT research and development has occurred in Europe, centred on Austria, where the bulk of CLT manufacturing is concentrated (90% of global CLT production, circa 800,000 m^3 per annum) [25]. However, CLT's use is growing worldwide, especially in Central Europe, but also in Scandinavia and Canada, where there is a long tradition of building with wood. Its popularity is increasing too in earthquake-prone regions such as the West coast of the US, Italy, Japan, and New-Zealand, due to the reduced seismic loads associated with this lightweight building system.

While timber in its many guises is a staple building material, the extended possibilities afforded by CLT and other mass-timber construction, combined with its eco-credentials, are inspiring designers worldwide to build ever-higher wooden structures. There are conceptual proposals for a 40-storey CLT building in Stockholm [26], a 70-storey high tower in Tokyo [27] and a 80-floor timber tower in central London [28][29]. An illustration of this tower in the current London skyscape is shown in Figure 2.1 [30]. There is a proposal in Sweden to develop a whole neighbourhood of wood, comprising 31 CLT towers [31][32]. Figure 2.2 shows Waugh Thistleton's 2009 landmark nine-storey residential block, Stadthaus/Murray Grove. It was the first multi-story building where the entire structure, with the exception of the ground floor, comprised CLT panels only. However, multi-storey timber buildings are less unusual now, with many global examples available [33], including a wide variety of CLT buildings in the UK [34].

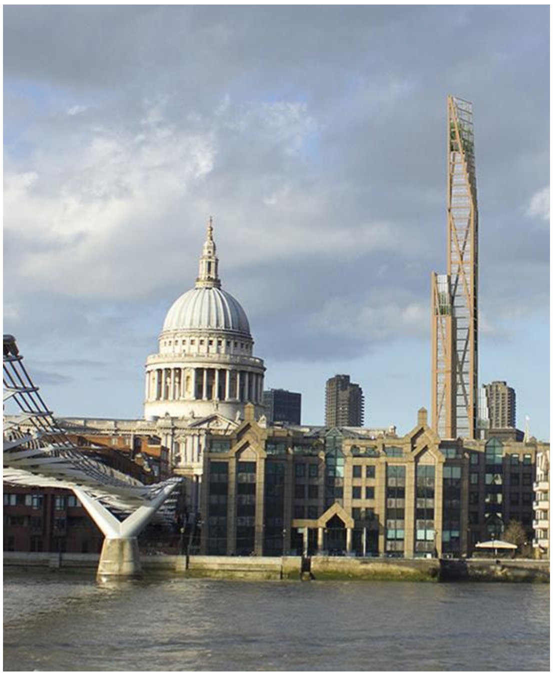

Figure 2.1 *Proposed 80-storey Oakwood timber tower for London [Image by PLP Architecture [30]]*

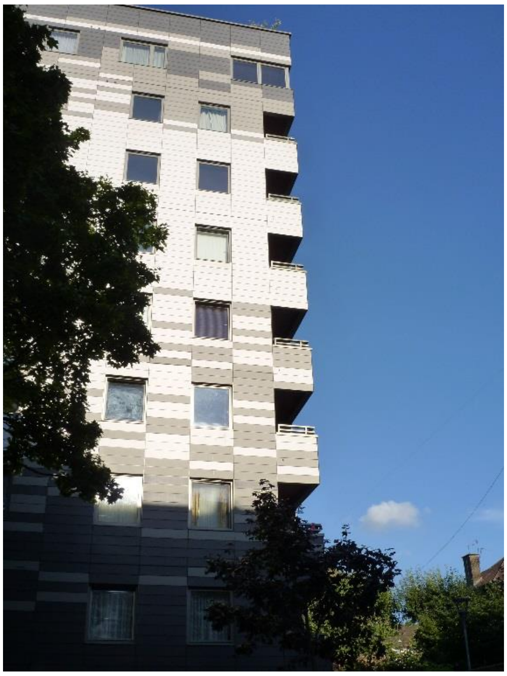

Figure 2.2 *Murray Grove, a nine-storey residential building in Hackney, London, 2009*

Murray Grove demonstrated the suitability of CLT to modular prefabricated construction, but this type of construction is equally suited to more ambitious design with a high proportion of nominations in recent years for UK's architectural RIBA awards comprising mass-timber buildings. Its principal award, the RIBA Stirling Prize, was awarded in 2017 to Hastings Pier, which is a CLT development. The 2018 RIBA award winning building by dRMM architects that houses the newest Maggie's cancer-care treatment centre in Oldham, Manchester is constructed with a hardwood CLT. Maggie's has a reputation for commissioning high-quality contemporary design, boasting world acclaimed architecture. Frank Gehry, Zaha Hadid, and Herzog & deMeuron designed the Dundee, Kirkcaldy, and Glasgow centres, respectively. The CLT panels for the Manchester centre were manufactured with sustainable American tulipwood. The base timber was selected due to its lower mass in comparison with other hardwoods, and higher strength characteristics compared with softwood [35]. A garden grows through a central glass core in the Maggie's Oldham building, which is illustrated in Figure 2.3.

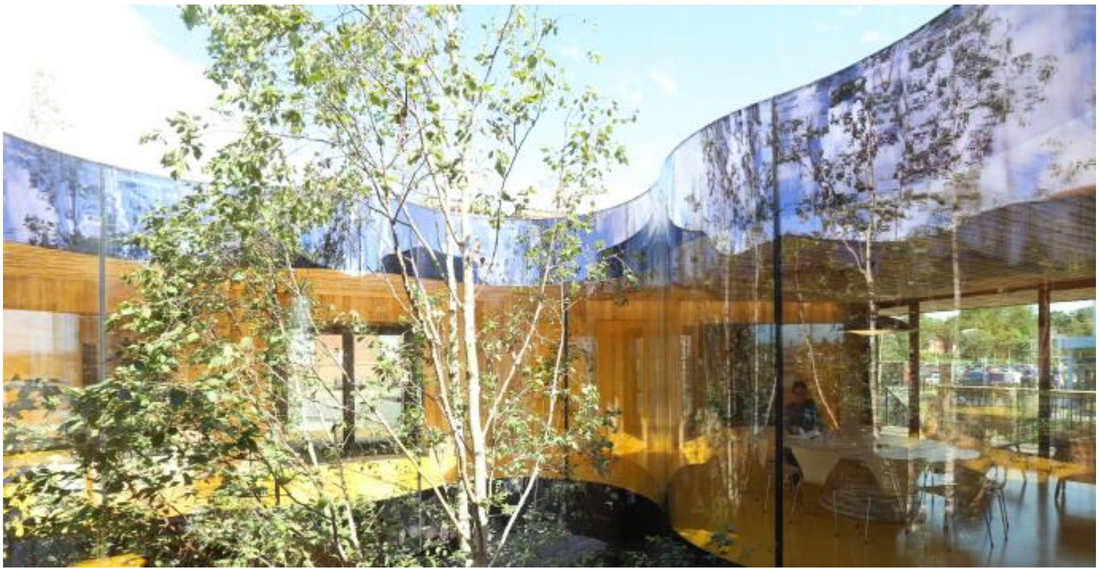

Figure 2.3 *dRMM's Maggie's Oldham building [Image by Alex de Rijke [36]]*

In 2012, the London borough of Hackney introduced a 'Timber first' policy, which is a testament in itself to timber's suitability for high-density development using CLT. A case study which illustrates this is Hackney's ten-storey Dalston Lane development [37], shown in Figure 2.4. Built adjacent to a high-speed railway line, with weight restrictions in place, an additional three storeys with potentially 35 extra units were possible by selecting CLT over a concrete structure. Similarly, using CLT construction for a redeveloped in-fill site in Kensington allowed for the reuse of the existing foundations. This was possible as the CLT structure of the new 43 unit housing development was much lighter than traditional construction [34].

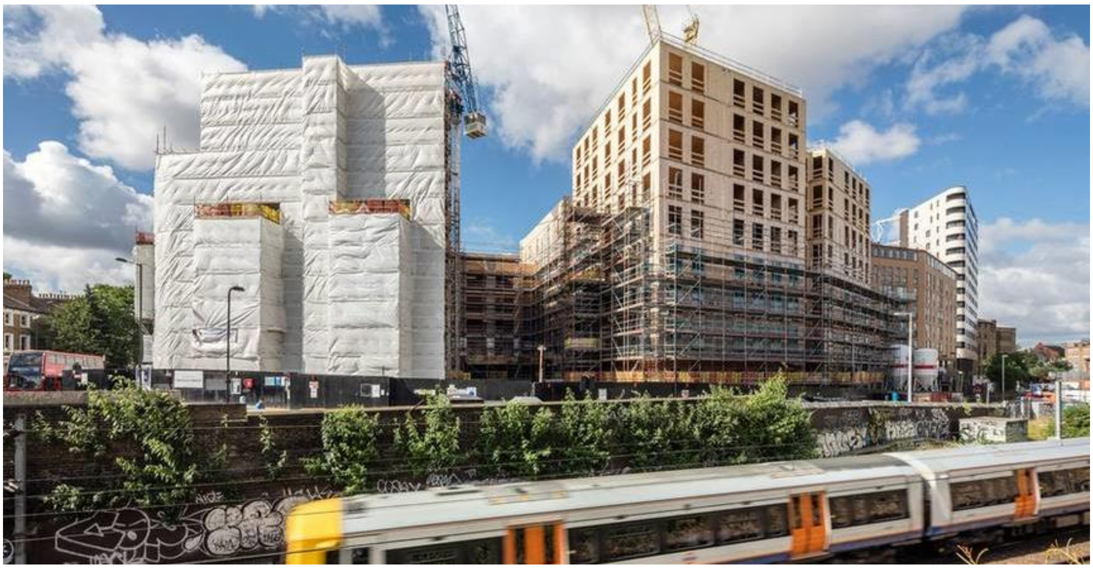

Figure 2.4 *Dalston Lane adjacent a high-speed railway line [Image by Daniel Shearing [38]]*

2.1.2 Hybrid CLT buildings

Like most construction methods, mass-timber construction can incorporate other building materials, meeting specific time, cost, or material characteristics, and are described as hybrid buildings. Until March 2019 the world’s tallest timber building was an 18-storey student residence for the University of British Columbia, Brock Commons. Its principal structural components comprised CLT flat slabs supported on glulam columns with concrete stairs and lift cores. Measuring 53 m high, the timber structure was erected in 8 weeks [39][40][41]. Brock Commons has since rescinded its title as the tallest timber building to Norway’s 85 m high, 18-floor, Mjøsa Tower.

2.1.3 CLT buildings in Ireland

Two examples of CLT construction in Ireland are the award winning projects by Bucholz McEvoy architects, Ballyogan Environmental Centre (Figures 2.5 and 2.6) constructed using CLT for the walls and floors, and the Samuel Beckett Civic Campus (Figure 2.7), which comprises CLT walls and concrete floors. The frame of both buildings is glulam.

CLT construction in Ireland is otherwise limited to a small number of one-off dwellings. An example of one dwelling during construction is shown in Figure 2.8.

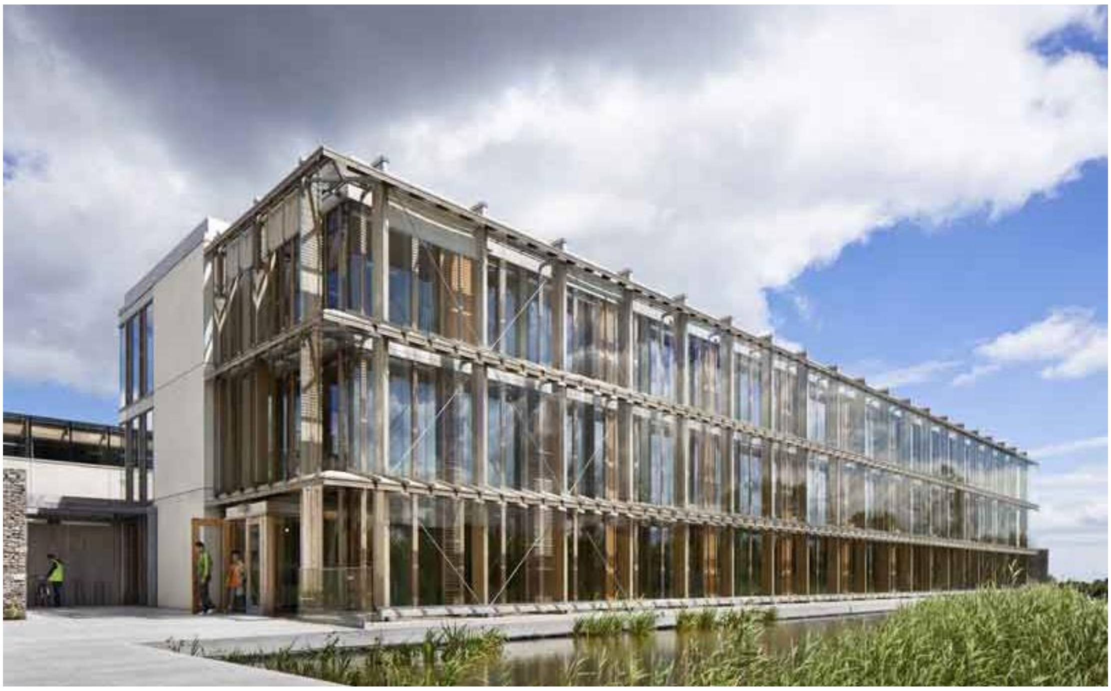

Figure 2.5 *Ballyogan Environmental Centre [Image by Michael Moran courtesy of Bucholz McEvoy]*

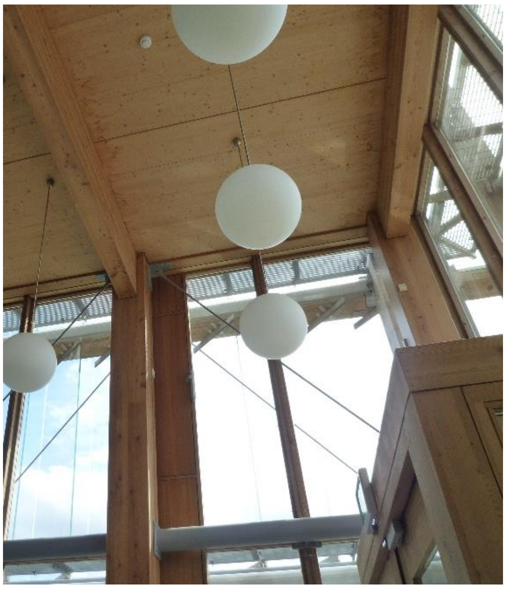

Figure 2.6 *Ballyogan Environmental Centre*

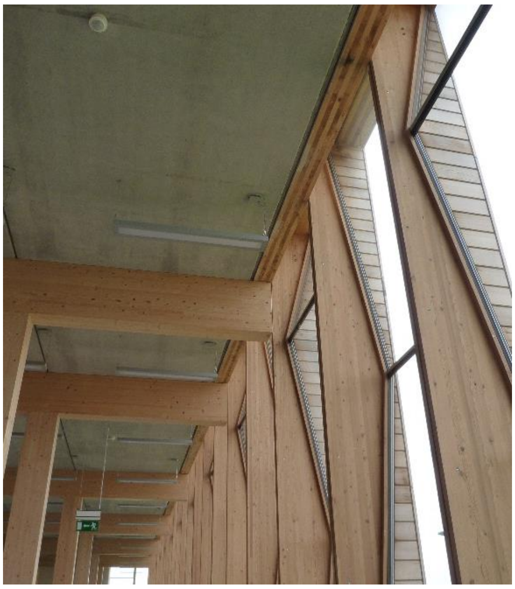

Figure 2.7 *Samuel Beckett Civic Campus*

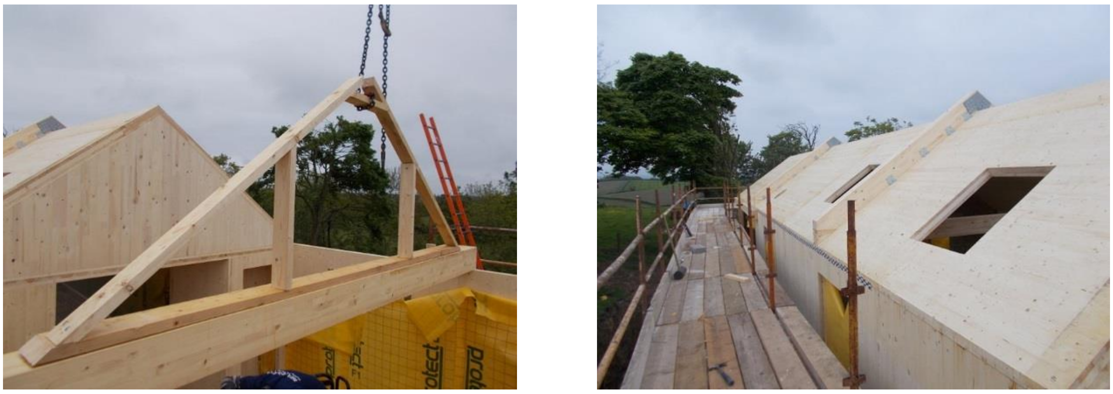

Figure 2.8 *Private house in Co. Down [Images courtesy of G-Frame Structures]*

Bearing in mind Ireland's current urban deficit in housing and school resources, due to a depleted construction industry in recent years and a growing population, a time-efficient building system which is suited to high density development may be an attractive option in meeting this shortfall.

With investment recently allocated to school buildings in Ireland [42], it is worth noting that timber in the form of CLT and glulam is considered a viable material in school development globally [43][44][45][46][47]. In a recent restructuring of a 1970's concrete building to create a new elementary school in New South Wales, Australia, BVN Architects selected glulam and CLT throughout the refurbishment of the school. The timber structure was generally left exposed in the interests of promoting wellness and improving the building's acoustic performance, which are additional benefits to timber's established environmental credentials [48].

The offsite manufacturing and sequenced building approach used in CLT construction make it an appropriate choice where there is a requirement to maintain access and use of the existing facilities during the build time. The fixed school year make this a critical consideration for any building works to, or adjacent educational buildings. The standardised school dimensions, with room sizes regularly spanning over seven meters, generally rule-out the use of traditional timber-joist floors, but are very possible with CLT.

2.2 CLT design

Although CLT panels can be used in tandem with traditional concrete, steel-frame, or even masonry construction, integrating CLT with other structural systems may reduce its time, mass, and space benefits [34]. For mid-rise development, it is recommended to primarily build the whole structure with CLT panels, using glulam or steel beams locally, if necessary. It is very common however that the external façade does not reflect the building's structure. Dalston Lane (Figure 2.4), for example, now has a red-brick external façade.

In the main, CLT mid-rise building structures, may be categorised as either balloon construction, shown in Figure 2.9, or platform construction, which is illustrated in Figures 2.10 and 2.11. In the case of balloon construction, the walls are erected spanning more than one storey and intermediate floors are attached thereafter. Due to limitations on the panel length and propping requirements during erection, this type of approach is usually limited to low-rise construction or specific compartments in a building, such as the stairwells or lift shafts.

Alternatively for multi-storey development, specific proprietary multi-point connection systems have been developed [49][50], such as that illustrated in Figure 2.12. However, as is generally the case with modular proprietary building systems, integration with other structural building materials in this case is more complicated.

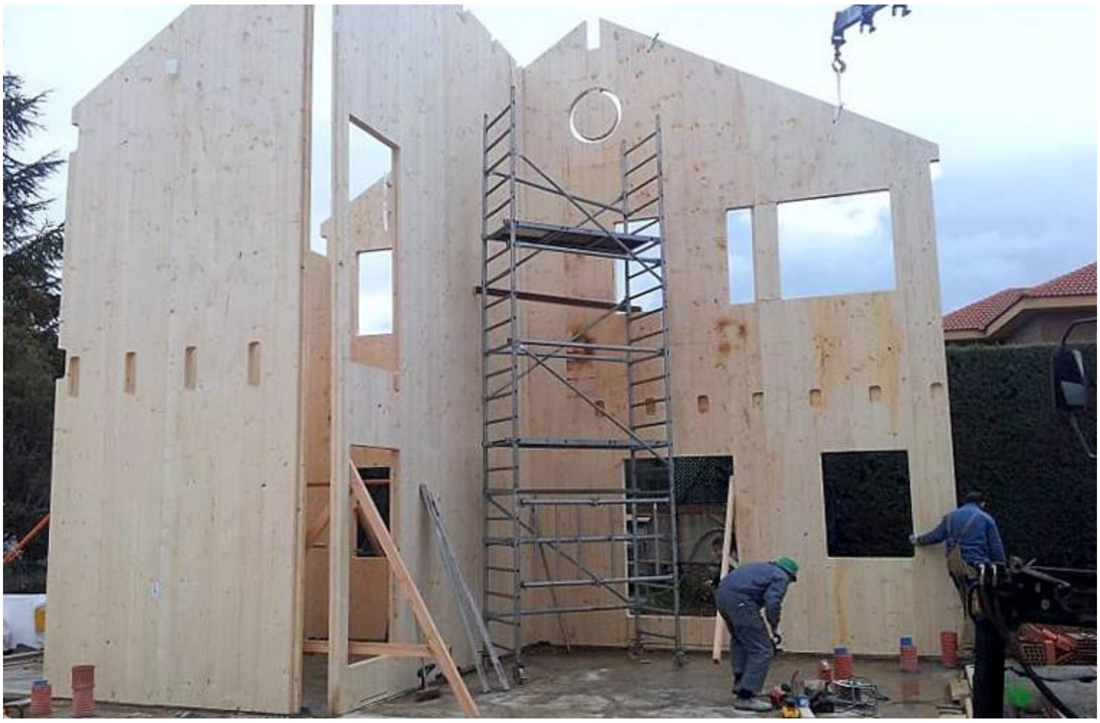

Figure 2.9 *CLT balloon construction [Image by GB-Legname [51]]*

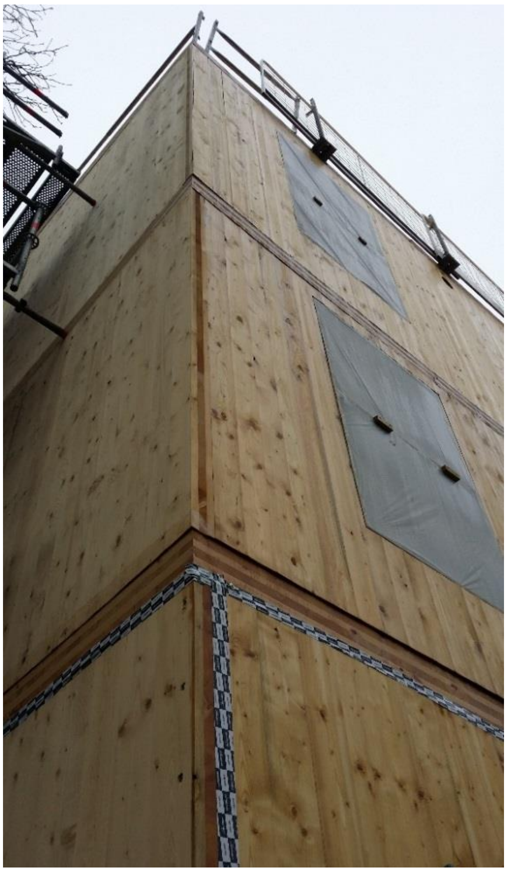

Figure 2.10 *CLT platform construction*

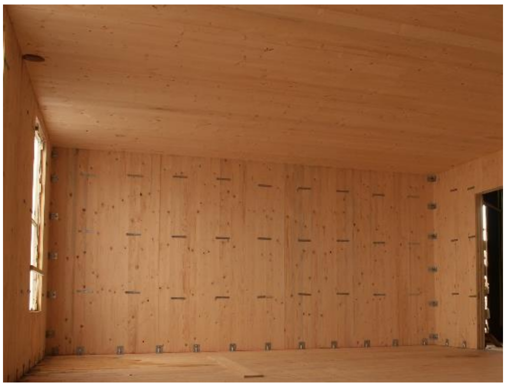

Figure 2.11 *CLT platform construction*

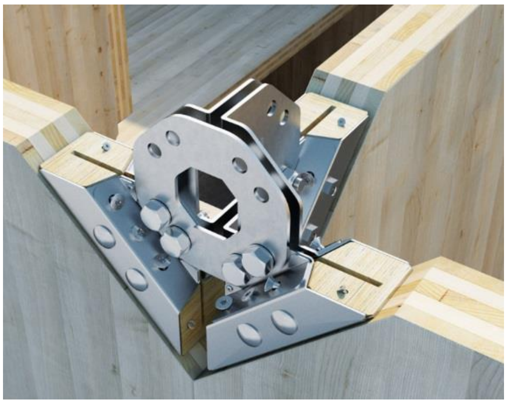

Figure 2.12 *Proprietary multi-point CLT connection system [Image by Rothoblaas [52]]*

The more popular CLT assembly method is platform construction, where the building is erected storey by storey, and each successive floor is supported and fixed to the walls below (Figures 2.10 and 2.11). This method is preferred as the connection assemblies are straightforward and the load paths are well defined. The phased approach theoretically facilitates an infinite number of storeys, although taller buildings require a more tailored connection design [37][39][53][54][55][56].

2.2.1 CLT design standards

Currently a building design standard for CLT construction is not available in Europe [23]. The existing European timber design standard, EC-5 [22] does not provide specific guidance on CLT structural design. The standard is currently under revision and CLT design will be included in the updated revision [57][58]. While the European product standard for CLT, EN 16351: 2015 [59], sets out provisions in relation to the production and performance characteristics of CLT panels, guidance on detailed building and connection design are not available [60]. Incidentally, CLT producers in Europe at present generally follow their own individual European Technical approvals (ETA) and therefore the material characteristics and design loads of the CLT panels are specific to each manufacturer [61].

Meanwhile, structural engineers when designing with CLT rely on a combination of particular timber national standards, namely the German and Austrian National Annexes to EC-5 [62] [63][64], research-based manuals, along with manufacturers technical specifications. The principal research manuals include the “BSP-Handbuch” by Schickhofer et al. [65] and “Cross-laminated timber design” by Wallner-Novak et al. [66]. There are also a number of software design tools available. One example that includes common CLT load situations, developed in Graz University, is CLT Designer [67][68]. CLT manufacturers also provide software to assist the CLT design process. An example is KLHdesigner, which can be integrated with the more general structural engineering software, Dlubal. Standard construction details with respect to fire, sound, cold-bridging, and moisture ingress are presented by Mayr-Melnhof Holz [69]. Design guidance in Canada and the US can be found in the respective CLT Handbooks [70][71]. Australia and New Zealand refer to the European standards and also an XLam Design Guide based on the specific material properties of New Zealand grown

Radiata Pine and Douglas Fir timber which incorporates criteria from the New Zealand Building Codes [72].

2.2.2 Commercial CLT panel mechanical characteristics

Commercial European CLT panels are manufactured in sizes that range between 50 mm and 300 mm thick, 2000 mm to 3000 mm wide, and up to 16500 mm in length. The panel length is generally limited by transport and delivery constraints. CLT lamina layup must be symmetrical with a minimum of three layers. The maximum number of layers, or plies, is nine.

Standard commercial panels in Europe use softwood C24 grade in accordance with EN 338: 2009 [73], while a lower grade (C16/18) may be substituted for the transverse layers, up to 10% of the boards per layer EN 15497: 2014 [74]. Defects in the panel baseboards are reduced by cutting away and re-joining using standardised finger joints in accordance with EN 15497: 2014 [75]. The baseboards typically measure 20, 30, or 40 mm thick, their breadth ranging between 40 mm and 300 mm, usually 150 mm, with a breath-to-thickness ratio greater than four recommended by the product standard, EN 16351: 2015 [59], to avoid rolling shear failure. The base timber is conditioned to a moisture content of 12% +/- 2%. The boards in a lamina layer may or may not be bonded along their edges, with a minimum gap of 2 mm to 3 mm recommended between the boards on the outside lamina and up to 4 mm to 6 mm for core layers. A bond line thickness of 0.1 mm and 0.2 mm is recommended between lamina. Most commonly the bonding adhesive is a one-component Polyurethane, (1K-PUR, 1C-PUR). Alternatively, Melamine Urea Formaldehyde (MUF) is used. While MUF has a better resistance to higher temperatures and is found to have better gap-filling performance, the possible emission of formaldehyde is cited as a disadvantage [76]. The bond press equipment pressure can range between 0.01 N/mm^2 and 1.00 N/mm^2.

The material properties of CLT panels vary depending on the base material, adhesive, and production, but the characteristics provided by Schickhofer et al. [77] shown abridged in Table 2.1 serve as an initial reference. American CLT performance characteristics and guidelines on its material properties can be found in ANSI/APA PRG 320: 2011 [78].

Table 2.1 *Proposed characteristic properties for homogeneous CLT, base material strength class T14, CV[$f_{t,0,l}$] 25 ± 5% Schickhofer et al. [77].*

Property	*Symbol*	*CLT strength class CL 24h*	*Units*
Bending strength	$f_{m,CLT,k}$	*24*	*N/mm²*
Tensile strength	$f_{t,0,CLT,\ net,k}$	*16*	*N/mm²*
Compression strength	$f_{c,0,CLT,\ net,\ k}$	*24*	*N/mm²*
Shear strength in-plane (Shear & torsion)	$f_{v,\ CLT,\ IP,\ k}$	*5.0*	*N/mm²*
Shear strength out-of-plane	$f_{v,\ CLT,\ OP,\ k}$	*3.0*	*N/mm²*
Modulus of elasticity	$E_{0,\ CLT,\ mean}$	*11 000*	*N/mm²*
Shear modulus	$G_{CLT,\ mean}$	*650*	*N/mm²*
Rolling shear modulus	$G_{r,CLT,\ mean}$	*65*	*N/mm²*
Density	$\rho_{CLT,\ k}$	*350*	*kg/m³*
	$\rho_{CLT,\ k}$	*385*	*kg/m³*

When calculating the shear stress distributions in CLT panels, the loaded out-of-plane modulus of elasticity is usually considered negligible. The distributions of normal and shear stresses through the thickness of a CLT panel loaded out-of-plane are shown in Figure 2.13 [67]. Only the layers oriented in the span direction are to contribute to the structural resistance. The maximum shear stress occurs at the neutral axis.

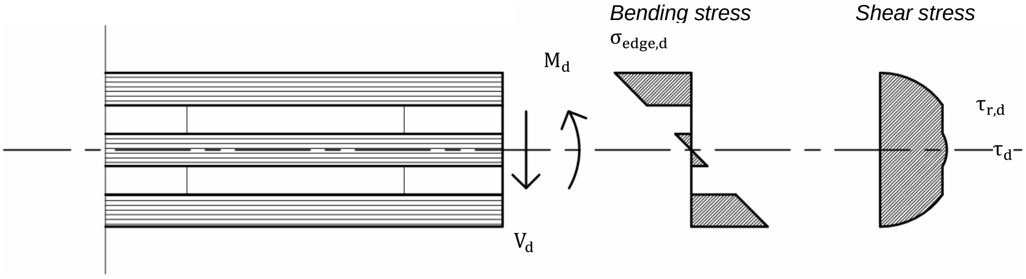

Figure 2.13 *Cross section of a five-layer CLT element loaded out-of-plane showing normal and shear stress distributions [67].*

As Euler-Bernoulli theory neglects shear deformations, the high shear flexibility of the transverse layers in CLT panels prescribes that theories other than Euler-Bernoulli must be applied in determining bending and shear stresses. Examples of approaches currently used include the γ-method, the shear analogy method, and the Timoshenko transverse shear-flexible beam theory. The implications of each have been compared by Bogensperger [79], and all approaches were found to be applicable. However, a preferred method with verified consistency between design calculations and experimental results is to be selected. The γ-method found in Annex B of the European timber design standard, EC-5 [22] calculates the effective bending stiffness of mechanically jointed beams, and is commonly adapted for CLT panels. Equation (2.1) outlines the adapted γ-method to determine the effective bending stiffness of a five-ply CLT panel as outlined by Bogensperger [79].

$$(EI)_{ef} = \sum_{i=1}^{3}(E_i . I_i + \gamma_i . E_i . A_i . a_i^2) \tag{2.1}$$

Using mean values of E, in kN/mm^2, the area A_i, in mm^2, and the second moment of area I_i, in mm^4 are determined using Equations (2.2) and (2.3) below.

$$A_i = b_i \, h_i \tag{2.2}$$

$$I_i = b_i . h_i^3/12 \tag{2.3}$$

Where b_i and h_i, are the lamina width and thickness in mm, respectively. γ_i is determined using Equations (2.4) and (2.5).

$$\gamma_1 = \gamma_3 = 1/\Big(1 + (\pi^2 . E_0 . h_i^2 / G_{90} . l^2)\Big) \tag{2.4}$$

$$\gamma_2 = 1 \tag{2.5}$$

With the parameter a_i defined in Equations (2.6) and (2.7)

$$a_1 = a_3 = h_1/2 + h_{1,2} + h_2/2 - a_2 \tag{2.6}$$

$$a_2 = 0 \tag{2.7}$$

Although most commercial CLT is manufactured from spruce in Europe, and pine in Canada and the US, it is possible to manufacture CLT using alternative timber base products, (as illustrated with the Manchester Maggie building). Bearing in mind the trend towards minimising the construction industries carbon footprint and increasing sustainability generally, it is not surprising that there are studies ongoing globally to establish the performance properties and feasibility of CLT using the respective local timber species [80][81][82][83][84][85]. At present commercial forestry in Ireland comprises mostly Sitka spruce (60%) and Douglas fir which, due to our damp and temperate weather, yields a fast-growing, low-density softwood with a high juvenile wood content. It is readily identified by its large ring-widths [86]. The best quality

Irish timber is structural grade C16 suitable for medium span, internal carpentry. But a large proportion of Irish wood is also used in the timber post, palette, and fencing industry. The bi-lateral strengthening from cross-lamination and the facility to trim away defective base product during production gives an opportunity in CLT to upgrade indigenous Irish and UK timber to a more robust and versatile building product. Studies examining the viability of manufacturing mass-timber using Irish or British timber are ongoing. The likely material characteristics of native Irish CLT have been investigated at NUI Galway [87][88] [89][90].

2.2.3 CLT connection design and fastener selection

In addition to bespoke connection design necessary for high-rise timber buildings, which generally incorporates glued-in rods and plates, there are specific CLT multi-point connection systems available, including X-RAD [49][91][52] (Figure 2.12) or SHERPA CLT [50] which are suitable for use in balloon construction (Figure 2.9).

However, the majority of the floor-to-wall panel connections in CLT mid-rise development are platform construction (Figure 2.10 and 2.11), with balloon construction used locally only. The preferred fastenings used in both cases are combinations of large diameter self-tapping screws, partially or fully-threaded, along with metal brackets. These brackets include angle brackets to transfer shear loads and hold-down brackets that transfer uplift tensional forces to the foundations.

In platform construction, the floors are supported and fixed to the walls below with self-tapping screws, the walls in turn are connected to the floor with angle brackets. Washer-head, large diameter self-tapping screws transfer the load of the upper storeys through the floor onto the walls below. A typical platform junction at an external wall is illustrated in Figure 2.14.

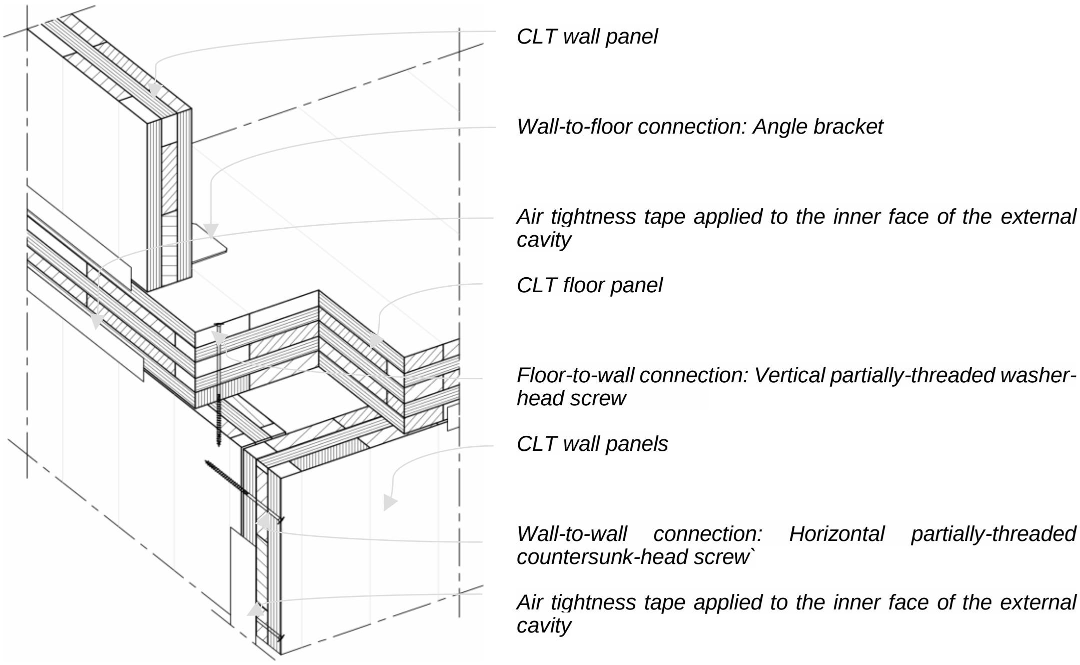
CLT wall panel
Wall-to-floor connection: Angle bracket
Air tightness tape applied to the inner face of the external cavity
CLT floor panel
Floor-to-wall connection: Vertical partially-threaded washer-head screw
CLT wall panels
Wall-to-wall connection: Horizontal partially-threaded countersunk-head screw`
Air tightness tape applied to the inner face of the external cavity

Figure 2.14 *Standard wall to upper floor to wall detail*

CLT floors generally comprise a number of panels spanning in parallel. The parallel panels are connected with: (a) a half-lap joint using partially threaded screws, (b) a broad top-joint that incorporates a ply insert using pairs of partially threaded screws, or (c) a butt joint using pairs of inclined fully-treaded screws, as illustrated in Figures 2.15. All screws within the floor space have counter-sunk heads.

To satisfy particular design criteria these typical junction details may be modified. For example, a half-lap and broad-top detail can be combined. Some common variations of panel-to-panel connection assemblies are illustrated in Figures 2.16 (d), (e), and (f).

The Common wall-to-floor panel configurations which are at present the favoured fixing solution for the majority of CLT low- to mid-rise construction are illustrated later in Figures 5.9 to 5.17.

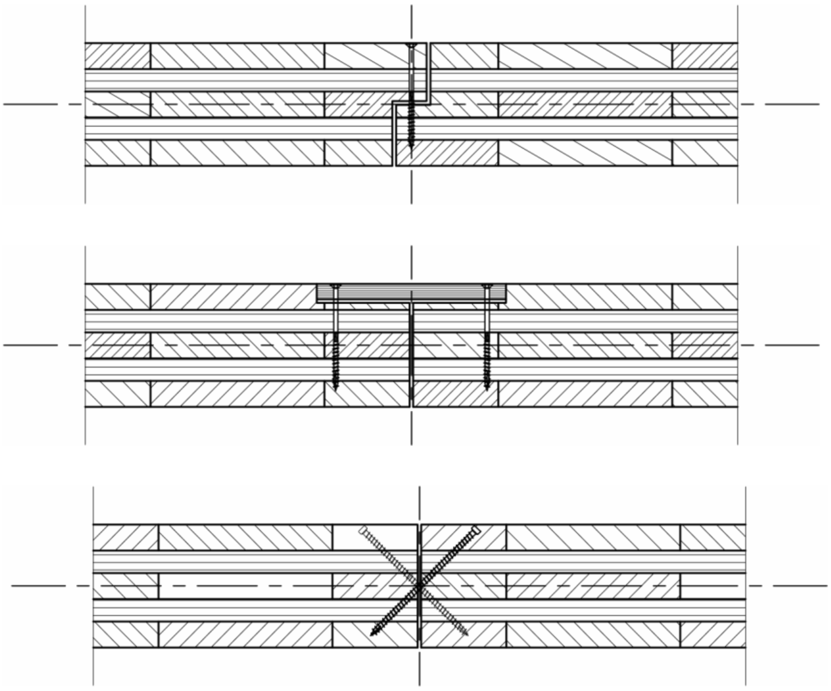

(a) Half-lap joint

(b) Broad-top joint

(c) Butt joint with inclined pairs of screws

Figure 2.15 *Typical CLT floor-to-floor panel junctions*

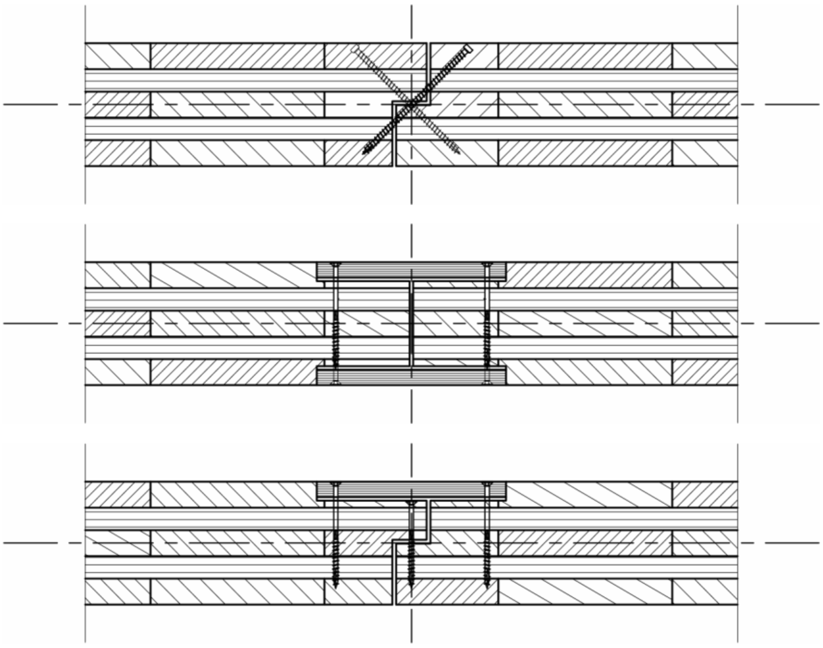

(d) Half-lap joint with inclined pairs of fully-threaded screws

(e) Broad-top joint with ply insert top and bottom

(f) Half-lap joint and broad-top joint combined

Figure 2.16 *Alternative CLT floor-to-floor panel junction assemblies*

The fixing solutions for CLT have been adapted in the main from lightweight timber design and are compatible with existing carpentry practices. Leading timber connection producers provide support for their use in the form of characteristic performance tables and software design tools. However, product specification and performance can vary between connector producers, and lightweight timber-frame and

CLT construction is fundamentally distinct in many respects. The high shear strength and stiffness of CLT panels contrasts with the inherent ductility or movement of the equivalent timber-frame, so the bulk of the responsibility to dissipate energy will fall on the connectors in a CLT building.

Studies have shown that deformations, due to rocking and slip mechanisms, are most likely to occur at the connectors in CLT buildings [15][16]. Additionally the bond lines, gaps, or shrinkage, in a CLT panel distinguish it from solid timber or even glulam. According to CLT design engineers, Smith and Wallwork [92] ‘insufficient or inconsistent’ manufacturers technical data for connections along with a lack of detailed design guidance, especially with regard to vibration limit criteria for CLT floor slabs, poses a sizable challenge when designing CLT buildings. As the technical data and load capacities vary from manufacturer to manufacturer without a universal standard, both the CLT panel producer and specific connector types must be chosen before commencing any detailed design.

2.2.4 Revisions to EN 1995-1-1 (EC-5)

With observations like this in mind, the current Eurocodes are being revised [57], with the European Commission mandating explicitly the improvement of codes for practical day-to-day calculations [58]. The COST Action FP1402 compiled available scientific results [93] for incorporation by CEN TC250 into the proposed revised timber design guide. Through its working group on timber connections (WG3), a survey was undertaken via the Chambers of Civil and Structural Engineers to assess the opinion of practitioners on EC-5 [22] Section 8: Connections with metal fasteners. Replies to the survey comprised responses from 28 European countries and five non-European countries, including New Zealand and Japan [94]. It was widely agreed that the current timber fastener section of the European standard requires improvement. New guidance for inclusion to the code that were most requested, was guidance on large diameter self-tapping screws and fasteners in axial compression. When asked what parts of EC-5 [22] required the most effort to apply, connection design scored highest, followed by vibration and deflection calculations.

2.3 Conclusions

The state-of-the-art in CLT construction has been described and the current CLT floor design and panel-panel connection details were summarised. The panel-panel connections in CLT mid-rise development generally combine large diameter, self-tapping screws with metal angle brackets. Floor-to-wall panel connections in CLT mid-rise development are typically platform construction, with balloon construction used locally.

The screw and bracket connection details that are generally used have been adapted from lightweight timber design. However, as lightweight timber-frame and CLT construction deviate with regard to mass and stiffness, specific detailed design guidance and consistent manufacturer's technical data is needed for CLT connections. This is especially the case with respect to floor serviceability and determination of vibration and deflection limits.

Civil and Structural Engineers universally agree that EC-5 [22] needs improvement, specifically with respect to the connection and serviceability design of the code. the Additional guidance on the use of large diameter, self-tapping screws and vibration and deflection calculations for floors is also needed.

This thesis will endeavour to identify the influence on floor vibration and deflection with respect to alternative standard CLT connection details using large diameter screws and metal angle brackets. The study aims to specifically quantify the advantage of a particular fixing type or spacing with respect to the serviceability of the floor.

The following chapter will provide an outline of basic vibration theory. The current criteria on vibration tolerance in buildings at the design stage are also précised.

3 VIBRATION

3.1 Introduction

This chapter gives an overview of classic vibration theory to provide a basis of understanding of the dynamic behaviour of structures. A synopsis of the current timber serviceability limit design criteria and a summary of the International standards on vibration in buildings is then presented. Included are guidelines on human induced vibrations and the vibration comfort boundaries that are deemed appropriate in design.

3.2 Vibration theory

Vibrations are mechanical oscillations that occur about an equilibrium point. They are characterised by their frequency and amplitude. The frequency is the rate of oscillation while the amplitude is its magnitude. Vibration analysis generally aims to predict the magnitude and duration of a dynamic response due to external forces with the range of frequencies which is perceivable by occupants or especially vibrations that coincide with the natural frequencies of the structure. Natural frequencies are intrinsic characteristics of any system that depend on its mass and stiffness. They define the rate at which a structure will vibrate freely if set in motion by one input. An exciting force applied at the same rate as a natural frequency will resonate causing deflections much greater than as a result of static loading. The lowest natural frequency value is the fundamental frequency. A structure’s dynamic motion will generally comprise a combination of vibrations. Where the vibration is a multiple of the fundamental frequency, it will repeat after a time interval. This is termed periodic vibration. If the vibration is not periodic, it is termed complex.

Theoretical vibration analysis may be divided into modal and response models [95]. The modal model incorporates a spatial model which characterises a structures physical properties, including its stiffness, mass, and damping characteristics which then define a set of natural frequencies with corresponding mode shapes. The modal model is concerned only with how a structure will vibrate naturally without external forces. Based on the modal model, the response model examines how a structure will respond to defined excitations.

3.2.1 Free vibration without damping

Essentially, the alternating transfer of energy between its potential and kinetic forms causes a structure to vibrate. The means to store potential energy is dependent on a spring of stiffness, *k*, with the kinetic energy characterised by mass or inertia, *m*. According to Hooke's law, the change in length of a linear spring is proportional to the force acting along its length, illustrated in Figure 3.1 and Equation (3.1).

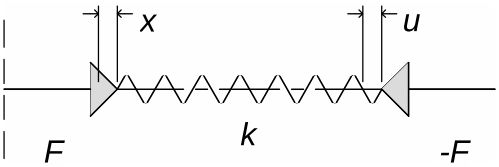

Figure 3.1 *Linear spring [96]*

$$F = k\,(x - u) \tag{3.1}$$

where *x* and *u* define the linear displacements. An ideal spring has no mass, hence forces acting at each end are equal and opposite. The constant proportionality, *k*, is termed the spring stiffness. According to Newton's second law, the acceleration of a rigid mass is proportional to all the resultant forces, *F*, acting on the mass, *m*. Newton's second law is represented in Figure 3.2 and Equation (3.2), where *x*, defines displacement.

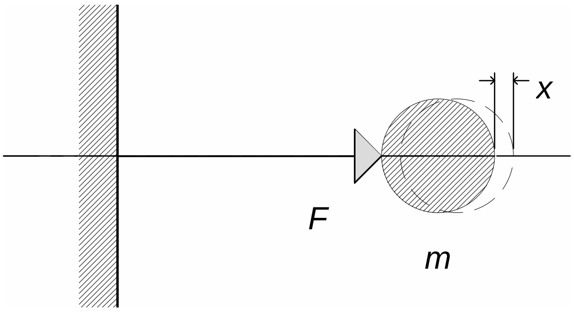

Figure 3.2 *Rigid mass*

$$F = m\,\ddot{x} \tag{3.2}$$

The simplest vibratory system consists of a mass attached to a fixed support via a spring. The mass is confined to translational motion along the x-axis, therefore any movement from the initial datum can be quantified completely in terms of one displacement variable, *x*. This is termed a single degree-of-freedom (SDOF) system, illustrated in Figure 3.3.

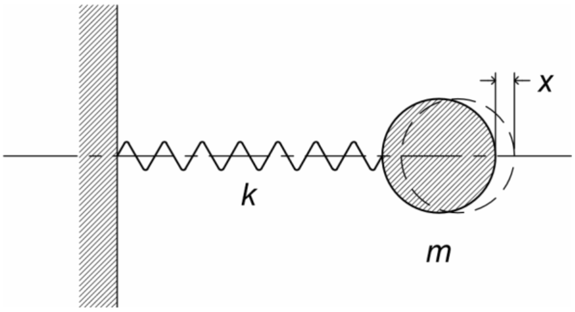

Figure 3.3 *Undamped single degree-of-freedom system*

This motion combines Hooke's law and Newton's second law, (Equations (3.1) and (3.2)) giving Equation (3.3). The natural oscillations of the mass, *m,* due to only one initial force displaces the mass from its equilibrium position. The displacing force is opposite in direction to the displacement. This motion is defined as free vibration or simple harmonic motion. The equilibrium position of the mass is given by $x = 0$. The rate of its oscillation is a natural frequency, f_n, measured in cycles per second, Hz.

$$m\ddot{x} + kx = 0 \tag{3.3}$$

As the behaviour of x with time has a sinusoidal or cosinusoidal dependence, the solution to Equation (3.3), in Equation (3.4), is given in terms of the angular natural frequency of the system.

$$x = A\sin\sqrt{k/m}\,(t) + B\,\cos\sqrt{k/m}\,(t) \tag{3.4}$$

The circular frequency ω_n, in rad/sec, is defined in Equation (3.5).

$$\omega_n = \sqrt{k/m} \tag{3.5}$$

The time interval of a full cycle of each sinusoidal oscillation of the mass is the period T, in seconds, which is the reciprocal of the natural frequency, given in Equation 3.6.

$$f_n = 1/T = \omega_n/2\pi = 1/2\pi\sqrt{k/m} \tag{3.6}$$

The oscillatory motion is fully dependent on the initial displacement and velocity conditions at $t = 0$, where $B = x$ and $A = \dot{x} / \omega_n$. The phase angle, is denoted by θ. The displacement at a given time is given by Equations (3.7a), or (3.7b).

$$x = A \sin \omega_n (t) + B \cos \omega_n (t) \quad \text{, or} \tag{3.7a}$$

$$x = C \sin (\omega_n (t) + \theta) \tag{3.7b}$$

where $C = \sqrt{A^2 + B^2}$ and $\theta = \tan^{-1} B/A$

The maximum value of sin $(\omega_n (t) + \theta)$ is unity. Therefore the constant, C, equates to the maximum value of x, known as the amplitude of displacement. The system oscillates between the values of $x = \pm C$. The phase relationship with time for displacement, velocity, and acceleration of simple harmonic oscillating motion is illustrated in Figure 3.4.

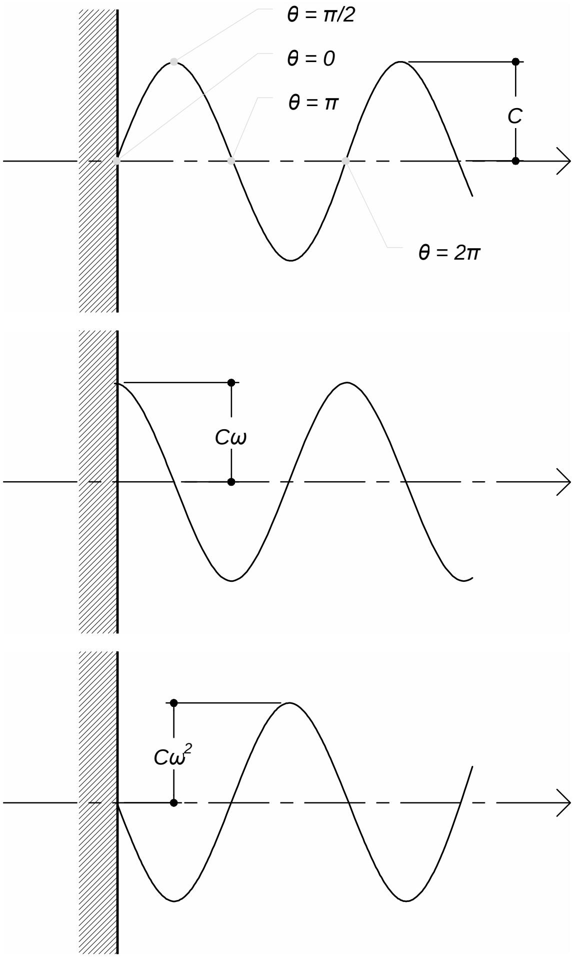

Displacement $x = C \sin [\omega (t) + \theta]$

Velocity $\dot{x} = C \omega \cos [\omega (t) + \theta]$

π / 2 out of phase with displacement

Acceleration $\ddot{x} = - C \omega^2 \sin [\omega (t) + \theta]$

π out of phase with displacement

Figure 3.4 *Variation with time, displacement, velocity, and acceleration* [97]

3.2.2 Damping

Damping is the rate a system set in motion will return to its steady state. If the total energy within an oscillating system remains constant, displacements will follow a sine curve indefinitely. In reality, a portion of energy will be lost. This resistance to motion indicates that another restoring force that is proportional, but opposite to the velocity acting in the system, is present in the system. The proportional damping force is characterised as the damping coefficient, c. An ideal viscous damper is described in Figure 3.5 and Equation 3.8.

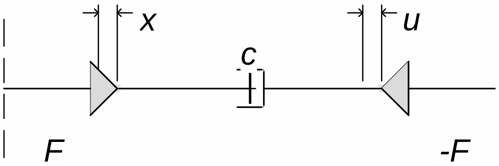

Figure 3.5 *Viscous damper*

$$F = c\,(\dot{x} - \dot{u}) \tag{3.8}$$

3.2.3 Free vibration with viscous damping: SDOF system

Figure 3.6 and Equation (3.9) defines the homogeneous equation to free vibration of a SDOF system with viscous damping.

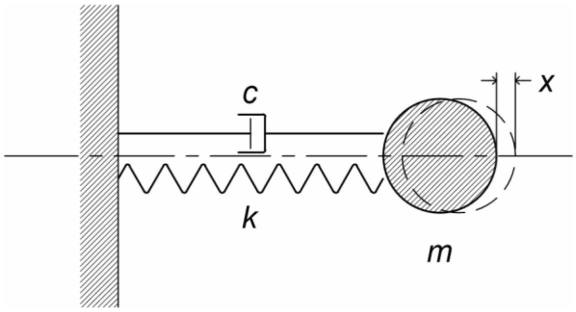

Figure 3.6 *Damped single degree-of-freedom system*

$$m\,\ddot{x}\,(t) + c\,\dot{x}\,(t) + k\,x\,(t) = 0 \tag{3.9}$$

The general solution to Equation (3.9) is given in Equation (3.10).

$$x\,(t) = X\,e^{st} \tag{3.10}$$

where s is a complex quantity termed the Laplace variable. Substituting the general solution in to Equation (3.9) yields Equation (3.11).

$$(m\,s^2 + c\,s + k)\,X\,e^{st} = 0 \tag{3.11}$$

The trivial solution ($x\,(t) = X\,e^{st} = 0$), results in no motion of the system. Equation (3.12) corresponds to the non-trivial solution.

$$m\,s^2 + c\,s + k = 0 \tag{3.12}$$

The roots of the characteristic Equation (3.12) are given by Equation (3.13).

$$s_{1,2} = -\,{}^{c}\!/_{2\,m} \pm \sqrt{\left({}^{c}\!/_{2\,m}\right)^2 - {}^{k}\!/_{m}} \tag{3.13}$$

Rewriting the general solution Equation (3.10) as,

$$x\,(t) = A\,e^{s_1 t} + \,B\,e^{s_2 t} \tag{3.14}$$

Where the initial imposed conditions at $t = 0$ determine the constants A and B.

The applicable solution to the homogeneous Equation (3.9) is reliant on the nature of s_1 and s_2 which are characterised by the damping coefficient.

If $\left[\left({}^{c}\!/_{2\,m}\right)^2 > {}^{k}\!/_{m}\right]$ the damping forces will govern the systems motion. This system is considered to be overdamped and the root solutions (s_1 and s_2) are both real.

If $\left[\left({}^{c}\!/_{2\,m}\right)^2 = {}^{k}\!/_{m}\right]$ the system is critically damped and the root solutions are equal and real.

If $\left[\left({}^{c}\!/_{2\,m}\right)^2 < {}^{k}\!/_{m}\right]$ inertia and elastic forces will govern motion. This system is termed underdamped. Both root solutions are therefore complex conjugate.

A coefficient derived from Equation (3.13) defines the critical damping on a system. The critical damping coefficient c_{cr}, is defined by Equation (3.15).

$$c_{cr} = 2\sqrt{km} = \,2\,m\sqrt{{}^{k}\!/_{m}} \,=\, 2\,m\,\omega_n \tag{3.15}$$

The damping ratio ζ, which is dimensionless, is determined using Equation (3.16).

$$\zeta = {}^{c}\!/_{c_{cr}} \tag{3.16}$$

where [$\zeta > 1$] the system is over-damped;

where [$\zeta = 1$] the system is critically damped;

where [$\zeta < 1$] the system is underdamped.

The general solution in the case of an overdamped system [$\zeta > 1$] is determined using Equation (3.17), with Equation (3.18) incorporating the initial conditions.

$$x\,(t) = e^{-\,\zeta\,\omega_n t}\,\left[A\,e^{\omega_n t\,\sqrt{(\zeta^2-1)}} \quad + B\;e^{\omega_n t\,\sqrt{(\zeta^2-1)}}\quad\right] \qquad (3.17)$$

$$x\,(t) = e^{-\,\zeta\,\omega_n t}\left[x\,(0)\cosh\left(\omega_n t\,\sqrt{(\zeta^2-1)}\right) + \frac{\dot{x}\,(0)+\,\zeta\,\omega_n x\,(0)}{\omega_n\,\sqrt{(\zeta^2-1)}}\,\sinh\left(\omega_n t\,\sqrt{(\zeta^2-1)}\right)\right] \qquad (3.18)$$

In the case of a critically system [$\zeta = 1$] the general solution is evaluated using Equation (3.19), with the initial conditions applied in Equation (3.20).

$$x\,(t) = e^{-\,\omega_n t}\,[A\;+B\;(\mathrm{t})] \qquad (3.19)$$

$$x\,(t) = e^{-\,\omega_n t}\,[x\,(0)(1+\;\omega_n t) +\;\dot{x}\,(0)(t)] \qquad (3.20)$$

In the case of overdamped or critically damped systems, motion returns to static equilibrium. Oscillatory motion is only possible where a system is underdamped.

The underdamped system solution [$\zeta < 1$] is determined using Equation (3.21), where$\left[\,\mathrm{i} = \sqrt{-1}\,\right]$. Equation (3.22) considers the initial conditions of the system.

$$x\,(t) = e^{-\,\zeta\,\omega_n t}\,\left[A\,e^{i\,\omega_n t\,\sqrt{(1-\zeta^2)}} \quad + B\;e^{-i\omega_n t\,\sqrt{(1-\zeta^2)}}\quad\right] \qquad (3.21)$$

$$x\,(t) = e^{-\,\zeta\,\omega_n t}\,\left[x\,(0)\cos\left(\omega_n t\,\sqrt{(1-\;\zeta^2)}\right)\;+ \frac{\dot{x}\,(0)+\,\zeta\,\omega_n x\,(0)}{\omega_n\,\sqrt{(1-\zeta^2)}}\,\sin\left(\omega_n t\,\sqrt{(1-\;\zeta^2)}\right)\right] \qquad (3.22)$$

If there is no damping [$\zeta = 0$], the motion is harmonic with a constant amplitude at a natural frequency. Where the damping is less than the critical value [$0\; < \zeta < 1$], the motion is defined as damped oscillating motion tending exponentially towards zero. The frequency of oscillation, termed the damped natural frequency ω_{d}, given by Equation (3.23).

$$\omega_d =\;\omega_n\,\sqrt{(1-\;\zeta^2)} \qquad (3.23)$$

By evaluating the exponential decay of free damping of the oscillating motion, the damping ratio ζ may be determined. Figure 3.7 illustrates a sample record of free damping in an oscillating system. From the time domain plot, a peak amplitude value X_i, is measured and another subsequent peak amplitude value X_{i+1}, taken after a number of cycles, n.

The logarithmic decrement, from which the damping is derived is given in Equation (3.24).

$$\lambda = \ln {}^{X_i}/_{X_{i+1}} = {}^{2\,n\,\pi\,\zeta}/_{\sqrt{(1-\zeta^2)}} \qquad (3.24)$$

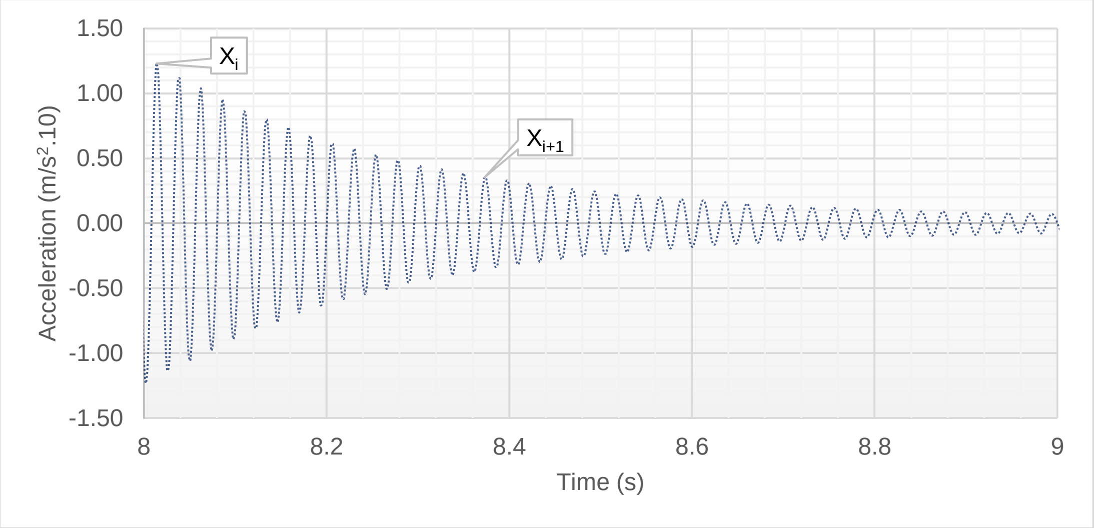

Figure 3.7 *Sample FRF free decaying damped oscillation (Assembly P)*

3.2.4 Forced vibration with viscous damping: SDOF system

In the case of forced vibration of a single degree-of freedom system with viscous damping, illustrated in Figure 3.8, and described by Equation (3.25).

$$m\,\ddot{x}\,(t) + c\,\dot{x}\,(t) + k\,x\,(t) = f(t) \qquad (3.25)$$

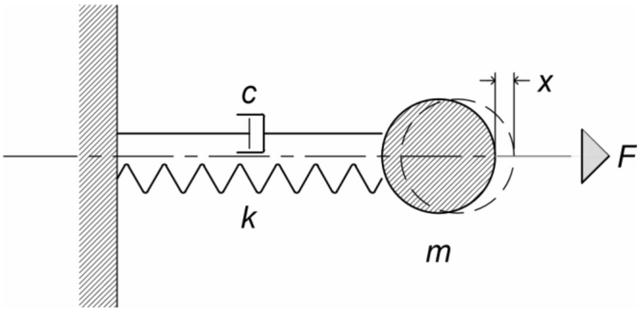

Figure 3.8 *Forced vibration applied to a damped single degree-of-freedom system*

Where $f(t) \neq 0$ denotes the time dependent excitation force applied to a system. The forcing function may be defined by Equation (3.26), where F denotes the amplitude of a harmonic exciting force and ω, in rad/sec, is its frequency.

$$f\,(t) = F\,e^{i\omega t} \qquad (3.26)$$

The particular solution to Equation (3.25) is given in Equation (3.27). The complex amplitude defined in Equation (3.28), termed a phasor $\overline{X}$, which incorporates the phase angle of the response with respect to the exciting force.

$$x\ (t) = \bar{X}\ e^{i\omega t} \tag{3.27}$$

$$\bar{X}\ = X\ e^{i\theta} \tag{3.28}$$

Substituting into Equation (3.25) gives Equation (3.29).

$$\bar{X}\ = \ {}^{F}\!/_{(k-\ \omega^2\ m) + i\ \omega\ c} \tag{3.29}$$

Which may be rewritten as,

$$\bar{X}\ = \ {}^{F}\!/_{\sqrt{(k-\ \omega^2\ m)^2 + (\ \omega\ c)^2}}\ e^{i\theta} \tag{3.30}$$

Where $\tan\theta\ = \ {}^{-\omega\ t}\!/_{k-\ \omega^2\ m}$ (3.31)

Therefore the particular solution for Equation (3.25) for the forcing function defined in Equation (3.26) is given by Equation (3.32) which represents a harmonic steady-state solution for the response $x\ (t)$ due to an exciting force of constant amplitude. The response is delayed with respect to the forcing phase angle, θ.

$$x\ (t)\ = \ {}^{F}\!/_{\sqrt{(k-\ \omega^2\ m)^2 + (\ \omega\ c)^2}}\ e^{i(\omega\ t+\ \theta)} \tag{3.32}$$

Combining the force solution Equation (3.32) with the underdamped homogeneous solution of the system Equation (3.22) gives the complete solution given in Equation (3.33).

$$x\ (t) = e^{-\ \zeta\ \omega_n t}\left[A\ e^{i\ \omega_n t\ \sqrt{(1-\zeta^2)}} + B\ e^{-i\omega_n t\ \sqrt{(1-\zeta^2)}}\right] + {}^{F}\!/_{\sqrt{(k-\ \omega^2\ m)^2 + (\ \omega\ c)^2}}\ e^{i(\omega\ t+\ \theta)} \tag{3.33}$$

The complete solution combines both transient and the steady-state vibrations of the system. The transient vibration dissipates after an initial time period, leaving only the steady-state vibration of the forced vibration.

The steady-state part of the complete solution may be represented using a dimensionless parameter Ω, termed the amplification ratio, defined in Equation (3.34).

The term $\beta = {}^{\omega}/_{\omega_n}$, represents the ratio of the forcing frequency to the systems natural frequency.

$$\Omega = {}^{X}\!\Big/\!\left({}^{F}/_{k}\right) = \; {}^{1}\!\Big/\!\sqrt{(1-\ \beta)^2 + (\,2\,\zeta\beta)^2} \qquad (3.34)$$

A sample illustration of the amplification ratio *(Ω)*, (denoted by *A (ω)*), and the phase of the *x (t)* response, (denoted by *φ (ω)*), relative to the forcing function *f (t)*, are plotted against the frequency ratio $\beta = {}^{\omega}/_{\omega_n}$, in Figures 3.9 (a), and 3.9 (b), respectively. This representation is valid for any SDOF system [98].

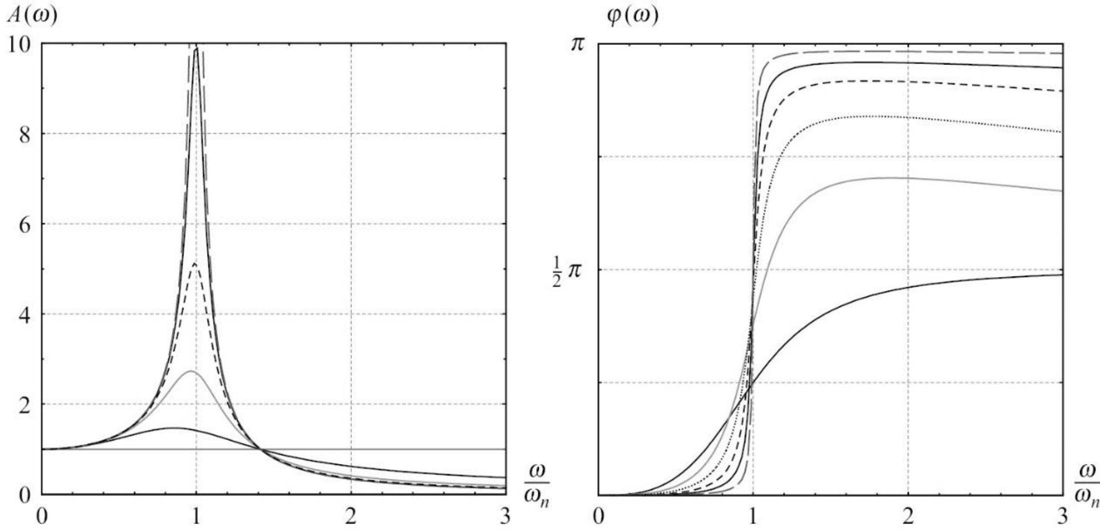

(a) (b)

Figure 3.9 *Amplification ratio (a) and phase angle (b), plotted against the frequency ratio [99]*

The maximum dashed-line curve depicts a damping ratio ζ near zero. The minimum curved line represents approximately half the critical damping ratio ζ. Note, the amplification at the natural frequency is maximum, regardless of the magnitude of the forcing function. This phenomenon is termed resonance. If the damping ratio ζ is equal to zero, the amplification of the response is potentially infinite. Also noteworthy from the curve Figure (3.9(a)) is that the response curves coincide away from the natural frequency, inferring that damping is only effective at or near resonance frequencies [98]. Figure (3.9(b)) illustrates the phase shift of the response as it passes through resonance at 90˚. The sharpness of the phase change reduces with increased damping ratio ζ values. The maximum dashed-line curve again depicting a damping ratio near zero where [$\beta \ll 1$] the displacement response is in phase with the excitation force. As displacement is dependent on stiffness, the response magnitude of the system is stiffness dependent;

where [$\beta \sim 1$] damping dominates the response;

where [$\beta \gg 1$] the phase of the displacement response lags the forcing frequency, the response tending toward 180˚. The system is therefore inertia dependent [96].

Rewriting Equation (3.29) with respect to the dynamic output to input quantities, Equation (3.35) represents the Frequency Response Function (FRF) denoted by $H\,(\omega)$ [98].

$$\bar{X}/_{F} = H\,(\omega) = {}^{1}/_{(k - \omega^2\, m) + i\,\omega\, c} \tag{3.35}$$

3.2.5 Vibrations of real systems: MDOF

Real civil engineering structures are not defined by just one mass moving in one direction of translation or rotation. The degrees-of freedom are infinite. However, analysis may be reduced to a discrete number of degrees-of freedom that sufficiently represent the behaviour of a given system. By means of superposition, the multiple degrees-of freedom (MDOF) of the dynamics of any system may be reduced to a SDOF system [95], [98]. The governing equations of motion of a MDOF system are written in matrix form, given in Equation (3.36).

$$\begin{pmatrix} m_1 & \cdots & 0 \\ \vdots & \ddots & \vdots \\ 0 & \cdots & m_N \end{pmatrix} \begin{Bmatrix} \ddot{x}_1 \\ \vdots \\ \ddot{x}_N \end{Bmatrix} + \begin{pmatrix} c_1 & \cdots & 0 \\ \vdots & \ddots & \vdots \\ 0 & \cdots & c_N \end{pmatrix} \begin{Bmatrix} \dot{x}_1 \\ \vdots \\ \dot{x}_N \end{Bmatrix} + \begin{pmatrix} k_1 & \cdots & 0 \\ \vdots & \ddots & \vdots \\ 0 & \cdots & k_N \end{pmatrix} \begin{Bmatrix} x_1 \\ \vdots \\ x_N \end{Bmatrix} = \begin{Bmatrix} f_1 \\ \vdots \\ f_N \end{Bmatrix} \tag{3.36}$$

Represented more concisely by Equation (3.37).

$$[M]\,\{\ddot{x}\,\} + [C]\,\{\dot{x}\} \; + [K]\,\{x\} = \{f\} \tag{3.37}$$

where $[M]$, $[C]$, and $[K]$, respectively, represent the mass, damping and stiffness N x N matrices, N representing a finite number of degrees-of freedom. The N x 1 vectors $\{\ddot{x}\,\}$, $\{\dot{x}\}$ and $\{x\}$ represent acceleration, velocity, and displacement, respectively. The N x 1 vector $\{f\}$ represents external excitation forces on the system with respect to time.

Equation (3.38) depicts the free vibration of an undamped MDOF system.

$$[M]\,\{\ddot{x}\,\} + [K]\,\{x\} = \{0\} \qquad (3.38)$$

Solutions to Equation (3.38) are in the form:

$$\{x\,(t)\} = \{\bar{X}\}\,e^{i\omega t} \qquad (3.39)$$

Where $\{\bar{X}\}$ represents an N x 1 vector of the time-independent response amplitudes.

Substituting into Equation (3.38) gives,

$$[K] - \,\omega^2\,[M]\,\{\bar{X}\}\,e^{i\omega t} = \{0\} \qquad (3.40)$$

which reduces to Equation (3.41), as $e^{i\omega t} \neq 0$ for any instant of time.

$$[K] - \,\omega^2\,[M]\,\{\bar{X}\}\; = \{0\} \qquad (3.41)$$

The non-trivial solutions to Equation (3.41) are given by Equation (3.42).

$$det\,\big[[K] - \omega^2[M]\big]\; = 0 \qquad (3.42)$$

Solving for Equation (3.42) may provide N possible real positive solutions $\omega_1^2\,, \omega_2^2\,, \ldots .\,\omega_N^2$, termed eigenvalues, where the values $\omega_1, \omega_2, \ldots .\,\omega_N$ represent the undamped natural frequencies of the system. Substituting each natural frequency value into Equation (3.41) provides N possible solutions in the form of vector solutions $\{\psi_1\}, \{\psi_2\}, \ldots\ \{\psi_N\}$, the eigenvectors or mode shapes of the system, which are orthogonal and therefore linearly independent. Each eigenvector contains N real components. The components may be positive or negative, indicating the direction of the mode, but not the magnitude. Pairing the corresponding natural frequency values and the modes shapes represented by the eigenvectors $(\,\omega_1\{\psi_1\})$, $(\,\omega_2\{\psi_2\}), \ldots (\,\omega_N\{\psi_N\})$ describe the N modes of vibration. The complete free vibration solution, the eigensolution, or the Modal matrix, may be expressed with two matrices, Equations (3.43) and (3.44).

$$\boldsymbol{\omega^2} = \begin{pmatrix} \omega_1^2 & \cdots & 0 \\ \vdots & \ddots & \vdots \\ 0 & \cdots & \omega_N^2 \end{pmatrix} \qquad (3.43)$$

$$\Psi = (\{\psi_1\}, \{\psi_2\}, \ldots\ \{\psi_N\}) \qquad (3.44)$$

The presentation of the mode shape vectors is always subjected to a normalisation procedure, depending on the particular eigensolution but often based on making the largest element in each vector equal to unity. When mapping the shape of the vibrations for each natural frequency of a structure, the static equilibrium position is usually depicted together with a grid of coordinates displaced proportionally to the values of the eigenvector for each natural frequency of interest.

Figures 3.10 and 3.11 show graphical normalised representations of the first two mode shapes of a uniform plate.

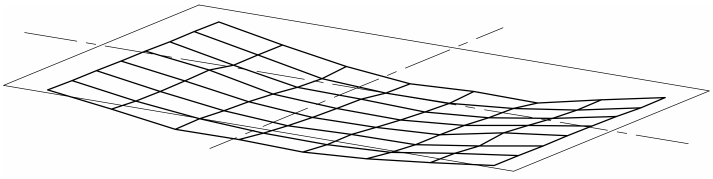

Figure 3.10 *First bending mode of a homogeneous plate*

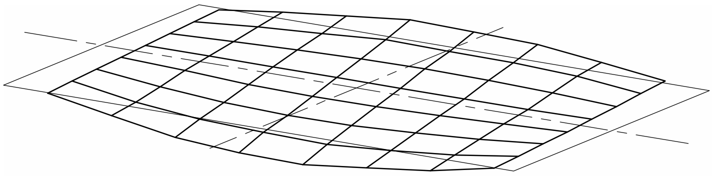

Figure 3.11 *Second mode of a homogeneous plate, torsional*

Finite element models are commonly developed to predict the static and modal responses. A numerical modal model of a structure is especially worthwhile in anticipating the locations of the mode peaks, their maximum amplitude, and where the vibration is negligible. A response model may be developed by applying defined excitations to the calibrated finite element model. Any variation of the static mass or dynamic forces will alter the spatial characteristics of the structure, consequently affecting the modal and response models also.

3.3 Floor vibration design criteria

Floor vibration induced by occupants' everyday activity is a persistent design problem [17][18]. With the exception of manufacturing or industrial building use, where machinery can often dominate noise and vibration, internal dynamic actions in commercial buildings are otherwise due to walking or other cyclic movements by people [100]. As modern building design trends towards longer spanning and slender floors, the perceivable vibration performance of the floor may be compromised as a consequence. Open un-interrupted spaces is commonplace in contemporary offices which, combined with quiet working environments, provides a challenge to architects and engineers in respect to floor design [17]. For dwellings too, an open-plan layout is synonymous with modern living. Surveys on the most common grievances regarding building performance generally found that the second most frequent source of complaints from building users relates to the building floors [21][101]. Annoying human induced vibrations are considered the most common floor serviceability design challenge, with pedestrian excitation cited as the primary significant source of disturbing vibrations [102]. A rise in the number of negative comments for newly constructed floors cited by Hudson and Reynolds [103] inspired their investigation on the benefits of applying active vibration control to problem floors, especially where passive vibration control involving tuned mass dampers [104], or viscoelastic interlayers was not possible or had not been successful. Active vibration control involves applying a force in response to the floors motion to improve vibration serviceability, therefore meeting acceptable comfort limits. However, there are several codes and guidelines available to designers to mitigate uncomfortable floor vibration at the design stage with the verification and assessment of a floor’s dynamic response achieved in many ways [22], [70], [111]–[116], [71], [78], [105]–[110].

As the aim of this study is to examine the serviceability response of CLT floors, current serviceability limit design criteria and recommendations, which are applied at present for timber floor design and by CLT design engineers, are outlined in the following paragraphs.

3.3.1 Human tolerance to floor vibration

As natural frequencies are inherent properties of any system, contingent on mass and stiffness, so too for the human body, with distinct natural frequencies for each body member and organ. Therefore, there are standards that define human comfort boundaries [116] [114] [113] [105][108]. They bound the frequency range of vibration exposure that most impacts on a person’s comfort, perception, and health at 0.5 Hz to 80 Hz, with a person’s sensitivity to vertical, foot-to-head, vibration bounded between 4 to 12.5 Hz and between 1 and 2 Hz for horizontal acceleration [117]. Vertical acceleration is deemed most acute between 4 and 8 Hz [115] [21][118]. Ohlsson [13] examined the dynamic response of different light-weight floors and human perception of floor vibrations, in parallel with experimental evaluations on dynamic footfall forces. It was observed that tolerance to vibration depends on proximity and awareness of the source, and the person's own activity level. The longer the duration of the vibration, the greater the discomfort. With regard to footfall measurements, it was found that the components of force due to a person walking dominate at 0 to 6 Hz, with the force intensity falling away almost linearly until 50 Hz, and dissipating rapidly thereafter. As the frequency of everyday footfall coincides with the frequency range which is most uncomfortable, it was suggested by Ohlsson that light-weight floor's resonant frequencies should be greater than 6 Hz to ensure that footfall does not resonate with the floor. However, if the resonant frequencies of the floor are greater than 50 Hz, further investigations of floor vibrations from human footfall would not be required. With regard to the damping ratio ζ, a value of 1% was observed for the lower resonances of laboratory floors, with ratios two to four times greater obtained with field test floors. Subsequently, Ohlsson issued a design guide [119] for light-weight floors with resonant frequencies greater than 8 Hz. Design calculations were proposed to estimate a floor's first natural bending mode, the fundamental frequency (f_1), with calculations and limits for static point load deflection (maximum 1.5 mm deflection per 1 kN static point load) and impulse velocity responses in the frequency range of 8 to 40 Hz, and guidance on dynamic continuous loading for frequencies, again up to 40 Hz. A damping ratio ζ of 1% was proposed for traditional timber floor construction, with a lower value of 0.8% suggested for floors in open plan construction or heavy floors with mass greater than 150 kg/m^3. The vibration criteria set out in EC-5 [22] are principally based on those suggested by Ohlsson.

3.4 European floor vibration design criteria EN 1995-1-1 (EC-5)

EC-5 (Section 7.3) [22] specifies that any actions, which can reasonably be anticipated on a structure, do not cause vibrations that can impair the function of the structure or cause unacceptable discomfort to the users. The code instructs that vibration should be estimated by measurements or by calculation, taking into account the expected stiffness of the structure and the modal damping ratio. A modal damping ratio ζ of 1% is to be assumed, unless other values are proven more appropriate. The Irish National Annex (NA) to EC-5 [111], for example, requires that the damping ratio ζ is to be taken as 2%. Additionally, there is general guidance pertaining to vibrations from machinery with regard to the design loads and continuous vibration levels and acceleration acceptance criteria. ISO 2631-2: 1989 [105] is referenced in the code [22], however the relevant criteria were omitted from its latest revision, ISO 2631-2: 2003 [113], as the range of potential applications was deemed too extensive. However, continuous vibration levels and acceleration acceptance criteria have been included in ISO 10137: 2007 [115]; both standards are discussed in more detail later.

EC-5 [22] then sets out design guides for residential timber floors, stating that a special investigation should be made for floors with a f_1 less than 8 Hz ($f_1 \leq 8$ Hz). Further guidance or recommendations on this are not given. For floors where f_1 is greater than 8 Hz ($f_1 \geq 8$ Hz), limits for static point load deflection and impulse velocity responses from 8 to 40 Hz should be satisfied as described in the following sections.

3.4.1 Fundamental frequency limit

In calculating f_1, the floor should be assumed to be unloaded, and only the self-weight of the floor and any permanent actions are to be considered. Equation (3.45) is provided to approximate f_1 for a rectangular simply supported floor of timber beam construction.

$$f_1 = {}^{\pi}/_{2\,l^2} \left({}^{(EI)_l}/_{m}\right) \tag{3.45}$$

Where l is the timber beam floor span, in m, m is the mass per unit area, in kg/m^2, and $(EI)_l$ is the equivalent plate bending stiffness of the floor about an axis perpendicular to the beam direction, in Nm^2/m.

3.4.2 Static unit point load deflection limit

The maximum instantaneous vertical deflection w, in mm, due to a vertical concentrated static force, F, in kN which can be applied at any point on the floor, taking into account load distribution should be less than the permissible limit a, in mm/kN Equation (3.46).

$$ {}^{w}/_{F} \leq a \tag{3.46}$$

The values of a vary depending on the national criteria, set out in the respective National Annexes to EC-5 [22]. The value ranges from 0.5 mm to 4.0 mm/kN as charted in Figure 3.12.

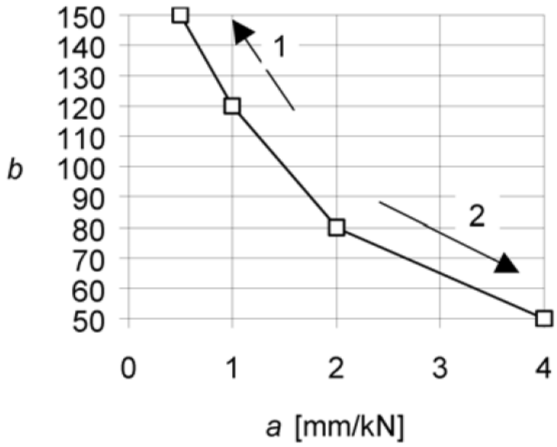

Figure 3.12 *Limits and relationships between parameters a and b, [EC-5_7.3.3 [22]]*

1. *Better performance* **2.** *Poorer performance*

3.4.3 Unit impulse velocity response limit

The unit impulse velocity response is a measure of the maximum initial value of the vertical floor vibration velocity, in m/s, caused by an ideal impulse of 1Ns which is applied at the point of the floor giving maximum response in the frequency range 8 Hz to 40 Hz. The unit impulse velocity response limit, v, in m/ (Ns^2), is determined using Equation (3.47). The limit is related to f_1, the fundamental frequency, ζ the damping ratio, and the parameter b which is directly related to the local permissible deflection limit a, found using the EC-5 [22] chart shown in Figure 3.12.

$$v \leq b^{f_1^{\zeta-1}} \tag{3.47}$$

For design purposes, Equation (3.48) is provided to estimate the unit impulse velocity response (v, in m/ (Ns^2)) of a rectangular floor of span l and breadth x, in m, simply supported along all four edges and m, in kg/m^2 is the mass of the floor.

$$v = {}^{4\,(0.4 + 0.6\,n_{40})}\!\Big/_{m\,b\,l + 200} \tag{3.48}$$

The number of first-order modes with natural frequencies up to 40 Hz, n_{40}, may be calculated using Equation (3.49).

$$n_{40} = \left(\left(\left({}^{40}\!/_{f_1} \right)^2 - 1 \right) \left({}^{b}\!/_{l} \right)^4 \, {}^{(EI)_l}\!/_{(EI)_b} \right)^{0.25} \qquad (3.49)$$

$(EI)_x$ is the equivalent plate bending stiffness, in Nm^2/m of the floor about an axis parallel to the beams, where $(EI)_b < (EI)_l$.

In addition to the provisions outlined in EC-5 [22], additional regional design criteria are applicable. They are described in the national annexes to the code.

3.4.4 Irish national annex to EC-5

The first significant difference to be noted in the vibration criteria of the Irish National Annex to EC-5 [111], is that the damping ratio ζ is to be taken as 2%. This reflects that Irish building practice has a reduced timber joist spacing to elsewhere in the EU. This is true of the UK also, where the damping ratio is also increased. Limits for static point load deflection and impulse velocity responses are applicable where $f_1 \geq 8$ Hz. However, in calculating $f_{1,}$ Equation (3.45), and the unit impulse velocity response limit, v, in m/ (Ns^2), Equation (3.48), the quasi-permanent part of the imposed floor load should be included when calculating the floor mass m, in kg/m^2 using Equation (3.50).

$$m = mG_k + \psi_2 \, mQ_k \qquad (3.50)$$

Where mG_k, in kg/m^2, is the characteristic permanent action, the mass of the floor, and mQ_k, in kg/m^2, is the characteristic variable action on the floor. The factor ψ_2, is taken from Table A1.1 of EN 1990 (EC-0 [120]). Domestic and office loading values for ψ_2 are 0.3, while a value of 0.8 for ψ_2 is applies for storage areas.

With regard to Equation (3.46) the value of the instantaneous force F, is 1kN and the permissible deflection limit, a, should not exceed 1.8 mm for spans equal to or less than 4000 mm, or $[16500/\text{span}]^{1.1}$ where the span is greater than 4000 mm. When calculating the unit impulse velocity response limit, v, (in m/ (Ns^2), Equation (3.48)), the constant b, is 180-60*a, where a is equal or less than 1 mm and 160-40*a where a is greater than 1 mm. In determining $(EI)_b$, (in Nm^2/m equation (3.45)), where plasterboard is fixed to the underside of the floor joists, discontinuities of the plasterboard at the floor edges may be ignored, but the rigidity of the plasterboard should not be included.

When calculating the maximum deflection of the whole floor, the deflection of a single floor joist may be calculated, and multiplied by parameters that allow for the joist type, spacing, and transverse stiffening, Equation (3.51).

$$u = u_1 \, k_{dist} \, k_{amp} \qquad (3.51)$$

Where u, in mm, is the maximum instantaneous vertical deflection due to vertical concentrated static force, and k_{amp} ranges from 1.05 to 1.30 depending on the make-up of the joists. Equation (3.52), may be used to compute u_1 the deflection of a single joist.

$$u_1 = {1000\, l^3} \Big/ {48\, (EI)_{joist}} \qquad (3.52)$$

Parameter k_{dist} is determined using Equation (2.53).

$$k_{dist} = \max \begin{matrix} k_{strut} \left(0.38 - 0.8\ \ln\left[14\, {(EI)_b} / {s^4} \right] \right) \\ 0.30 \end{matrix} \qquad (3.53)$$

Where k_{strut} relates to cross bridging and ranges between 0.97 and 1.0. The term s, in mm, representing the joist spacing.

3.4.5 Other EC-5 national annexes

A study of the vibration design criteria of thirteen EU countries is presented by Zhang et al. [121], wherein the alternative equations and parameters for each country are outlined. Additionally the different standards are applied to a range of timber beam floor constructions and compared. The most notable differences between the national annexes are that Ireland and the UK allow a damping ratio ζ of 2%. Finland's f_1 limit is 9 Hz while Austria and Finland both use more comprehensive equations to calculate f_1. Austria and Finland include the quasi-permanent action when determining the floor mass calculated using Equation (3.50), and Finland, Germany, Norway, and Spain disregard the unit impulse velocity response criteria completely.

Zhang et al. [121] concluded that the unit point load deflection criterion is the most critical in timber floor design, but that there is at present a large disparity between calculated deflection methods and the limits applied by the various countries. Ireland and the UK were found to have the most comprehensive formula, as it considers shear deflection, the stiffening effect from transverse floor members, and the effect of floor joist spacing. Finland was found to currently have the strictest design requirements. Discussing the suitability of current EC-5 [22] criteria, Zhang et al. [121] observed that alternative international vibration design guides including ISO 2631[114] [113] [108], ISO 10137: 2007 [115], and BS 6742-1: 2008 [117], discussed below, often require experimental measurements, thus requiring a degree of expertise not necessarily available to structural engineers. The criteria prescribed in EC-5 [22] and its National Annexes can, in the main, be applied by all qualified building designers.

3.5 International vibration design criteria

The international standards ISO 2631-1 (1997 [116], 2010 [114]), ISO 2631-2 (2003 [113]), and ISO 10137 (2007 [115]), and ISO 2631-4 (2010 [108]) provide guidance on mechanical vibration and shock, together with evaluation of human exposure to whole-body vibration. Additionally the standard ISO 2631-2 (1989 [105]) is superseded but is referenced in EC-5 [22]. The standards define comfort boundaries for lateral, and vertical axes of standing, sitting, and recumbent persons and they bound the frequency range of vibration exposure that most impacts on a person's comfort, perception, and health between 0.5 Hz and 80 Hz. Based on those comfort boundaries, ISO 10137: 2007 [115] provides design guidelines with regard to the serviceability of structures, including buildings and walkways against vibrations. BS 6472-1: 2008 [117] provides guidance on evaluating human exposure to non-blasting vibration, including weighting curves with respect to human tolerance to vibration.

3.5.1 Common forcing frequencies

ISO 10137: 2007 [115] presents design values for coordinated human activities. The dominant fundamental harmonic design value of common forcing frequencies for up to six persons per m^2 in a stationary location ranges between 0.5 Hz to 3.5 Hz. The forcing frequency of vertical actions of seated audiences is bound between 1.5 Hz and 3.0 Hz, and up to 3.5 Hz for coordinated jumping or dancing. Design parameters for one person moving can vary between 1.2 Hz and 12.0 Hz for the first five harmonics. A harmonic, in this case, refers to a positive integer multiple of the fundamental frequency. The pace of walking is typically between 1.5 Hz and 2.5 Hz [20].

3.5.2 Damping ratios

The energy dissipation that is caused by restorative internal forces, which include tension, compression, or shear, and/or external friction or gravity forces, is defined as the damping of a structure. It is the damping that regulates the magnitude of vibration and response, most critically at or near resonance. The damping of a building element is principally dependent on the material characteristics of each of the element components together with their assembly construct. However, a range of other non-structural factors may impact on its effect and magnitude. In the case of floors, the floor and ceiling finishes, internal non-structural walls, furniture, and the people occupying the rooms can all considerably impact the floors damping value. People moving have been found to influence damping more than people standing and even a person's posture and gait has been found to affect their influence on a floors dynamic response and damping ratio ζ [122][123]. ISO 10137: 2007 [115] asserts that accurate damping ratio ζ estimates are not possible, recommending that a designer refer to prior knowledge of the response of similar construction types to assume appropriate values. Damping ratios ζ from 1.5% to 4.0% are given as an estimate range for a timber-joisted floors spanning two to nine meters, and 2.0% is proposed as a preliminary ζ design value.

3.5.3 Acceptance criteria

When quantifying vibration, the peak-to-peak displacement, maximum peak displacement, or vibration velocity, are all applicable parameters. However, accelerometers are deemed the most viable instruments for measuring small dynamic movement. It is accepted therefore that when assessing vibration, particularly for continuous and lower frequencies, a criterion expressed in terms of vibration acceleration (m/s^2 or g) is deemed appropriate [100]. The root-mean-square (rms) value is often taken in preference to the peak value, so that any uncharacteristic spikes in the recording are attenuated over time.

3.5.4 Vibration perception

While people's activities influence their tolerance to vibration, many factors may contribute to a person's awareness of vibration in a building. Some common factors that influence human perception are outlined in BS 6472-1: 2008 [117]. They include structural-borne or airborne noise, induced rattling, visual effects that include periodic displacement of suspended features or reflected images, or an adverse comment from a third party. Other influencing factors outlined in ISO 10137: 2007 [115] include the occupants familiarity with the vibration, structural appearance, confidence in the building structure, and height above ground. All are contingent to the tolerance of each of the building occupants. Two parameters that can be measured and are found to frequently impact on a person’s awareness and tolerance to vibration are the vibration direction and its magnitude. ISO 2361-1: 1997 [114] illustrates the distinct vibration directions that are considered, shown in Figure 3.13.

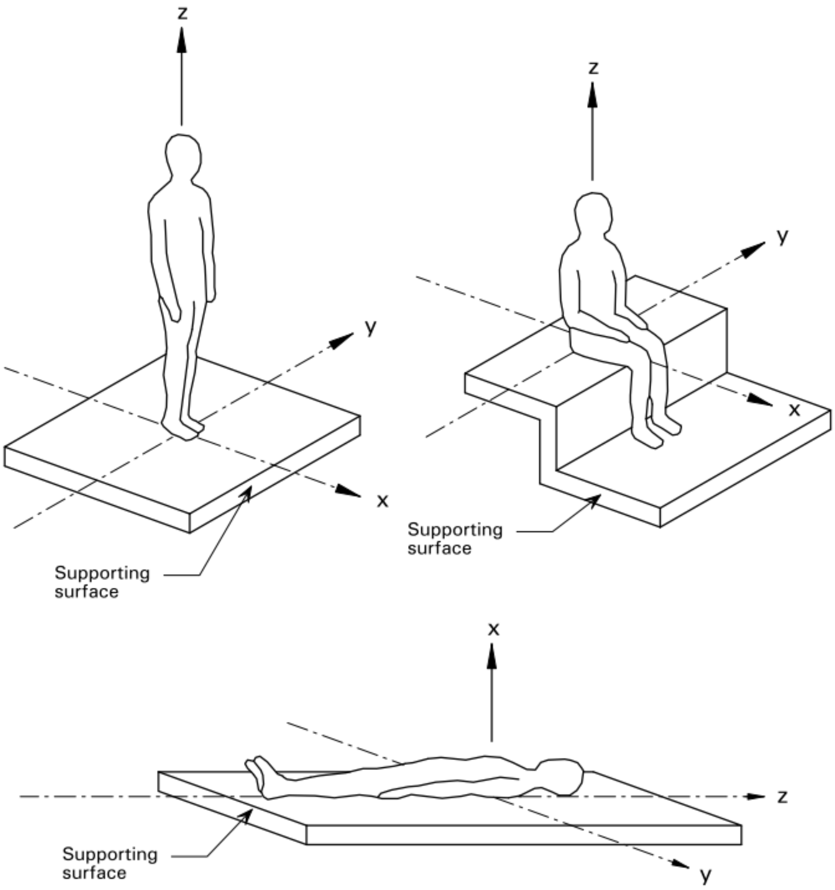

Figure 3.13 *Basicentric axes (x, y, and z) for vibration defined in ISO 2631-1. Image [19]*

Acceleration weighting curves are defined in BS 6472-1: 2008 [117]. The weighting curves are further simplified in ISO 10137: 2007 C.1, C.2, and C.3 [115]. They are termed base curves and are presented in Figures 3.14 to 3.16. The base curves bound the maximum human sensitivity for vertical acceleration between 4 Hz and 8 Hz, and between 1 Hz and 2 Hz for horizontal vibration.

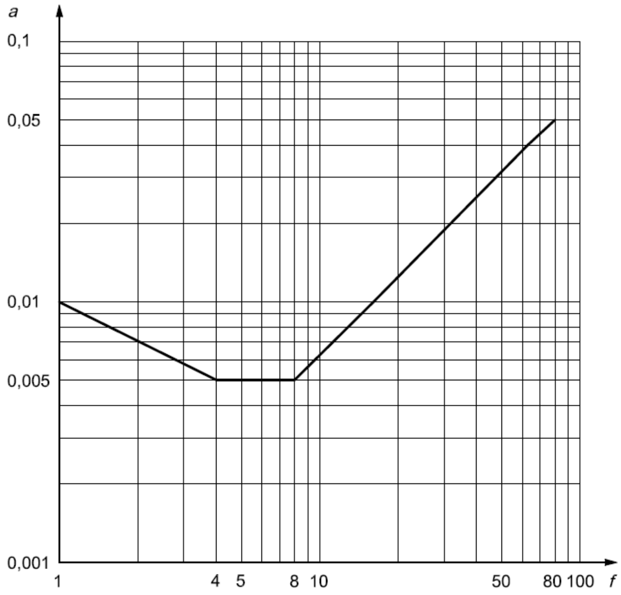

Figure 3.14 *Building vibration z-axis base curve for acceleration (foot-to-head) ISO 10137 [115]*

ɑ acceleration (rms), m/s² *ƒ frequency, Hz*

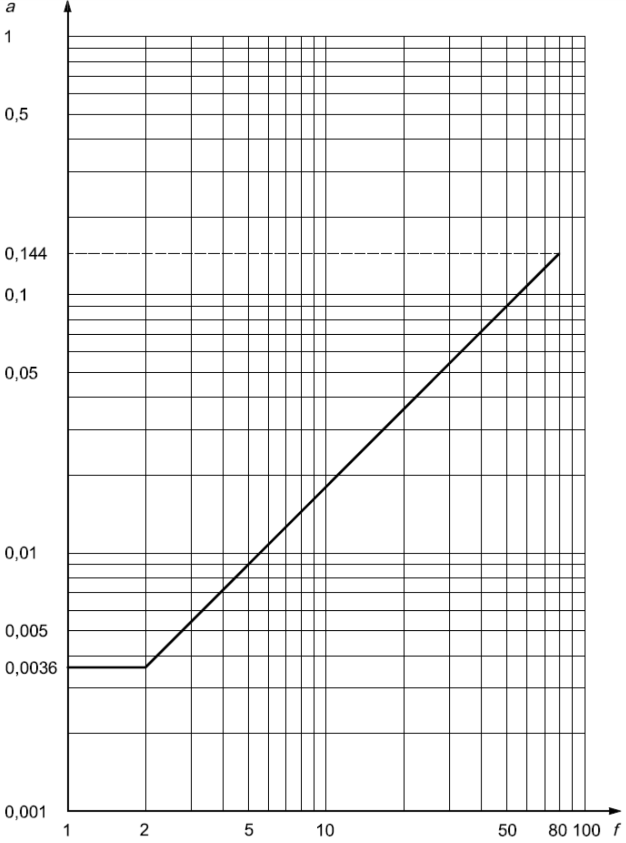

Figure 3.15 *Building vibration x- and y-axis base curve for acceleration (side-to-side and back-to-chest) ISO 10137 [115]*

ɑ acceleration (rms), m/s² *ƒ frequency, Hz*

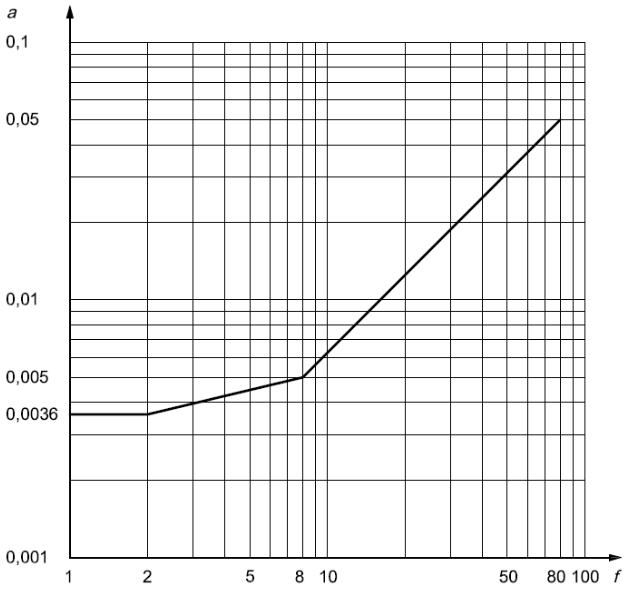

Figure 3.16 *Building vibration x-, y-, and z-axis base curve for acceleration, ISO 10137 [115]*

a acceleration (rms), m/s^2 *f frequency, Hz*

Applying the base curves, the value for z-axis vibration below which vibration is deemed negligible, is 0.005 m/s^2 in the frequency range of 4 Hz to 8 Hz. For x- and y-axis vibration, the base value is 0.00357 m/s^2 for frequencies less than 2 Hz. Looking at different frequency responses using the base curves, a continuous vibration of frequency 6 Hz in the foot-to-head direction (z-axis) is considered insignificant below 0.005 m/s^2, while vibration at 20 Hz in the same direction may be considered negligible at two and a half times the amplification at 0.013 m/s^2. Applying the base curve (Figure 3.15 (ISO 10137: 2007 C.2 [115])) for the same 20 Hz vibration from side to side (y-axis) is considered insignificant at over seven times the magnitude at 0.036 m/s^2.

Pedestrian traffic constitutes a common vibration source in domestic, office, and school floors. The maximum pace of footfall for one person is found to be 3.2 Hz [100]. Taking an average walking pace of 2 Hz, a base value of 0.007 m/s^2 is applicable [20].

3.5.5 Continuous, intermittent, and occasional vibration

BS 6472-1: 2008 [117] classifies the time history of building vibrations which are perceptible by its occupants as:

- Continuous, vibration which is uninterrupted for an assessment period;

- Intermittent, a vibration perceived in separate identifiable repeated bursts;
- Occasional, which occurs less often to intermittent and may be less predictable.

Further characterised as having:

- Constant amplitude;
- Variable amplitude; or
- Impulsive, identified by a rapid build-up to a peak followed by decay, which may or may not, comprise a number of cycles of vibration.

3.5.6 Tolerance of vibration

As people's acceptance of vibrations is subjective, contingent largely on their own level of activity [13], multiplying factors specifying satisfactory magnitudes of building vibrations are applied to the base curves. They are dependent on the type of vibration, the time of day, and the building use. The multiplying factors adapted from ISO 10137: 2007 Table C.1 [115] are charted in Table 3.1. The factors constitute vibration magnitudes below which the probability of adverse comment is low.

Table 3.1 *Multiplying factors from Table C.1 ISO 10137: 2007 [115]*

Place	***Time***	*Multiplying factors to base curves Figures C.1, C.2, and C.3 ISO 10137: 2007* [115]	
		Continuous and intermittent vibration	*Impulse vibration excitation with several occurrences per day*
Critical working areas (Hospital operating-theatres, precision laboratories, etc.)	*Day*	*1*	*1*
	Night	*1*	*1*
Residential (Flats, homes, hospitals)	*Day*	*2 to 4*	*30 to 90*
	Night	*1.4*	*1.4 to 20*
Quiet office (Open plan)	*Day*	*2*	*60 to 128*
	Night	*2*	*60 to 128*
General office (Schools, offices)	*Day*	*4*	*60 to 128*
	Night	*4*	*60 to 128*
Workshops	*Day*	*8*	*90 to 128*
	Night	*8*	*90 to 128*

Continuous vibration is defined as having a duration of more than 30 minutes per 24 hours. Intermittent vibration refers to occurrences of more than 10 events per 24 hours. Using the previous example of a continuous foot-to-head vibration of frequency 6 Hz, an acceleration amplitude below 0.040 m/s^2 would be considered negligible, night or day in a workshop environment, while this value is reduced to below 0.007 m/s^2 a in an apartment building at night. A vibration magnitude of up to 6.400 m/s^2 may be considered satisfactory for impulse vibrations, depending on the frequency.

3.5.7 Low and high frequency floors

The definition of a low or high frequency floor relates to the floors response to human dynamic excitation. Floors with fundamental frequencies below 7 Hz to 10 Hz are regarded as low frequency floors, while floors with a fundamental frequency above this range are considered high frequency floors. A low frequency floor is vulnerable to excitation and resonant build-up due to walking, running, and jumping. The magnitude of the dynamic responses are relative to the floor’s mass and damping. The greater the mass the lower the response to excitation [117]. When evaluating footfall in low frequency floors, the response is regarded as a resonant response and is quantified in terms of acceleration, however, the duration of the vibration should be considered [115].

In the case of high frequency floors, the dynamic response from human activity can be considered as a series of transient responses to the individual impulses of the footfall, BS 6472-1: 2008 [117]. Applying the multiplying factors for continuous vibration when assessing a high frequency floor response due to walking and running is considered conservative. It defines the most critical limit of vibration tolerance.

The response of a structure to resonant excitation is very dependent on its damping characteristics. If the natural frequency of a floor is within four times the pace of footfall, resonance is possible; however, if the fundamental frequency of the floor is greater than four times the pace of footfall the floors vibration response will not appreciably exceed the impulse response of one step. Impulsive response magnitudes are much less sensitive to damping. The impulse velocity of a footstep is proportional to the floors fundamental frequency, the frequency of the footfall, and the modal mass of the floor [20].

3.5.8 Dynamic actions of groups of people

When considering the dynamic action of groups of people in a building, their mass and their coordination is important. The more complex the activity, the lower the coordination and a lower level of synchronisation is expected for the higher harmonics. A group's familiarity of the activity is also considered. A group of individuals in a gymnasium may be regarded as highly coordinated, while crowds attending a concert are expected to have low coordination. Medium coordination is expected from spectators at a sports event. Correction factors are provided for groups of over 50 people with respect to the comfort of observers or non-participants to activities of the crowd. A moving crowd is deemed less sensitive to the vibrations they are propagating. The correction factors range from 0.30 to 0.80, depending on the groups likely coordination (ISO 10137: 2007 Table A.2 [115]). A correction factor of up to 0.14 may be applied for an uncoordinated group, depending on the group size, with a group of up to five people deemed to act in harmony.

3.5.9 Concrete and steel floor vibration design criteria

Uncomfortable floor vibration is not confined to timber buildings. To mitigate poor serviceability in steel deck or slender concrete floors both the British Steel Construction Institute and Concrete Society have produced design handbooks, namely, Smith et al.'s (SCI P354) [19] Design of floors for vibration: A new approach, and Willford and Young's (CCIP016) [20] Design guide for footfall induced vibration of structures, respectively. Within these design guides, a rule-of-thumb parameter to determine initial vibration acceptability for different building uses is described in terms of the response factor, R. Essentially this is the ratio between the measured or calculated weighted rms acceleration or velocity and the base value charted in Figures 3.14 to 3.16. For constant vibration of a constant amplitude in the z-axis, the response factor R is determined using Equation (3.54).

$$R = {}^{a_{w,rms}}/_{0.005\ m/s^2} \tag{3.54}$$

For similar continuous vibration in the x- and y-axis, the response factor R is determined using Equation (3.55).

$$R = {}^{a_{w,rms}}/_{0.00375\ m/s^2} \tag{3.55}$$

Where $a_{w,rms}$, in m/s^2 is the weighted rms acceleration. The proposed values for R, which is dimensionless, equate to the multiplying factors for continuous vibration outlined in Table 3.1. In the case of impulse vibration, footfall on high frequency floors, a constant rms velocity R criterion is applied, outlined in Equation (3.56).

$$R = {}^{v_{rms}}\!/_{0.0001\ m/s} \tag{3.56}$$

Where, $v_{,rms}$, in m/s, is the rms velocity of a single impulse.

Willford and Young's (CCIP016) [20] design guide provides calculations for different floor assemblies, where the effective impulse is empirically related to the pace of walking and the floors fundamental frequency. Applying a calculation that is applicable to a floor of regular shape and constant thickness, gives the footfall impulse response for the first mode of the floor. It considers only the fastest walking pace. Equation (3.57) may be used to determine the effective design impulse value.

$$I_{eff} = {}^{54\, f_w^{1.43}}\!\Big/_{f_n^{1.30}} \tag{3.57}$$

Where I_{eff}, in Ns, is the effective impulse value, f_w and f_n, measured in Hz, are the pace of walking and the structures fundamental mode, respectively. Dividing the impulse value by the modal mass gives a peak velocity, Equation (3.58).

$$\hat{v} = {}^{I_{eff}}\!/_{\hat{m}} \tag{3.58}$$

Where $\hat{v}$, is the peak velocity, in m/s, and the modal mass $\widehat{m}$, in kgm^2 is determined using Equation (3.59).

$$\hat{m} = {}^{mLW}\!/_{4} \tag{3.59}$$

where m, in kg, is the mass per unit area of the floor and L and W are the floor width and length, measured in m.

The root mean square velocity is calculated using Equation (3.60)

$$v_{rms} = \sqrt{\frac{1}{T} \int_0^T v\,(t)^2\, dt} \tag{3.60}$$

where T, in s, is the period of one footfall and $v\ (t)$ is proportional to $f_w^{1.43}$, the rate of footfall. The peak velocity, $\hat{v}$ occurs at the fastest walking pace, therefore only the fastest pace is considered.

In a low frequency floor excitation due to pedestrian traffic may resonate with the floor. CCIP016 [20] provides a calculation approach to determine the maximum steady-state acceleration that is likely. The modal frequencies of the floor, their modal mass, and the damping ratio of each mode is included. The calculation is outlined in Equation (3.61).

$$a = {}^{\mu_{e,m}\ \mu_{r,m}\ F_h} \big/ {}_{2\ \zeta_m\ m} \tag{3.61}$$

Where $\mu_{e,m}$ and $\mu_{r,m}$ are the mode shape values at the point of excitation and response for each mode. F_h, in N is the harmonic force due to walking. ζ_m is the modal damping and m, in kg, is the mass.

The calculation is repeated for all potential walking paces to establish the maximum excitation response. The maximum response is compared with a base acceleration value to determine the floor's R-value. The calculations are deemed valid for all floors with a natural frequency greater than 4 Hz. All of the natural modes of the floor that occur between the fundamental frequency f_1 and two times the fundamental frequency of the floor, $2\ (f_1)$ should be considered.

US steel floor design criteria

The American Institute of Steel Construction design guide to floor vibration due to human activity by Murray et al. [21] proposes baseline rms and peak vibration acceleration recommendations for human comfort due to human activities for different building uses. The values are charted in % of gravitational acceleration, shown in Figure 3.17.

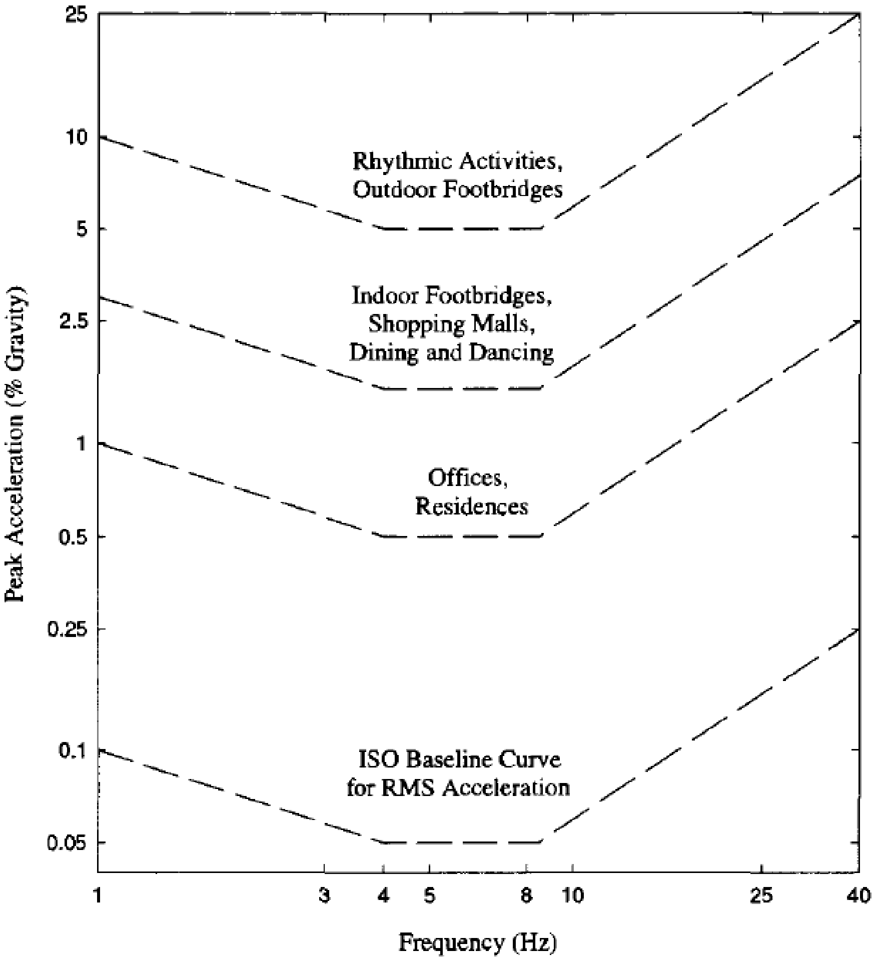

Figure 3.17 *Recommended peak acceleration for human comfort for vibrations due to human activity. Steel Design Guide Series 11: Floor Vibrations due to Human Activity [21]*

The baseline threshold is similar to the vertical acceleration base curve from ISO 10137: 2007 C.1 [115]. The minimum rms acceleration tolerance is set below 0.005 m/s^2 in the frequency range between 4 Hz and 9 Hz. The acceptable minimum peak acceleration values are set below 0.049 m/s^2 for office and residential occupancy and below 0.147 m/s^2 for dining, dancing, and shopping areas in the 4 Hz and 9 Hz frequency range.

3.5.10 Vibration dose values

Human induced vibrations have neither a steady magnitude nor are they continuous. Footfall can be regarded as a series of transient impulses where the pace and amplitude are ever changing. A vibration dose value (VDV) quantifies vibration responses over a longer time frame to integrate the varied values. It is based on the fourth power of acceleration, providing a greater emphasis on the vibration magnitude than the vibration duration. Increasing the magnitude of a vibration by two would also increase the VDV by two. If the duration of the vibration was increased by two, the VDV would increase by only 19% [20]. The VDV is determined using Equation (3.62) [116] [117] [118].

$$VDV = \left(\int_0^T a\,(t)^4\,dt\right)^{0.25} \tag{3.62}$$

The vibration dose value VDV is expressed in m/s$^{1.75}$, a (t), in m/s^2, is the weighted acceleration, and the duration of the measurement, T, is recorded in seconds.

BS 6472-1: 2008 [117] and ISO 10137: 2007 [115] provide guidance on maximum VDV for residential buildings during the daytime and during the night. The values are charted in Table 3.2. Where these values are exceeded, adverse comments would be expected.

Table 3.2 *Vibration dose values (m/s$^{1.75}$) [115][117]*

Place	*Low probability*	*Possible*	*Probable*
Residential *16 h day*	*0.2 to 0.4*	*0.4 to 0.8*	*0.8 to 1.6*
Residential *8 h night*	*0.13*	*0.26*	*0.51*

3.6 US and Canadian CLT floor vibration design criteria

The US and Canadian CLT Handbook criteria [70][71] regard CLT floors as high frequency floors, and therefore are deemed unlikely to resonate with footfall. Only the transient vibration caused by individual heel impact is considered. As the floor's stiffness and mass limit the peak values of transient vibration, the American CLT floor serviceability criteria is focused on acceptable parameters for static deflection and fundamental frequency only. Equations (3.63) and (3.64) describe the combined deflection and frequency criterion. As each equation is the inverse of the other, either equation may be applied. Imperial units are used in the American handbooks, for clarity, the metric versions, which were presented at the World Conference on Timber Engineering in 2012 (WCTE 12) [124] are shown here.

$$f_1/_{d^{0.7}} \geq 13.0 \tag{3.63}$$

$$d \le {f_1}^{1.43} / 39 \tag{3.64}$$

Where f_1 is the fundamental frequency, in Hz, of a 1m wide CLT simply supported panel, calculated using Equation 3.45, and *d*, in mm, is the static point load deflection mid-span of a simple beam. Its value may be calculated using Equation (3.65).

$$d = {}^{(1000\, P\, l^3)} \big/ {}_{(48\, (EI)_{eff})} \tag{3.65}$$

Where *l*, in m, is the span. *(EI)* *eff*, is the effective characteristic stiffness value along the span of a 1m wide panel, in Nm^2, as defined by the CLT manufacturer's technical data. *P* is a 1 kN load. By combining these equations a span limit can be determined using Equation (3.66).

$$l \le {}^{1}/_{9.15} \left({}^{(EI)^{0.293}} \big/ {}_{(\rho A)^{0.123}} \right) \tag{3.66}$$

Where *ρ*, is the density in $\mathrm{kg/m}^3$, and *A* is the unit cross sectional area, in m^2.

Field studies of occupant's expectations with regard to the serviceability of residential floors by Onysko's [125] found that the fundamental frequency and 1 kN static point load deflection criteria provided the best correlation with consumer satisfaction. Similar studies by Hu and Gagnon [124] on five and seven ply CLT floors found the same criteria also correlated well with occupant's expectations of CLT floors.

Hu et al. [126] compared various floor vibration and serviceability criteria that included Canadian, American, and European codes. It was found that applying a criterion based on the fundamental frequency and point load deflection only was the simplest to apply. Homb and Kolstad [127] found better accuracy using the American static deflection and fundamental criteria compared with European criteria with regard to perception of low frequencies on traditional joisted floors. Further comparison studies on engineered timber joisted floors by Hu [128] found that the deflection and fundamental frequency limits correlated as well as other vibration performance standards with regard to human comfort tolerance.

3.7 Conclusions

Annoying human induced vibrations are considered the most common floor serviceability design challenge, with pedestrian excitation cited as the primary significant source of disturbing vibrations [102]. Moving people are generally more tolerant to vibration, but a number of people moving in unison may intensify the dynamic effect on a structure.

A building’s use and the time of day are weighed when assessing acceptable vibration levels. Where a vibration is not continuous, a vibration dose value (VDV) may be applied to assess the tolerance level. A VDV quantifies vibration responses over a longer time frame, providing a greater emphasis on the vibration magnitude than the vibration duration.

The frequency range of vibration exposure that most impacts on a person’s comfort, perception, and health is between 0.5 Hz to 80 Hz. A person’s sensitivity to vertical vibration is most acute between 4 and 8 Hz.

The response of a structure is strongly dependent on the similarity between the natural frequencies of the structure and the frequency of the exciting force. Where the exciting force is less than the natural frequency, the response is stiffness dependent. Where the excitation force is higher than the nearest natural frequency, the response is inertia or mass dependent, with excitation decreasing with greater disparity between both frequencies. If the excitation force is resonant with a natural mode, maximum displacements will occur and the system response is damping dependent. However, damping is only effective at or near resonant frequencies.

A preliminary design damping ratio value ζ of between 1% and 2% is generally recommended for traditional timber floors, with a lower value of 0.8% suggested for floors in open plan construction or heavy floors with mass greater than 150 kg/m^3.

The dynamic response of a floor due to pedestrian traffic is largely dependent on if it is a low or high frequency floor. A low frequency floor’s fundamental frequency is in the range of four times the pace of footfall and is therefore vulnerable to resonant excitation from human activity. The response is quantified in terms of acceleration.

In the case of high frequency floors, the fundamental frequency is greater than four times the pace of footfall and the dynamic response from human activity can be considered as a series of transient impulses. The response is quantified in terms of impulse velocity which are much less sensitive to damping and peak velocity occurs at the maximum footfall pace.

The maximum force due to a person walking is less than 6 Hz and negligible over 50 Hz. An average walking pace is 2 Hz.

European design standards (EC-5 [22]) recommend a fundamental frequency greater than 8 Hz for timber floors. Guideline limits are prescribed for static point load deflection and impulse velocity responses between 8 Hz to 40 Hz and a damping ratio value ζ of 2% is recommended in the Irish NA. The deflection limit criteria ranges between 0.5 mm/kN and 4.0 mm/kN.

The Canadian and US CLT design standards [70][71] regard all CLT floors as high frequency floors, with the serviceability criteria focused on acceptable parameters for the fundamental frequency and static point load deflection only.

The following chapter will give an overview of measurement and analysis methods that are used to determine the dynamic behaviour of floors. Included also is a review of field and laboratory studies made on timber floors with respect to serviceability and some of the FE approaches applied to modelling timber and CLT.

4 LITERATURE REVIEW

4.1 Introduction

The previous chapter outlined basic vibration theory and the principal static and dynamic acceptance criteria. In this chapter the primary methods used to measure and predict a structures serviceability response are précised. Prevailing static and dynamic measurement methods and the applicable data analysis are reviewed with respect to their appropriateness to laboratory and field measurement of floors. Included is a review of the current provisional European testing standard for timber floor deflection and vibration prEN 16929:2015 [112] and alternative testing approaches appropriate to traditional timber and CLT floor serviceability are examined.

Numerical FE analysis is widely applied in dynamic evaluation of structures. It is used to preliminary appraise a structures dynamic characteristics in advance of experimental testing, informing the data measurement range. FE models that are calibrated with experimental data can then predict the influence of structural modifications. A review of FE modelling of timber, CLT, and timber and CLT assembly with respect to linear and non-linear dynamic loading is outlined in this chapter.

4.2 Static and vibration measurement

4.2.1 Static deflection measurement

Usually the simplest parameter to measure, particularly in the laboratory, is the static point load deflection. The static deflection establishes a floor’s flexural stiffness, which significantly influences a floors dynamic behaviour [112][128]. Therefore, it is generally ascertained when assessing a floors serviceability performance [13][129][130][14][124][131][132]. The measurement is taken by applying a concentrated dead load, usually 1kN, to the position on a floor where the largest deformation is expected and recording the deflection change. As the deflections recorded may be relatively small, the only real challenge is to ensure that the accuracy of the measurement is appropriate, and that the necessary apparatus is positioned and mounted such that it does not influence the results. Providing a suitable mounting to the measurement device is especially challenging in the case of field tests.

4.2.2 Dynamic measurement

The objective of a vibration measurement determines the data type measured, which subsequently governs the measurement and equipment requirements.

Vibration measurement may be divided into two categories, the measurement of operating or modal data. Operating data is the measurement of the vibration response only. This data is most useful to provide an actual depiction of a structures behaviour in use. Modal data describes the inherent modal characteristics of a structure, determined by measuring the dynamic excitation and response concurrently to comprise a modal data set. The modal data set is then used to define a mathematical model of the structure's dynamic characteristics and is commonly referred to as the modal model. Either data set may relate to the entire structure or discrete component parts.

The data accuracy required in testing is influenced by the precision requirement of its end application. To reduce the scope of testing to a succinct data set, an outline numerical model is commonly developed first, before modal testing is instigated. The numerical model may then be refined to correlate with the test data as necessary. A numerical modal model verified by modal testing may then be used to predict responses to given excitations. Validation of the major modes by the modal model can usually provide confidence in the validity of the numerical model [95].

With regard to damping, it is generally not possible to corroborate theoretical damping predictions with the modal model. However, damping results from modal testing may be incorporated into a numerical model to approximate results [95].

4.2.3 Operating data

Operating data comprises the measurement of the response of a structure to an existing or applied excitation. It is especially suited to measuring the serviceability of a floor in use. Common excitation techniques where only the response is measured include the heel-drop or impulse methods, footfall, or brush and trolley excitation. Accelerometers are generally used to measure vibrations. They are placed either where the natural mode shapes are estimated to have maximum amplitude or in areas of a floor considered to be most critical with respect to occupants' perception.

Heel-drop / impulse load test

The heel-drop test comprises the measurement of the response of the impulse produced by an adult standing on their toes on the floor, then quickly dropping their heels as illustrated in Figure 4.1. Alternatively, the impulse may be imparted by a quick release of an attached dead weight from below the floor, a free drop [112], or from the bounce of a heavy rubber ball to simulate an adult jumping [124][133][134][135][136], as illustrated in Figure 4.2. An impulse may also be produced by a suitably sized hammer, illustrated in Figure 4.3. In all cases the objective is to excite a floor in order to measure its dynamic response. A transducer, placed where the natural frequency mode shapes are maximum, records the response of the structure.

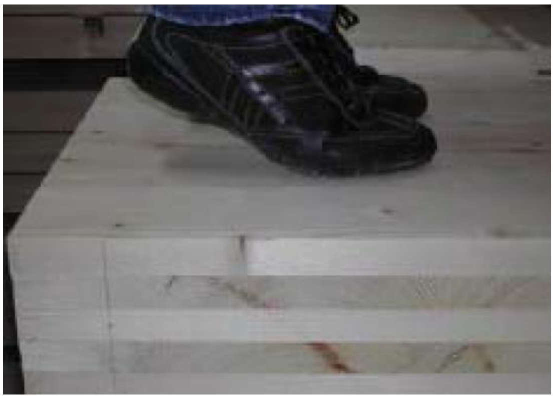

Figure 4.1 *Impulse provided by a heel drop [137]*

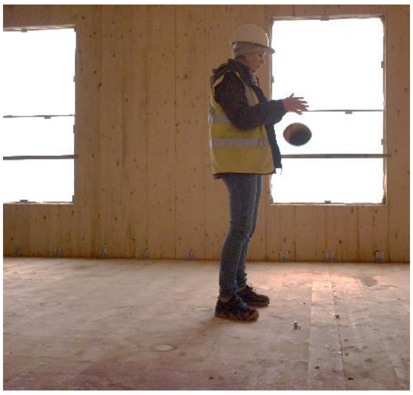

Figure 4.2 *Impulse provided by a heavy rubber ball*

For field studies, the free drop method may raise difficulties with regard to its attachment where access to the underside of a floor is not convenient or possible. Breaking the fall of the weight to avoid damage or injury may also pose a problem. The size of an impulse hammer is critical to providing a sufficiently strong response, which may raise concerns of damage to an in-situ floor and the replication of the impulse can also be a challenge. The only real advantage of using a hammer is that when using a specific impulse hammer, the force is also recorded. This is discussed later in Section 4.2.4. The heel-drop impulse is considerably more convenient in field measurement, however, the rubber ball method is equally convenient and may provide better replicability.

The damping ratio may be measured using an impulse load; however, prEN 16929: 2015 [112] suggests that the continuous and steady excitation of an electromagnetic shaker is more suited to damping measurements.

Footfall excitation

Alternatively, a floor may be excited with footfall or walking persons [138][139][123]. It can be argued that this approach will most accurately simulate the most common annoying source of floor vibration, with numerous studies aimed at accurately simulating footfall and jumping load excitation [140][141][142][143][144][145][146][147][148]. Although Ohlsson [13], when investigating light-weight floors, measured the modal properties by exerting a controlled dynamic force, the mode excitation capacity was measured from human induced footfall. It is often the case that a number of measurement techniques are applied in dynamic analysis [13][124][149][131][132], defining the structure's characteristics using various different measurements. Figure 4.3 shows images from footfall and impulse hammer field tests of timber floors, in Italy.

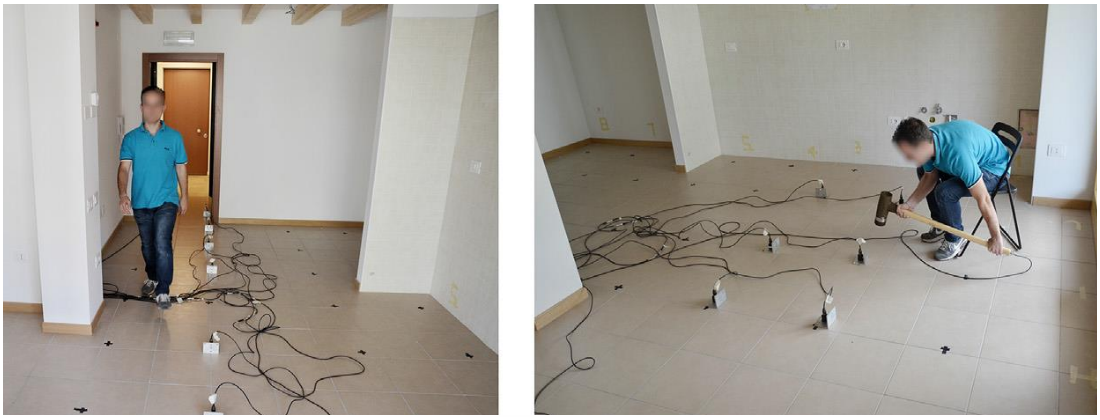

Figure 4.3 *Walking and impulse hammer field tests on timber floors [132]*

Brush and trolley excitation

A floor may also be excited manually by means of a brush and trolley [130][150][131]. The mass of the trolley can range between 5 kg and 10 kg. Using a brush, while walking adjacent to or above the floor on a bridge structure, the trolley is moved over the entire floor exciting all natural modes simultaneously. Roving transducers on a grid of equally spaced points measure the output-only response.

4.2.4 Modal data

In testing a structure, if only the response is measured it cannot be known whether a particularly large response level is due to a strong force excitation or due to resonance [95]. In the case of modal data measurement, both the force input and vibration response are measured simultaneously, so that the frequency response function (FRF) can be determined. The FRF is the ratio of the output response due to an applied input excitation force. It is usually the case that the relative responses are recorded at points on a grid in order to map the value and shape of each natural mode. Modal data is best suited to correlating with numerical modelling. This data is also suited to the investigation of modifications to a structure to mitigate dynamic responses.

Two approaches for measurement of the dynamic characteristics of a structure are Phase-Resonance, and Phase-Separation. Phase-Resonance methods involve the excitation of one vibration mode using several shakers at independent variable force levels, suited to measuring non-linear behaviour in a structure. When investigating a linear structure such as a floor, the Phase-separation approach is more appropriate. With Phase-separation methods, single point test strategies can be applied, including broadband testing, where the excitation is provided by an electromagnetic shaker or single impact testing using an impulse hammer.

Hammer impulse

The main advantage to using an impulse hammer is that the equipment is relatively small, light, and very portable. It is therefore widely used in dynamic analysis [151][152][14][131][153][132]. However, the hammer impulse signal is hard to control precisely, and its duration is very short in comparison with the measurement time. The size and mass of the hammer must be proportional to the structure under investigation. It is hence more suited for diagnostic purposes rather than for precise measurement of FRF properties [98] [154].

Electromagnetic shaker

As the excitation due to an electromagnetic shaker is regulated and can be precisely replicated, modal excitation is often applied by means of a shaker [155][122][156][157][158][159]. For broadband testing, the structure is excited using the shaker with a signal containing energy over a range of frequencies. Generally the excitation locations are fixed, and a series of fixed, or roving accelerometers, on a grid are used to capture the vibration response. The Fast Fourier Transform (FFT) method transforms the time data to the frequency domain. Using the frequency data, the FRF can be computed. Broadband measurement and analysis techniques vary depending on whether the excitation and response signals are periodic, random, or transient. The quickest and most successful types of excitation signal, which can be applied with an electrodynamic shaker to a floor, are the transient types, which includes burst swept sine signals [160], also referred to as chirp signals. Figure 5.30 shows an electromagnetic shaker attached to a CLT test floor in NUI Galway.

4.2.5 SISO, SIMO, and MIMO vibration measurement

Where a roving transducer records the single input vibration of a shaker, or impulse hammer, this is termed SISO (Single Input-Single Output). If multiple accelerometers are recording the excitation due to a single input vibration, the term is SIMO (Single Input-Multiple Output). Multiple shakers with multiple transducers capturing the vibration response are MIMOs (Multiple Input-Multiple Output), or Multiple-Reference tests. The analysis varies considerably depending on whether there are multiple exciters or transducers feeding the FRF analysis. A comprehensive guide to alternative single- and multiple-FRF measurement methods and the implications of each is provided by Maia et al. [98]. However in brief, SISO, single-FRF methods are applicable to most FRF data sets with light modal density and should be applied whenever possible [153]. A variety of frequency domain mathematical curve fitting analysis methods are applicable to SISO measurements, including the Peak Amplitude, the Quadrature Response, and the Maximum Quadrature Component methods. The Peak Amplitude is the simplest modal identification method, where the natural frequencies are observed from peaks on the magnitude response graphs. Damping is calculated from the sharpness of the peaks [161], and the mode shapes are determined from the ratios of peak amplitude at various points on a structure. The Quadrature Response method finds the natural frequencies at the locations where the in-phase component of the response, the real part, is zero. The Maximum Quadrature Component method identifies the natural frequencies where the quadrature component, the imaginary part of the response, is maximum or minimum; the response is 90° out-of-phase with the forcing function in both cases. Other appropriate methods include the Kennedy-Pancu and the Circle-Fitting methods [95][98].

Single-FRF SISO modal analysis is appropriate for a laboratory-scale floor, with a regular plan layout, but as SISO methods can be very time-consuming when measuring larger data sets, multiple-FRF, i.e. SIMO or MIMO methods may be preferable. For SIMO and MIMO measurement, more sophisticated multiple channel recording and processing equipment is required in comparison to that used in SISO modal methods. An accumulation of small discrepancies that accumulate in the measured data may be problematic in multi-FRF methods [95]. Some analysis methods applied to SIMO data include the Global Dobson's method, an extension of Dobson's method which considers complex modes, itself an extension of the Inverse method, and the Advanced Characteristic Response Function (ACRF) method developed by Maia et al. [98], which is based on the Inverse and Dobson's methods combined. Reasons for choosing MIMO testing may include cases where all modes of interest are not detected using a single excitation, or if a structure cannot be sufficiently excited from one reference point, or, an additional reference may be needed to identify closely-coupled modes [153].

FRF and the coherence function

The ratio of the Fourier transforms of both the excitation and the response signals is used to derive the FRF for periodic vibration signals, as described in Equation (4.1).

$$H(\omega) = {}^{X(\omega)}\!/_{F(\omega)} \qquad (4.1)$$

Where *H (ω),* denotes the complex frequency response function, the system's FRF, which characterises the dynamic response to a given forcing function; X *(ω),* denotes the Fourier transform of the response and *F (ω),* represents the Fourier transform of the excitation.

In the case of quasi-permanent transient vibration signals, including burst swept sine, where the excitation and response signals are effectively zero at the start and end of the sample, they are computed as discrete Fourier transform (DFT) solved in the same way as periodic vibration. Figure 4.4 illustrates a traditional measurement-system model used to describe FRF measurement when noise is present on both measured force and response signals.

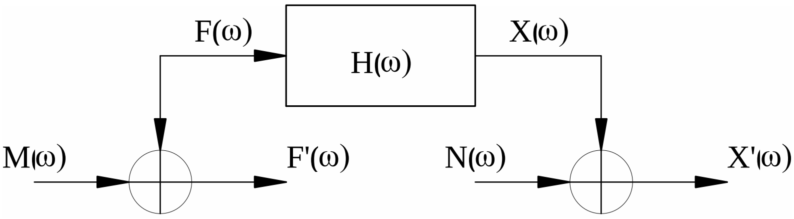

Figure 4.4 *Traditional measurement-system model, where noise is present in the system, basic SISO model [98][95]*

In the figure, $M(\omega)$ and $N(\omega)$ represent noise present on the force and response signals, respectively. Conventionally, FRF is found by using the cross input-output spectrum $S_{f'x'}(\omega)$ and the input auto-spectrum $S_{f'f'}(\omega)$. The FRF $H_1(\omega)$ *is* expressed in Equation (4.2).

$$H_1(\omega) = {S_{f'x'}(\omega)} \Big/ {S_{f'f'}(\omega)} \tag{4.2}$$

Alternatively, the FRF may be estimated by normalising the output auto-spectrum $S_{x'x'}(\omega)$ by the cross input-output spectrum $S_{x'f'}(\omega)$, using for Equation (4.3) to define $H_2(\omega)$.

$$H_2(\omega) = {S_{x'x'}(\omega)} \Big/ {S_{x'f'}(\omega)} \tag{4.3}$$

As the result of both estimators $H_1(\omega)$ and $H_2(\omega)$ should be equal, finding the ratio of both estimates will indicate of the quality of the analysis, as expressed in Equation (4.4).

$$H_1(\omega) \Big/ H_2(\omega) = \left(S_{f'x'}(\omega)\right)^2 \Big/ \left(S_{f'f'}(\omega)\, S_{x'x'}(\omega)\right) = \gamma^2(\omega) \tag{4.4}$$

Where $\gamma^2(\omega)$ is referred to as the ordinary coherence function, a normalised coefficient of correlation between the measured force and response signals evaluated at each frequency, where $0 < \gamma^2(\omega) < 1$. Monitoring the coherence function ensures adequate signal-to-noise ratio. If its value is less than unity, at least one of the following conditions exists in the system.

- Peripheral noise is present in the FRF measurements;
- Bias errors are present in the resolution of the spectral estimates;
- The force input or the response in the system are not linear; or
- The measured response is a result of other external inputs aside from the force input.

4.3 Provisional EU testing standard for timber floors prEN 16929

Currently the provisional European Standard prEN 16929:2015 [112] provides guidelines on testing procedures to measure and report the vibration properties of timber floors. The testing parameters for measurement comprise the static point load deflection, the fundamental frequency, damping ratio, and acceleration amplification. There are alternative procedures depending on whether the floor is in a laboratory or in the field, with guidance on the test set-up, support detailing, and apparatus. Guidance on the accuracy of the apparatus, post-processing and recording of results is also provided. All methods are non-destructive.

Procedures are given on determining dimensions of the floor, its moisture content, in accordance with EN 13183: 2002 [162] and EN 322: 1993 [163], its mass, and the environmental conditions.

Static unit point load deflection measurement: prEN 16929:2015

The static deflection is determined by applying a concentrated dead load on a load pad at the location where the maximum deflection is expected. The load pad may be a square 100 mm x 100 mm pad, or a circular disk of radius 113 mm. The deflection is to be measured with a linear variable differential transformer (LVDT), having an accuracy 1% of the maximum deflection reading, or with a dial gauge of accuracy 0.01 mm. Results are normalised to a 1kN load. At least 1 minute should pass between successive tests and additional tests are required if there is a variance greater than 5% between deflection values. The definitive deflection value is taken as the mean of three satisfactory measurements.

Deflection measurements may be taken either from the top surface or from underneath the floor. A caveat is included in relation to in-situ testing with respect to accessibility to the main floor structure or possible spurious measurements that may be recorded due to the deformation of non-structural elements, including a floor underlay or finished floating floor, for example.

Fundamental frequency measurement: prEN 16929:2015

The current testing guidelines suggests an impulse-load test to measure the floor's fundamental frequency using an impact hammer, heel-drop, or free drop. The impulse is introduced at the geometrical centre of the floor, with the response measured also in the centre of the floor by an accelerometer of an accuracy ranging between 0.5 Hz and 1 kHz, a non-linearity of ± 1 dB, and a relative transverse sensitivity less than 3%.

The use of additional accelerometers is suggested if there is an interest in higher modes, but only the frequencies below 40 Hz to 50 Hz are considered significant. A sample rate of 10 times the highest estimated natural frequency is proposed. A minimum of three successive measurements is required with the mean value of the lowest natural frequency to be taken as the measured fundamental frequency. The fundamental frequency is established from an FFT of the collected time domain. It is recommended to log both the time domain signal and the FFT.

Damping ratio measurement: prEN 16929:2015

To find the damping ratio, providing excitation using a mechanical exciter attached to the floor is preferred. The exciter acts in resonance with the floor and is stopped when a steady-state vibration is reached. The damping ratio ζ is calculated from the logarithmic decrement of the decreasing vibration (Equation (3.24)). The mounting of the mechanical exciter is critical to the clarity of vibration response when using an electronic shaker. Lateral movement of the exciter should be restricted. Additionally, any vertical bounce of the exciter may create cross interference between the structures dynamic response and the forcing vibration, resulting in poor signal measurements. For smaller vibration analysis, the mechanical exciter is isolated from the structure by way of a drive rod or stringer. In the case of a floor, however, where the exciter to structure mass ratio is relatively small, the exciter may be fixed to the floor.

Where it is not possible to attach a mechanical exciter, the guidelines suggest that the floor may be excited by a person stepping at half- or one-third of the fundamental frequency of the floor. However, as the pace of human walking, running, and jumping, ranges between 0.5 Hz and 3.5 Hz [115] [100] this approach is only possible with low-frequency floors, confined to floors with a fundamental frequency below 10 Hz.

The mean of the logarithmic decrement of three successive measurements of a resonant frequency is recorded as the floors damping ratio in prEN 16929:2015 [112].

Acceleration amplification measurement: prEN 16929:2015

A mechanical exciter is again required to determine the acceleration amplification. The exciter is fixed on the floor at mid-span and a trial-and-error approach is used until an adequate signal-to-noise ratio and clear FRF signals are achieved, which is indicated by a coherence function close to unity. The exciter should produce sine wave signals of loads ranging between 50 N and 200 N. To characterise the full mode shape of each mode of interest, a grid consisting three equally spaced rows along the span direction is recommended for a joisted floor. The FRF determines the acceleration amplification, taking the mean of three successive measurements.

In the case of an in-situ floor, the practical difficulties in fixing an exciter to the floor are noted again, and excitation by stepping at half- or one-third the fundamental frequency of the floor for 10 seconds is suggested as an alternative. The maximum amplitude of the accelerations during steady-state vibration should be recorded as the acceleration amplification in this case. This approach is only possible with low-frequency floors, as before.

prEN 16929:2015 [112] is currently under review by the European Technical Committee CEN/TC 124, (May 2019).

4.4 Laboratory and field floor vibration studies

A review of laboratory and field testing studies on the static and dynamic behaviour of timber floors is presented in following sections.

4.4.1 Traditional timber floor serviceability studies

Ohlsson [13], when investigating footfall and the dynamic response of light-weight floors, tested eight timber floors under laboratory conditions and undertook four field tests of one-family timber framed houses. Two of the buildings were furnished. A concentrated static force was used to find the local stiffness, while the modal properties were measured by exerting a controlled dynamic force. Human induced footfall was used to establish the mode excitation capacity. The floors generally comprised 45 mm x 200 mm beams at 600 mm centres, spanning up to 5000 mm. The fundamental frequencies measured were greater than 12 Hz for the laboratory floors and over 19 Hz in field tests. The static deflection results averaged at 1.0 mm/kN and 0.41 mm/kN for the laboratory and field measurements, respectively. The laboratory floors provided a mean damping ratio ζ of 0.9%, while ζ-values of 3.4% were measured in-situ. Ohlsson's design guide [119] based on his results later suggested a ζ–value of 1% for standard timber construction reduced to 0.8% for heavy floors with a mass greater than 150 kg/m^3.

Eriksson [100] asserted that resonant frequencies are closely spaced in traditional timber joisted floors due orthotropic characteristics of the floors. Smith and Chui [164] found that adequate strutting between joists and provision of a support to all sides of a rectangular floor improved the separation of the natural frequencies. Solid-block strutting performed better than herring-bone bridging. No significant correlation was measured between the joist-end rigidity and the vibrational response of traditional floors. Variations in the modulus of elasticity did not significantly influence the results.

Khokhar examined the influence of the lateral element stiffness of a wooden floor on its dynamic performance [129]. A laminated veneer lumber (LVL) joisted floor with oriented strand board (OSB) deck spanning 4200 mm was examined. A 1 kN point load applied midspan resulted in a 1.30 mm deflection for a non-laterally braced floor. This improved by 30% to 0.90 mm with LVL bracing. Five natural modes with a value below 70 Hz were recorded for each floor assembly tested. Neither solid block nor cross-bridging influenced the natural frequency values to any significant degree. However, cross-bridging combined with 19 mm x 89 mm strapping to the underside of the joists improved results from 19.25 Hz to 21.80 Hz for the fundamental frequency. A greater difference was observed in the fifth mode, which was increased from 66 Hz to 70 Hz.

Zhang et al. [150] studied the vibrational performance of nine laboratory floors. The floors consisted of timber metal-web joists, all measuring 5250 mm in length. The dynamic influence of alternating the joist spacing, along with various types and arrangements of strongback bracing, and the provision of a ceiling were examined. Modal testing consisted of output-only modal analysis, where excitation was provided with a brush and trolley. Roving transducers on a grid of 25 equally spaced points on the floors were used to measure the response. The natural frequencies, their mode shapes, and damping ratios up to 40 Hz were measured. All floors were found to have fundamental frequencies over 14 Hz with corresponding damping ratios ζ measuring 0.9% on average, which is less than the recommended 1% value in EC 5 [22]. It was found that including a ceiling, alternative joist spacing, or various strongback bracings had no significant influence on the fundamental frequencies, nor their corresponding damping ratios. However, higher modes were impacted. Increasing the number and size of strongback bracings was found to significantly reduce the number of first-order modes below 40 Hz, improving compliance with EC-5 [22] velocity response criteria. Reducing joist spacing or increasing the number and size of strongback bracings both improved the point load deflection results, as did the inclusion of a ceiling. Floors without bracing or a ceiling were found not to comply with EC-5 UK NA criteria [165].

Labonnote [152] [151], when comparing two 2400 mm x 2880 mm traditional timber joisted laboratory floors using screwed or nailed connections, found a marginal influence in stiffness for the screwed floor. The connections were glued also in both cases. The floors consisted of 225 mm glulam joisting at 600 mm spacing, with 22 mm and 13 mm thick particleboard for top and bottom decks, respectively. Each floor was simply supported at the four corners of the floors by means of 4 mm x 133 mm diameter steel cylinders positioned along the 225 mm x 67 mm edge joists. Fundamental frequencies between 28.5 Hz and 29.7 Hz were recorded. The difference between damping ratios ζ was minor, measuring less than 2% for the fundamental modes and below 3% for the second and third natural frequency modes.

Field testing of timber-joisted floors by Xiong et al. [166] on an elementary school in China measured average damping ratios ζ of 0.95% for ambient vibration and 5.05% for an impulse load. The large disparity between results from these tests question if the ambient vibration was resonant or alternatively the results reinforce prEN 16929: 2015 [112] recommendation that measuring damping using an impulse load is not appropriate.

In Ebadi et al.'s [131] ambient vibration tests, nine laboratory glulam beam-and-deck floors were excited by means of a 10 kg trolley. The vibration response was recorded via roving accelerometers on points of a predetermined grid. The measured fundamental frequency and corresponding damping ratio ζ for a 5000 mm span floor were 11.1 Hz and 1.3%, respectively. The maximum deflection recorded was 0.58 mm due a 1kN point load applied midspan. Introducing a non-structural concrete topping to a 3800 mm spanning floor resulted in a damping ratio value of 3.1%, and a significant reduction in deflection to a value to 0.07 mm. The topping decreased the fundamental frequency of the floor from 20.2 Hz to 18.8 Hz.

Homb and Kolstad [127] measured the fundamental frequencies, damping ratios, and the static point load deflections of over twenty timber-joisted floors, including four in-situ floors. The floors comprised solid-wood, glulam, engineered I-beam, and metal-web joists, with transverse stiffening provided to longer spanning floors. Spans ranged from 3600 mm to 7500 mm. A rubber ball excited the floor for the dynamic testing, with the damping ratios found using the half-power bandwidth method on the FRF spectra. The fundamental frequency results ranged between 9 Hz and 21 Hz. There was a broad scatter of results when recording the damping ratios, with results ranging between 1.5 and 15%. In-situ measurements of damping ratios ζ recorded values at least 4%, with a damping ratio of over 7% recorded where there was additional support from a load bearing wall. The high ζ-values measured from the impulse load again bring to mind prEN 16929: 2015 [112] comment regarding steady excitation in preference to an impulse load when measuring damping. The static point load deflection results ranged between 0.2 mm and 2.3 mm.

Experimental investigations of the point load static deflection and vibration performance of laboratory floors with various timber-engineered joist arrangements were made by Weckendorf [130]. The timber floors comprised metal-web joists, laminated veneer lumber (LVL) / OSB I-joists, and solid timber / OSB I-joists, and the static deflection, natural frequencies, and damping ratios ζ were measured. For the dynamic tests the floor was excited manually with a brush and 5 kg trolley. Roving transducers on a grid of 25 equally spaced points on the floors were used to measure the output-only responses. For the metal-web joisted floors spanning over 5000 mm, the deflection and fundamental frequency results ranged between 0.86 mm/kN and

1.80 mm/1 kN, and 13.4 Hz to 15.5 Hz, respectively. The damping ratio ζ values ranged between 0.82% and 1.28%. Supporting timber joisted floors along all edges was found to increase the frequency spacing, while timber I-joists generally outperformed the metal-web floors with regard to damping.

4.4.2 CLT and composite floor serviceability studies

A single and a double panel 5-ply CLT floor were tested in the laboratory by Weckendorf and Smith [167]. Alternative support fixity and different supporting materials were examined. The panels were both 5500 mm x 2280 mm. A half-lap joint was used to connect the panels in parallel. The natural frequencies and mode shapes below 90 Hz and the corresponding damping ratios ζ were measured. There was negligible difference between the single- and double-panel floors fundamental frequency value. However, the number of modes was increased, reducing the mode separation. The average value was reduced from 11.4 Hz to 12.0 Hz. All fundamental mode damping ratio ζ results for bare single and double panel CLT floors were less than 1%. A person standing on the floor improved the damping performance of the floors by up to three times the value for the bare floors; however, the person's influence varied depending his position on the floor and the mode shape examined.

In general, it can be accepted that occupants affect the dynamic response of a floor [168], with many studies investigating the influence of people's movements on floor vibration or crowd induced dynamic loading relative to the response [139][147]. For example, the effect of walking traffic on a laboratory concrete floor in comparison with people standing was found to improve damping ζ results significantly [122].

Dynamic tests of exposed and unfurnished in-situ CLT floors in the Sky's multi-storey gymnasium building [159] gave average damping ratio ζ value in the order of 2%. Campbell et al. [159] surmised from the field test results that the stiffness and therefore the modal performance of the floors could be improved by increasing the continuity of the floor panel-to-panel connections in the non-spanning direction of the floor. The commonly used CLT half-lap joint (Figure 2.15 (a)) was replaced with connection that combined a half-lap with a broad-top joint (Figure 2.16 (f)).

Hamm et al. [137] studied in-situ timber floors, including traditional and CLT floors with, and without screed topping to investigate why annoying vibrations continue to be a problem, even though EC-5 [22] and the German NA DIN 1052 [63] are generally adhered to. The extensive study found that in-situ frequency measurements and calculated values did not sufficiently correlate. This anomaly was attributed to the assumed boundary conditions used in calculations that did not include the torsional spring influence of the walls above, nor any non-bearing partitions which positively influenced vibration behaviour in all cases. Frequency measurements and perceived vibration annoyance also did not agree. However, the static deflection criterion was found to be equally as important as the frequency parameter. It was suggested when designing timber floors that any mass due to a live load on the floor should be neglected, contrary to DIN 1052 and BSP-Handbuch [63][65], but that the stiffness of a screed, if existing, should be included. It was recommended to incorporate into design calculations if the floor was spanning in two directions.

Maldonado and Chui [169] examined the vibration response of 5-ply CLT floors consisting of one, two, three, and four panels each 132 mm thick, 1020 mm wide, spanning 4870 mm. The floors were tested spanning one- and two-ways. Adjacent panels were connected with inclined screw pairs at 300 mm spacing. The study found negligible influence of adding additional panels on the first and second natural frequencies of the one-way spanning floor with results averaging 11.5 Hz and 42.5 Hz, respectively. In the case of the two-way spanning floors, the removal of support screw fixings reduced the natural frequency results by an average of 5%. Investigating the rotational stiffness of the floor supports of a 1000 mm wide 3-ply CLT panel showed an improved fundamental frequency and static deflection response with increased rotational support stiffness [14]. Alternative one-way spans were examined up to a 4500 mm span, with increased rotational stiffness of the support along with an added load on each support. The fundamental frequencies in each case measured between 9.4 Hz and 12.3 Hz, damping ratios ζ ranged between 0.51% and 1.96% for the same floor. The static deflections measured between 2.54 mm/kN and 3.32 mm/kN.

Hu and Gagnon [124], when developing the design equations for CLT floor spans that now form the basis of the US and Canadian CLT Handbook vibration criteria [70][71], conducted subjective and dynamic tests of laboratory CLT floors of different thicknesses. The floors were 230 mm, 182 mm, and 140 mm thick, each comprising of three 2000 mm wide panels. The floors were tested with the three panels connected in parallel using a half-lapped joint with vertical 8 mm diameter self-tapping screws at 320 mm spacing and alternatively using a top-joint, also known as a spline-joint. Pairs of 5 mm diameter self-tapping screws at 200 mm spacing through a continuous LVL top-strip represented the spline-joint. No significant difference was found for either panel-to-panel connection assembly with regard to the floors natural frequencies nor the static point load deflection results. The damping ratio ζ-values of the bare CLT floors consistently measured near 1%.

Before building the University of British Columbia’s 18 storey student residence, many experimental studies were made on the building design [39][40][41]. This included the bespoke CLT on glulam column floor support assembly [154]. The design comprised four corner, and two intermediate edge supports on circa 8000 mm x 3000 mm CLT floors. Dynamic and static tests were made on full size floor specimens with, and without openings. The dynamic tests comprised a roving impact hammer providing the excitation with a fixed accelerometer recording the response. Four-point loading tests were used to measure the bending and failure loads. The average fundamental frequency was found to be 17 Hz, which reduced to 15.8 Hz in the floors with openings.

Jarnerö [157][158] investigated the fundamental frequencies and damping ratio ζ values of a 3100 mm x 5100 mm intermediate floor of an eight storey residential timber-frame building. The floor consisted a CLT panel and glulam beam floor system, simply supported on four sides. The CLT deck consisted a 73 mm thick panel and the glulam beams were 276 mm deep. The floor was tested in-situ at different stages of construction and compared with a similar floor configuration in the laboratory, with, and without an elastic interlayer. The elastic interlayer generally improved damping performance from 2.2% to 3.1% for the first bending mode. The damping ratio ζ of the same floor in-situ improved two-fold to 6.5%. Integration of the floor in the building significantly influenced the damping behaviour of the floor. The fundamental frequency of the in-situ floor at all stages was greater than 21 Hz.

Smith and Chui suggested that neither the variation in the degree of end fixity of traditional timber joists nor the use of an elastomeric adhesives in lieu of low-density nailing would significantly influence the vibrational response of traditional floors [164], but studies in Graz on CLT floors [138] found that although elastomers alone did not significantly influence low natural frequencies, they lowered the clamping effect of a superimposed load, such as that from upper storeys. As increased rigidity of the floor support leads to higher natural frequencies and lower excitability [170], the benefit of increased support rigidity due to clamping might be negated [138]. It was observed that although added mass decreased the resonant frequency values, it also reduced the sensitivity to excitation and improved damping. It was concluded that non-load bearing intermediate walls add stiffness to floors, increasing the frequency values of the natural modes. However, the inclusion of the effect of these walls are not considered in the various design codes as they may be moved or removed completely at any stage of a buildings lifespan.

Zimmer and Augustin [138], in laboratory and in-situ CLT floor studies, also measured the rms acceleration of the floors. They recorded values between 0.6 m/s^2 and 0.8 m/s^2 in CLT floors without added mass, which reduced to values between 0.2 m/s^2 and 0.4 m/s^2 when a dead load was applied to the floors. The damping ratio ζ values of bare CLT floors improved from 0.5 % to 3.5 % when a person was present on the floor.

Casagrande et al. [132] tested two similar five-storey timber buildings. One building constructed with timber frame, the other building constructed using CLT floors and walls. The timber frame floors comprised 120 mm x 200 mm glulam beams at 580 mm spacing with a 50 mm concrete slab. The CLT floors comprised 153 mm five-ply panels. The CLT floors spanned 4200 mm and 3100 mm. The research, which also referred to preliminary studies [171][172], compared experimental results of in-situ floors and laboratory models of similar floors. A 5.5 kg impact hammer provided the impulse for the frequency tests. Higher frequency values were recorded in the case of the field tests for both floor types, the first two modes recorded on the glulam-concrete floor were 13.1 Hz, and 14.1 Hz in the laboratory compared with 23.3 Hz and 28.0 Hz in the case of the in-situ floors. There was a small variation observed when comparing the glulam-concrete with the CLT floors. The first two modes recorded on the CLT floors were 13.3 Hz and 15.7 Hz in the laboratory and 26.2 Hz and 29.1 Hz in the field tests. Damping ratios ζ measured in the laboratory ranged between 0.84% and 1.38%, generally lower in the case of the glulam-concrete floor. The in-situ damping ratios ζ were increased for both floors, ranging between 2.4% and 4.3%, with no clear trend favouring either building method. The variation between the laboratory results and those found on site was attributed to intermediary partition walls, which were not included in the laboratory model. A non-structural load was included in the laboratory dynamic test set-up. The added mass comprised 24 evenly distributed steel plates on both the glulam-concrete and CLT laboratory floors. In the case of the 158 mm x 2900 mm x 4200 mm laboratory CLT floor tested, it was simply supported with an evenly distributed non-structural added mass of 1.38 kN/m^2. A 1kN point load applied midspan resulted in a 0.11 mm deflection. A fundamental frequency of 13.3 Hz was recorded. The damping ratio ζ of the first mode was 0.95%. These values increased for the floor integrated into the building to frequency and damping values of 26.2 Hz and 3.5%, respectively. It was concluded that the shortest span which was defined by non-structural partitions determined the frequency and mode shapes of the in-situ floors. The acceleration from people walking was measured for both the laboratory and in-situ floors. No clear trend favoured either building method.

4.5 Finite element modelling approaches to timber

Finite element approaches that have been applied when modelling floors, timber-to-timber connections, and CLT assemblies is presented in following section.

Gasparri et al. [54] developed FE models of CLT panels in ANSYS using homogeneous solid elements. The timber material behaviour was assumed isotropic and non-linear. Hernández Maldonado and Chui’s [14] also used isotropic linear elastic material properties to examine the effect of support conditions on the vibrational performance of three-ply CLT panels. Meghlat et al.’s [173] FE examination of nailed and screwed timber connections and Sejkot and Ormarsson [174] timber beam-to-beam nailed bracket connection FE investigation represented timber beams with solid elements using orthotropic elastic material properties.

Jarnerö et al. [175][157] compared in-situ and laboratory modal tests on timber floors with FE modal analysis. The floors comprised prefabricated timber sections that consisted a three-ply CLT deck. The CLT panels were created using linear brick elements with reduced integration. The separate layers of the CLT panel were defined as orthotropic and linear elastic with full interaction between the layers. Pinned junctions represented the floor supports. Labonnote's [151][152] study on the damping of timber floors used linear shell elements for a timber floor deck with rigid tie constraints simulating the connections between all timber elements, therefore, the degrees-of-freedom in the rotational and translational directions were equal for adjacent surfaces.

Campbell et al.'s [159] study of the Sky gymnasium building compared experimental field and FE modal results of bare CLT floors using Arup Oasys GSA 8.7 FE software. The CLT panels were modelled using shell elements with alternative stiffness's attributed to each orthogonal layer. The floor supports were defined as pinned connections.

Glisovic and Stevanovic's [176] traditional timber joisted floor model also assumed all floor joists to be simply supported. Rinaldin et al., Gavric et al., Izzi et al. [177][178][179] and Casagrande et al. [172][132] modelled CLT panels as linear elastic shell elements with orthotropic layers when analysing the seismic behaviour of CLT construction. Mpidi Bita and Tannert's [55] FE study also defined CLT panel lamina using orthotropic elastic material properties and shell elements, each lamina oriented at 90°and uniformly and fully bonded along the width of the panel.

Bogensperger et al.'s [79] FE analysis compared the γ-method, the shear analogy method, and the Timoshenko transverse shear-flexible beam theory. The study contributed to the development of the CLT software design tool from Graz University, CLT Designer [67][68]. It was found that the computational cost of 3D models was not justified in their FE analysis of CLT panels, therefore 2D planer models in ABAQUS were developed. Orthotropic linear elastic material properties were used in accordance with GL24h [180].

Xu et al. [181] developed a subroutine to represent a history dependent nailed wood joints. The connections included stiffness and strength degradation and pinching. Investigating seismic loading of CLT construction, Rinaldin et al. [179] and Gavric et al. [178][182] modelled typical steel CLT connections using non-linear multi-spring elements with hysteretic behaviour. The springs were integrated in the ABAQUS model as external subroutines.

Considering the connection between parallel CLT panels, Hu and Gagnon's [124] study of laboratory multi-panel CLT floors found that the choice of connection assembly between parallel panels had little effect on the natural frequencies and the static point load deflection results. Ussher et al. [183] defined CLT panel-to-panel half-lap junctions with hinge joints that allowed rotation only along one axis, while Lewis et al. [184] represented CLT half-lap floor junctions using a matrix element connection of two nodes, defining the degrees-of freedom at each node separately.

Fernández Martínez et al.'s [139] study required the inclusion of non-structural added mass in their investigation of jumping load models on a concrete gymnasium floor. The floor was defined using shell elements. The density of the floor slab was increased locally to account for discrete masses on the floor at the applied jumping load positions, increasing the mesh density also.

4.6 Conclusions

From the literature, some recurring parameters that impact on the serviceability of timber floors were identified. A summary of the main issues noted with respect to CLT design are outlined below.

Support rigidity, elastomeric interlayers, building integration

It is well-established that the rotational stiffness of supports can significantly influence a beam or plate's static and dynamic response [96][97][185][170]. Hence, with respect to floor design the question arises as to what degree the rigidity of the support conditions is influenced by the fixing assembly method or the floors integration in a building. Weckendorf et al. [186] outlines the challenge of uncoupling the vibration influence of a floors substructure and the building generally with that of the floor. Weckendorf and Smith [167] when comparing timber and steel supports observed that greater stiffness in the support structure increased the frequency values of higher modes in timber floors.

Labonnote [152][151], compared glued and screwed, and glued and nailed connections of timber-joisted floors in the laboratory. The screwed floor was found to be stiffer. A marginally higher frequency result was recorded, however, the differences in the damping ratios ζ were negligible. It was asserted that there was a gap in the knowledge with regard to the dynamic influence of alternative connectors in timber floors and that accurate dynamic performance prediction required accurate numerical estimations of the fixing details.

Hernández Maldonado and Chui’s laboratory studies of the influence of the rotational stiffness of the supports of a 3-ply CLT floors [14] found that providing an additional load, and additional screw fixings along the supported edges increased the rotational stiffness of the floor supports. This resulted in an improved serviceability performance in the floor; increasing the fundamental frequency value and reducing the point load static deflection. Based on these experimental results, Zhang et al. [187] later developed analytical coefficients for the purpose of mass timber design, though it was observed, with regard to the test results outlined in [14], that the rotational stiffness alters with the span of the floor panel. It can be interpreted from this that the influence of fixings or load on the rotational stiffness of the floor is also influenced by the weight and span of the floor.

Ohlsson’s [13] recorded that in-situ floor serviceability performance improved with respect to all serviceability criteria tested, while Hamm et al. [137] suggested that the torsional spring influence due to loads applied by upper storey walls was a possible reason for anomalies between in-situ frequency measurements and the calculated design values.

Jarnerö’s dynamic study of a third storey floor in Växjö, Sweden [157][158] found varying degrees of influence due to the integration of the floor into the eight-storey building at different phases of construction. While changes were observed in the dynamic response over the duration of the construction period, the frequency values at completion were essentially equal for the first two modes compared with the initial results. The influence on higher modes was more pronounced. The parameter which was most affected due to the floor’s integration into the building was the damping ratio ζ. Its value generally increased, most significantly in the case of the second mode from 5.5% to 7.9%. The subtle differences observed in the frequency results by Jarnerö imply that although the different forces that can be expected on a floor and its supports may each affect its rotational stiffness, the disparate influences may be conflicting consequently negating any overall natural mode value change. A more concerted study on the individual dynamic effects of alternative floor and support variations would serve to establish the most optimum fixing choice with respect to serviceability criteria.

Smith and Chui's [164] investigation of lightweight timber floors recorded that neither the degree of end rigidity of the joists nor the use of elastomeric adhesives in lieu of low-density nailing significantly influenced the vibrational performance of the floors. Studies in Graz on CLT floors [138] concluded that although elastomers alone did not significantly influence low natural frequencies, they lowered the clamping effect of a superimposed load, such as from upper storeys. By reducing the clamping effect of the connection, the rigidity of the support was also reduced. Weckendorf and Smith [167] found a clamped support detail had a moderate influence on the fundamental frequency, more significant for higher modes, although the damping ratio of the first modes decreased in the case of the clamped fixing detail. Jarnerö [175] also attributed improved damping to an elastomer interlayer.

Two-way support and floor shape

Hamm et al.'s [137] recommends always incorporating into design calculations whether a floor is supported in two directions. Weckendorf's [130] laboratory investigation of various timber joisted floors found that where floors were supported on four sides, the mode separation is influenced by the overall width of the floor. Hu and Gagnon [124] agree that the whole stiffness of the floor, both longitudinally and laterally, influences its static deflection and acceleration amplitude response.

The findings imply that while the shortest span will dictate the fundamental frequency value, the stiffness and support in the alternative span direction can have notable impact on a floors overall serviceability behaviour. Weckendorf and Smith [167] identified that the direction of the floor support may greatly influence the interaction of the natural frequencies in CLT floors. Studies concluded that an efficient approach to numerically modelling of floors of various geometries is required to provide accurate prediction on floor serviceability [164].

Added mass and dynamic loading

It was observed by Zimmer and Augustine in Graz [138] that although added mass decreased the resonant frequency values, it also reduced the sensitivity to excitation and improved damping. Thus, where the fundamental frequency was not critical, added mass could be considered to have a positive effect. Casagrande et al. [132] found non-structural elements significantly influenced the dynamic behaviour of timber-concrete composite (TCC) and CLT floors. Ebadi et al. [131] measured an improvement in damping and static deflection results by introducing a non-structural concrete topping on laboratory glulam beam-and-deck floors. However, the topping decreased the fundamental frequencies values also. Smith and Chui [164] recommended investigating how typical objects in dwellings may impact on the perception of accelerations to a human observer.

It is accepted also that occupants, due to their mass or movement, affect the dynamic response of floors [168]. One person standing on a CLT floor was found to improve the damping ratios ζ by up to three times. The degree of influence varying depending on the position of the person on the floor and the mode shape examined, observing that annoying vibration is not confined to a floors centre (the maximum deflection of the fundamental mode of a rectangular floor) [167]. Studies on the dynamic mechanical interaction of crowds on structures found that groups of people reduced the structural response of vertical low-frequency dynamic behaviour [147]. People walking in comparison with people standing have been found to improve damping results, with the influence on the modal parameters of a structure increasing with increasing crowd size [122].

Additional transverse panels

There are few CLT floor layout designs that will only require one panel. Assessing the influence of multiple panels in CLT floor construction, Weckendorf and Smith's laboratory study of CLT floors [167] found that the influence of a second CLT plate on the floors overall fundamental frequency was small, but that the number of modes below 90 Hz was increased. This had the added negative effect of reducing the separation between adjacent natural mode values. Hu and Gagnon's [124] subjective and dynamic tests of laboratory multi-panel CLT floors found that the choice of connection between parallel panels had little effect on the natural frequencies and the static point load deflection results, while Hernández Maldonado and Chui's [169] study on the vibration response of single and multiple five-ply CLT floor panels recorded a negligible influence on the first and second natural frequencies comparing the single- and multiple-panel one-way spanning floors.

The studies suggest that that the type of fixing system applied to connect the panels in parallel does not strongly impact on the static or vibration response. Although multiple CLT panels connected in parallel generally did not influence the fundamental harmonic, the number of higher modes within the perceptible range of interest was increased, which consequently reduces a floor’s compliance with EC-5 [22] velocity criteria.

Ohlsson [13] concluded that accurate analysis of timber floors with respect to footfall loading requires consideration of natural modes higher than the fundamental frequency. Smith and Chui [164] recommended investigation of the transmission of vibrations in floors. Both parameters are highly dependent on the natural mode separation in floors, hence the influence of parallel connections of CLT panels is required in addition to appropriate and calibrated numerical modelling approaches to multi-panel CLT floors.

Non-load bearing intermediate walls

Jarnerö [158] concluded that it is the installation of partitions on a floor that most affects the frequency reponse. Casagrande et al.’s vibration studies of TCC and CLT in-situ and laboratory floors [132][172], asserted that in-situ intermediary partition walls greatly influence the natural frequency, their mode shapes, and damping ratio ζ-values. Hamm et al. [137] found that non-loadbearing internal walls positively influenced vibration behaviour in all cases. While Zimmer and Augustine [138] recorded that non-structural intermediate partitions added stiffness to floors hence increasing the natural frequency values. Numerous studies imply that all floor supports improve serviceability performance generally. However, internal non-structural walls are not considered in the various design codes as they may be moved or removed completely at any stage in a buildings lifespan. It could be argued, however, that in high density development, the floor layout is optimised to a degree that any significant reconfiguration is unlikely without a comprehensive design audit. While a spacious residence or large commercial or office space may undergo many renovations and refurbishments, therefore, making it foolhardy to rely on internal partitions in the design; in the case of a modest studio apartment, a hotel twin room, or standard student accommodation, the optimised floor area of these generic designs make it unlikely that the internal layout will be remodelled to any significant degree. Modal and static analysis to assess the implications on serviceability, particularly with respect to frequency and stiffness criteria of standard internal wall positions would provide a better prediction of the serviceability of such rooms. Consequently, better confidence of occupant’s satisfaction in accommodation of this type constructed with CLT.

Openings in the floor

Weckendorf et al. [186] found one of the challenges facing designers with respect to predicting timber floor vibration is the difficulty of simply representing perforations in a floor. Preliminary design investigations of UBC’s Brock Commons floor support assembly [154] found the average fundamental frequency was reduced in the floors with openings. Smith and Chui [164] recommended developing a straightforward approach to numerical modelling of the dynamic behaviour of floors that included floor voids.

Static stiffness criterion

Hamm et al. [137] asserted that the static stiffness criterion of a floor was deemed as important as the modal characteristics of a floor. It was recommended that the stiffness of a screed should be incorporated into design calculations. Jarnerö [157][158] found that the midspan point load deflection criterion best predicted occupants acceptance of the floor serviceability.

Numerical analysis approach

In the case of modal analysis of floors, 2D shell elements are generally considered cost efficient and appropriate. The density of the shell elements may be adjusted locally to simulate discrete non-structural loads. The orthogonal characteristics of timber is generally represented, therefore, the orientation of the lamiae is significant to the accuracy of the results in CLT analysis. It has been found that representing the layers uniformly fully bonded is also appropriate.

Where FE analysis of timber and timber junctions is concerned with ultimate limit design loads or seismic loads, the inclusion of the hysteretic behaviour of the timber and steel is warranted. The ductility or plasticity of each connection element and the slip behaviour of all the components is pertinent to the accurate representation of the junction. However, the displacements resulting from serviceability analysis are relatively small and can be defined as linear. An accurate representation of intermediate supports to floors is necessary to correctly predict the mode shape and frequency values of floors. Edge-to-edge junctions of plates may be defined with hinge connections that allow rotation only along one axis.

5 EXPERIMENTAL METHODS

5.1 Introduction

The preceding chapter outlined the established testing methods used in determining a structure’s serviceability response, focusing specifically on static and dynamic testing of floors. Notable results from various field and laboratory timber floor studies were summarised. In this chapter a laboratory and field CLT floor testing programme is presented. The study is focused on the vibration behaviour of CLT floors in response to the everyday activities of building occupants within the structural vibration frequency range of people’s perception.

As there may be a large disparity in cost and practical on-site assembly between alternative CLT assembly details, the laboratory study aims to assess the effect on dynamic behaviour of alternative connection design, examining many common variations of industry standard CLT floor-to-wall connection details. To ensure any variance measured is a consequence of the individual connection detail, the same CLT floor panel is used for each laboratory test configuration and the test procedure is replicated exactly for each fixing assembly. The sequence and spacing of the various fixing components were designed to minimise damage to the test CLT panels. The objective of field tests are to examine the influence of the number of panels connected in parallel and a floor’s integration in the building on the dynamic response of CLT floors.

The results of both the laboratory and field experimental data will serve to refine numerical models so an appropriate numerical approach to CLT serviceability performance may be developed.

5.2 Overview of experimental testing programme

A single-panel five-ply CLT floor panel supported on CLT rising walls was tested in the laboratory. Multiple panel five-ply CLT floors integrated into a three storey CLT building were studied in the field studies.

The laboratory testing programme considered:

- Alternative floor support orientation, spanning the CLT floor panel in one and two directions,
- CLT platform and balloon construction,
- Alternative screw fixing, including vertical and inclined screw pairs at variable spacing,
- Bracket only and alternative bracket-screw fixing assemblies at variable spacing,
- The inclusion of a resilient interlayer, and
- The influence of a non-structural added mass evenly distributed over the floor area.

The CLT panels and fixing components comprised standard industry units sized in accordance with residential, office, and school floor design loads [188]. The connection assemblies selected comprised platform and balloon construction details observed in mid-rise CLT building field studies, and that recommended from CLT construction experts. In some cases the test assembly configurations were modified with respect to screw spacing, following recommendations from a leading CLT fixing system provider to match similar CLT studies on acoustic performance [189]. The results of which have since been incorporated into their design manuals [190].

The laboratory testing programme incorporates the serviceability assessment guidelines outlined in prEN 16929:2015 [112] and alternative techniques (outlined in 4.2) that are appropriate to measure the vibration response of upper-storey timber floors. The testing programme was designed to assess key influencing parameters of floor serviceability performance. Namely, (i) a floor's flexural stiffness, determined by measuring the static 1 kN point load deflection, (ii) establishing low or high frequency floor, by measuring the fundamental frequency value of the floor, with sample time domain footfall excitation recorded to confirm transient or resonant excitation. The magnitude and duration of resonant vibrations are predicted by determining (iii) the natural frequencies and their mode shapes in the 0 to 80 Hz range, (iv) accelerance values of the natural modes, (v) and their damping ratio ζ values.

The field test programme measures parameters (i), (ii), including the natural modal frequencies of the floors below 80 Hz, examining the influence of the number of panels connected in parallel, and a floor's integration in the building on dynamic excitation of the floor. All test methods are non-destructive.

5.3 Laboratory CLT test assembly

5.3.1 CLT floor and wall panels

For the laboratory measurements a leading CLT manufacturer provided the CLT floor and wall panels. Their floor and ceiling panel sizes range between 60 mm to 320 mm thick 3-ply to 8-ply panels (comprising double-ply laminae in the principal span of the 8-ply panels), respectively, with standard 3-ply to 5-ply wall panel thickness' ranging from 57 mm to 158 mm. All panels are available in widths ranging from 2400 mm to 2950 mm, with a maximum panel length of 16500 mm. Vertical permanent and imposed loads of 60 kN/m are possible with standard wall sizes measuring up to 2950 mm high. A maximum imposed load of 5 kN/m^2 is recommended with floor and ceiling panels.

The standard panel dimensions have been updated since the time of testing, with 3-ply to 5-ply wall panel thickness' now ranging from 60 to 180 mm [191].

The floor geometry was chosen to be representative of typical CLT floor panels, while keeping the size and mass within the restrictions of the laboratory space and lifting apparatus available. Comparing design loads for residential, office, and school floors, a maximum imposed load of 3 kN/m^2 applies to school floors (Category C1: Table NA2. [188]). A 162 mm thick 5-ply floor panel of a lamella structure of 34, 30, 34, 30, 34 mm, with an effective stiffness of 3460 kNm^2, is appropriate to span 4000 mm at this load. Therefore, a 5-ply CLT floor panel measuring 162 mm x 2400 mm x 4000 mm was selected. The mass of the floor panels, the largest component of the test assembly, was estimated to be no greater than 778 Kg, just below the laboratory crane capacity of 800 Kg. The mass was subsequently measured to be 727.5 kg.

To investigate the influence of standard CLT floor to wall connection assemblies CLT support walls were required. As neither the test floor nor any loads resulting from testing would approach the capacity of standard CLT wall panels, a dimension width of 94 mm was selected as a representative size commonly used in mid-rise development. Four 94 mm 3-ply wall panels, with 34, 30, and 34 mm lamellas, were used to support the floor. The walls were 1200 mm high to accommodate access above and below the CLT floor. A 750 mm wide x 900 mm high opening in the longer support walls was provided to facilitate the mounting and access of testing apparatus during the two-way span testing, illustrated in Figure 5.1.

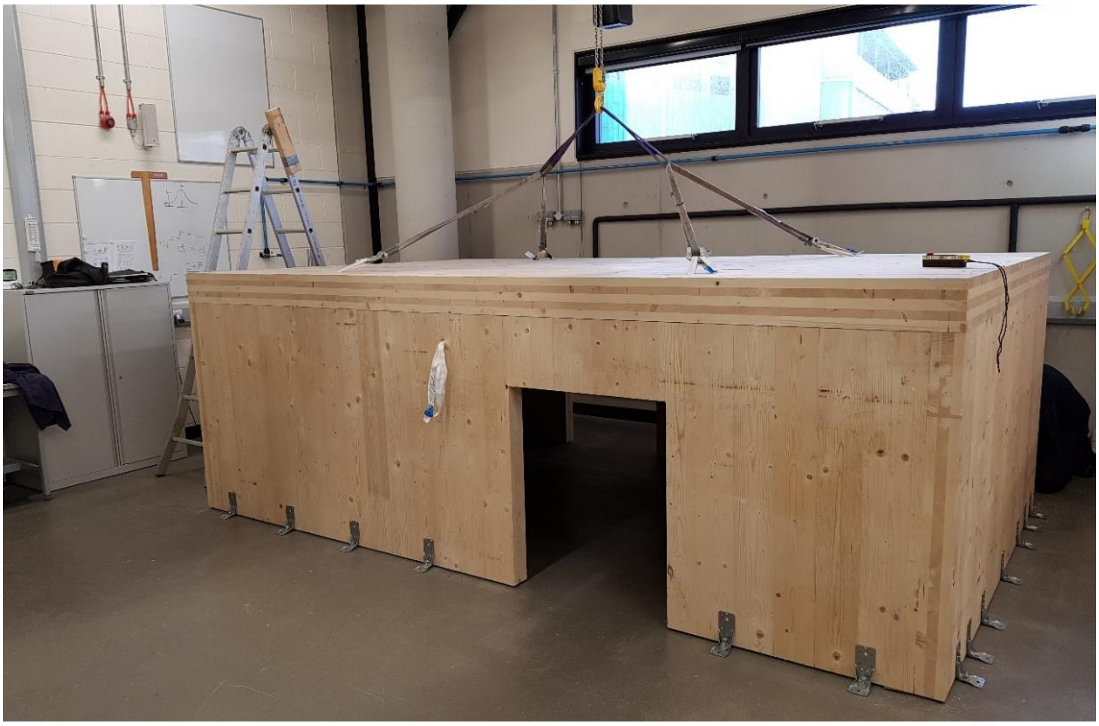

Figure 5.1 *Assembly of the two-way span platform construction @ NUI Galway*

5.3.2 Floor orientations

In all, sixteen variations of CLT floor construction were examined. They can be categorised into four groups:

- One-way long span platform construction
- One-way long span balloon construction
- One-way short span platform construction
- Two-way platform construction

One CLT floor panel was used for all the laboratory testing, without modification. The support walls were moved as necessary. The longest span measured was 4000 mm.

Figures 5.2 to 5.5 illustrate the orientations of the panels for each of the four categories.

Figure 5.6 shows balloon construction in the NUI Galway laboratory during assembly.

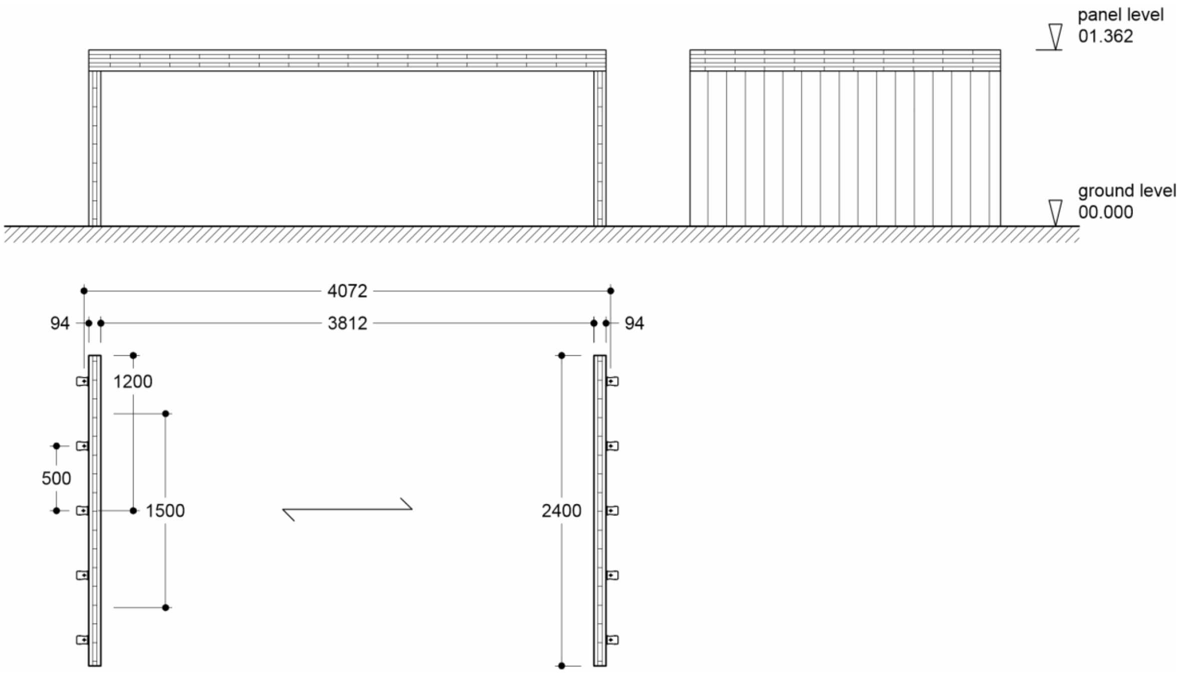
panel level
01.362
ground level
00.000
4072
94
3812
94
1200
500
1500
2400

Figure 5.2 *One-way long span platform construction (3812 mm span)*

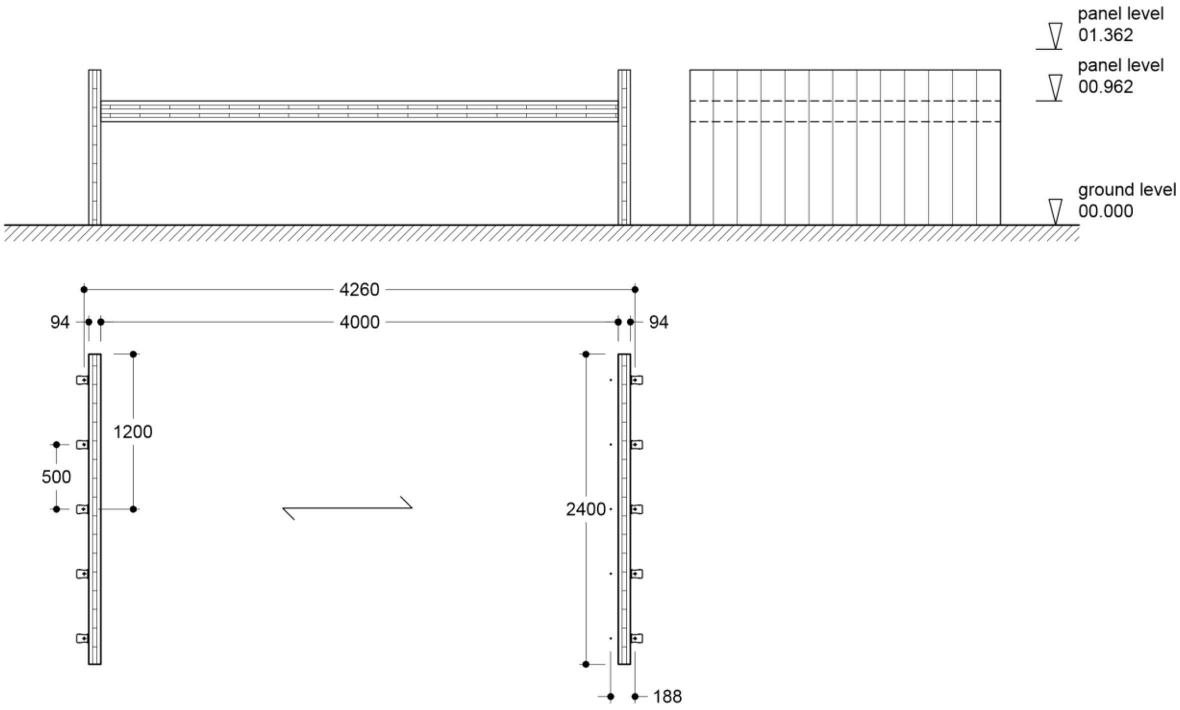
panel level
01.362
panel level
00.962
ground level
00.000
4260
94
4000
94
1200
500
2400
188

Figure 5.3 *One-way long span balloon construction (4000 mm span)*

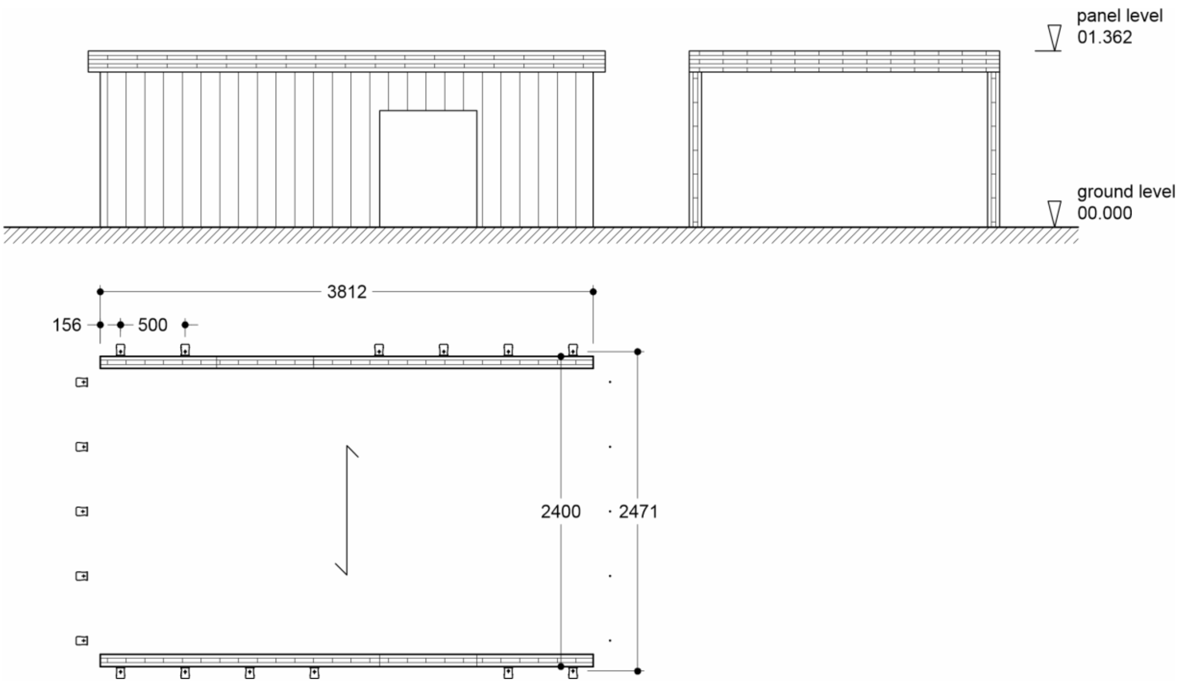
panel level
01.362
ground level
00.000
3812
156
500
2400
2471

Figure 5.4 *One-way short span platform construction (2212 mm span)*

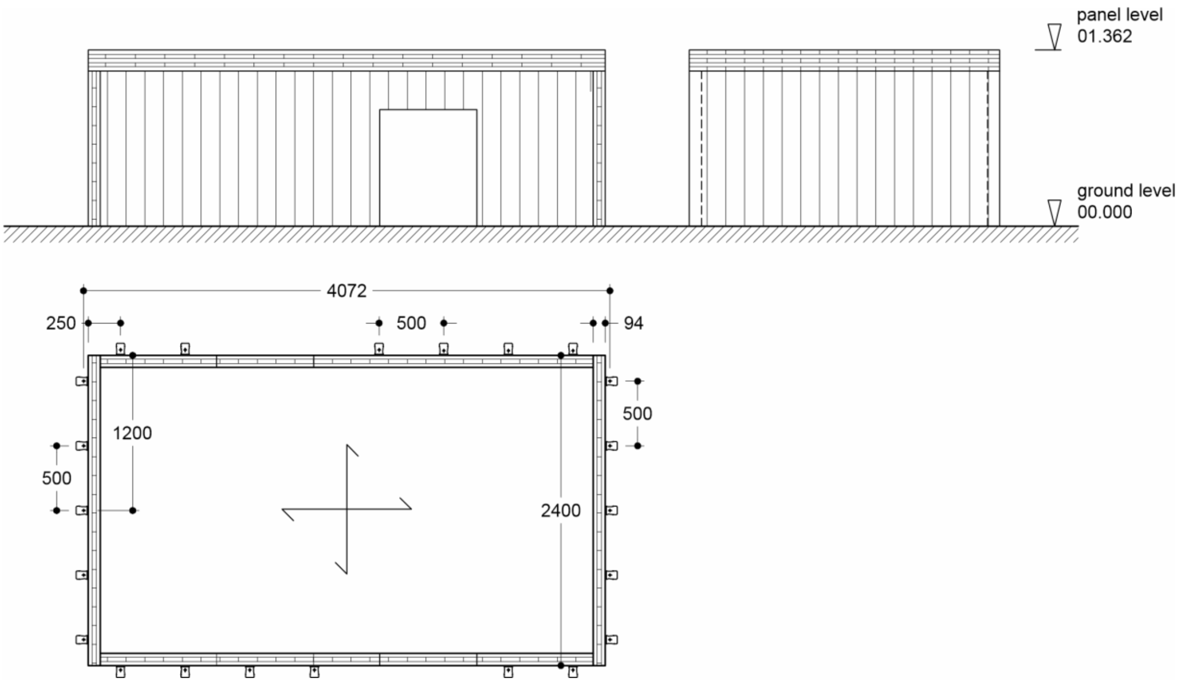
panel level
01.362
ground level
00.000
4072
250
500
94
500
1200
500
2400

Figure 5.5 *Two-way spanning platform construction (3812, 2212 mm span)*

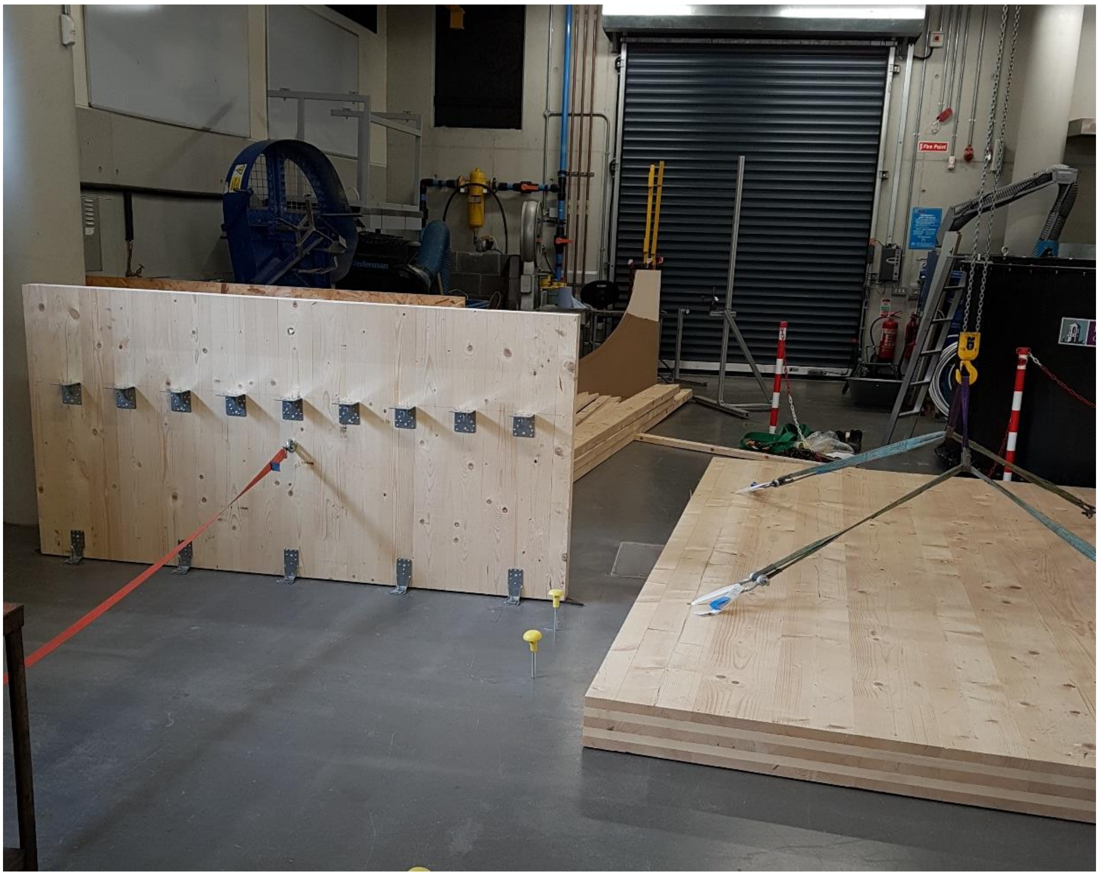

Figure 5.6 *Erection of one-way span balloon construction @ NUI, Galway*

5.3.3 Laboratory test assembly

All the brackets, screws, and the separating interlayer were provided by Rothoblaas srl. [190]. Hold-down brackets connected the CLT support walls to the laboratory floor (Figures 5.7 and 5.8), while various combinations of screws and brackets were used to connect the CLT floor to the CLT support walls (Figures 5.9 to 5.17).

5.3.4 Bracket and screw schedule

The CLT support walls were fixed to the concrete laboratory floor using the following anchors, brackets, and screws:

	Product Ref.	
• Reinforced hold-down angle brackets	WKR	13530
• Ø 5 x 50 mm round-head (LBS) screws	PF	603550
• M12 threaded steel rods with washers and nuts		
• Epoxy chemical anchor	EPOPLUS	

The fixing assembly is detailed in Figures 5.7 and 5.8.

The brackets and screws used in the alternative CLT floor-to-wall fixing assemblies (Figures 5.9 to 5.17) tested comprised:

• Ø 8 x 260 mm washer-head partially threaded screws	TBS	8260
• Ø 9 x 200 mm cylindrical-head fully threaded screws	VGZ	9200
• Ø 9 x 400 mm cylindrical-head fully threaded screws	VGZ	9400
• Titan shear-angle brackets	TTN	240
• Reinforced angle brackets	WBR	100
• Ø 5 x 50 mm screws	PF	603550
• Separating interlayer XYLOFON 35 (100 x 6 mm)	XYL	35100
• Ø 5 x 50 mm round-head (LBS) screws	PF	603550

5.3.5 CLT support walls to concrete floor

The use of base connectors spaced at 300 mm to 500 mm centres is the conventional hold-down detail for multi-storey mid-rise development. These are designed to transfer shear loads and uplift forces. The stiffening flanges to the brackets transfer uplift without increasing the load on the anchor [92]. A minimum 10 mm gap is maintained between the wall panels and the concrete floor. This gap accommodates any level variation in the concrete floor slab and facilitates waterproofing and structural grout between the concrete ground floor and timber panels. Figure 5.7 shows this detail applied in practice. Figure 5.8 details the laboratory CLT wall-to-concrete floor connection.

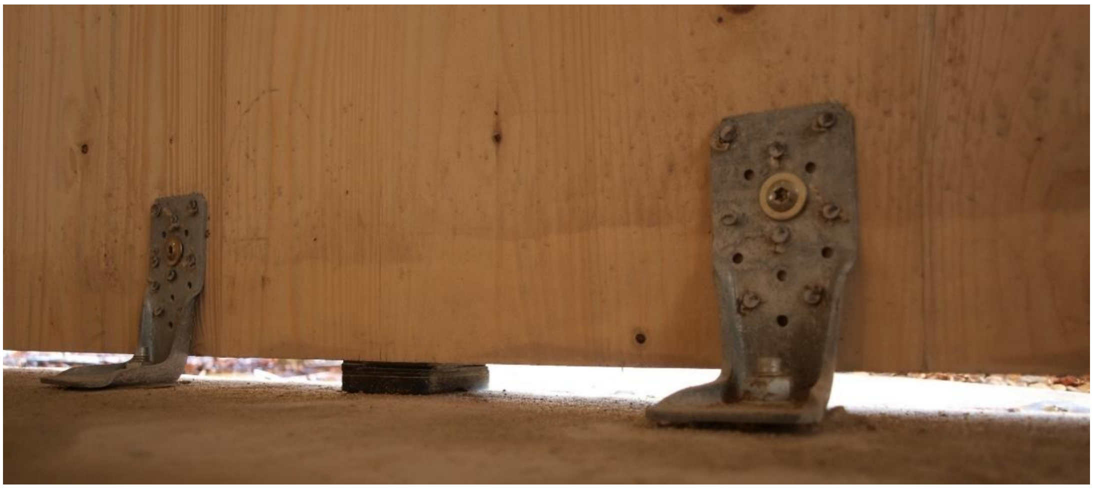

Figure 5.7 *Hold-down brackets in-situ, Bishop's Stortford, UK. A 10 mm gap is maintained between concrete ground floor and vertical timber wall panel.*

The laboratory CLT wall panels were fixed to the concrete laboratory floor using reinforced hold-down angle brackets (WKR 13530) at 500 mm spacing. This fixing arrangement can be regarded as conservative. The total expected load on the brackets, including the test assembly and equipment with three operatives is calculated as less than 1500 kg. The brackets were fixed to the floor using M12 threaded rods secured into 14 mm diameter pre-bored holes with an epoxy chemical anchor. The brackets were fixed to the rising walls using 5 mm x 50 mm diameter round-head screws (PF 603550), detailed in Figure 5.8. Three 5 mm diameter screws per bracket were calculated as sufficient for the applied loads, however a minimum of seven screws per bracket were used to better replicate field conditions.

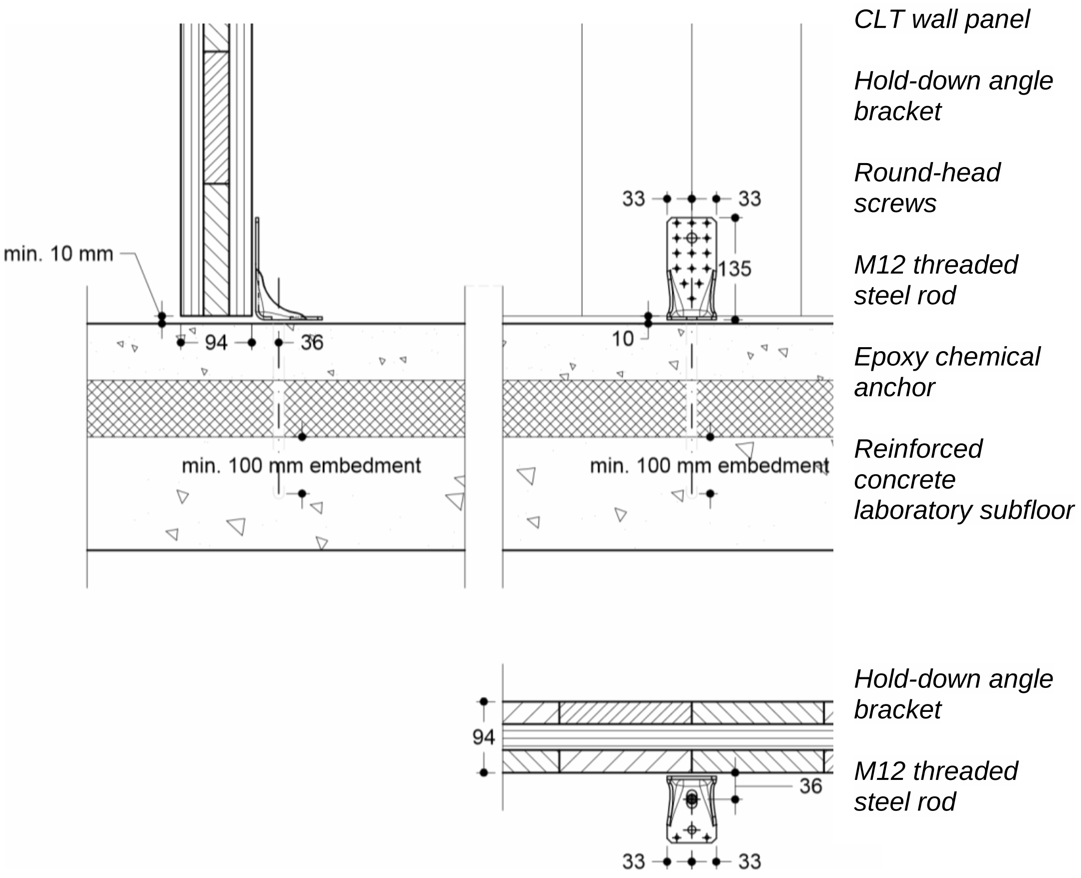
CLT wall panel
Hold-down angle bracket
Round-head screws
M12 threaded steel rod
Epoxy chemical anchor
Reinforced concrete laboratory subfloor
min. 10 mm
94
36
10
33
33
135
min. 100 mm embedment
min. 100 mm embedment
Hold-down angle bracket
M12 threaded steel rod
94
36
33
33

Figure 5.8 *Hold-down brackets fixed to concrete laboratory floor @ 500 mm c/c with epoxy chemical anchor, min. 100 mm embedment in the structural floor slab.*

5.3.6 CLT floor to CLT wall assembly

In the case of one-way long span platform construction, eight assembly variations were tested as detailed in Table 5.1, Figures 5.9 to 5.13. The test assemblies compare alternative spacing of vertical partially threaded washer-head screws (TBS 8260), the influence of adding alternative angle brackets types (TTN 240, WBR 100) at different centres, and assemblies comprising inclined pairs of fully threaded cylindrical-head screws (VGZ 9200).
Two examples of one-way long span balloon construction included, an assembly using inclined pairs of fully-threaded cylindrical-head screws (VGZ 9200) and an assembly with reinforced angle brackets (WBR 100). The assemblies are charted in Table 5.2 and Figures 5.14 and 5.15.

For the one-way short span platform construction, alternative spacing of partially threaded washer-head screws (TBS 8260), and shear-stress brackets (TTN 240) at different spacing were compared (Table 5.3).

Cross bracing for all one-way spanning assemblies was provided so that any lateral movement could be discounted in results. Dial gauges were placed on each supporting wall to monitor any horizontal displacement. Table 5.4 outlines the tested two-way platform construction configuration using vertical partially threaded washer-head screws (TBS 8260).

Additionally, one connection configuration examined the influence of introducing a resilient interlayer (Assembly C, Table 5.1), while the effect of an evenly distributed added mass was explored in four floor assemblies (Assemblies D, K, and O, Tables 5.1, 5.2, and 5.3).

The alternative CLT floor-to-wall fixing assemblies tested are outlined in Tables 5.1 to 5.4 and Figures 5.9 to 5.17.

An overview of the laboratory test schedule is outlined in Table 5.5.

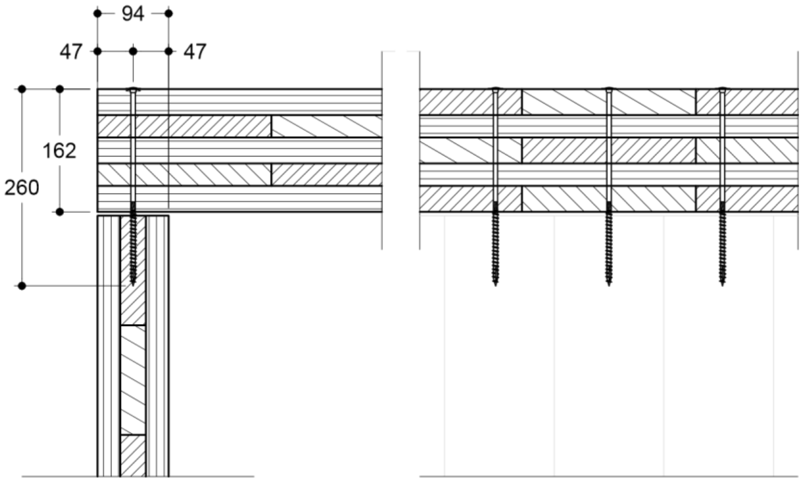

162 mm CLT floor panel
Ø 8 x 260 mm partially threaded washer-head vertical screws @ 150 mm c/c
94 mm CLT wall panel

Section **Elevation**

Figure 5.9 *Platform construction partially threaded vertical screws @ 150 mm c/c*

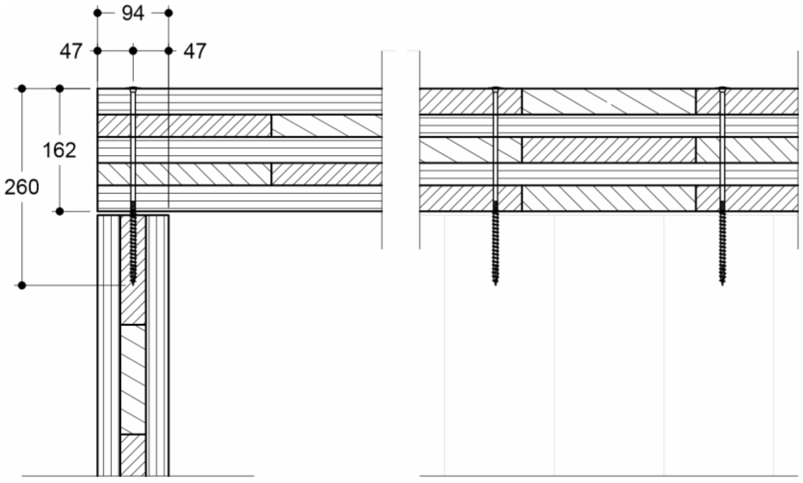

162 mm CLT floor panel
Ø 8 x 260 mm partially threaded washer-head vertical screws @ 300 mm c/c
94 mm CLT wall panel

Section **Elevation**

Figure 5.10 *Platform construction partially threaded vertical screws @ 300 mm c/c*

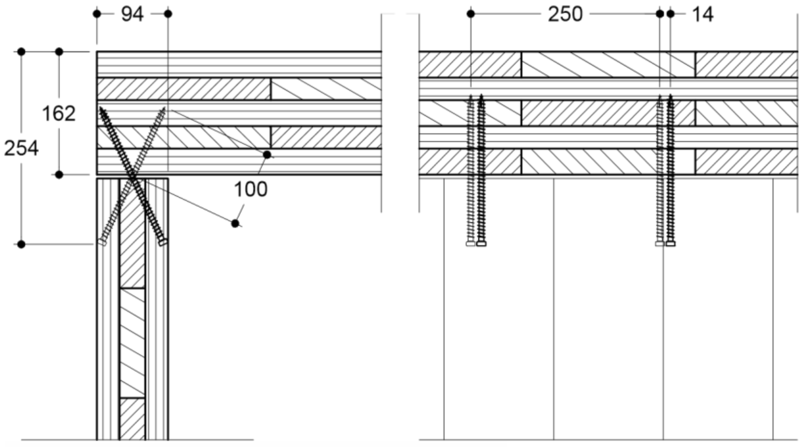

162 mm CLT floor panel
Ø 9 x 200 mm fully threaded cylindrical-head inclined screw pairs @ 250 c/c
14 mm clear between screws
94 mm CLT wall panel

Section **Elevation**

Figure 5.11 *Platform construction fully threaded inclined screws, 250 mm c/c*

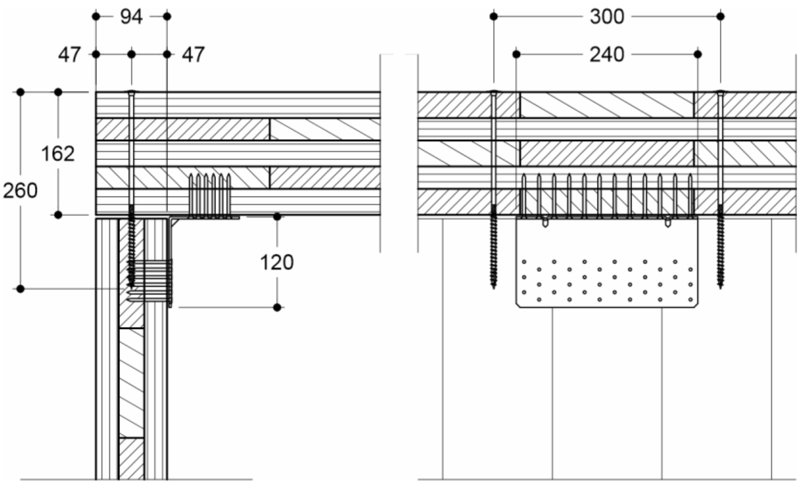

162 mm CLT floor panel
Ø 8 x 260 mm partially threaded washer-head vertical screws @ 300 mm c/c
240 x 93 x 120 mm angle shear-stress brackets @ 800 mm c/c
94 mm CLT wall panel

Section **Elevation**

Figure 5.12 *Platform construction with partially threaded vertical screws @ 300 mm c/c with shear-stress brackets*

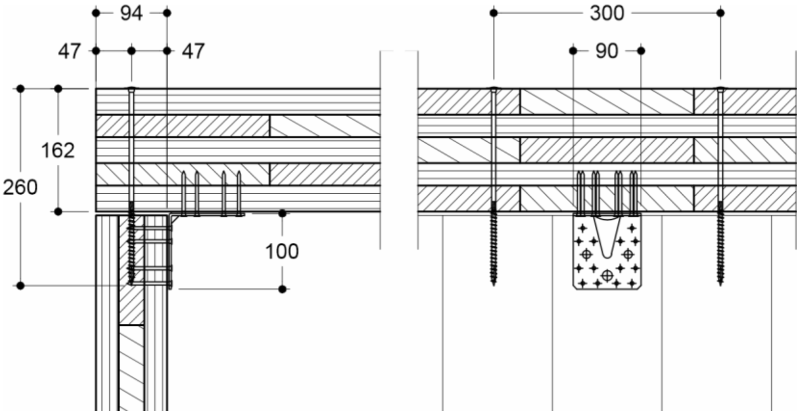

162 mm CLT floor panel
Ø 8 x 260 mm partially threaded washer-head vertical screws @ 300 mm c/c
100 x 100 x 90 mm reinforced angle brackets @ 800 mm (G), 200 mm (H) c/c
94 mm CLT wall panel

Section **Elevation**

Figure 5.13 *Platform construction with partially threaded vertical screws @ 300 mm c/c with reinforced angle brackets*

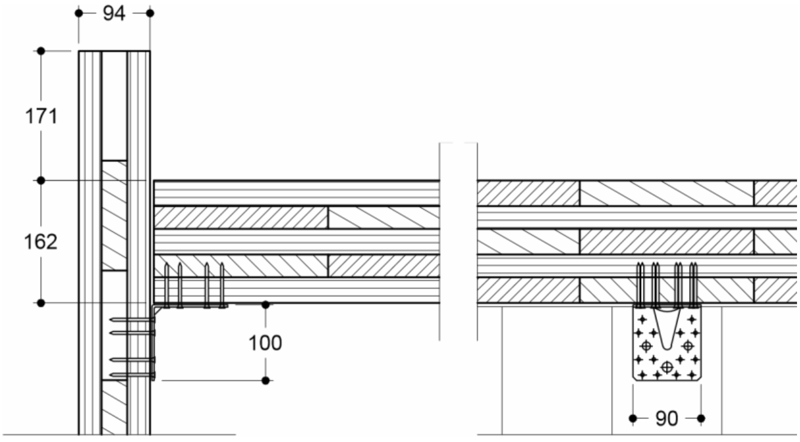

94 mm CLT wall panel
162 mm CLT floor panel
100 x 100 x 90 mm reinforced angle brackets @ 250 mm c/c

Section **Elevation**

Figure 5.14 *Balloon construction with reinforced angle brackets @ 250 mm c/c*

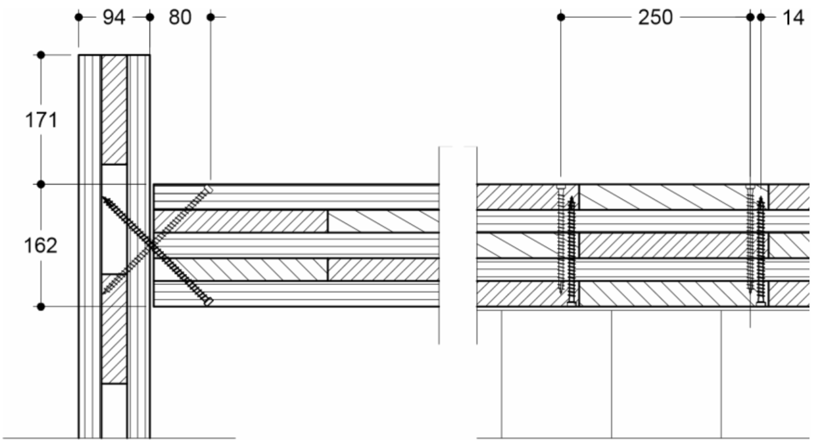

94 mm CLT wall panel
162 mm CLT floor panel

Ø 9 x 200 mm fully threaded cylindrical-head inclined screw pairs @ 250 c/c
14 mm clear between screws

Section **Elevation**

Figure 5.15 *Balloon construction with inclined screws, 250 mm c/c*

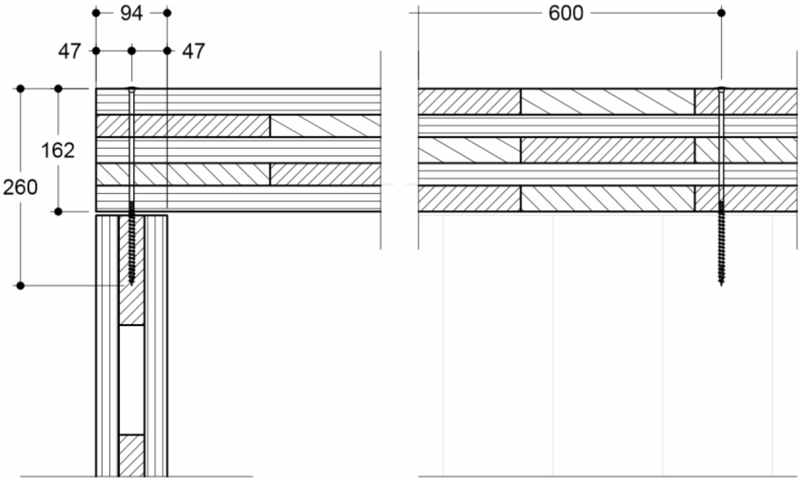

162 mm CLT floor panel
Ø 8 x 260 mm partially threaded washer-head vertical screws @ 600 mm c/c

94 mm CLT wall panel

Section **Elevation**

Figure 5.16 *Platform construction partially threaded vertical screws @ 600 mm c/c*

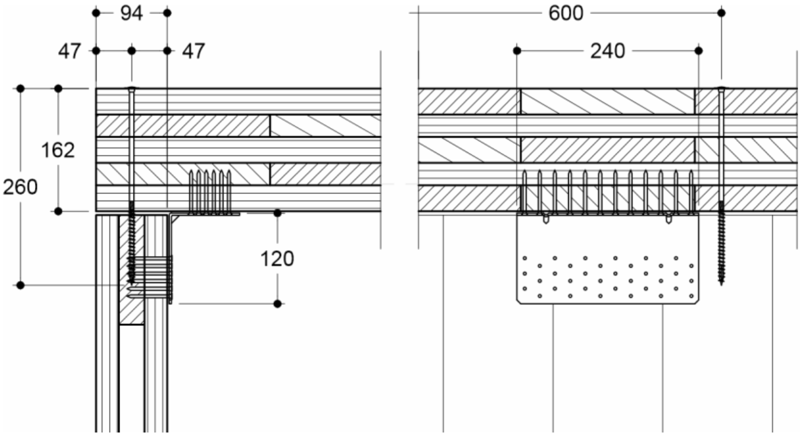

162 mm CLT floor panel
Ø 8 x 260 mm partially threaded washer-head vertical screws @ 600 mm c/c
240 x 93 x 120 mm angle shear-stress brackets @ 800 mm c/c
94 mm CLT wall panel

Section **Elevation**

Figure 5.17 *Platform construction partially threaded vertical screws @ 600 mm c/c and shear-stress brackets*

Table 5.1 *One-way long span platform construction: Assemblies A-H*

Assembly	*Screw fixing*	*Bracket fixing*	*Added load*	*Resilient interlayer*
A	*Ø 8 x 260 mm partially threaded washer-head vertical screws (TBS 8260)* *Spacing @ 150 mm c/c* ***Figure 5.9***			
B	*Ø 8 x 260 mm partially threaded washer-head vertical screws (TBS 8260)* *Spacing @ 300 mm c/c* ***Figure 5.10***			
C	*Ø 8 x 260 mm partially threaded washer-head vertical screws (TBS 8260)* *Spacing @ 300 mm c/c* ***Figure 5.10***			•
D	*Ø 8 x 260 partially threaded washer-head vertical screws (TBS 8260)* *Spacing @ 300 mm c/c* ***Figure 5.10***		•	
E	*Ø 9 x 200 mm fully threaded cylindrical-head inclined screws (VGZ 9200)* *Spacing @ 250 mm c/c* ***Figure 5.11***			
F	*Ø 8 x 260 mm partially threaded washer-head vertical screws (TBS 8260)* *Spacing @ 300 mm c/c* ***Figure 5.12***	*240 x 93 x 120 mm shear-stress bracket (TTN 240)* *Spacing @ 800 mm c/c* *Ø 5 x 50 mm screws* *2 x 36 no. per bracket*		
G	*Ø 8 x 260 mm partially threaded washer-head vertical screws (TBS 8260)* *Spacing @ 300 mm c/c* ***Figure 5.13***	*100 x 100 x 90 mm angle bracket (WBR100)* *Spacing @ 800 mm c/c* *Ø 5 x 50 mm screws* *2 x 7 no. per bracket*		
H	*Ø 8 x 260 mm partially threaded washer-head vertical screws (TBS 8260)* *Spacing @ 300 mm c/c* ***Figure 5.13***	*100 x 100 x 90 mm angle bracket (WBR100)* *Spacing @ 200 mm c/c* *Ø 5 x 50 mm screws* *2 x 7 no. per bracket*		

Table 5.2 *One-way long span balloon construction: Assemblies I-K*

Assembly	*Screw fixing*	*Bracket fixing*	*Added load*	*Resilient interlayer*
I	***Figure 5.14***	*100 x 100 x 90 mm (WBR100) angle bracket* *Spacing @ 250 mm c/c* *Ø 5 x 50 mm LBS screws 2 x 7 no. per bracket*		
J	*Ø 9 x 200 mm fully threaded cylindrical-head inclined screws pairs (VGZ 9200)* *Spacing @ 250 mm c/c* ***Figure 5.15***			
K	*Ø 9 x 200 mm fully threaded cylindrical-head inclined screws pairs (VGZ 9200)* *Spacing @ 250 mm c/c* ***Figure 5.15***		●	

Table 5.3 *One-way short span platform construction: Assemblies L-O*

Assembly	*Screw fixing*	*Bracket fixing*	*Added load*	*Resilient interlayer*
L	*Ø 8 x 260 mm partially threaded washer-head vertical screws (TBS 8260)* *Spacing @ 300 mm c/c* ***Figure 5.9***			
M	*Ø 8 x 260 mm partially threaded washer-head vertical screws (TBS 8260)* *Spacing @ 600 mm c/c* ***Figure 5.16***			
N	*Ø 8 x 260 mm partially threaded washer-head vertical screws (TBS 8260)* *Spacing @ 600 mm c/c* ***Figure 5.17***	*240 x 93 x 120 mm shear-stress bracket (TTN 240)* *Spacing @ 800 mm c/c* *Ø 5 x 50 mm screws 2 x 36 no. per bracket*		
O	*Ø 8 x 260 mm partially threaded washer-head vertical screws (TBS 8260)* *Spacing @ 600 mm c/c* ***Figure 5.17***	*240 x 93 x 120 mm shear-stress bracket (TTN 240)* *Spacing @ 800 mm c/c* *Ø 5 x 50 mm screws 2 x 36 no. per bracket*	●	

Table 5.4 *Two-way platform construction: Assembly P*

Assembly	*Screw fixing*	*Bracket fixing*	*Added load*	*Resilient interlayer*
P	*Ø 8 x 260 mm partially threaded washer-head vertical screws (TBS 8260)* *Spacing @ 300 mm c/c* ***Figure 5.9***			

Resilient interlayer

The effect of introducing a resilient interlayer was studied. The 100 mm x 6 mm XYLOFON 35 separating layer in roll form and during the construction of Assembly C (Table 5.1) applied to the top of the supporting wall are shown in Figures 5.18 and 5.19, respectively.

XYLOFON35
100x6x3,66
XYLOFON35
100x6x3,66

Figure 5.18 *XYLOFON 35*

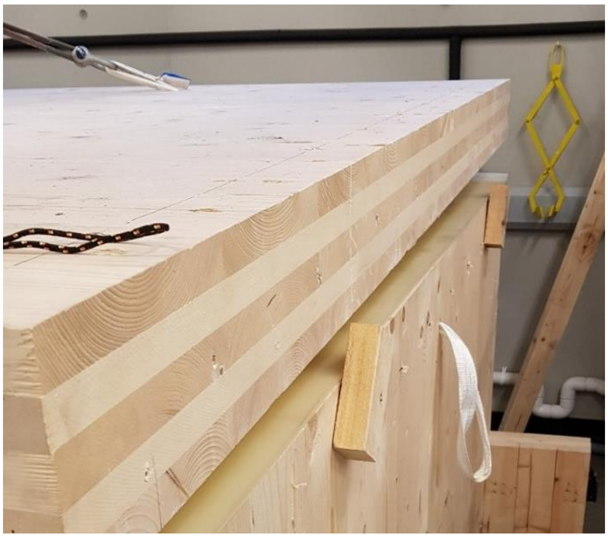

Figure 5.19 *Assembly C during construction*

Added mass

An evenly distributed mass was applied to floor Assemblies D, K, and O. The masses consisted 49 loads, each averaging 12.45 kg distributed on a 500 mm x 300 mm grid over the area of the floor. The distribution of the loads are illustrated in Figure 5.20.

Each mass comprised a 150 mm diameter x 300 mm cylindrical load. The total added mass was 610 kg, which was representative of un-bonded dry liquid non-structural screed, of density 2050 kg/m^3 over the area of the floor [192]. Assembly D is illustrated in Figure 5.21.

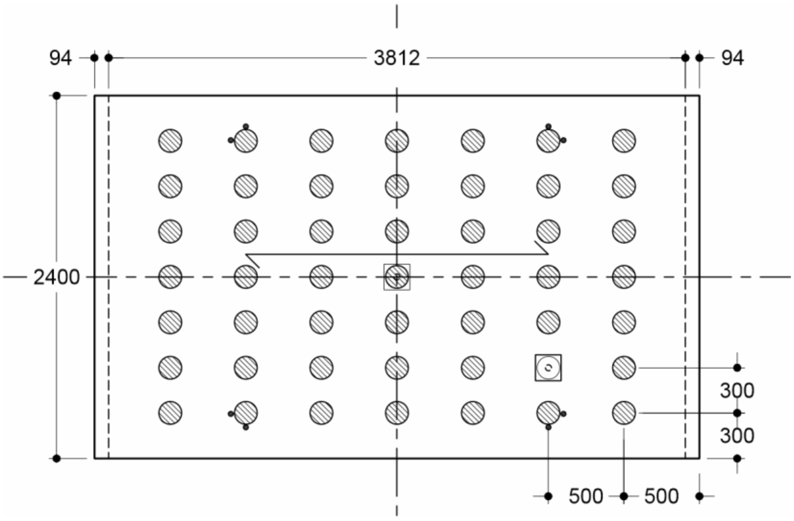
94
3812
94
2400
300
300
500
500

Figure 5.20 *Applied mass on a 500 mm x 300 mm grid*

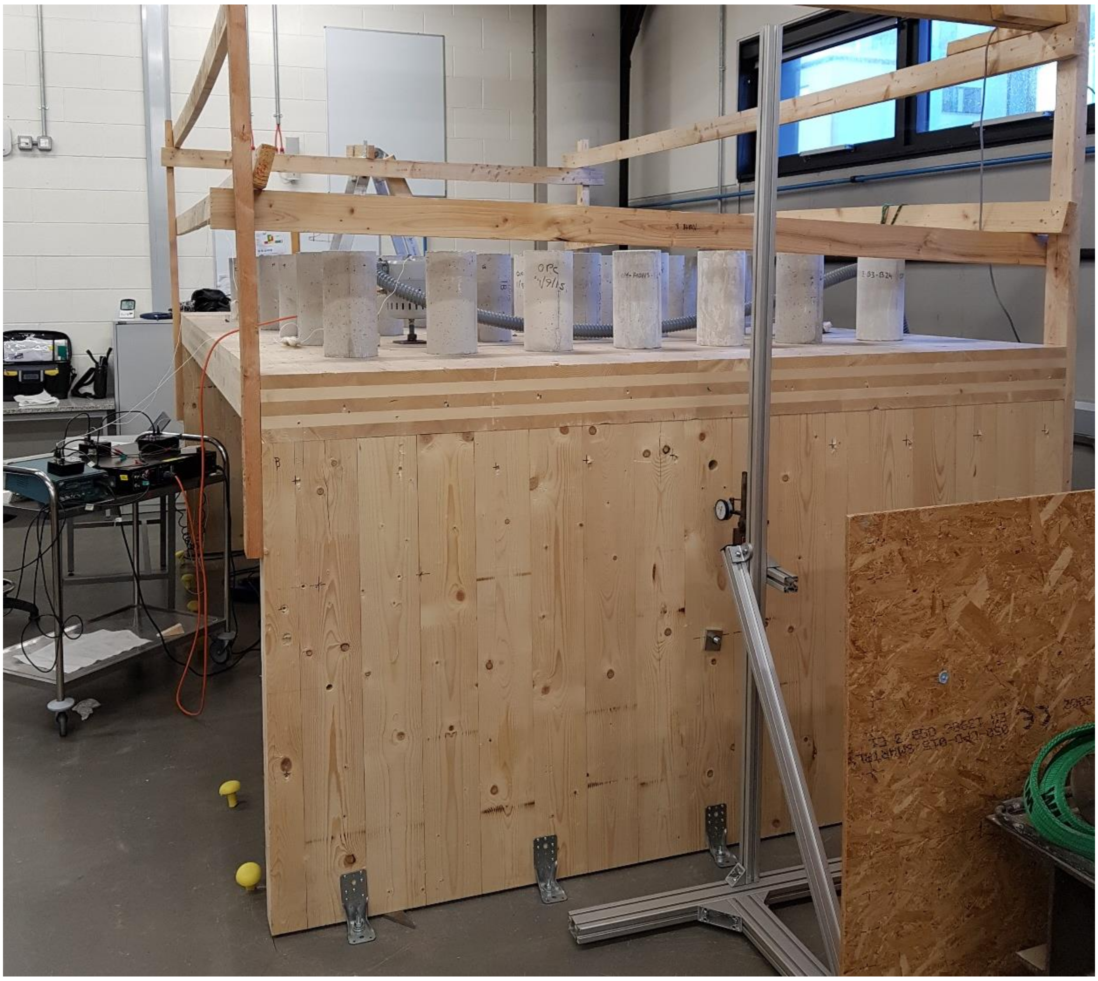

Figure 5.21 *Long span platform construction dynamic testing with evenly distributed added mass, Assembly D*

Safe access during testing

As testing required working at a height, statutory Health and Safety regulations necessitated safe access and egress from the floor. Any raised working area required a suitable handrail and balustrade or fall arrest system [193]. The guarding to waist height, which can be observed in Figures 5.21, (and later in Figures 5.23, 5.28, and 5.30), was erected in accordance with the Code of Practice: Access and working on scaffolds, guidelines [194]. Access below the floor panel during testing was provided by a 750 mm x 900 mm wide opening incorporated in both longer support wall panels, shown in Figure 5.1.

5.4 Laboratory testing programme

The span, width, and depth of the CLT floor was measured to an accuracy of 1 mm in accordance with prEN 16929:2015 [112]. An average of three measurements of the floor panel thickness taken 150 mm from the floor edge, determined the floors depth. The floor’s moisture content was measured with a moisture meter in accordance with EN 13183-2 [162]. The floor mass was measured to an accuracy 0.1 kg using a dedicated scales suspended from the overhead crane.

5.4.1 Environmental conditions

The room’s temperature and relative humidity were recorded at the time of each test.

5.4.2 Overview of testing

Testing included static and dynamic measurements of each of the sixteen floor assemblies, A to P outlined in Tables 5.1 to 5.4. Each test was repeated a minimum of three times and the average was taken as the test result.

Table 5.5 summarises the alternative floor-span orientations and different floor-to-wall connection assemblies that were considered.

Table 5.5 *Laboratory testing schedule*

Laboratory test floor *162 mm x 2400 mm x 4000 mm five-ply CLT floor panel of mass 727.5 kg*	
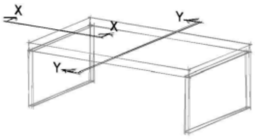	*One-way long span platform construction: Assemblies A-H*
*Vertical screws @ **150** mm c/c*	*Assembly A*
*Vertical screws @ **300** mm c/c*	*Assembly B*
*With **resilient interlayer***	*Assembly C*
*With added **mass***	*Assembly D*
***Inclined** screw pairs @ **250** mm c/c*	*Assembly E*
Vertical screws @ 300 mm c/c ***Shear** brackets @ **800** mm c/c*	*Assembly F*
Vertical screws @ 300 mm c/c ***Angle** brackets @ **800** mm c/c*	*Assembly G*
Vertical screws @ 300 mm c/c ***Angle** brackets @ **200** mm c/c*	*Assembly H*
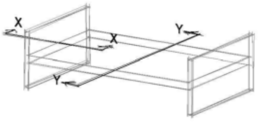	*One-way long span balloon construction: Assemblies I-K*
***Angle** brackets @ **250** mm c/c*	*Assembly I*
***Inclined** screw pairs @ **250** mm c/c*	*Assembly J*
*With added **mass***	*Assembly K*
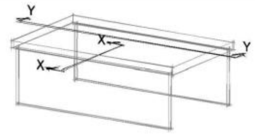	*One-way short span platform construction: Assemblies L-O*
*Vertical screws @ **300** mm c/c*	*Assembly L*
*Vertical screws @ **600** mm c/c*	*Assembly M*
Vertical screws @ 600 mm c/c ***Shear** brackets @ **800** mm c/c*	*Assembly N*
*With added **mass***	*Assembly O*
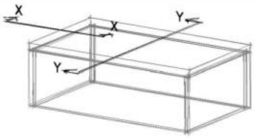	*Two-way span platform construction: Assembly P*
*Vertical screws @ **300** mm c/c*	*Assembly P*

Testing comprised applying the current European guidelines, prEN 16929:2015 [112], which provide procedures to measure the static point load deflection, determining the fundamental frequency due to an impulse, damping ratio and vibration acceleration amplification measurement as summarised in Section 4.3. Additionally, SISO modal testing was used to measure the dynamic response using roving transducers on a predetermined grid. An electromagnetic shaker fixed to the floor provided a dynamic force, as described in Section 4.2.4. The SISO testing allowed the mode shapes of the floor for each floor support configuration to be mapped (Section 4.2.5). Only the modes considered to be within the range of human perception were measured (0 to 80 Hz). Mapping the mode shapes permitted measurement of the resonant vibration amplification and damping ratio ζ at the points of maximum acceleration for each mode.

5.4.3 Apparatus

Static measurement

The static point load deflections were measured with:

- 3 no. Mitutoyo MT2119S-10 dial gauges of range 5 mm, revolution 0.2 mm, and graduation 0.001 mm
- 10 no. 1 kg steel masses
- 1 no. 100 mm x 100 mm load pad, in accordance with prEN 16929:2015 [112]
- An overhead crane, with detachable scales.

Dynamic analysis

The impulse and modal testing equipment included:

- Tektronix AFG 1000 signal generator, Sine waveform range: 1 µHz–60 MHz
- Electrodynamic shaker TIRA S 51125-IN, frequency range: 2-2 kHz
- Amplifier TIRA BAA 500
- Cooling blower TIRA TB 0080
- DAQ NI USB-6009
- 1 no. LIVM accelerometer, Dytran model 3055B2, sensitivity 104.34 mV/g

- 2 no. LIVM accelerometers, Dytran model 3100D24, sensitivity's 1002.27 mV/g and 1026.97 mV/g with relative transverse sensitivity less than 3 %, frequency range 0.6 to 1 kHz, and nonlinearity of ± 1 dB
- 2 no. Battery powered single channel IEPE supply, with gain, model 4105C
- 1 no. Battery powered three channel IEPE supply, unity gain, model 4103C
- 2 kg Ø 300 mm rubber ball

Figure 5.22 illustrates the modal test set-up assembly. The signals were recorded and analysed with a programme developed using NI LabVIEW 2014 software.

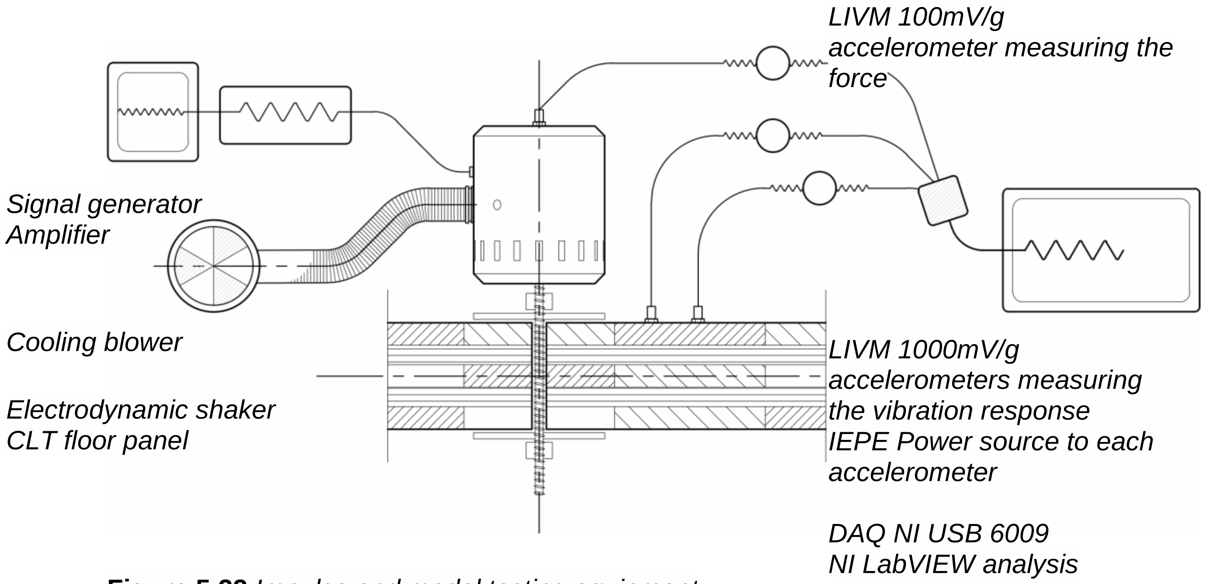
LIVM 100mV/g accelerometer measuring the force
Signal generator
Amplifier
Cooling blower
Electrodynamic shaker
CLT floor panel
LIVM 1000mV/g accelerometers measuring the vibration response
IEPE Power source to each accelerometer
DAQ NI USB 6009
NI LabVIEW analysis

Figure 5.22 *Impulse and modal testing equipment*

5.4.4 Deflection measurement

For each assembly the static point load deflection was determined by applying a concentrated dead load to the position on a floor where the largest deformations were expected and recording the deflection. Using an overhead crane, ten 10 kg steel masses were mounted on a 100 mm x 100 mm load pad positioned midspan on the floor. Deflections were measured directly below the applied masses on the floor soffit with a dial gauge. The test set-up is outlined in Figure 5.23.

The dial gauge was removed completely between each re-assembly of the alternative fixing configurations (Assemblies A to P: Table 5.5) and then re-positioned to the floor soffit midspan and re-zeroed for each test. This was also the case for Assemblies, D, K, and O where the effect of adding additional non-structural mass was examined.

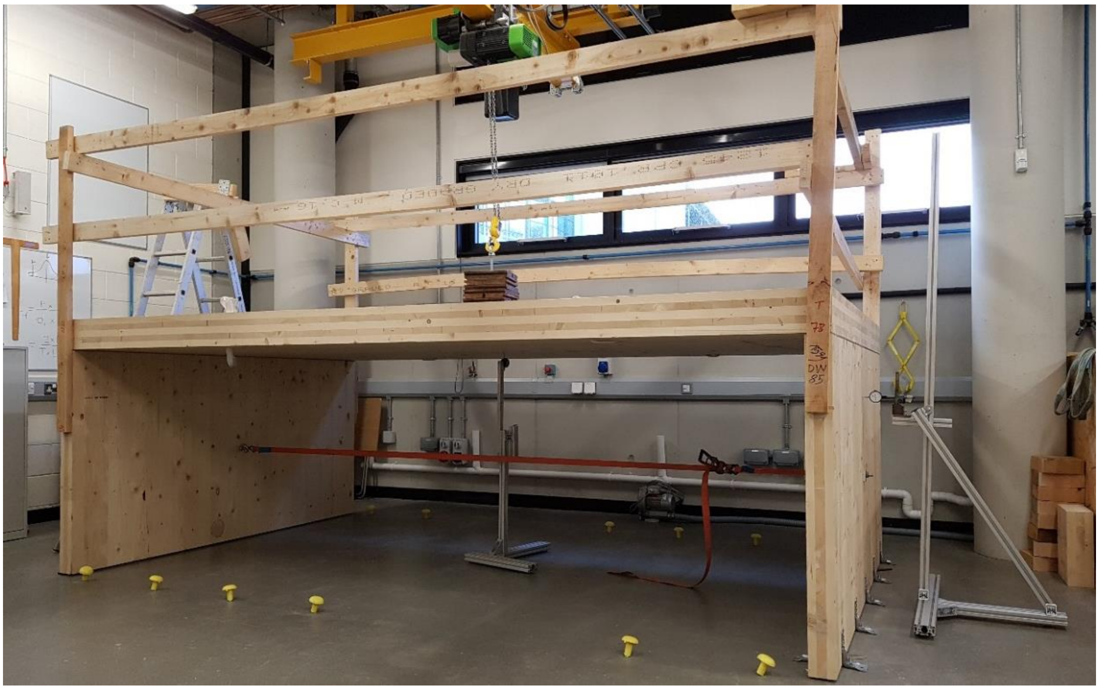

Figure 5.23 *Static point load deflection measurement, one-way long span platform construction @ NUI Galway*

Without changing the position of the load nor the measurement device, the test was repeated three times. The differences between successive readings of each floor assembly was less than 5%, and the time between successive readings was greater than 1 min., in accordance with prEN 16929:2015 [112]. Two additional dial gauges of the same type and graduation were placed on each supporting wall to monitor any spread or sway during testing. The applied mass including the load pad and a connection assembly to the overhead crane measured 106.15 kg. The deflection results were normalised to a 1 kN load.

5.4.5 Initial frequency analysis and impulse measurement

To refine the scope of the modal testing and as a posterior check on the reliability of the modal data, a preliminary analytical calculation using the effective bending stiffness from the gamma method [79] adapted from EC-5 [22] was used to determine the fundamental frequency of the CLT floor panel simply supported. Numerical FE models were then developed to predict the number, shape, and value of all the natural modes in the range of interest. Both the minimum and maximum rotational support conditions, simply supported and fully fixed, were examined to establish the range of modal values likely, bearing in mind that the support conditions in practice will be semi-rigid.

As discussed in Section 3.5, international standards define the frequency range of vibration exposure that most impacts on a person’s comfort, perception, and health for lateral, and vertical axes of standing, sitting, and recumbent persons between 0.5 and 80 Hz [116] [114] [113] [105][108]. Therefore, all analytical, modal, and diagnostic impulse measurements focused on determining the natural modes below 80 Hz.

Impulse test

Diagnostic impulse measurements were then taken to confirm qualitatively the frequency predictions. The natural frequencies of one test configuration were determined. The assembly selected for the initial comparison was a balloon construction assembly. The floor was supported on reinforced angle brackets at 250 mm spanning in one direction between the supporting walls (Assembly I, Table 5.2, and Figure 5.14).

A response transducer, an LIVM 1000 mV/g accelerometer, was placed on the floor at midspan and attached with a thin layer of wax. The impulse excitation was provided by dropping a 2 kg rubber ball from 1100 mm above the floor on a point pre-marked 300 mm away from the accelerometer, in accordance with prEN 16929:2015 [112]. The impulse and transducer locations are illustrated in Figure 5.24. The vibration responses were converted to a digital representation using an analog-to-digital converter, recorded at a sample rate of 512 Hz. A band-limited filter was applied to the signal in the range of 1 Hz to 90 Hz, with an exponential window applied to the FFT. The Peak Amplitude method was used to compute the natural mode values. Measurements were repeated, recorded three times, and the result was averaged. The specific NI LabVIEW 2014 software program developed to record and process the data is outlined in Appendix A.

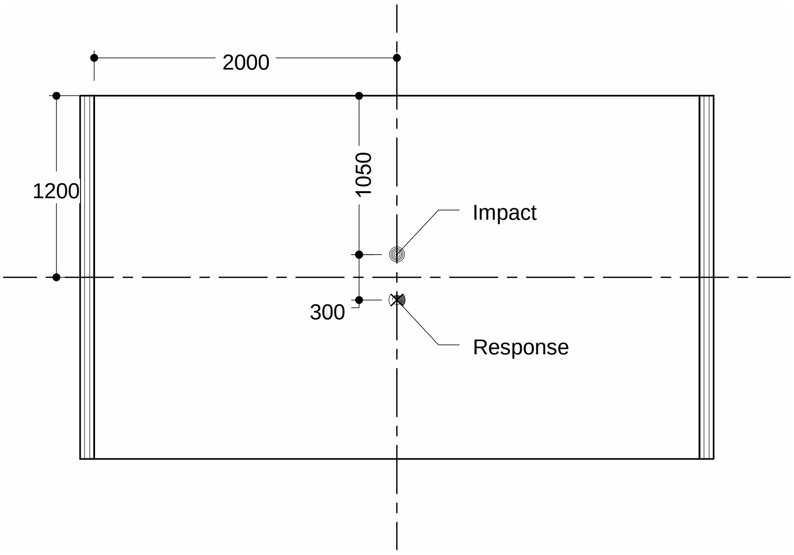

Figure 5.24 *Diagnostic impulse impact and response locations on a one-way long span balloon construction, Assembly I*

For the impulse testing, a walking platform was built above the test floor to avoid any influence on measurements due to the weight or movement of the person applying the excitation. The platform was supported independently of the test assembly, as seen in Figure 5.25.

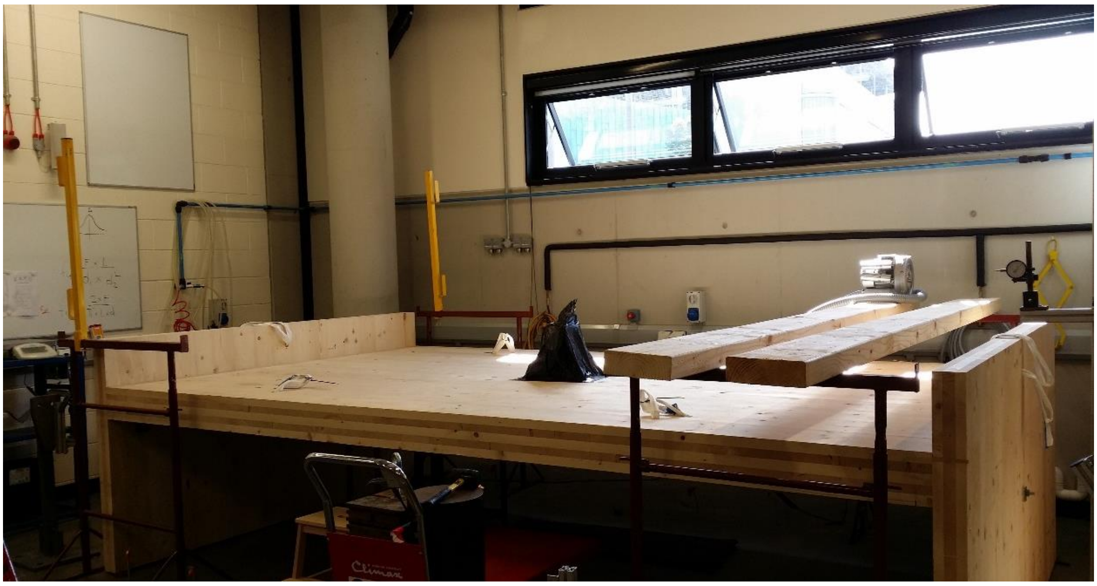

Figure 5.25 *Independent scaffold erected for diagnostic impulse tests @ NUI Galway*

5.4.6 Modal measurement

Having validated the numerical modal model, the natural frequencies and their corresponding mode shapes in the frequency range of interest were measured for each of the laboratory floor assemblies, A to P. A single excitation was provided by an electrodynamic shaker and roving response transducers measured the response. The shaker was fixed to the floor panel as outlined in Figure 5.26. To characterise the full shape of each of the modes, the transducer locations were predetermined on a grid of 64 measurement points, illustrated in Figure 5.27.

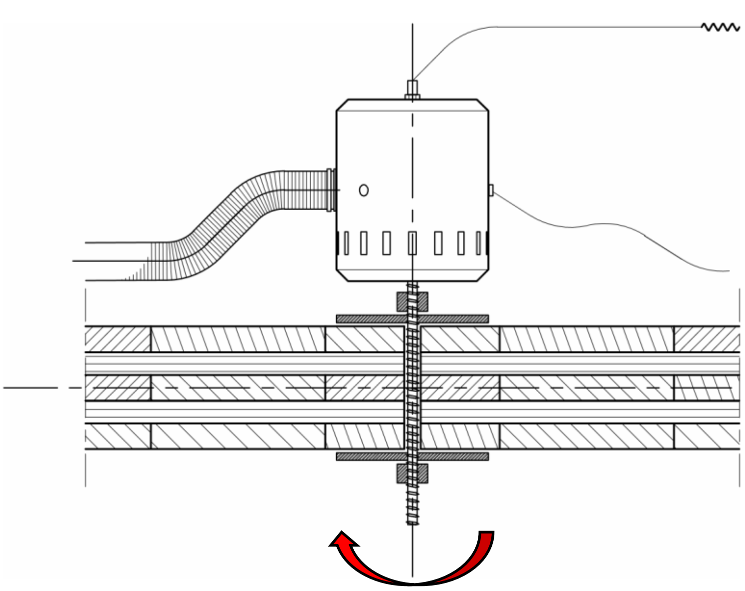

LIVM 100mV/g accelerometer measuring the force

Electrodynamic shaker threaded onto a steel rod through the floor

Power source

Blower to maintain temperature of the shaker

162 mm CLT floor panel

Ø 12 mm threaded rod with 2 no. washer and nuts tightly fixing onto the steel plates

10 x 200 x 200 mm steel plates top and bottom of the floor panel

Figure 5.26 *Fixing of shaker to the floor*

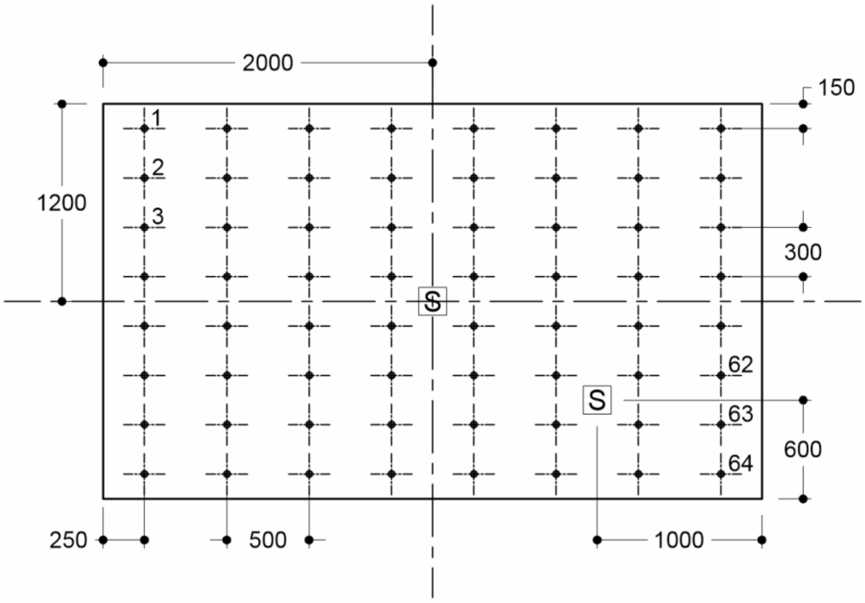

Figure 5.27 *Transducer locations: 500 x 300 mm grid of 64 measurement points. Two alternative shaker locations, midspan and quarter-span*

The force input measurement and roving response transducers comprised three accelerometers. To measure the input force, an LIVM 100mV/g accelerometer was attached to the top of the electrodynamic shaker, illustrated in Figure 5.26. A signal generator supplied a burst swept sine signal to the shaker and two SISO measurements were taken simultaneously, with two LIVM 1000 mV/g accelerometers measuring the vibration response. The response was measured starting at transverse corners of the floor (points 1 and 64), then moving systematically to the next adjacent points (2 and 63), repeating the test to record two more modal measurements and so on until each response accelerometer had recorded 32 locations on the grid, half the floor panel. An analog-to-digital converter, with a sample rate of 512 Hz, converted the signals to digital format and these were recorded and processed using NI LabVIEW 2014 software. The discrete Fourier transforms gave the FRF. The coherence function was monitored as a check on the reliability of the data measured. Measurements were repeated and recorded three times, and the results were averaged for each point on the grid. Figure 5.28 shows the modal testing apparatus in use (Assembly D).

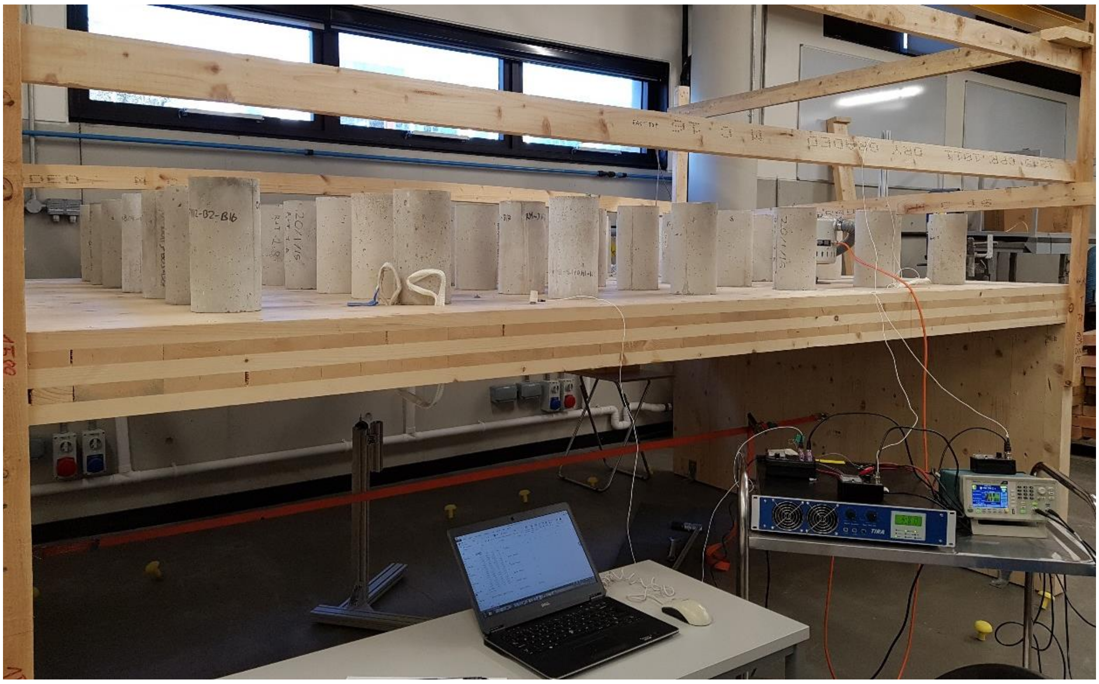

Figure 5.28 *Modal testing in the laboratory with mass added to the floor panel (Assembly D)*

The maximum deflection of the first and fourth modes were found at the floors midspan, hence the shaker was fixed to the floor panel at this point. However, this location coincided with a node of the second, third, and fifth mode, so when the 64 response points were recorded three times, the shaker was moved and fixed to an alternative location, at the quarter span that did not coincide with a modal node, and the measurements were repeated. The mode shapes were extracted from the data using the Maximum Quadrature Response method which is outlined in Section 4.2.5. The shaker positions, marked S, are also illustrated in Figure 5.27.

The modal measurements necessitated the frequent movement of the response transducers. As the room temperature was found to be consistently moderate, noted in Appendix B, and vibrations were of a low frequency, a thin layer of wax was used to attach the transducers. Comparison measurements were taken for transducers attached with a suitable threaded connection and with wax as illustrated in Figures 5.29a and b. The wax proved equally appropriate for the transducer attachment.

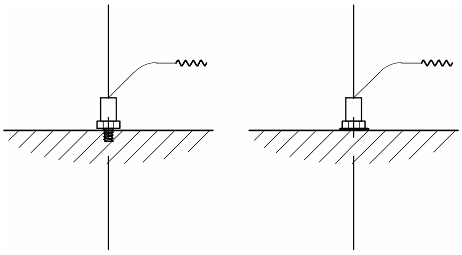

(a) (b)

Figure 5.29 *Accelerometer fixing to floor: Threaded (a), and wax (b)*

5.4.7 Acceleration amplification measurement

The FRF, which is the ratio of vibration response to an applied input excitation force, determined the acceleration magnitude. An LIVM 100mV/g accelerometer fixed to the top of the electrodynamic shaker measured the force input. The response was measured twice concurrently using two LIVM 1000 mV/g accelerometers. One was positioned at the point of maximum deflection identified in the mode shape measurements with another control measurement recorded at midspan for all the modes. The shaker was positioned at midspan when measuring the amplitude of the first and fourth modes or at the quarter span for the second, third, and fifth mode measurement. Figure 5.30 shows the shaker fixed to the CLT floor at midspan, as detailed in Figures 5.22 and 5.26.

The cooling blower is supported separately from the test set-up to avoid interference with measurements.

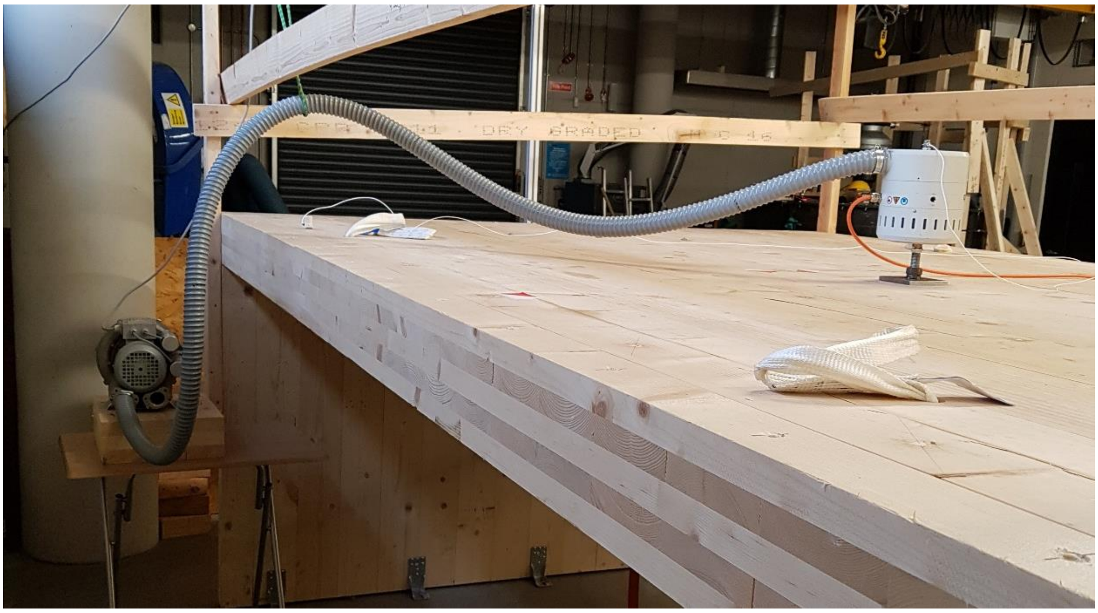

Figure 5.30 *Electromagnetic shaker fixed to floor midspan, with cooling blower supported separately from the CLT test floor*

The signal generator supplied a discrete sinusoid signal to the exciter, with a fixed amplitude. The signal frequencies corresponded to the resonant frequencies which were determined from the modal analysis for each assembly, A to P. An analog-to-digital converter, with a sample rate of 512 Hz, converted the force and response signals to digital format and these were recorded and processed using NI LabVIEW 2014 software. Measurements were repeated and recorded for each natural mode three times, with the result averaged.

5.4.8 Footfall acceleration measurement

An excitation that can be expected on any floor is that of pedestrian traffic. A number of walking tests were made measuring the vibration response on a bare one-way spanning CLT floor (Assembly A). Vibration measurements were taken of a single person walking in a random way. Three measurement were recorded of the footfall. A different adult was recorded each time. Additional time domain responses were recorded of the three adults walking on the floor and one person walking with a stick. The adult’s masses ranged between 70 kg and 90 kg. A response transducer, an LIVM 1000 mV/g accelerometer, was placed on the floor at midspan and attached with a thin layer of wax. The vibration responses due to walking were converted to a digital representation using an analog-to-digital converter, recorded at a sample rate of 512 Hz.

5.4.9 *Damping ratio measurement*

In order to determine the damping ratio ζ for each mode, the floor was again excited with the mechanical exciter at a resonant frequency. The exciter was positioned at either the midspan or quarter span, depending on the mode shape, recording the response at the point of maximum acceleration. An additional control measurement recorded the responses at midspan. The signal supplied to the exciter was a discrete, fixed amplitude, sinusoid signal with the frequency value corresponding to each resonant mode value. An analog-to-digital converter, with a sample rate of 512 Hz, converted the force and response signals to digital format. After a steady-state vibration was reached, the forcing vibration was stopped and the decreasing response vibration was recorded. The damping ratio was calculated from the logarithmic decrement of the exponentially decreasing response peaks (Equation 3.24). Figure 5.31 shows a sample damping recording.

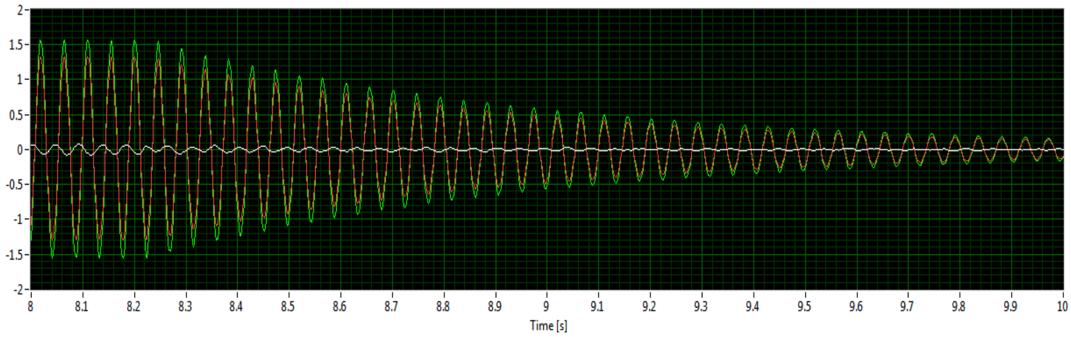

Figure 5.31 *Sample damping measurement. Control measurement in red.*

Measurements were repeated and recorded for each natural mode three times, with the result averaged.

Where the influence of a distributed added mass was investigated (Assemblies D, K, and O), one of the 12.45 kg masses was exchanged with the 15.54 kg exciter depending on the mode shape measured.

5.5 Field testing programme

The field studies comprised static deflection and dynamic frequency measurements of upper floors in a three-storey CLT building. The building was one of two, constructed to provide student living accommodation for a school in Bishop’s Stortford, UK. The building in which the measurements were taken is shown in Figure 5.32, the other adjacent CLT building is shown in Figure 5.33.

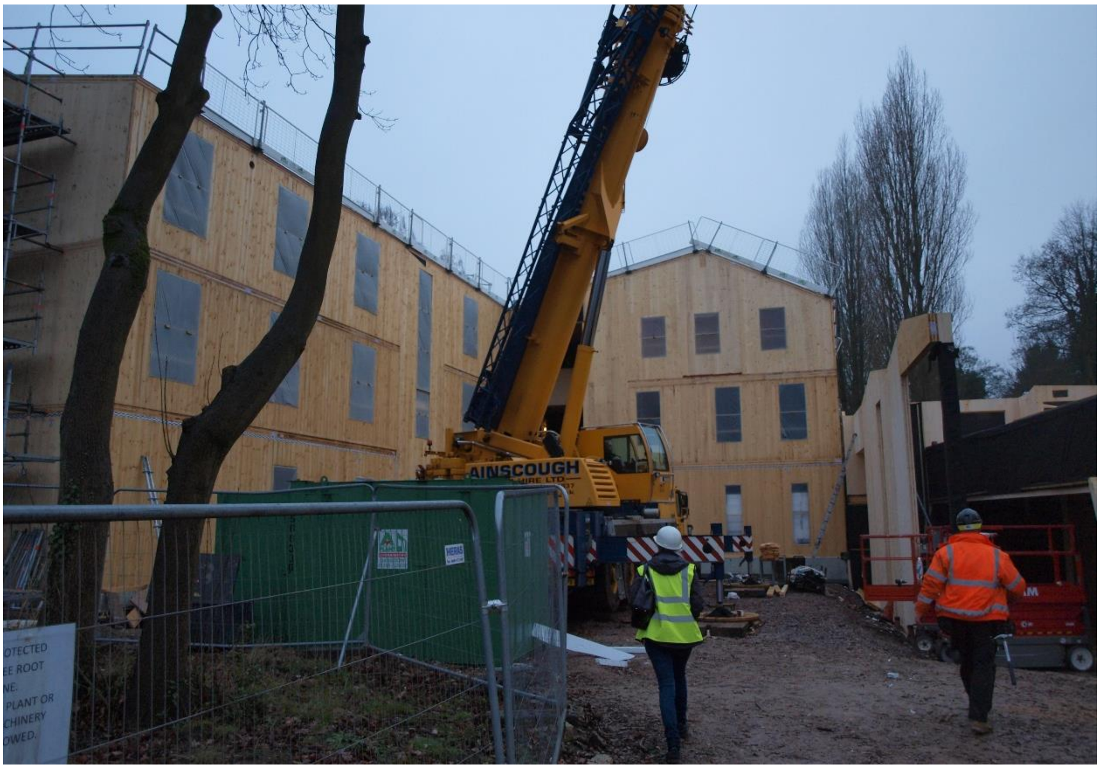

Figure 5.32 *CLT construction in Bishop’s Stortford, UK: Test building*

The structure of both buildings predominately comprised CLT platform construction with some balloon construction at stairwells and lift shafts. Glulam beams and columns, or steel beams were incorporated at one large void space in each building, however, measurements were not taken in this area.

All testing was completed in three days in late December 2016. The CLT structure was in its final stages of construction with fit-out of the internal partition walls in progress. Testing was confined to three rooms on the top floor. The relevant section of the third floor plan that includes the rooms tested is shown in Figure 5.34.

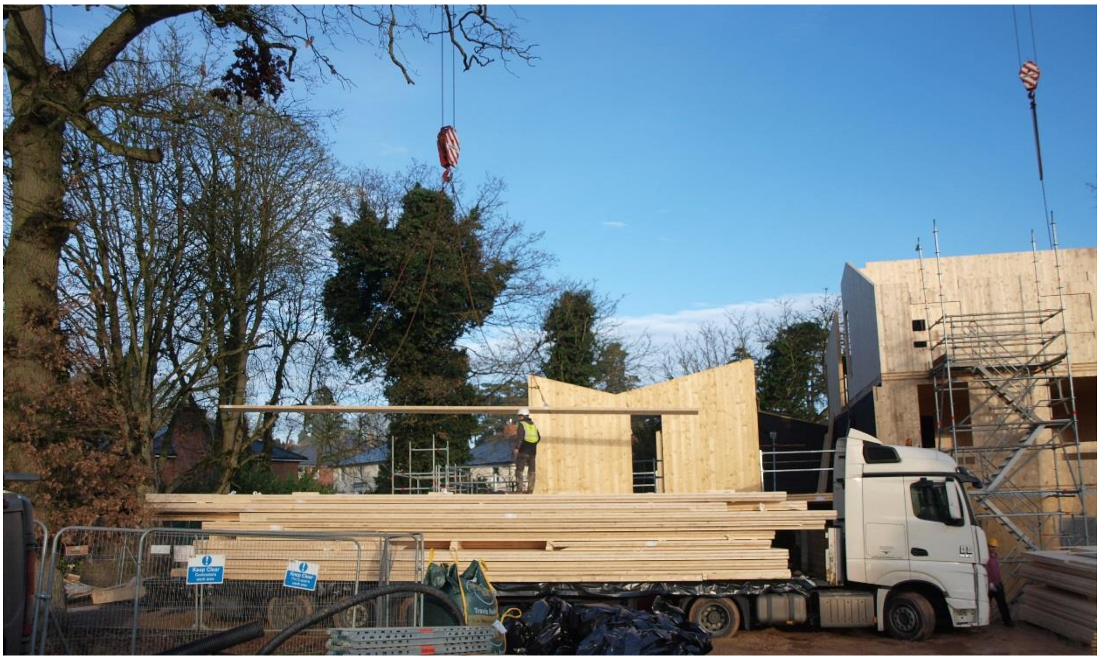

Figure 5.33 *CLT construction in Bishop's Stortford, UK*

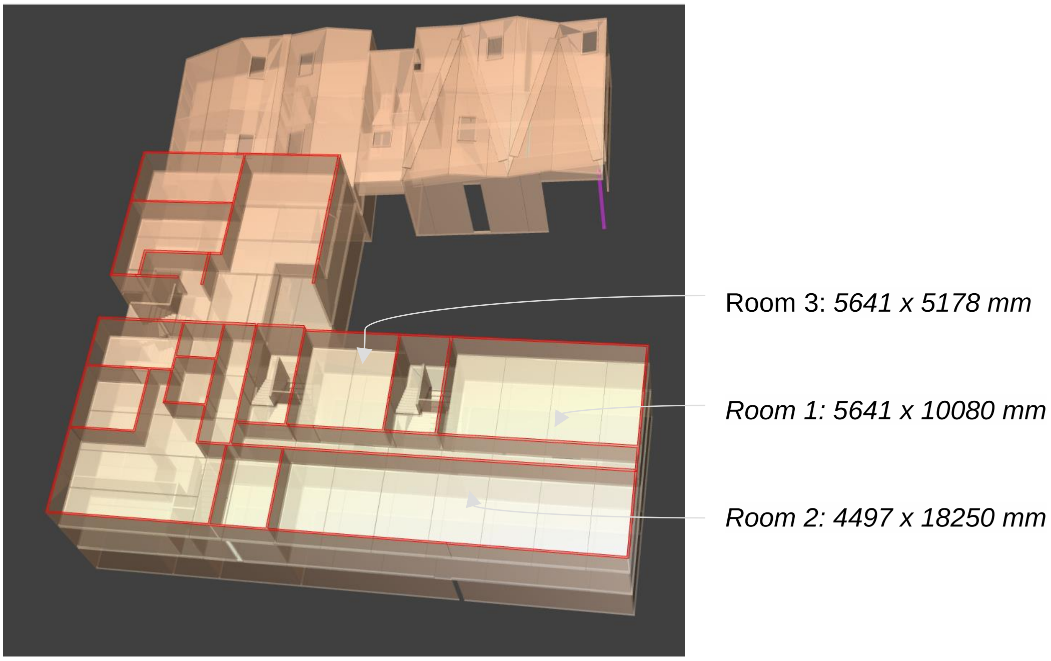

Room 3: *5641 x 5178 mm*

Room 1: 5641 x 10080 mm

Room 2: 4497 x 18250 mm

Figure 5.34 *CLT building in Bishop's Stortford, UK [Image courtesy of KLH UK]*

5.5.1 Room geometries and floor supports

The rooms share seven 180 mm thick 5-ply CLT floor panels that span the breadth of the building north-south. The total span of the panels is 11767 mm, accommodating two rooms either side of a central corridor. The panel widths ranged from 2181 mm to 2897 mm, transversely connected with half-lap joints using vertical 8 x 160 mm diameter countersunk-head, and partially threaded screws at 250 mm spacing (Figure

1.15). The CLT floor panels were connected to the CLT walls below with vertical partially-threaded, washer-head screws 8 mm diameter x 280 mm, generally at 250 mm spacing. Wall panels were connected to the floor using 100 mm x 100 mm angle brackets at 500 mm spacing. For internal walls the brackets alternated each side of the wall. A sealing tape was applied along all panel joints externally.

Rooms 1 and 3 are located either side of a stairwell on the north side of the corridor, while Room 2, the largest room is situated on the south side of the building. The floor below had a similar floor layout. The subdivision of this larger room on the lower floor was underway at the time of testing. The division of the rooms was provided by partition walls comprising a lightweight metal frame structure with gypsum plaster and skim or tape finish.

Static point-load deflections measurements were recorded in all three rooms, while the natural frequencies were also recorded for two floors, in Rooms 1 and 2. The surrounding noise due to general building works that continued during the course of the testing made damping ratio ζ and acceleration measurements unfeasible.

5.5.2 Test scope

Room 1

Room 1 measured 5641 mm x 10080 mm and had four 180 mm five-ply CLT floor panels. The supporting walls of this corner room comprised external 94 mm three-ply CLT walls on two sides, a corridor wall measuring 128 mm, with a 140 mm five-ply CLT wall to the stairwell.

Room 2

Room 2, measured 4497 mm x 18009 mm. This was the largest room tested and had seven 180 mm five-ply CLT floor panels connected in parallel. The supporting walls comprised 94 mm three-ply CLT walls on three sides and a 128 mm five-ply CLT corridor wall.

Room 3

The third room was located between two stairwells and measured 5641 mm x 5178 mm. The floor was supported by three 95 mm three-ply walls and a 128 mm five-ply CLT corridor wall.

5.5.3 Environmental conditions

The room's temperature and relative humidity were recorded at the time of each test.

5.5.4 Apparatus

Static measurement

The static point load deflections were measured with:

- FOIF EL302A Digital level ± 0.01 mm with tripod and receiver staff
- 10 no. 1 kg steel masses
- 1 no. 100 x 100 mm^2 load pad, sized in accordance with prEN 16929:2015 [112]

Dynamic analysis

The impulse testing equipment included:

- DAQ NI USB-6009
- 1 no. LIVM accelerometers, Dytran model 3100D24, sensitivity 1026.97 mV/g with relative transverse sensitivity less than 3 %, frequency range 0.6-1 kHz, and nonlinearity of ± 1 dB
- 1 no. battery operated LIVM current sources, gains: X1, X10, X100, model 4105C
- 2 kg Ø 300 mm rubber ball

Signals were recorded and analysed using NI LabVIEW 2014 software.

5.5.5 Initial static and modal analysis

In advance of the site visit preliminary numerical models were developed. The characteristic properties were obtained from construction drawings, which were provided by KLH UK and the project design engineers Smith and Wallwork. Finite element models were developed to estimate the static point load deflection value and the natural modes of the floors within the perceivable range of interest, between 0.5 and 80 Hz in accordance with human exposure to vibration standards [116] [114] [113] [105][108]. Both the minimum and maximum rotational support conditions, simply supported and fully fixed, were examined for each likely modal value, as it was assumed that the support conditions in-situ would be neither truly pinned nor rigid.

5.5.6 Deflection measurement

The static point load deflection was determined in each room by applying a concentrated dead load to pre-defined positions on a floor and recording the deflection change. A total mass of 100 kg was mounted on a 100 mm x 100 mm load-pad midspan in each room. Deflections were measured using a digital level mounted outside the room at a doorway in the corridor with the receiver staff mounted using a tripod at the load location, shown in Figures 5.35 and 5.36. (Note: Figure 5.35 depicts the receiver staff adjacent a supporting wall along the same panel as the level. It is shown to clearly outline the apparatus used. The actual deflection measurements were recorded midspan in each room where the level was not mounted along the same CLT panel as the receiver staff.)

The deflection was measured to an accuracy of ± 0.01 mm. Without changing the position of the mass or the measurement device, the test was repeated three times and the results were averaged. The differences between successive readings at each test location were less than 5% and the time between successive readings was greater than 1 min., in accordance with prEN 16929:2015 [112]. The mass applied was increased to 183 kg and the tests were repeated. A person standing adjacent to the steel masses constituted the additional 83 kg.

5.5.7 Frequency measurement

An impulse excitation was provided by dropping a 2 kg rubber ball from 1100 mm above the floor on a point pre-marked on the floor, shown in Figure 5.37. The response was recorded with an LIVM 1000 mV/g accelerometer placed on the floor 300 mm away from the pre-marked impact point, in accordance with prEN 16929:2015 [112]. As the room temperatures were found to be moderate and the vibrations were of a low frequency the transducer was attached with a thin layer of wax.

The vibration responses were converted to a digital representation using an analog-to-digital converter, recorded at a sample rate of 512 Hz. A band-limited filter was applied to the signal in the range of 1 Hz to 90 Hz with an exponential window applied to the FFT. Measurements were repeated and recorded three times. The response transducer was then moved to alternative locations on the floor to capture modes with a node coinciding with the initial location. Alternative impact locations were also selected, for the same reason.

The Peak Amplitude method was used to compute the frequencies, with results averaged. The specific NI LabVIEW 2014 software program developed to record and process the vibration data is outlined in Appendix A.

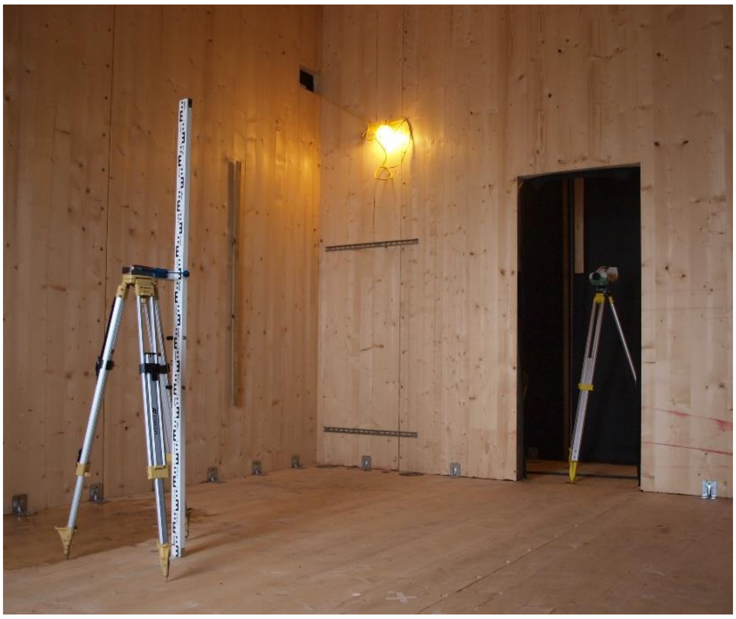

Figure 5.35 *Static point load deflection testing*

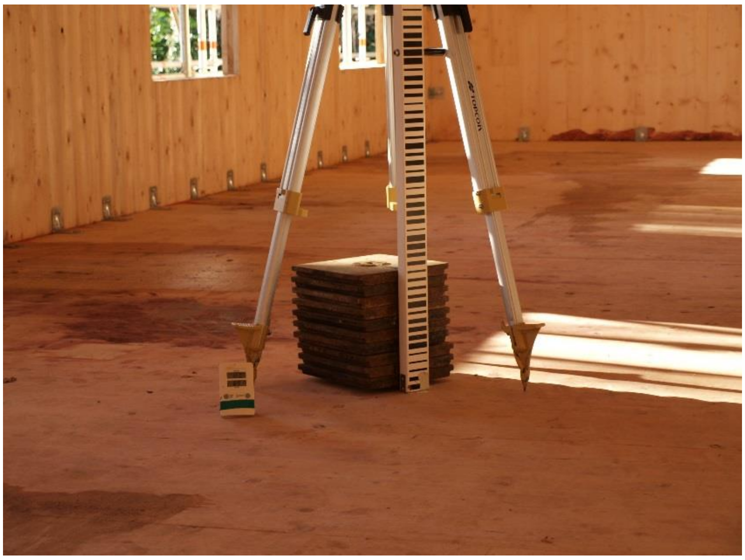

Figure 5.36 *Static point load applied midspan*

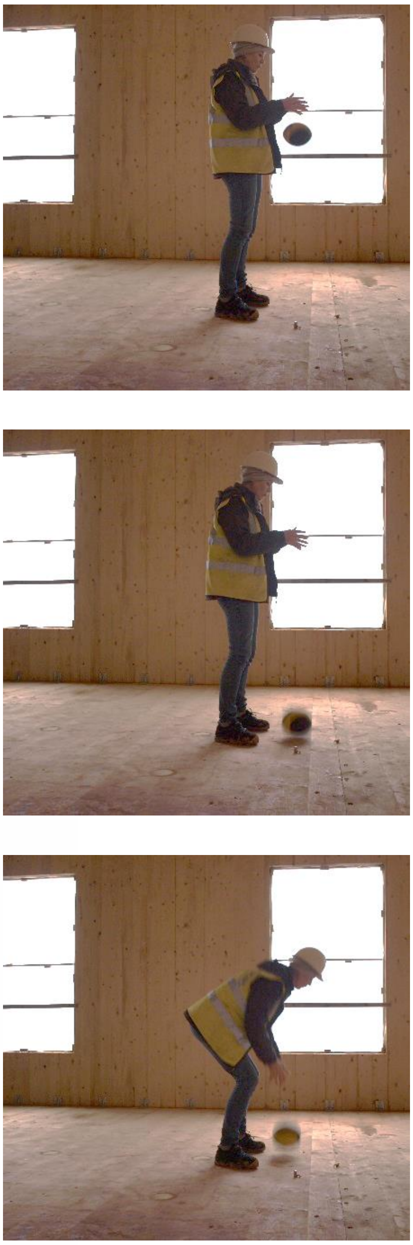

Figure 5.37 *Impulse testing using a 2 kg ball*

5.6 Conclusions

In this chapter the experimental testing programme of CLT floors in the laboratory and in the field were presented. The testing programme focused on deflection and vibration measurement of CLT floors supported with industry standard fixing details.

A variety of alternative support details in keeping with contemporary mid-rise CLT assembly included alternative large-diameter screw assemblies, screw and bracket details, and alternative bracket types. An investigation of the effect of increased fixing spacing and the inclusion of an elastomer interlayer are accommodated in the experimental testing programme (summarised in Table 5.5). The influence of added mass was also examined.

The testing programme included the measurement of static deflection and natural frequency values in the laboratory and in the field. The laboratory testing schedule also comprised the measurement of the natural mode shapes within the frequency range, 0 to 80 Hz, and the resonant vibration accelerance values. Sample time domain footfall excitations were recorded to confirm transient or resonant responses, and the damping ratio ζ values of the natural modes were also included in the laboratory test schedule.

The following chapter gives the detailed results of the laboratory and in-situ field testing.

6 EXPERIMENTAL RESULTS

6.1 Introduction

In this chapter, the results of the testing programme of CLT floors in the laboratory and in the field, outlined in Chapter 5, are presented. These include laboratory testing to quantify the influence of (i) connector type and spacing (Objective 1), (ii) a resilient interlayer in a floor-to-wall junction (Objective 2) and (iii) a distributed added-mass on the panel (Objective 3) on the static and dynamic performance of the system. Additional variables included in the laboratory testing are the support type (balloon or platform) and the span type (one-way or two-way). Results presented include the static deflection, natural frequency values, the mode shapes in the 0 to 80 Hz range, acceleration amplification of the natural modes, and their damping ratio ζ-values. The field tests address Objective 4.

6.2 Laboratory test results

A single-panel CLT floor panel supported on CLT rising walls was tested in the laboratory. The effect of separate combinations of vertical or inclined pairs of large diameter self-tapping screws, with, and without, angle brackets of different types at varied spacing was measured. The effect of alternative span directions, the inclusion of a resilient interlayer at supports, and the addition of an evenly distributed mass were also explored. The laboratory testing was conducted uninterrupted over six months in NUI Galway, completed in March 2018.

Static deflection and initial impulse frequency measurements were taken using the non-destructive test guidelines outlined in the European Standard on the test methods for determining the vibration performance of timber floors, prEN 16929: 2015 [112]. More comprehensive SISO modal testing established the modal frequencies and mode shapes, their acceleration amplifications and damping ratios ζ for sixteen floor assemblies (Section 5.3.6: Figures 5.9 to 5.17, Tables 5.1 to 5.5).

The measured mode shapes, corresponding frequencies, vibration amplitudes, damping values, and midspan deflections are charted for each laboratory test assembly in Appendix B. The environmental conditions of the room and the floor at the time of each test are included.

6.2.1 Floor geometry, moisture content, mass and room environment

The span, width, and depth of the CLT floor was measured to an accuracy of 1 mm in accordance with prEN 16929:2015 [112]. An average of three measurements of the floor panel thickness were taken 150 mm from the floor edge which determined the floors depth. The 5-ply CLT floor panel measured 162 mm x 2400 mm x 4000 mm. The floor mass was measured to an accuracy 0.1 kg using a dedicated scales suspended from the overhead crane. The average result of the floor mass from three consecutive measurements was 727.5 kg. The floor’s moisture content and the temperature and relative humidity of the laboratory room was recorded each day of testing. The floor’s moisture was determined with a moisture meter in accordance with EN 13183-2 [162]. The values fluctuated between 10.9% and 13.7%, averaging at 11.5%. The room temperature ranged between 17.5˚C and 20.6˚C, averaging at 19.4˚C, with relative humidity measurements ranging from 38.4% to 65.0 %, averaging 50.0% over the duration of all the laboratory testing. The relative test values are noted Appendix B.

6.2.2 Static point load deflection results

A 1 kN point load was applied midspan to measure the static deflection for each of the floor assemblies described in Chapter 5 (Section 5.3.6: Figures 5.9 to 5.17, Tables 5.1 to 5.5). The average deflection result from three consecutive measurements for each floor assembly are presented in Table 6.1 and Figures 6.1 to 6.4.

Table 6.1 *Static 1kN point load applied midspan deflection results, Assemblies A to P*

Floor to wall Assembly	*Resilient layer*	*Added mass*	*Deflection (mm)*
			1kN Static point load applied at midspan
	One-way long span: Platform construction		
A			*0.179*
B			*0.178*
C	●		*0.185*
D		●	*0.178*
E			*0.176*
F			*0.172*
G			*0.177*
H			*0.158*
	One-way long span: Balloon construction		
I			*0.219*
J			*0.201*
K		●	*0.202*
	One-way short span: Platform construction		
L			*0.111*
M			*0.113*
N			*0.103*
O		●	*0.104*
	Two-way span: Platform construction		
P			*0.098*

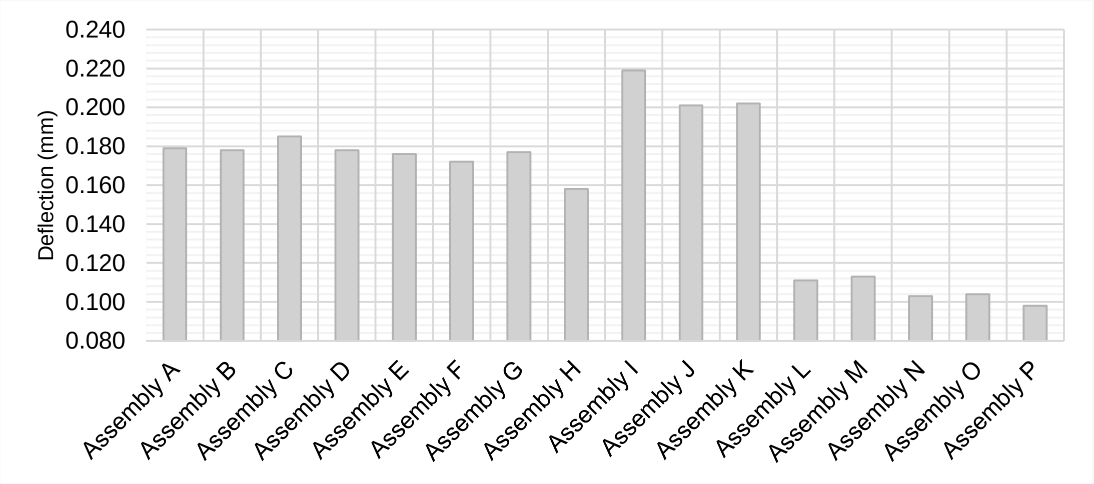

Figure 6.1 *Static 1kN point load applied midspan deflection results, Assemblies A to P*

The maximum deflection value recorded, 0.219 mm, coincided with the maximum balloon constructed span in one direction of 4000 mm (Assembly I). A CLT Designer software estimate for a similar panel, spanning 4000 mm simply supported was 0.190 mm. The minimum deflection of 0.098 mm was recorded for the two-way spanning floor (Assembly P), as expected.

One-way long-span platform construction *(Assemblies A to H)*

The deflection results for the different platform fixing assemblies used to support the floor spanning in one direction along the length of the floor (3812 mm) are presented in Figure 6.2.

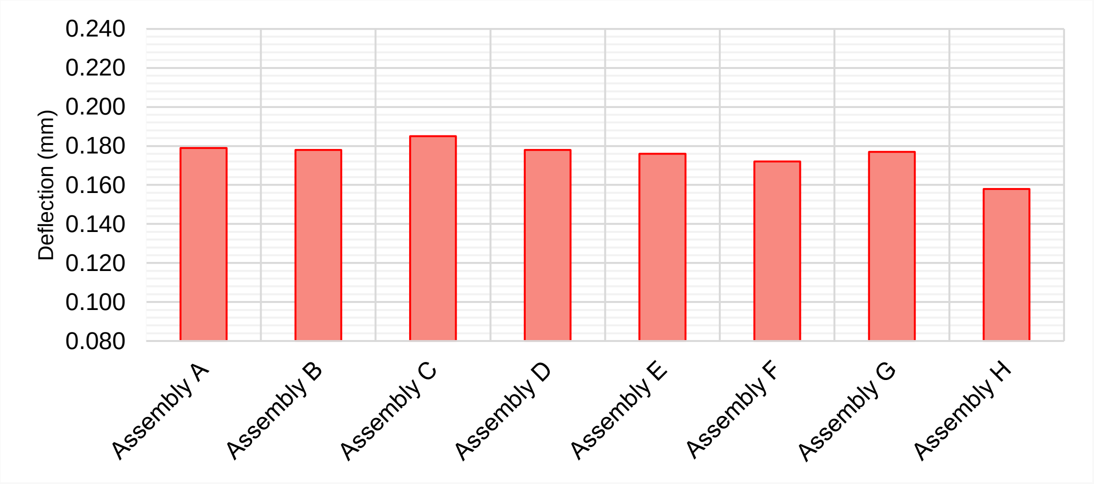

Figure 6.2 *Deflection results for Assemblies A to H, One-way long span platform construction*

Comparing alternative screw assemblies without brackets was generally negligible. Reducing the spacing of vertical screws from 300 mm (Assembly B) to 150 mm spacing (Assembly A) had no effect on the deflection results (± 0.001 mm). Using an alternative configuration of inclined fully threaded cylindrical-head screws (Assembly E) was also negligible.

Comparing vertical partially-threaded screws at 300 mm spacing (Assembly B) with the same configuration with the addition of angle brackets of different types at 800 mm spacing had no sizeable influence on the deflection results. The 240 mm x 93 mm x 120 mm (TTN 240) shear-angle brackets performed better than the 100 mm x100 mm x 90 mm (WBR 100) angle brackets (Assemblies F and G, respectively). However, the difference of 0.005 mm could be regarded as inconsequential. Reducing the bracket (WBR 100) spacing to 200 mm (Assembly H) reduced the CLT floor panel deflection by 11%.

The addition of a non-structural mass evenly distributed across the floor (onto the baseline Assembly B), (Assembly D) equally did not influence the point load deflection of the floor. Note: the dial gauge was re-zeroed before measuring each alternative fixing configuration (Assemblies A to P: Table 5.5).

Introducing a resilient interlayer (Assembly C) increased the deflection of the floor panel from 0.178 mm (for the baseline Assembly B), to 0.185 mm.

One-way long-span balloon construction *(Assemblies I to K)*

The 4000 mm span balloon assembly deflection results are shown in Figure 6.3.

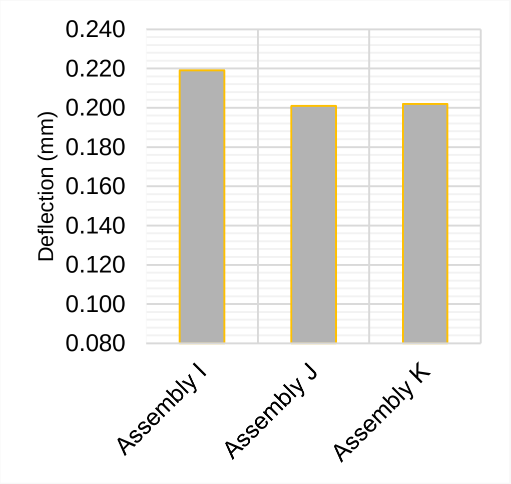

Figure 6.3 *Deflection results for Assemblies I to K, One-way long span balloon construction*

The balloon construction fixing arrangement that used inclined screw pairs at 250 mm spacing (Assembly J) in comparison with supporting the floor with angle brackets only (Assembly I), reduced the point load deflection by 8%. Adding an evenly distributed mass to the floor (Assembly K) did not influence the midspan deflection.

One-way short-span platform construction *(Assemblies L to O)*

The point load deflection results for the CLT floor spanning in one direction, 2212 mm span and in two directions (Assembly P) are illustrated in Figure 6.4.

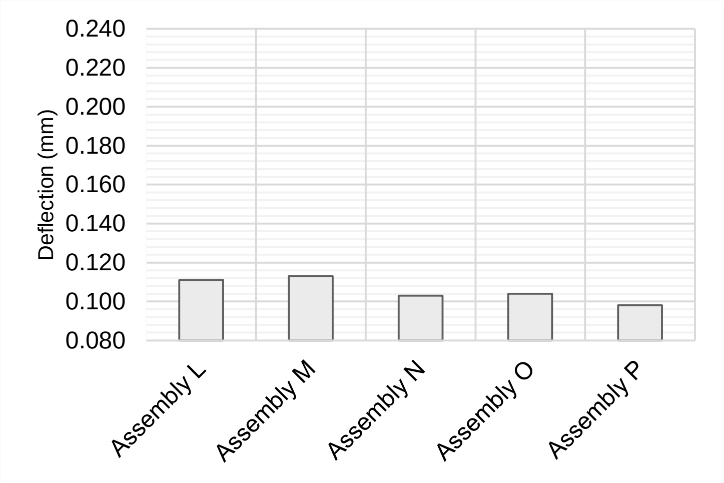

Figure 6.4 *Deflection results for Assemblies L to P, one-way short span and two-way spanning platform construction*

Supporting the floor in the alternative direction (Figure 5.4), reduced the span to 2212 mm, which therefore reduced the deflection results, as expected. Results ranged from 0.158 mm to 0.185 mm for the 3812 mm span floor and ranged from 0.103 mm to 0.113 mm for the 2212 mm spanning floor.

The influence of using alternative fixing configurations in the floor could again be regarded as insignificant. Increasing the spacing of vertical screws from 300 mm centres (Assembly L) to 600 mm centres (Assembly M) resulted in a 0.002 mm increase in the midspan deflection. Adding 240 mm x 93 mm x 120 mm (TTN 240) angle brackets at 800 mm spacing (Assembly N) reduced the deflection of the floor by 0.01 mm. The addition of a distributed non-structural mass on the floor (onto the baseline Assembly N), (Assembly O) did not influence the point load deflection of the floor.

Two-way platform construction *(Assembly P)*

Spanning in two directions using vertical partially-threaded screws at 300 mm spacing (Assembly P) compared with the same fixing configuration for a short span floor (Assembly L) improved the deflection of the floor by 12% from 0.111 mm to 0.098 mm.

Summary of deflection results

The Irish national annex to the current European timber design criteria [111][22] limit deflection due to a 1 kN point load at 1.800 mm for a single-span floor spanning 4000 mm or less. The limiting deflection values across Europe range between 0.500 mm/kN and 4.000 mm/kN [121]. The maximum 1 kN point load deflection recorded in the laboratory floor assemblies, all spanning 4000 mm or less, was 0.219 mm. As the European standards currently relate to traditional timber floor construction, it may be inferred from the laboratory CLT deflection results that the flexural stiffness of CLT floors is greater than what is expected from traditional timber floor construction.

The deflection of the floor was not significantly influenced by increasing the number of vertical screw fixings in the platform construction assemblies. Replacing vertical screws with inclined screw pairs did not notably impact on the deflection of the floor midspan either.

Adding 240 mm x 93 mm x 120 mm (TTN 240) shear-angle brackets at 800 mm spacing (Assemblies F and N) improved the flexural stiffness of the floor marginally (an improvement of 0.006 mm and 0.008 mm, respectively). Adding angle brackets (WBR 100) at 800 mm spacing (Assembly G) was negligible, however, providing the same angle brackets at 200 mm spacing (Assembly H) gave the best deflection improvement due to fixings (from 0.178 mm to 0.158 mm).

Adding a resilient interlayer increased deflection midspan, but the influence of any compression that may have occurred in the floor support was not monitored.

Overall, the laboratory deflection results suggest that the alternative fixing configurations do not notably affect the flexural stiffness of the floor. Providing angle brackets spaced at 200 mm provided the best improvement due to fixings of 11%, while using inclined screw pairs in preference to angle brackets in balloon construction improved the midspan deflection by 8%. Non-structural evenly distributed added mass did not influence the flexural stiffness of the CLT floor.

Lateral deflection in the supporting walls

Measurements of sway in supporting walls, due to the applied static point load, were negligible, recording values between 0.003 mm to 0.016 mm in the case of one-way spanning platform construction, and between 0.040 mm and 0.061 mm for all one-way spanning balloon construction assemblies. Sway ranged between 0.001 mm and 0.014 mm for short spanning platform assemblies, with a maximum value of 0.001 mm recorded where the floor panel was supported in both directions.

6.2.3 Initial theoretical and impulse frequency results

Theoretical frequency estimates

To refine the scope of the modal testing and to later provide a check on the reliability of the modal data, preliminary analytical and numerical models were developed. Using the effective bending stiffness from the gamma method [22][65] incorporating the measured dimensions and mass value along with the characteristic properties provided by the CLT manufacturers technical data sheets, the fundamental frequency of the 4000 mm spanning CLT floor panel simply-supported was calculated. The results were compared with CLT Designer software predictions for a similar 5-ply panel, of the same 4000 mm span, simply-supported (Assembly I or J).

Preliminary FE models were developed to predict the number, shape, and value of all the natural modes in the 0 to 80 Hz range. The FE analysis estimated five modes. Both the minimum and maximum rotational constraint conditions at the supports were examined to establish the range of modal values likely, bearing in mind that the support conditions in practice will be semi-rigid. The first five natural frequency values from the FE analysis and the fundamental frequency value of a simply-supported floor calculated using the analytical gamma method and using CLT Designer software are given in Table 6.2 and charted in Figure 6.5. The corresponding FE mode shapes are outlined Table 8.2.

Table 6.2 *Initial theoretical frequency estimates for Assembly I: Modes 0 to 80 Hz*

Floor to wall Assembly	*Support conditions*	*Natural frequencies (Hz)*				
		Mode 1	*Mode 2*	*Mode 3*	*Mode 4*	*Mode 5*
	Impulse: Balloon construction					
FEM	*Fully-fixed*	*35.60*	*38.79*	*79.27*	*74.19*	*83.72*
FEM	*Simply-supported*	*19.58*	*25.32*	*65.84*	*68.80*	*71.13*
CLT Designer		*17.84*				
γ-method		*19.47*				

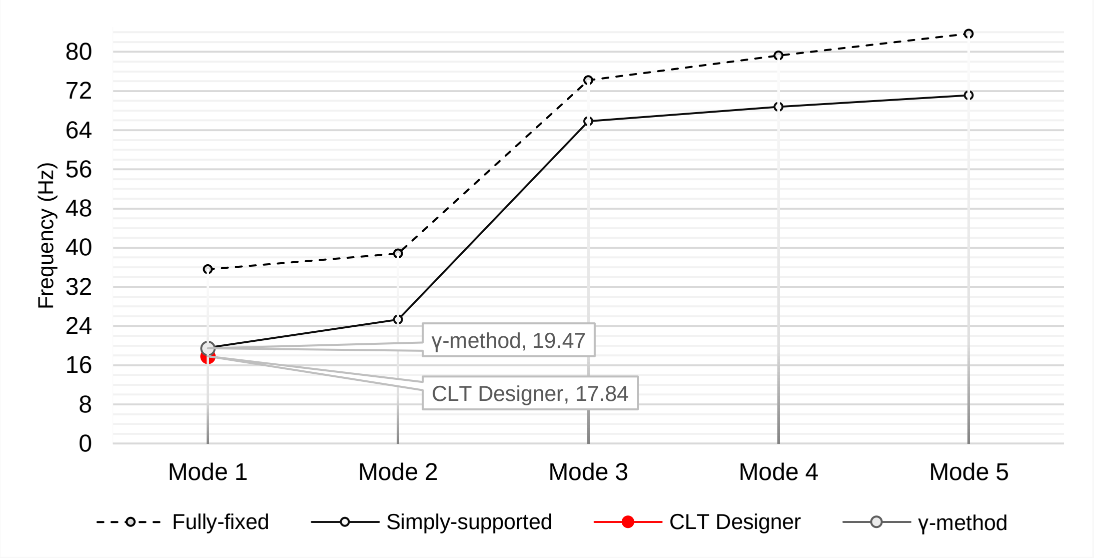

Figure 6.5 *Initial theoretical frequency estimates for Assembly I: Modes 0 to 80 Hz*

Experimental impulse frequency results

Initial impulse measurements were taken to determine the natural frequency values of the one-way balloon construction using angle brackets at 250 mm spacing (Assembly I). A response transducer was placed midspan on the floor while an impulse excitation was provided by a person standing on a scaffold constructed above the floor, which was supported independently. A 2 kg rubber ball dropped on a point pre-marked 300 mm away from the transducer provided the impulse. The location of the transducer and impulse are illustrated in Figure 5.24. The output measurements of three impulse responses were recorded and are charted in Table 6.3, with the average values plotted in Figure 6.6. The FE frequency values with maximum rotation at the supports are also represented by a dotted line in Figure 6.6 (previously also depicted in Figure 6.5).

Table 6.3 *Impulse test results for natural frequencies 0 to 80 Hz, Assembly I*

Floor to wall Assembly	*Support conditions*	*Natural frequencies (Hz)*				
		Mode 1	*Mode 2*	*Mode 3*	*Mode 4*	*Mode 5*
I	*One-way long span: Balloon construction*					
1st reading	*Bearing angle-brackets*	*20.10*	*25.20*	*61.60*	*70.08*	*75.75*
2nd reading		*20.10*	*25.20*	*61.75*	*70.50*	*75.75*
3rd reading		*20.10*	*25.20*	*61.75*	*70.65*	*75.90*
Average		*20.10*	*25.20*	*61.60*	*70.40*	*75.80*
FEM	*Simply-supported*	*19.58*	*25.32*	*65.84*	*68.80*	*71.13*

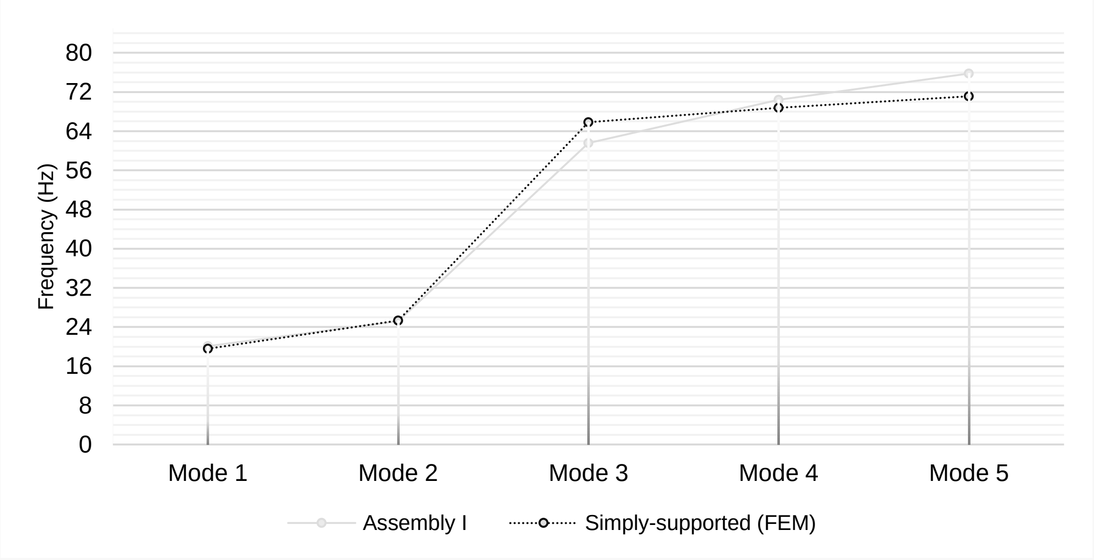

Figure 6.6 *Impulse test results for natural frequencies 0 to 80 Hz, Assembly I. A dotted line indicates the FEM simply-supported frequency values*

The correlation between the analytical gamma method, CLT Designer software estimate, FE modal analysis, and the impulse frequency measurements (Figures 6.5 and 6.6) provides reassurance on the reliability of the dynamic data recorded and defines the general range of frequency values and mode shapes that are to be expected in the subsequent experimental FRF modal analysis.

6.2.4 Modal frequency analysis results

FRF and impulse frequencies *(Assembly I)*

The experimental FRF modal analysis requires that an electromagnetic shaker of mass 15.54 kg be fixed to the floor (Figures 5.26 and 5.27). The initial impulse frequency measurements did not include the shaker. The natural frequency values from the initial experimental impulse tests and the FRF modal testing, that included the shaker mass, of the floor spanning 4000 mm in one direction (Assembly I) are shown in Table 6.4 and Figure 6.7.

Table 6.4 *Impulse and modal test results for natural frequencies 0 to 80 Hz, Assembly I*

Floor to wall Assembly	*Frequency measurement*	*Natural frequencies (Hz)*				
		Mode 1	*Mode 2*	*Mode 3*	*Mode 4*	*Mode 5*
	One-way long span: Balloon construction					
I	*Impulse*	*20.10*	*25.20*	*61.60*	*70.40*	*75.80*
I	*Modal*	*20.05*	*25.05*	*61.05*	*69.85*	*76.05*

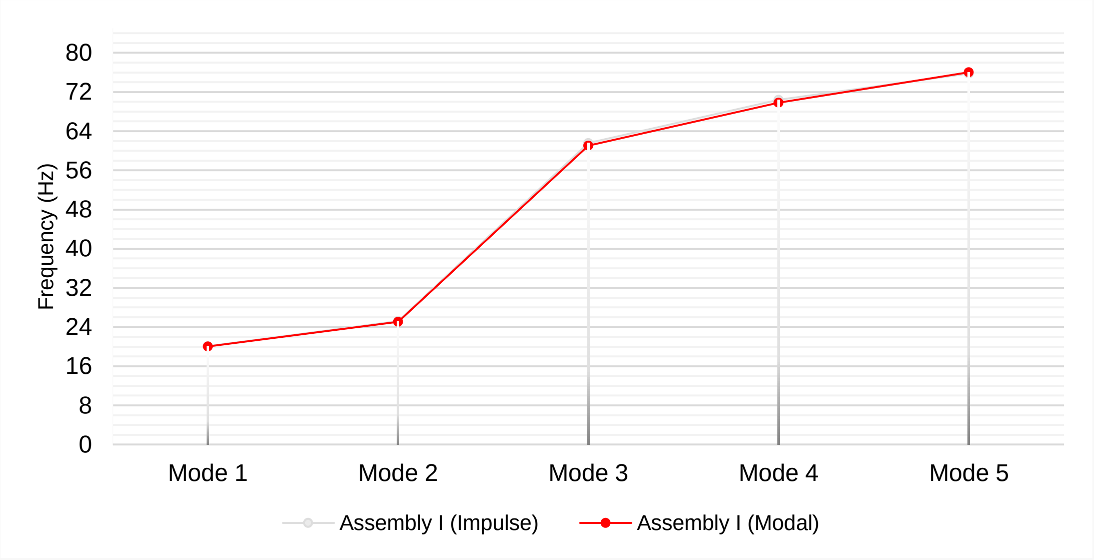

Figure 6.7 *Impulse and modal test results for natural frequencies 0 to 80 Hz, Assembly I*

Comparing both results indicates that the mass of the electromagnetic shaker did not notably affect the frequency values of the natural modes.

FRF modal analysis *(Assemblies A to P)*

To characterise the modal shapes, the responses at different locations on the floor were measured. An electromagnetic shaker fixed to the floor panel (Figures 5.26 and 5.27) provided the force across the frequency range of interest. Roving accelerometers on points on a predetermined grid captured the vibration response. The same excitation was provided for each measurement. The FRF of the FFT defined the magnitude of each mode at each measurement point, monitoring the coherence function throughout data acquisition. The measurements were repeated and recorded three times, and the results were averaged for each point on the floor grid. This was repeated for each assembly configuration. The measured mode shapes were normalised to unity displacement.

The measured mode shapes and corresponding frequencies are charted for each laboratory test assembly in Appendix B.

One-way long-span construction *(Assemblies A to K)*

The orientation of the floor panel and the addition of an imposed load most influenced the frequency and mode shape results. In the case of the platform and balloon construction single long-span floors, four natural modes were recorded in the frequency range between 0 to 80 Hz. An additional fifth mode was recorded for the one-way balloon constructions where the span of the floor was increased by 188 mm (Assemblies I to K). A fifth mode was also recorded on the one-way platform constructed floor panel where an evenly distributed mass was added (Assembly D). Examples of the five modes measured are illustrated in Figure 6.8.

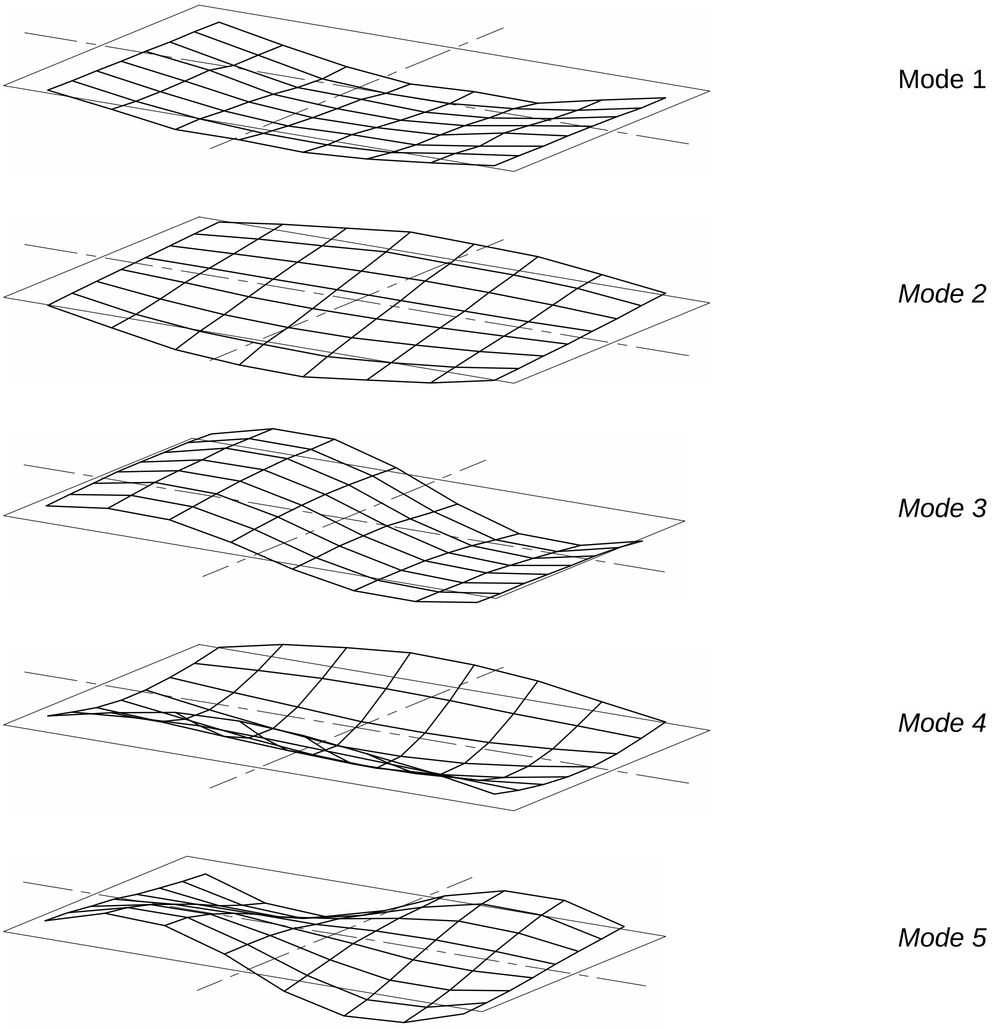

Figure 6.8 *Typical mode shapes for assemblies A to K*

One-way short-span platform construction *(Assemblies L to O)*

Modal testing of the one-way short-span platform assemblies measured up to four modes in the range of interest (Assemblies L to O). Examples from the modal testing measurements of the four modes are illustrated in Figure 6.9.

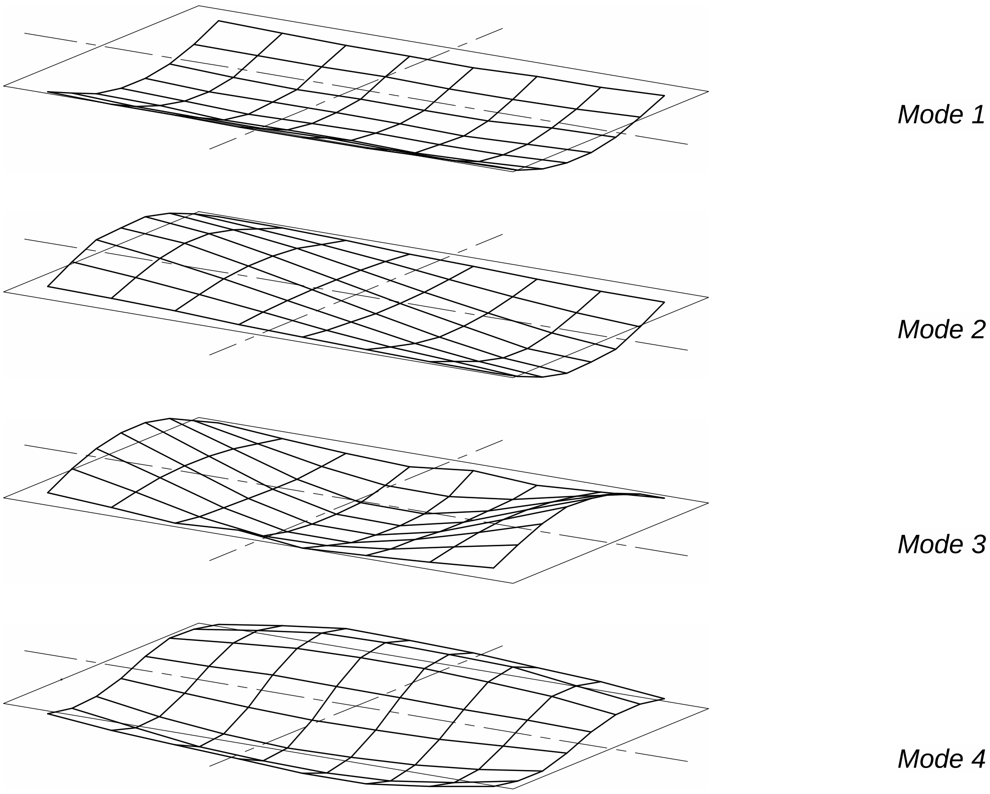

Figure 6.9 *Typical mode shapes for assemblies L to O*

Two-way span platform construction *(Assembly P)*

The two-way spanning floor (Assembly P) tests recorded only one mode at a frequency value less than 80 Hz. This mode is presented in Figure 6.10.

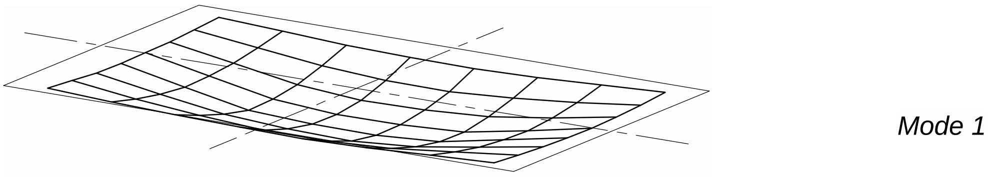

Figure 6.10 *Assembly P mode shape*

FRF frequency analysis *(Assemblies A to P)*

Table 6.5 with Figure 6.11 presents the average values from three measurements of the natural frequency values between 0 and 80 Hz for all of the floor assemblies tested. Comparisons between frequency results are further explored in Figures 6.12 to 6.18.

Table 6.5 *Natural frequencies 0 to 80 Hz range for floor to wall, Assemblies A to P*

Floor to wall Assembly	*Resilient layer*	*Load added*	*Natural frequencies (Hz)*				
			Mode 1	*Mode 2*	*Mode 3*	*Mode 4*	*Mode 5*
	One-way long span: Platform construction						
A			*22.35*	*28.75*	*73.10*	*78.35*	*-*
B			*21.90*	*28.20*	*72.65*	*78.05*	*-*
C	●		*21.50*	*27.30*	*70.35*	*78.25*	*-*
D		●	*16.35*	*21.45*	*53.95*	*69.25*	*65.35*
E			*22.05*	*28.55*	*73.10*	*78.35*	*-*
F			*22.30*	*28.35*	*72.95*	*78.20*	*-*
G			*22.00*	*28.25*	*72.75*	*78.15*	*-*
H			*23.40*	*29.70*	*74.10*	*78.90*	*-*
	One-way long span: Balloon construction						
I			*20.05*	*25.05*	*61.05*	*76.05*	*69.85*
J			*20.45*	*25.65*	*68.20*	*77.20*	*77.50*
K		●	*14.90*	*19.20*	*50.85*	*67.45*	*63.80*
	One-way short span: Platform construction						
L			*29.50*	*38.25*	*66.40*	*-*	*-*
M			*29.05*	*37.55*	*65.75*	*78.50*	*-*
N			*29.70*	*39.20*	*67.45*	*-*	*-*
O		●	*23.95*	*29.95*	*54.95*	*68.60*	*-*
	Two-way span: Platform construction						
P			*41.75*	*-*	*-*	*-*	*-*

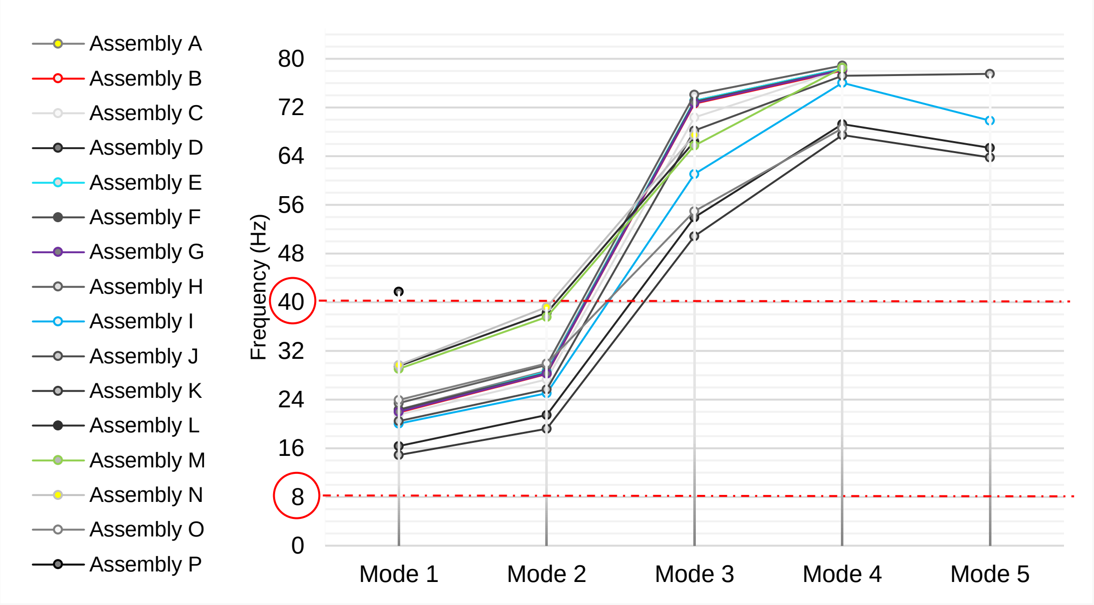

Figure 6.11 *Natural frequency results ranging between 0 and 80 Hz, Assemblies A to P*

The fundamental frequency results for all the assemblies tested ranged between 14.90 Hz and 41.75 Hz. The lowest natural mode was found for the floor assembly of the largest span 4000 mm with an evenly distributed added mass (Assembly K). The two-way spanning unloaded floor (Assembly P) recorded the highest fundamental frequency value, increased by 41% over the comparable one-way short-span floor using the same fixing configuration (Assembly L).

The fundamental frequency values recorded for all the floor assemblies tested were greater than the minimum recommended 8 Hz limit in EC-5 [22]. The frequency values increased with reduced floor span and decreased with the addition of a distributed load. With respect to the frequency mode separation, no more than one first-order mode, and one second-order mode was determined below 40 Hz. A reduced number of first-order modes below 40 Hz is important to ensure compliance with the unit impulse velocity criteria in EC-5 [22]. Bearing the floor in two directions significantly increased the natural frequency results, with no natural mode occurring below the 40 Hz unit impulse criteria limit.

One-way long-span platform construction *(Assemblies A, B, and E to H)*

The one-way long span platform construction results (Assemblies A, B, E to H) are plotted in Figure 6.12. The variations in frequency values between the different fixing configurations of the same floor orientation is small. Figures 6.13 and 6.14 examine the results more closely.

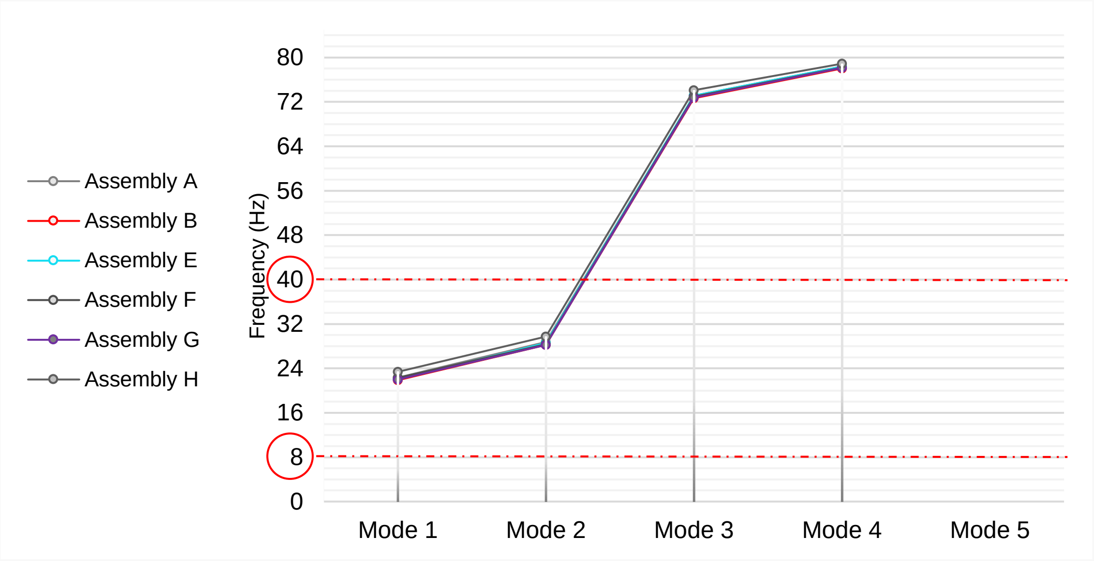

Figure 6.12 *Natural frequency results for the alternative bracket and screw configurations for one-way long span platform construction, without resilient interlayer or added load, Assemblies A, B, E, F, G, and H*

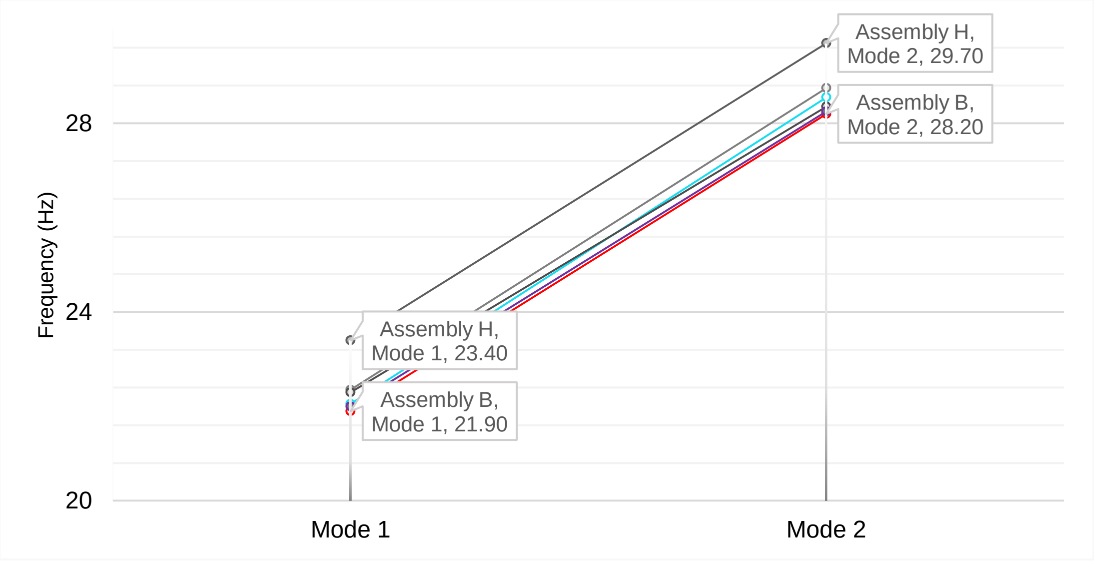

Figure 6.13 *Modes 1 and 2, Assemblies A, B, E, F, G, and H*

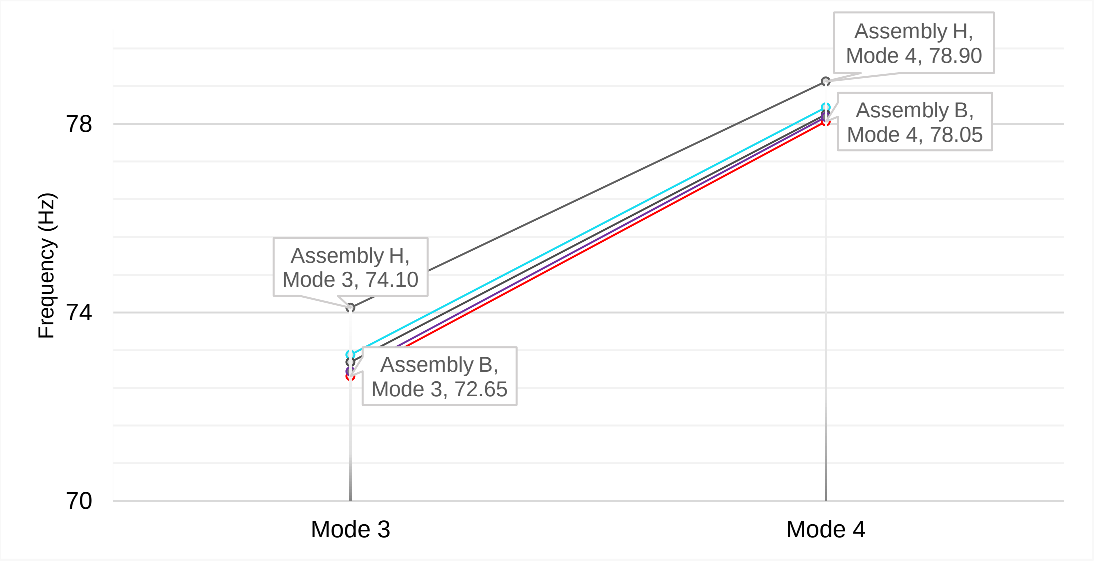

Figure 6.14 *Modes 3 and 4, Assemblies A, B, E, F, G, and H*

Comparing alternative screw assemblies without brackets was generally negligible. Reducing the spacing of vertical screws from 300 mm (Assembly B) to 150 mm spacing (Assembly A) provided little improvement in the frequency results, with less than a 1 Hz variance for all modes. Using an alternative configuration of inclined fully threaded cylindrical-head screws (Assembly E) was also negligible.

Two different angle brackets in addition to vertical screws at 300 mm spacing (Assembly B) were tested separately at 800 mm. The brackets used were 240 mm x 93 mm x 120 mm (TTN 240) and 100 mm x100 mm x 90 mm (WBR 100) angle brackets (Assemblies F and G, respectively). A negligible difference in the mode shapes and natural frequency values were recorded for all three assemblies (less than 1 Hz variance for all modes). Reducing the bracket (WBR 100) spacing to 200 mm (Assembly H) improved the frequency results, increasing the fundamental frequency by over 6%. This trend continued for the higher modes by a smaller margin.

Added mass and added resilient interlayer *(Assemblies B, C, and D)*

The influence of adding a resilient interlayer (Assembly C), and the addition of a non-structural mass evenly distributed across the floor (Assembly D) are charted alongside the baseline fixing configuration of vertical screws at 300 mm spacing (Assembly B) in Figure 6.15.

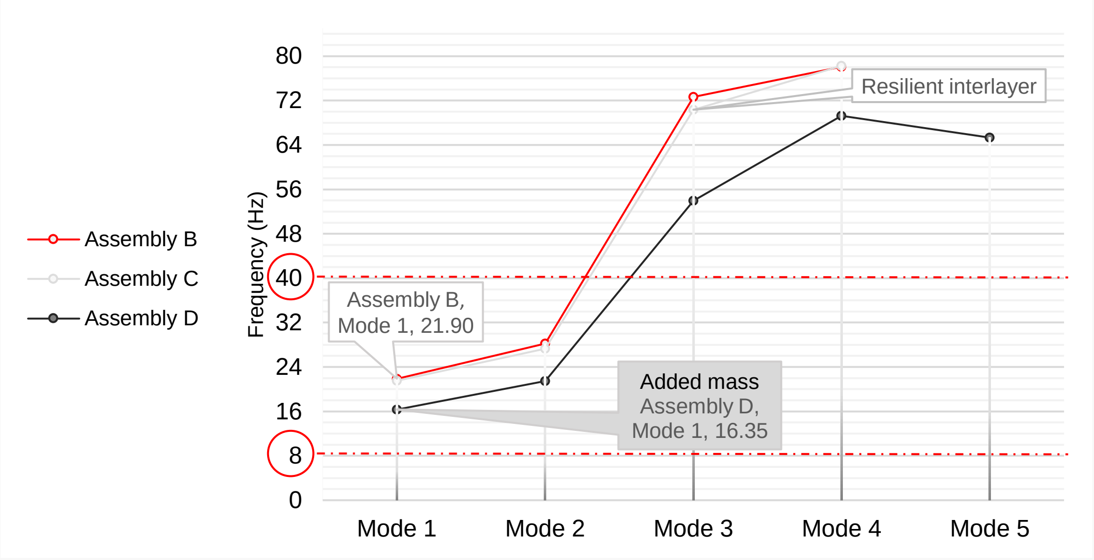

Figure 6.15 *Natural frequency results for the one-way long span platform construction, using partially threaded vertical screws @ 300 mm c/c (Assembly B), with resilient layer (Assembly C), and with added non-structural load (Assembly D)*

Introducing a resilient interlayer (Assembly C) reduced the frequency results for all modes. However, the difference was relatively small. The greatest variance was no more than 3% for the third natural mode.

The addition of a non-structural mass on the floor (Assembly D) significantly reduced all frequency mode values and increased the number of modes from four to five in the frequency range of interest (Figure 6.8). The first three mode values were reduced by up to 25%. The fundamental mode decreasing from 21.90 Hz to 16.35 Hz. The mode separation was marginally reduced for the loaded floor, however only a single first-order and second-order mode were measured below the 40 Hz range. All frequency values were greater than the EC-5 [22] 8 Hz limit.

One-way long-span balloon construction *(Assemblies I to K)*

The modal frequency results for the alternative balloon constructions one-way spanning floors, loaded and unloaded are charted in Figure 6.16.

Note: Mode 4 and Mode 5 are swapped in Figure 6.16 compared with Figure 6.7, so that the similar mode shapes are represented for each of the alternative assemblies.

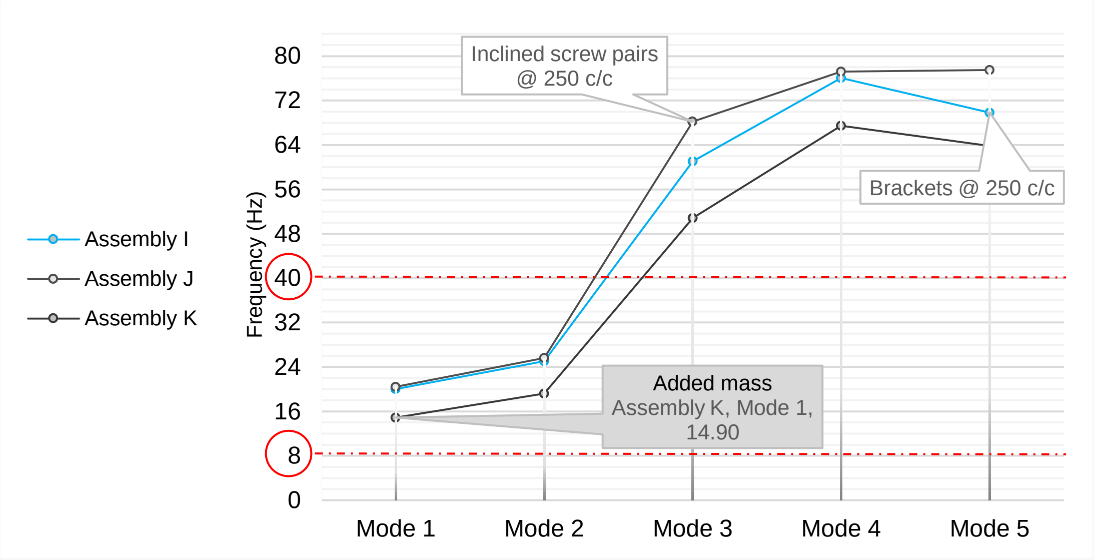

Figure 6.16 *Natural frequency results for the one-way long span balloon construction, using brackets and inclined fully threaded screws (Assembly J), and with added non-structural load (Assembly K)*

Comparing the floor panel supported on angle brackets at 250 mm spacing (Assembly I) with fixing the floor with inclined screws pairs of fully-threaded screws at 250 mm spacing (Assembly J) shows an insignificant variation between the first two mode values, less than 1 Hz in both instances. A more pronounced variation can be observed with the higher modes. Higher natural mode values were measured for the inclined screw pair assembly (Assembly J), an increase of over 10% for Mode 3 and Mode 5.

Adding mass again reduced the frequency results by over 25% for the first three modes, and by over 12% for the fourth and fifth modes. The fundamental frequency value decreased from 20.45 Hz to 14.90 Hz. This was the lowest fundamental frequency value measured in the laboratory testing. However, the floor assembly can be regarded as a high frequency floor (BS 6472-1: 2008 [117]), and therefore is unlikely to resonate with footfall excitation.

One-way short-span platform construction *(Assemblies L to O)*

Supporting the floor in the alternative direction (Figure 5.4), reduced the span to 2212 mm, which therefore changed the mode shapes and increased the natural frequency values. Four natural modes were recorded in the range of interest (Figure 6.9). However, the influence of using alternative fixing configurations in the floor could again be regarded as insignificant. The frequency values of the modes are shown in Figure 6.17.

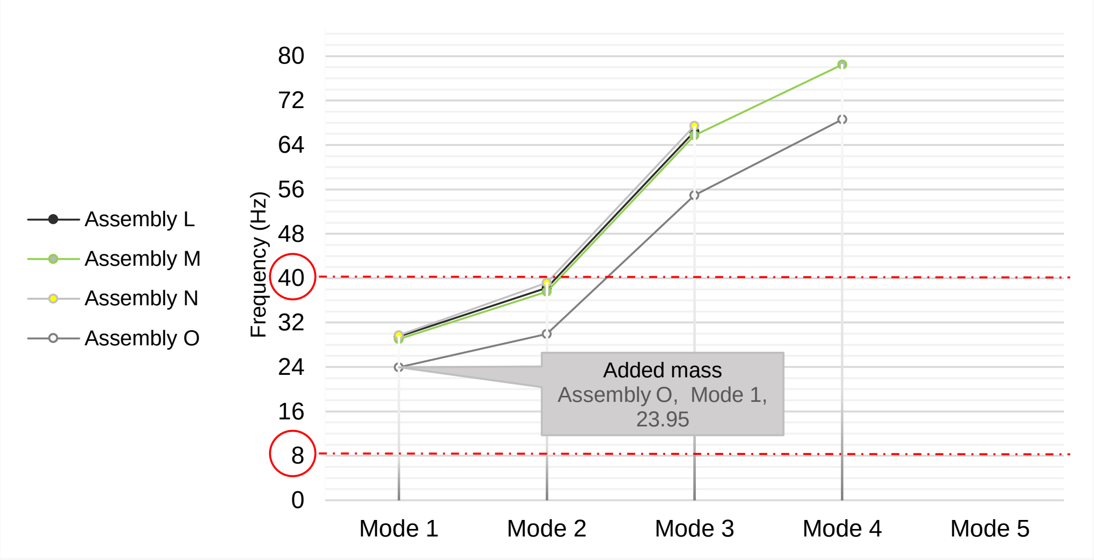

Figure 6.17 *Natural frequency results for the alternative bracket and screw configurations for one-way short span platform construction, and with added non-structural load (Assembly O)*

Increasing the spacing of vertical screws from 300 mm centres (Assembly L) to 600 mm spacing (Assembly M) resulted in a negligible difference in the natural mode shapes and frequency values. The variance was less than 1 Hz variance for all modes.

Similarly, the difference in frequency results was negligible due to the addition of 240 mm x 93 mm x 120 mm (TTN 240) angle brackets at 800 mm spacing (Assembly N) compared with the vertical screw only configuration (Assembly M).

The addition of a distributed non-structural mass on the floor (onto the baseline Assembly N), (Assembly O) reduced the frequency values by up to 23% (at Mode 2).

Values for the fundamental mode ranged between 29.05 Hz and 29.70 Hz for the floor assemblies without added mass, this value decreased to 23.95 Hz due to the addition of mass. A minimum mode separation of 8 Hz was recorded between the modes in the case of the floor spanning 2212 mm. Only one first-order and second-order mode were measured below the 40 Hz unit impulse criteria limit, and all natural frequency values were greater than the EC-5 [22] 8 Hz limit.

Two-way platform construction *(Assembly P)*

The recorded natural frequency results between 0 and 80 Hz for the CLT floor spanning in one direction and in two directions (Assemblies L and P, respectively) are illustrated in Figure 6.18.

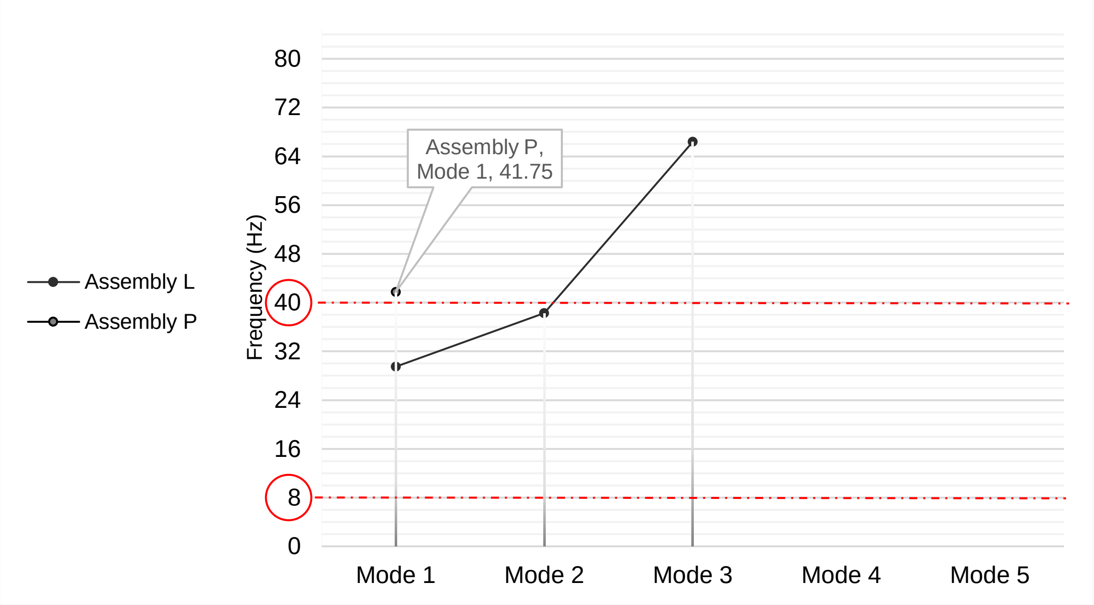

Figure 6.18 *Natural frequency results for the one-way short span and two-way span platform construction (Assemblies L and P)*

Spanning in two directions using vertical partially-threaded screws at 300 mm spacing (Assembly P) compared with the same fixing configuration for a short span floor (Assembly L) increased the natural frequency values considerably, from 29.50 Hz to a value of 41.75 Hz for the fundamental mode for the two-way spanning floor.

Summary of frequency results

All laboratory CLT floor assemblies tested performed well with regard to current European timber design frequency criteria (EC-5 [22]). The fundamental frequency values all measured above the 8 Hz limit and only one first-order and one second-order mode were measured below the 40 Hz unit impulse criteria limit. The mode separation between the first and second modes, and third and fourth modes were greater than 5 Hz for all assemblies. The frequency values of the second to third mode was generally much higher, ranging up to a 44 Hz difference between the mode values.

The 15.5 kg mass of the electromagnetic shaker was found to not notably affect the natural frequency values of the CLT floor (>700 kg) comparing the balloon constructed 4000 mm span floor.

Alternative fixings generally had negligible impact on the floor’s natural frequencies values. The most significant improvement was measured in the case of the assembly that provided angle brackets a 200 mm spacing. This assembly increased the natural frequency values of the floor by up to 6%. Adding a resilient interlayer reduced the frequency results for all modes. However, the difference was less than 3%.

The orientation of the floor panel and the addition of an imposed load most influenced the frequency and mode shape results. The frequency values increased with reduced floor span and decreased with the addition of a distributed load. Spanning in two directions increased the natural frequency values considerably, by over 40%. As the fundamental frequency was greater than 40 Hz, in the case of the two-way spanning floor assembly, the EC-5 [22] unit impulse velocity limit would not be applicable for this floor assembly.

6.2.5 Acceleration amplification results

FRF accelerance measurements *(Assemblies A to P)*

The resonant accelerance magnitude was measured in the case of each natural mode in the frequency range between 0 to 80 Hz for each assembly configuration. FRF was used to determine the vibration magnitude in response to a discrete sinusoid forcing signal of a fixed amplitude and frequency. The frequencies corresponded to the resonant values that were measured (Table 6.5). The excitation force was applied at either the midspan or quarter span depending on the mode shape. The responses were measured twice concurrently, one positioned at the point of maximum deflection identified in the mode shape measurements, with a control measurement recorded at midspan for all the modes. The average of three measurements of the accelerance at the point of maximum vibration for each mode are outlined in Table 6.6 and Figure 6.19, while comparisons between acceleration results of the various floor assemblies are explored in Figures 6.20 to 6.25.

The accelerance value and the point on the floor grid where the accelerance was measured for each mode is depicted for all assemblies in Appendix B.

Table 6.6 *Accelerance for floor to wall, Assemblies A to P*

Floor to wall Assembly	*Resilient layer*	*Load added*	*Acceleration amplification (m/s^2/N)*				
			Mode 1	*Mode 2*	*Mode 3*	*Mode 4*	*Mode 5*
	One-way long span: Platform construction						
A			*0.134*	*0.127*	*0.058*	*0.303*	-
B			*0.137*	*0.111*	*0.051*	*0.289*	-
C	●		*0.131*	*0.074*	*0.027*	*0.232*	-
D		●	*0.046*	*0.028*	*0.026*	*0.031*	*0.061*
E			*0.172*	*0.145*	*0.062*	*0.277*	-
F			*0.148*	*0.132*	*0.063*	*0.311*	-
G			*0.148*	*0.107*	*0.063*	*0.279*	-
H			*0.147*	*0.137*	*0.050*	*0.301*	-
	One-way long span: Balloon construction						
I			*0.108*	*0.117*	*0.051*	*0.157*	*0.057*
J			*0.116*	*0.099*	*0.055*	*0.294*	*0.125*
K		●	*0.038*	*0.018*	*0.011*	*0.027*	*0.019*
	One-way short span: Platform construction						
L			*0.024*	*0.101*	*0.215*	-	-
M			*0.026*	*0.108*	*0.197*	*0.015*	-
N			*0.013*	*0.105*	*0.225*	-	-
O		●	*0.035*	*0.027*	*0.040*	*0.026*	-
	Two-way span: Platform construction						
P			*0.158*	-	-	-	-

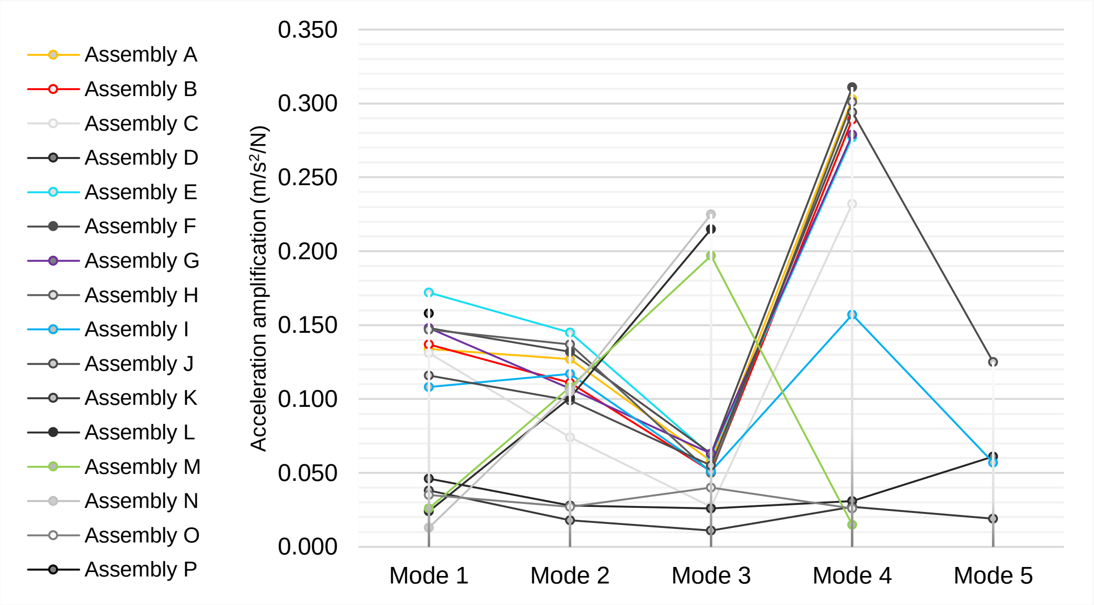

Figure 6.19 *Accelerance results for floor to wall assemblies A to P*

The overall FRF accelerance measurements ranged from 0.011 m/s^2/N to 0.311 m/s^2/N. The highest values were recorded in the case of the fourth mode, for both unloaded long spanning balloon and platform constructions. Adding additional mass to the floor generally improved vibration acceleration with the lowest accelerance value recorded for the third mode of the balloon construction with mass added (Assembly K).

One-way long-span platform construction *(Assemblies A, B, and E to H)*

The accelerance values for the one-way long-span platform construction results are shown in Figures 6.20 and 6.21.

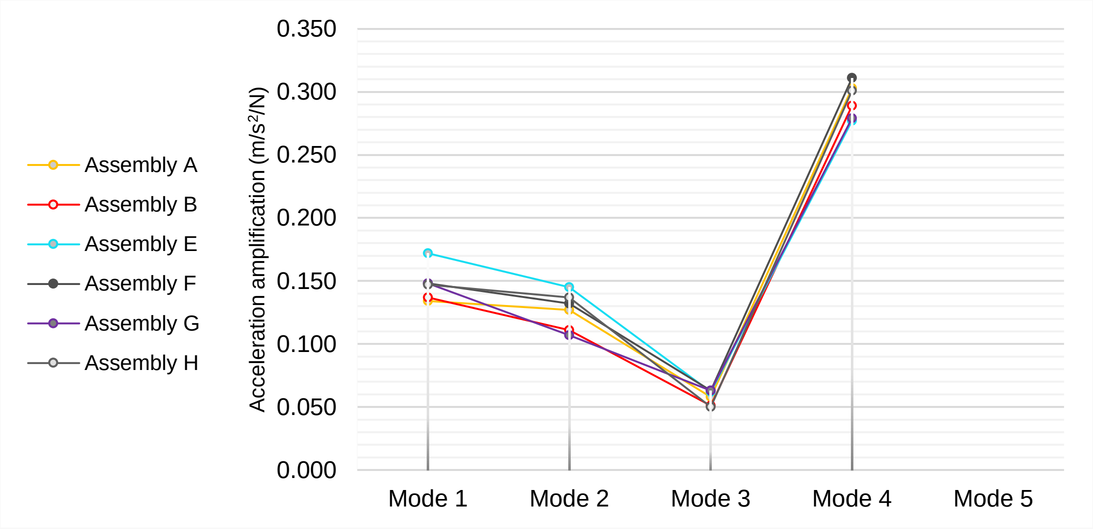

Figure 6.20 *Accelerations results for one-way long span platform construction, without resilient interlayer or added load, Assemblies A, B, E, F, G, and H*

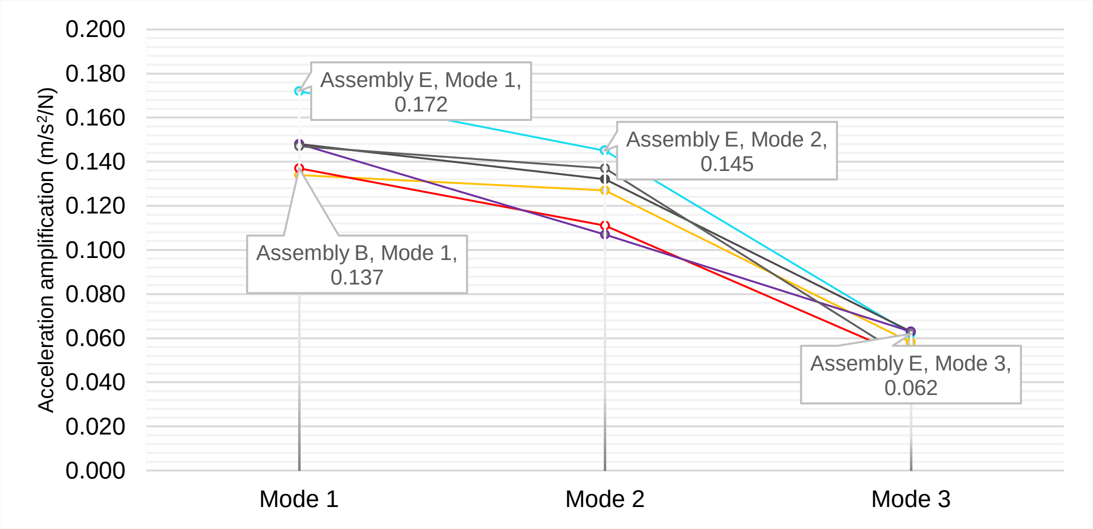

Figure 6.21 *Accelerations results of Assemblies A, B, E, F, G, and H Modes 1, 2, and 3*

The accelerance measurements in the case of the one-way long-span platform constructions ranged from 0.051 m/s^2/N to 0.311 m/s^2/N. From the modal frequency analysis the first and second modes of each assembly are most critical with regard to floor excitation as they occur below the 40 Hz footfall excitation frequency value defined in EC-5 [22]. Results ranged from 0.131 m/s^2/N to 0.172 m/s^2/N, for Mode 1 and from 0.107 m/s^2/N to 0.145 m/s^2/N, for Mode 2.

In the case of the alternative assemblies connected with screws and without brackets, reducing the spacing of vertical screws from 300 mm (Assembly B) to 150 mm spacing (Assembly A) had a negligible influence on accelerance values. Using an alternative configuration of inclined fully threaded cylindrical-head screws (Assembly E) recorded the highest FRF accelerance for the first two modes. An increase of 25% and 30%, respectively.

Comparing vertical partially-threaded screws at 300 mm spacing (Assembly B) with the same configuration with the addition of angle brackets of different types (TTN 240 and WBR 100) at 800 mm spacing generally increased the magnitudes of the resonant vibrations, marginally. Reducing the bracket (WBR 100) spacing to 200 mm (Assembly H) was found to increase the accelerance response, most notably at Mode 2 by 23%.

The variance was negligible between all assemblies for the third mode ranging between 0.050 m/s^2/N and 0.063 m/s^2/N. On average the lower vibration levels were recorded for the configuration consisting the vertical screws at 300 mm spacing (Assembly B).

The addition of angle brackets general increased accelerance values.

Added mass and added resilient interlayer *(Assemblies B, C, and D)*

The influence of adding a resilient interlayer and an evenly distributed mass (Assemblies C and D) are charted in Figure 6.22.

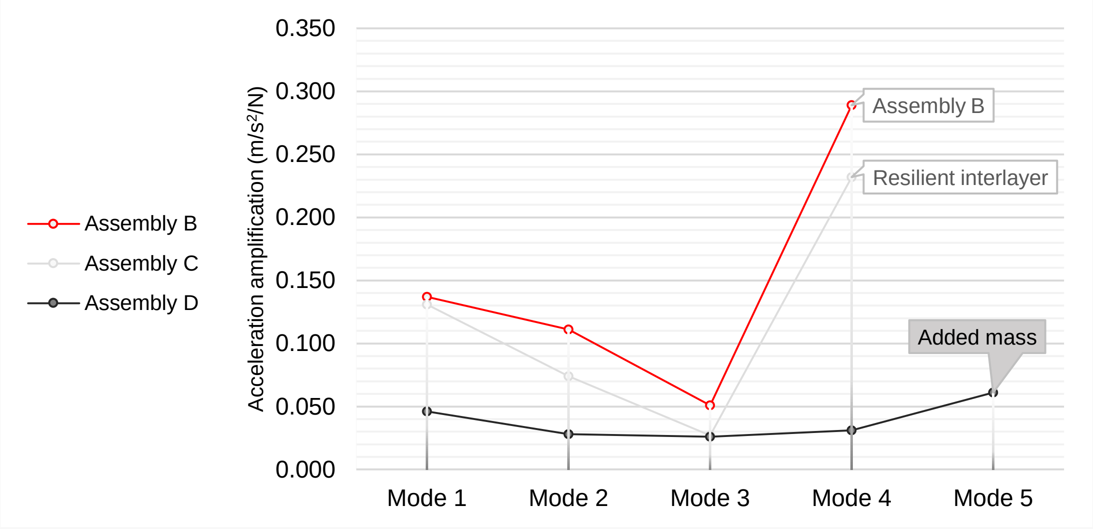

Figure 6.22 *Acceleration results of long span platform construction with vertical screws @ 300 mm c/c, with resilient layer (Assembly C), with added non-structural load (Assembly D)*

Introducing a resilient interlayer (Assembly C) improved the vibration magnitudes. The improvement to the vibration levels was relatively minor in the case of the fundamental frequency, but improved results by over 19% for the higher resonant modes. Adding a non-structural mass (Assembly D) reduced accelerance values significantly, improving the results by over 49% compared with the floor without mass added (Assembly B).

One-way long-span balloon construction *(Assemblies I to K)*

The FRF accelerance at the resonant frequencies of the one-way balloon construction assemblies are shown in Figure 6.23.

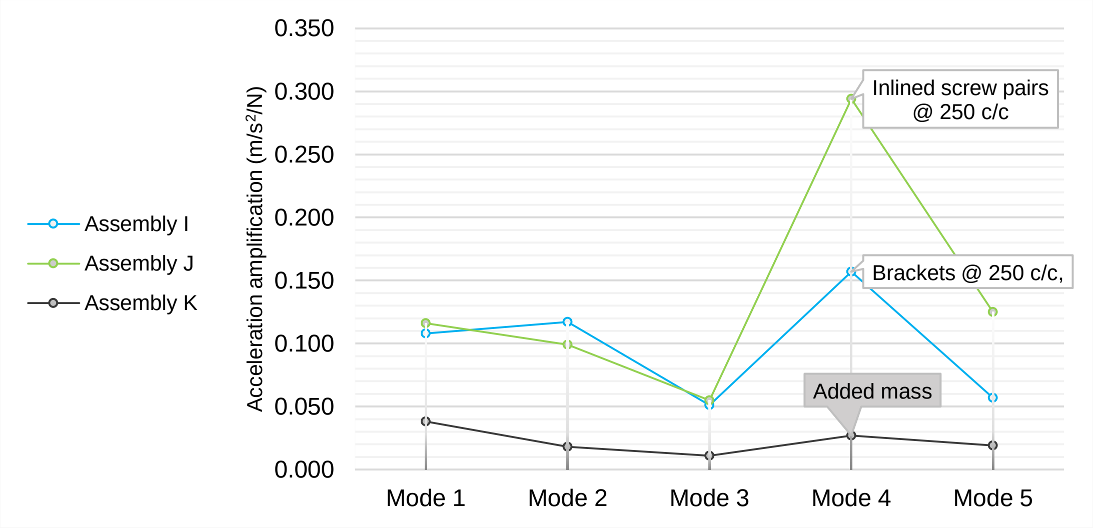

Figure 6.23 *Acceleration results for the balloon construction (Assemblies I, J, and K)*

Comparing the floor panel supported on angle brackets at 250 mm spacing (Assembly I) with fixing the floor with inclined screws pairs of fully-threaded screws at 250 mm spacing (Assembly J) found the bracket supported floor generally performed better with lower acceleration magnification values for all modes other than the second mode.

Adding an evenly distributed mass (Assembly K) reduced the vibration results for all modes, all measuring below 0.038 m/s^2/N. The acceleration magnitude results for the same floor configuration unloaded (Assembly J) ranged between 0.055 and 0.294 m/s^2/N.

One-way short-span platform construction *(Assemblies L to O)*

The FRF accelerance of the one-way short-span platform construction resonant modes are charted in Figure 6.24.

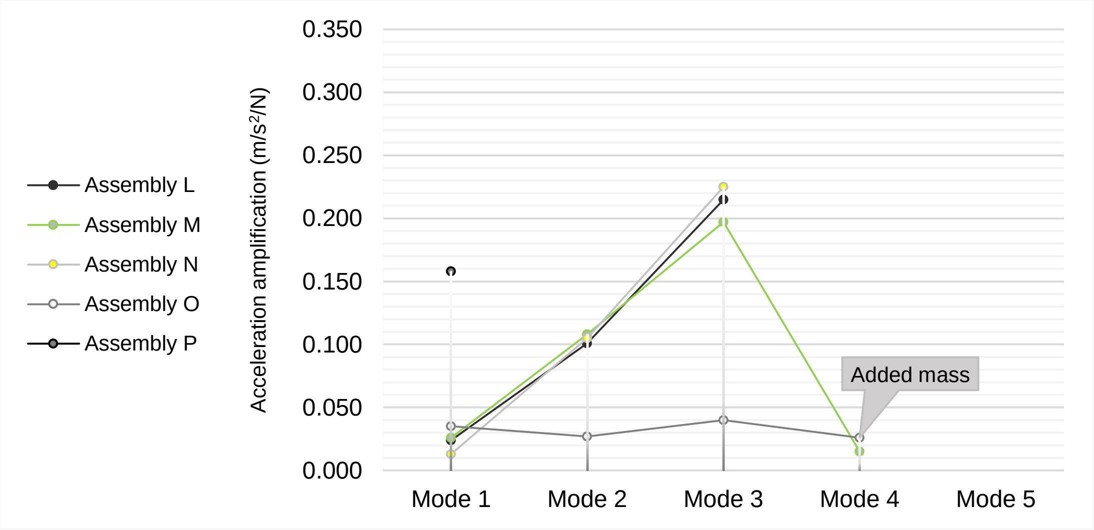

Figure 6.24 *Accelerance results for the alternative bracket and screw configurations for one-way short span platform construction (Assemblies L to N), and with added non-structural load (Assembly O)*

Increasing the spacing of vertical screws from 300 mm centres (Assembly L) to 600 mm spacing (Assembly M) resulted in a negligible difference in the accelerance values of the first two modes. The variance was more notable for the third mode, with a decrease of 8% recorded in the assembly with lesser screws (Assembly M).

Comparing the results due to the addition of angle brackets (TTN 240) at 800 mm spacing (Assembly N) with the vertical screw only configuration (Assembly M) showed a reduction in the vibration response for the first two modes but an increase of 14% was shown for the third mode, in the assembly that included brackets (Assembly N).

The addition of a distributed non-structural mass on the floor (onto the baseline Assembly N), (Assembly O) generally reduced the level of resonant vibration significantly, with levels measuring below 0.040 m/s^2/N as a result of all excitations resonant with the natural modes. One exception to this trend was in the case of the fundamental mode where the accelerance level was increased from 0.013 m/s^2/N to 0.035 m/s^2/N, respectively. The accelerance level for the floor without brackets (Assembly M) at this mode was recorded at 0.026 m/s^2/N.

Two-way platform construction *(Assembly P)*

The comparable one- and two-way floor configurations (Assemblies L and P, respectively) are charted in Figure 6.25.

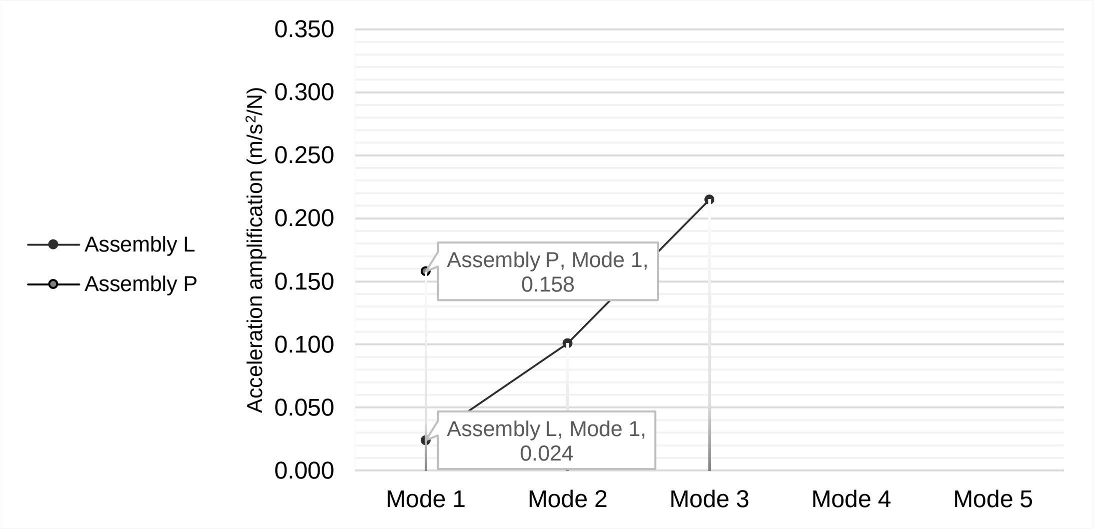

Figure 6.25 *Acceleration results of one- and two-way spanning platform construction acceleration values (Assemblies L and P, respectively)*

Spanning in two directions using vertical partially-threaded screws at 300 mm spacing (Assembly P) compared with the same fixing configuration for a short span floor (Assembly L) showed an increase in the magnitude of the vibration response, from 0.024 m/s^2/N to 0.158 m/s^2/N, respectively. An increase of six times the vibration response. However the modes are not the same shape nor are the frequency values similar.

Summary of FRF acceleration results

Alternative vertical screw spacing (Assemblies A and B) generally had negligible influence on accelerance values, with the assembly using inclined screw pairs resulting higher vibration response magnitudes (Assembly E).

The addition of angle brackets generally increased accelerance values, resulting in a poorer serviceability performance. Increasing the number of brackets was found to increase the accelerance response, by up to 23% when the angle brackets (WBR 100) were spaced at 200 mm (Assembly H).

Adding a resilient interlayer (Assembly C) reduced the vibration magnitude for all modes. Adding a non-structural mass reduced the magnitudes of vibration responses more significantly. Both cases improving the serviceability performance of the floor.

Spanning in two directions using vertical partially-threaded screws at 300 mm spacing showed an increase in the magnitude of the vibration response, which is not desirable in floor vibration. However, the frequency value was also substantially higher which would result in greater tolerance to vibrations resonant with that mode [115].

The acceleration weighting curves charted in BS 6472-1: 2008 [117] and ISO 10137: 2007 [115] bound the maximum human sensitivity for vertical acceleration between 4 and 8 Hz, with any floor acceleration in this range deemed to be tolerable below 0.005 m/s^2.

Human tolerance to vibration is always subjective. It depends on each occupant, their activity, the type of building occupied, and the time of day. Additionally the nature of the vibration, whether it is continuous, intermittent, or occasional, with a constant or variable amplitude are all considered when accessing the tolerance of vibration in buildings. The vibration responses that were measured in the laboratory were continuous with a constant amplitude. Only the resonant frequencies were considered. The same excitation force was applied to each mode measured, in so far as the mass and power to the exciter was constant. The frequency varied depending on the mode.

Considering acceleration tolerance criteria (ISO 10137: 2007 [115]), the magnitude of discomfort to a building occupant is relative to the frequency of the vibration.

For example, taking the lowest fundamental frequency value measured in the laboratory testing of 14.90 Hz. This value was recorded for the balloon constructed 4000 mm floor with added mass (Assembly K). Applying the weighting curves suggests that an acceleration value of 0.009 m/s^2 is most tolerable for vibration at this frequency in the vertical direction. Additionally applying a sample multiplying factor relative to the time of day and building use, this acceleration limit may be multiplied by four for residential and office buildings during the day. This improves the level which is tolerable to 0.036 m/s^2.

Then considering the fundamental frequency of the same floor assembly without added mass (Assembly J) which was recorded as 20.45 Hz. Applying the same weighting curves, gives a minimum tolerable vertical acceleration value of 0.013 m/s^2, again multiplied by four gives an acceptable vibration amplitude for a constant vibration of 0.052 m/s^2. The tolerance limit is greater for the floor without added mass, due to the increased resonant frequency value.

The permitted acceleration values relative to the frequencies of the natural modes (ISO 10137: 2007 [115]) for a daytime residential building are charted in Table 6.7 and Figure 6.26. The unit force acceleration results for both floor assemblies are included for comparison. The limit values are shown dotted.

Table 6.7 *Frequency dependant measured and permitted accelerations. Unit force measured values and residential daytime limits*

Floor to wall Assembly	*Resilient layer*	*Load added*	*Acceleration amplification (m/s^2/N)*				
			Mode 1	*Mode 2*	*Mode 3*	*Mode 4*	*Mode 5*
	One-way long span: Balloon construction						
J			*0.116*	*0.099*	*0.055*	*0.294*	*0.125*
K		●	*0.038*	*0.018*	*0.011*	*0.027*	*0.019*
	Acceleration limit ISO 10137: 2007 [115] *(m/s^2)*						
J'			*0.052*	*0.064*	*0.156*	*0.188*	*0.172*
K'		●	*0.036*	*0.052*	*0.120*	*0.168*	*0.160*

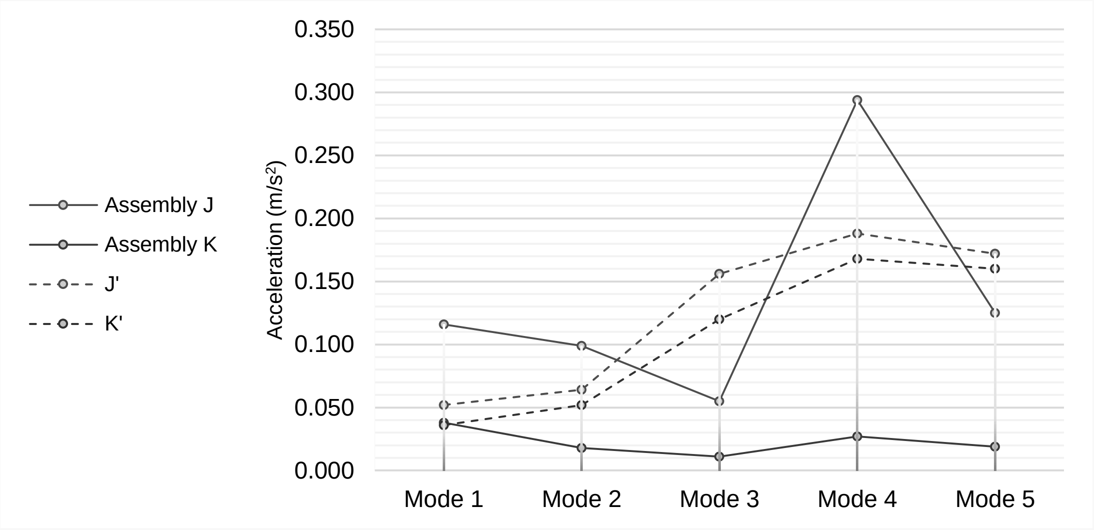

Figure 6.26 *Frequency dependant accelerance measured, with permitted residential daytime acceleration limit values*

As illustrated in the graph by the dotted lines, a higher tolerance is assumed in the severability criteria (ISO 10137: 2007 [115]) at the natural modes of the unloaded floor due to their higher frequency values. An accelerance level of 0.052 m/s^2 compared with 0.036 m/s^2 for the fundamental frequency. However, adding mass significantly improves the response of the floor. So although the acceleration limits are higher for the floor without mass, the vibration responses in the floor with mass are appreciably reduced. Hence, better compliance with the tolerance criteria in the floor with added mass despite the lower frequency values.

Similarly, Table 6.8 with Figures 6.27 and 6.28 illustrate the measured and possible permitted accelerance values (ISO 10137: 2007 [115]) in the case of the laboratory long and short span platform floors, Assemblies B and D, and Assemblies N and O, respectively.

Table 6.8 *Frequency dependant measured and permitted accelerations. Unit force measured values and residential daytime limits (Platform assemblies)*

Floor to wall Assembly	*Resilient layer*	*Load added*	*Acceleration amplification (m/s^2/N)*				
			Mode 1	*Mode 2*	*Mode 3*	*Mode 4*	*Mode 5*
	One-way long span: Balloon construction						
B			*0.137*	*0.111*	*0.051*	*0.289*	*-*
D		●	*0.046*	*0.028*	*0.026*	*0.031*	*0.061*
N			*0.013*	*0.105*	*0.225*	*-*	*-*
O		●	*0.035*	*0.027*	*0.040*	*0.026*	*-*

	Acceleration limit ISO 10137: 2007 [115] *(m/s²)*						
B'			*0.052*	*0.072*	*0.180*	*0.196*	-
D'		●	*0.036*	*0.052*	*0.120*	*0.180*	-
N'			*0.072*	*0.100*	*0.180*	-	-
O'		●	*0.060*	*0.072*	*0.152*	*0.180*	-

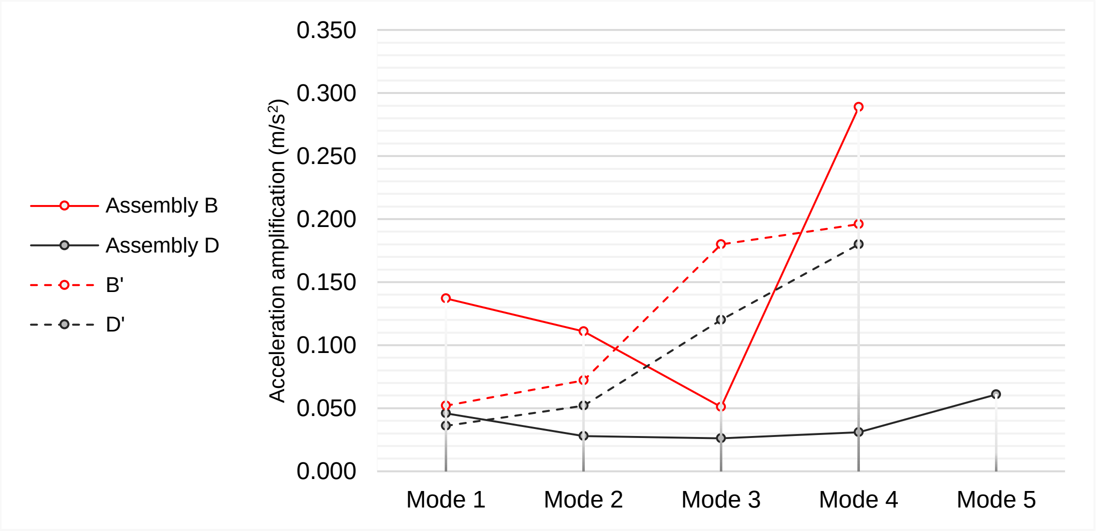

Figure 6.27 *Frequency dependant accelerance measured, with permitted residential daytime acceleration limit values (Assemblies B and D)*

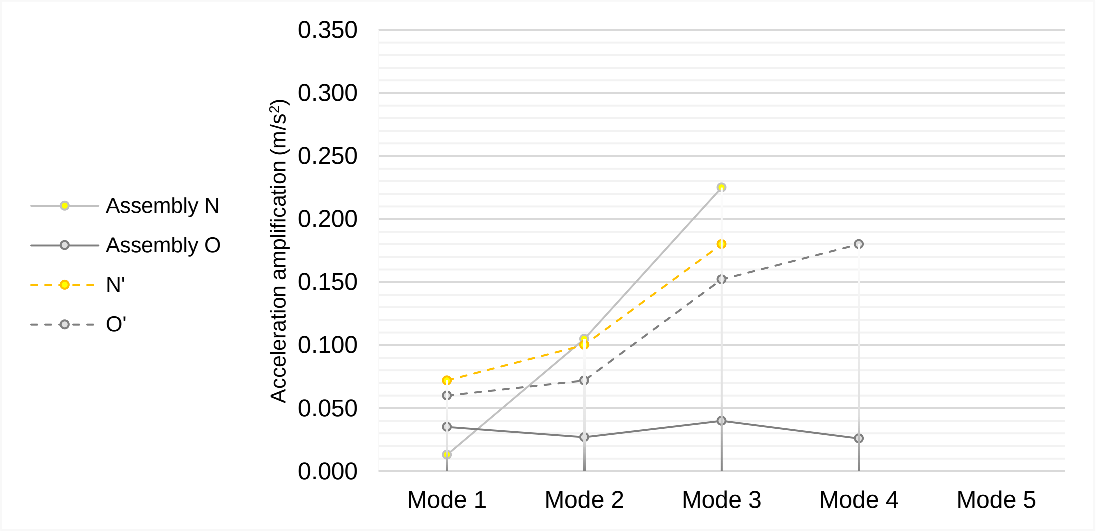

Figure 6.28 *Frequency dependant accelerance measured, with permitted residential daytime acceleration limit values (Assemblies N and O)*

6.2.6 Footfall acceleration results

Walking accelerance measurements *(Assembly A)*

A number of response measurements were taken of footfall on the CLT floor to observe the response of the floor due to a likely excitation.

Comparing the unit force accelerance values for each of the assemblies (A to P) due to the mechanical shaker excitation for each of the resonant modes (Modes 1 to 5) informs the knowledge on how the alternative parameters tested affect the magnitude of vibration in a CLT floor. However, predicting the response vibration level due to a non-mechanical and non-stationary excitation at the building design stage is not so straightforward. Footfall is one such excitation source. The magnitude of the response of the floor will be determined primarily by the floors fundamental frequency, which establishes whether it is a low or high frequency floor.

A low frequency floor is a floor with a fundamental frequency below 7 to 10 Hz and is susceptible to resonant build-up due to footfall. The resonant response is quantified in terms of acceleration with its magnitude determined by the floor’s mass and damping. The greater the mass the lower the response to excitation [117].

If the natural frequencies of the floor are greater than 8 to 12 Hz, the floor is described as a high frequency floor and the response from footfall can be considered as a series of transient responses to the individual impulses of the footfall impacts [117]. The response magnitudes are much less sensitive to damping and are quantified in terms of impulse velocity which is proportional to the floors fundamental frequency, the frequency of the footfall, and the modal mass and stiffness of the floor [20].

A number of walking tests were made measuring the vibration response on a bare one-way spanning CLT floor (Assembly A). Vibration measurements were taken of a single person walking in a random path. Three measurement were recorded of the footfall. A different adult was recorded each time. The adult’s masses ranged between 70 kg and 90 kg. A sample recording is illustrated in Figure 6.29.

Additionally, measurements were recorded of the three adults walking together and one person walking with the aid of a walking cane, shown in Figures 6.30 and 6.31, respectively. Figure 6.32 charts a sample response measurement of the mechanical exciter applying a force in resonance with the fundamental harmonic of the floor panel over a similar timeframe. The footfall responses were measured twice concurrently, positioning an accelerometer at the point of maximum deflection for the fundamental mode shape with a control accelerometer positioned midspan.

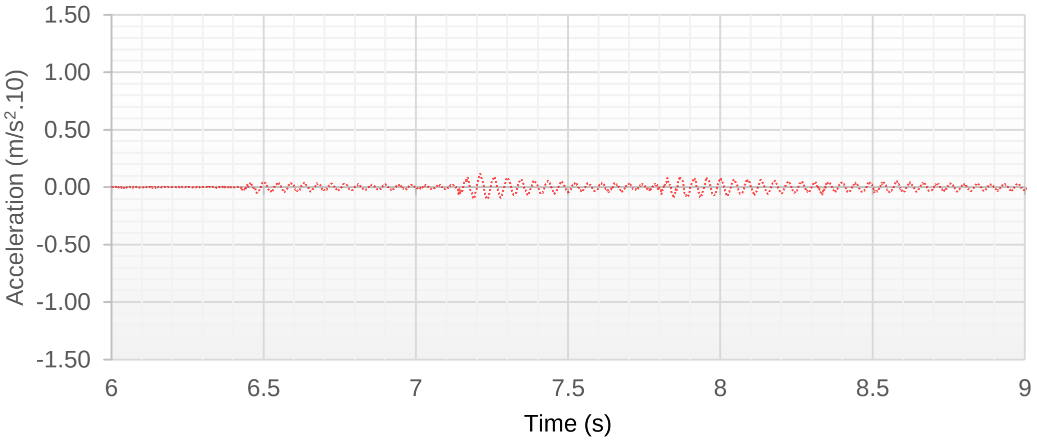

Figure 6.29 *Sample response measurement of one person walking (Assembly A)*

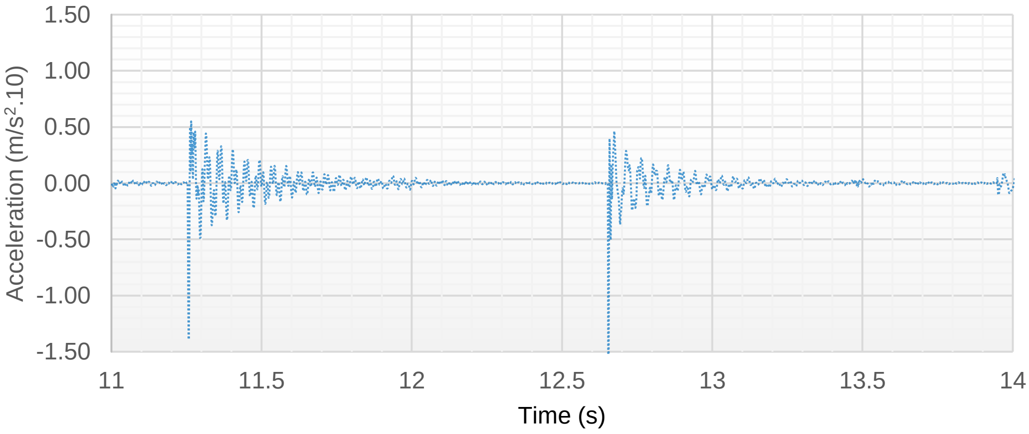

Figure 6.30 *Sample measurement of three adults walking (Assembly A)*

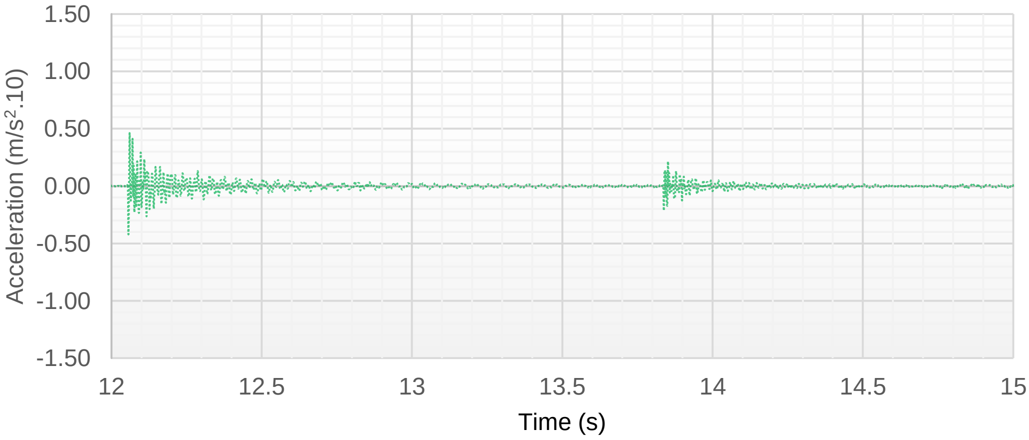

Figure 6.31 *Sample measurement of one person walking with a cane (Assembly A)*

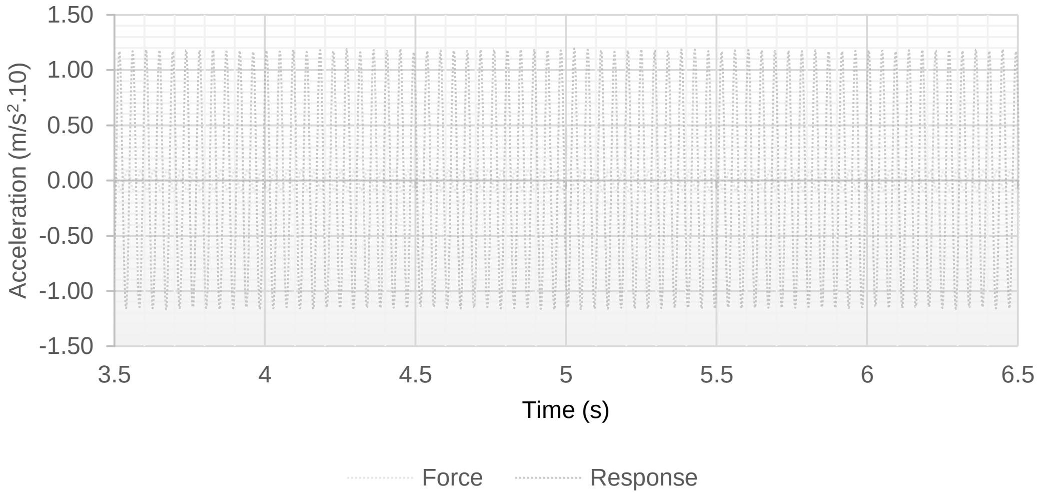

Figure 6.32 *Sample FRF accelerance fundamental frequency measurements (Assembly A)*

Each footfall is damped before the next impulse. There is no resonance build-up in the CLT floor. The measurements show clearly that assuming the response due to footfall to be a constant acceleration in this CLT floor assembly would be extremely conservative. More appropriate is to determine the impulse velocity of the footfall as outlined by Willford and Young's (CCIP016) [20].

The design calculations are outlined in Equations (3.56 to 3.60). Only the fastest walking pace and the fundamental frequency are considered in the calculation.

Applying the design equations and assuming the CLT floor to be of constant width and density, a unity value was taken for the flexural stiffness ratio in both orthogonal directions of the floor. The fundamental frequency value of the floor was measured as 22.35 Hz (Table 6.5, Assembly A). Estimating the fastest walking pace as 2.0 Hz and applying Equation 3.57 finds an effective design impulse value of 2.56 Ns for the first mode. Dividing the impulse value by the modal mass for the floor spanning in one direction gives a peak velocity of 0.007 m/s, equating to 0. 0021 m/s rms velocity.

Applying Equation (3.56), and dividing by 0. 0001m/s velocity baseline value gives an R-value of 21. The minimum limit allowed for impulse excitation with several occurrences per day in residential accommodation is 30 [115]. The minimum impulse vibration limit for offices is 60. The maximum limit for residential buildings at night is 20, therefore the calculated R-value of 21 may be deemed unacceptable, however from the accelerance values recorded due to the mechanical exciter (Table 6.6) the added mass reduced accelerance values by a third. The inevitable added mass on an in-situ floor due to fixtures and furniture can be expected reduce the vibration to within a tolerable range.

Alternatively if in the US or Canada, the CLT floor serviceability criteria [70][71] assume the vibration response due to footfall to be transient. Only the fundamental frequency of the floor and the 1 kN point load deflection are included in the acceptance criteria. Incorporating the measured fundamental frequency value of 22.35 Hz and midspan deflection of 0.179 mm (Tables 6.1 and 6.5, Assembly A), into Equations (3.63) and (3.64) shown below, shows that the CLT floor tested is substantially within the design parameters permitted.

$$f/_{d^{0.7}} \geq 13.0: \qquad 22.35\ Hz/_{0.179^{0.7}\ mm} = \mathbf{74.5} \qquad (3.63)$$

$$d \leq f^{1.43}/_{39}: \qquad 0.179\ mm \leq 22.35^{1.43} Hz/_{39} = \mathbf{2.18\ mm} \qquad (3.64)$$

6.2.7 Damping ratio results

***Damping ratio measurements** (Assemblies A to P)*

The damping ratios were measured for each floor assembly (A to P) at each natural frequency (Modes 1 to 5). An electromagnetic shaker fixed to the floor panel (Figure 5.26) provided a steady exciting force. After the vibration response reached steady-state the forcing vibration was stopped. The logarithmic decrement of the recorded decreasing vibration response determined the damping ratio values.

The responses were measured twice concurrently, one accelerometer positioned at the point of maximum deflection identified in the mode shape measurements with a control measurement recorded midspan for all the modes. The maximum vibration point for each mode is shown for all assemblies in Appendix B.

The forcing signal frequencies corresponded to the resonant values defined by the mode shape analysis (Table 6.5). The average of three measurements of each damping ratio values at the point on the floor of maximum acceleration are outlined in Table 6.9 and Figure 6.33.

Table 6.9 *Damping ratios for floor to wall, Assemblies A to P*

Floor to wall Assembly	Resilient layer	Load added	Damping ratios ζ (%)				
			Mode 1	Mode 2	Mode 3	Mode 4	Mode 5
	One-way long span: Platform construction						
A			0.94	0.90	1.32	0.61	-
B			0.98	0.93	1.54	0.68	-
C	●		1.05	1.28	1.52	0.82	-
D		●	1.66	2.79	1.56	1.74	1.17
E			0.85	0.82	1.18	0.66	-
F			0.92	0.88	1.30	0.65	-
G			0.96	0.91	1.36	0.63	-
H			0.87	0.84	1.20	0.63	-
	One-way long span: Balloon construction						
I			0.80	0.83	0.94	0.70	0.94
J			0.91	0.90	1.01	0.58	0.76
K		●	1.95	3.40	3.32	1.79	2.09
	One-way short span: Platform construction						
L			1.51	0.82	0.76	-	-
M			1.60	0.79	0.97	0.94	-
N			1.52	0.81	0.68	-	-
O		●	2.17	1.83	1.88	1.29	-
	Two-way span: Platform construction						
P			1.33	-	-	-	-

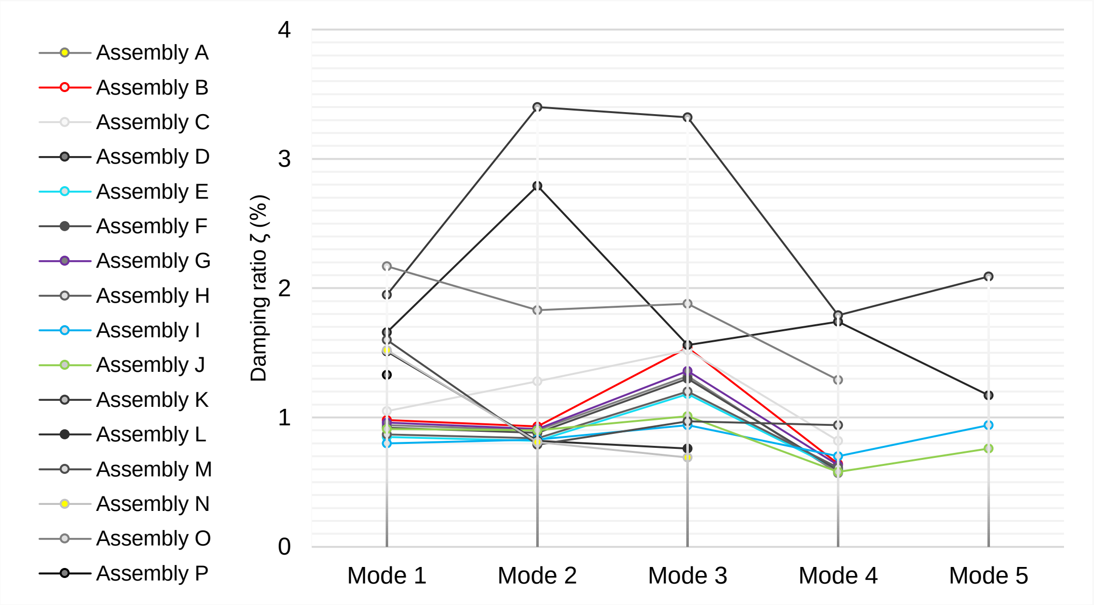

Figure 6.33 *Damping ratios results for floor to wall Assemblies A to P*

The damping ratio ζ results for all the assemblies tested ranged between 0.58% and 3.40%. The highest damping ratio ζ was found for the floor assembly of the largest span 4000 mm with an evenly distributed added mass (Assembly K). The corresponding balloon construction configuration without added mass (Assembly J) gave the lowest damping value ζ. Added mass to the floor generally improved damping results.

One-way long-span platform construction *(Assemblies A, B, and E to H)*

The damping ratio results for the one-way long-span platform construction without added mass or a resilient interlayer results are shown in Figures 6.34 and 6.35.

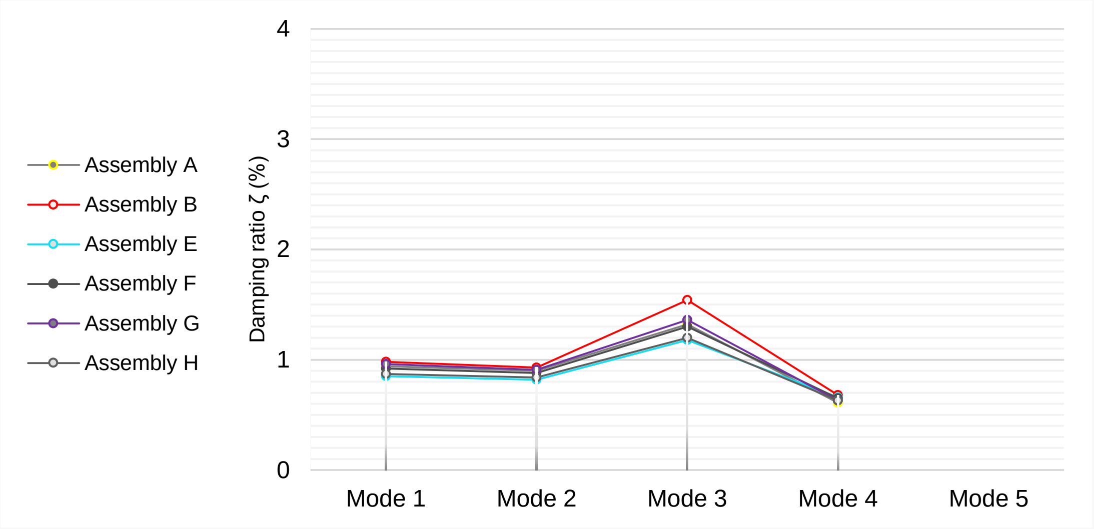

Figure 6.34 *Damping ratios results for one-way long span platform construction, without resilient interlayer or added load, Assemblies A, B, E, F, G, and H*

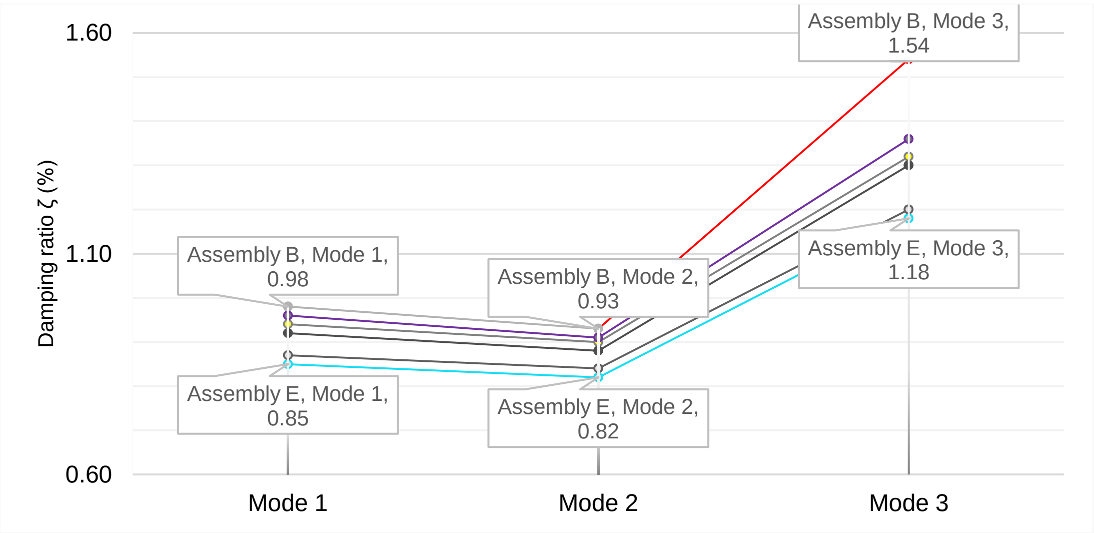

Figure 6.35 *Damping ratios results Assemblies A, B, E, F, G, and H: Modes 1, 2, and 3*

The damping ratio ζ measurements in the case of the one-way long-span platform constructions ranged from 0.61% to 1.54%. From the modal frequency analysis the first and second modes of each assembly are most critical with regard to floor excitation as they occur below the 40 Hz footfall value defined in EC-5 [22]. Results ranged from 0.85% to 0.98%, for Mode 1 and between 0.82% and 0.93%, for Mode 2.

The recorded measurements of the assembly with vertical screw spacing at 300 mm (Assembly B) were marginally higher than for the configuration using screws at 150 mm spacing (Assembly A). Values ranged from 0.98% to 0.94% and 0.93% to 0.90%, for the first two modes respectively. Using an alternative configuration of inclined fully threaded cylindrical-head screws (Assembly E) generally reduced the damping ratio ζ values, measuring 0.85% and 0.82% for the first and second mode, respectively.

Comparing vertical partially-threaded screws at 300 mm spacing (Assembly B) with the same configuration with the addition of angle brackets of different types (TTN 240 and WBR 100) at 800 mm spacing had a negligible influence on the damping ratio values ζ. Reducing the bracket (WBR 100) spacing to 200 mm (Assembly H) resulted in reduced damping ratio ζ values which were recorded at 0.87% and 0.84% for Modes 1 and 2, respectively.

In general, the damping ratio values ζ were improved with reduced number of fixings.

Added mass and added resilient interlayer *(Assemblies B, C, and D)*

The influence of adding a resilient interlayer (Assembly C), and the addition of a non-structural mass evenly distributed across the floor (Assembly D) are charted alongside the baseline fixing configuration of vertical screws at 300 mm spacing (Assembly B) in Figure 6.36.

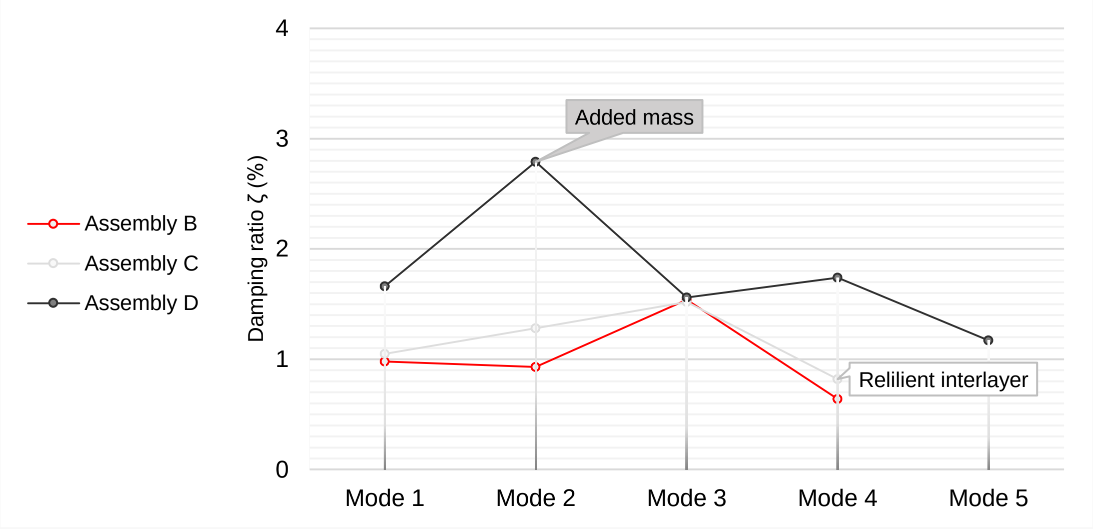

Figure 6.36 *Damping ratios results for one-way long span platform constructions (Assembly B), with a resilient layer (Assembly C), and with added mass (Assembly D)*

Introducing a resilient interlayer (Assembly C) improved the damping performance in the floor, however, the improvement was relatively minor in the case of Mode 1 and Mode 3, but improved from 0.93% to 1.28% for Mode 2 and from 0.68% to 0.82% for Mode 4. Adding a non-structural mass (Assembly D) generally improved the damping performance, increasing values by 69% for Mode 1 and by three times the damping ratio ζ for Mode 2.

One-way long-span balloon construction *(Assemblies I to K)*

The damping ratio values ζ at the resonant frequencies of the one-way balloon construction assemblies are charted in Figure 6.37.

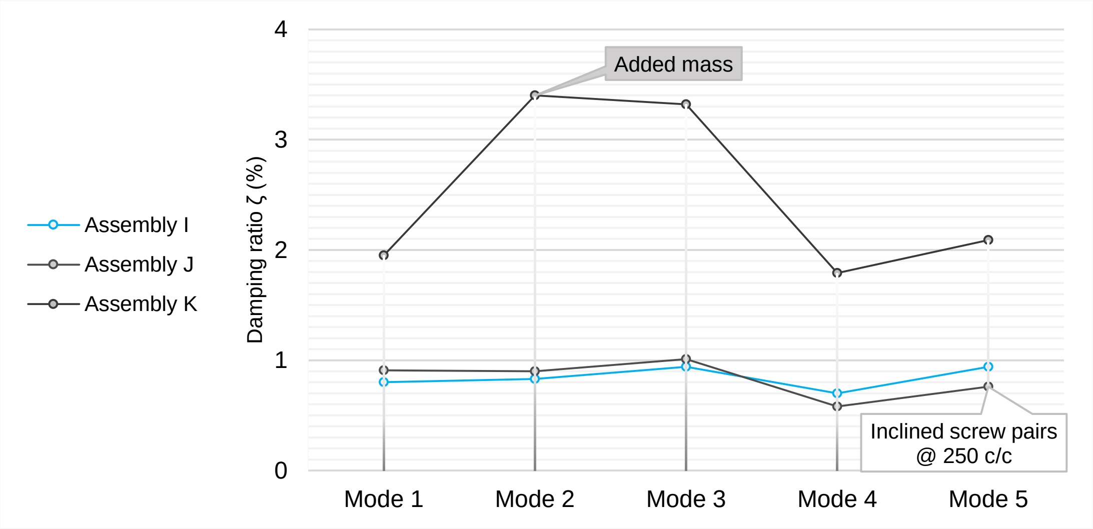

Figure 6.37 *Damping ratios results for the balloon construction (Assemblies I, J, and K)*

Comparing the floor panel supported on angle brackets at 250 mm spacing (Assembly I) with fixing the floor with inclined screws pairs of fully-threaded screws at 250 mm spacing (Assembly J) found the screw fixed floor generally performed better for Modes 1, 2, and 3. The damping for Modes 4 and 5 were improved in the bracket supported floor configuration (Assembly I). The variance was relatively small in all cases.

Adding an evenly distributed mass (Assembly K) significantly increased the damping results for all modes, with all damping ratio values ζ measuring in excess of 1.79% and up to 3.40%. The damping ratio ζ results for the same floor configuration unloaded (Assembly J) ranged between 0.58% and 1.01%.

One-way short-span platform construction *(Assemblies L to O)*

The one-way short span and two-way supported floor panel damping results are charted in Figure 6.38.

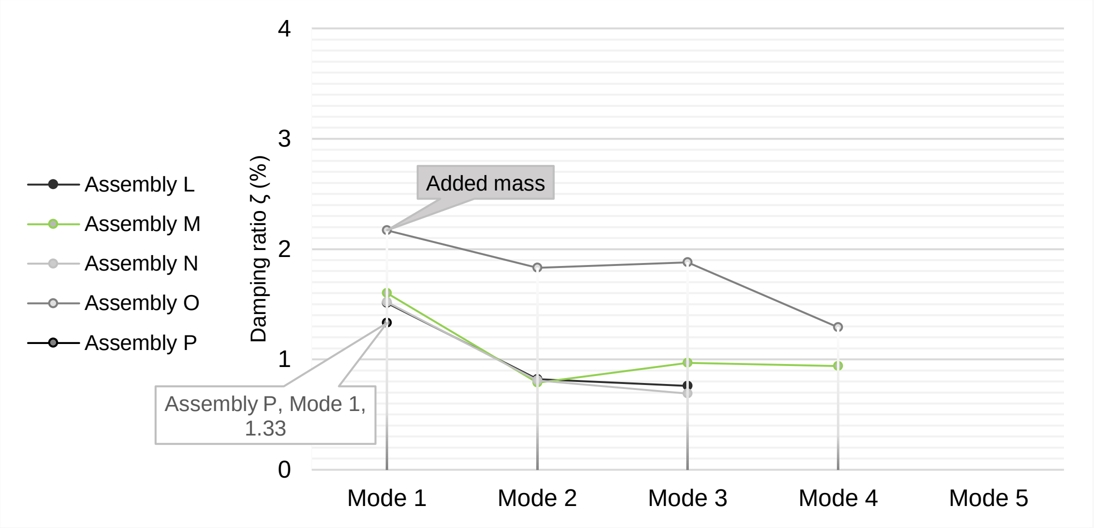

Figure 6.38 *Damping ratios results for the alternative bracket and screw configurations for one-way short span platform construction (Assemblies L to N), with added non-structural load (Assembly O), and the two-way spanning floor (Assembly P)*

Increasing the spacing of vertical screws from 300 mm centres (Assembly L) to 600 mm spacing (Assembly M) resulted in a negligible difference in the damping ratio values ζ. The difference was most significant for Mode 3 which improved from 0.76% to 0.97%.

Difference between the damping ratio ζ results with the addition of angle brackets (TTN 240) at 800 mm spacing (Assembly N) with the vertical screw only configuration (Assembly M) was negligible.

In general, the damping ratio values ζ were marginally improved with a reduced number of fixings.

Adding an evenly distributed mass (Assembly O) significantly increased the damping results for all modes, with all damping ratio values ζ measuring in excess of 1.29% and up to 2.17%. The damping ratio ζ results for the same floor configuration unloaded (Assembly N) ranged between 0.68% and 1.52%.

Two-way platform construction *(Assembly P)*

The damping ratio ζ of the natural mode that was recorded for the two-way floor configuration (Assembly P) is also charted in Figure 6.38. The ζ-value of 1.33% was less than the ζ-value for the fundamental mode of the one-way short span floor which ranged between 1.51% and 1.60%. However, the fundamental modes of the one-way short span and two-way supported floor panel are not the same shape nor are the frequency values similar.

Summary of damping ratio results

Results for all laboratory assembly configurations for ζ-values ranged between 0.58% and 3.40%. Changing the spacing of vertical screws (Assemblies A and B) generally had negligible influence on damping performance, but the alternative use of inclined screw pairs (Assembly E) resulted in a lower damping performance of the floor. Lower damping ζ values equate with poorer serviceability performance.

The addition of angle brackets of different types, in combination with vertical screws at 300 mm spacing, at 800 mm spacing also had a negligible influence on the damping ratio ζ results. Increasing the number of brackets by reducing the spacing to 200 mm (Assembly H) resulted in a further reduction of the damping ratio ζ of the floor. In general, increasing the number of fixing components reduced the damping performance of the floor.

The addition of a resilient interlayer (Assembly C) increased damping generally. Adding a non-structural mass improved damping results in all cases, with values for ζ ranging between 1.17% and 3.40% compared with the floor assemblies without an added mass that ranged from 0.58% to 1.54%.

Spanning the floor in two directions using vertical partially-threaded screws at 300 mm spacing (Assembly P) compared with the same fixing configuration for a short span floor (Assembly L) reduced the damping performance of the floor from 1.51% to 1.33%.

ISO 10137: 2007 [115] building serviceability guidelines assert that accurate damping ratio predictions are not possible, advocating to use measured data from similar construction types. ISO 10137: 2007 [115] proposes 2.0% as a preliminary ζ-value in floor design. EC-5 [22], which is currently based on timber-joist floor construction, recommends damping ratios of 1% and 2%. Ohlsson [13] recorded a mean damping ratio of 0.9%, for traditional timber floors in the laboratory. Similar floor constructions that were tested by Ohlsson [13] in-situ, were found to have mean ζ-value of 3.4%. The subsequent Swedish design guide [119] suggested a ζ-value of 1% for standard timber construction, reduced to 0.8% for floors with a mass greater than 150 kg/m^3.

The experimental results recorded in this study suggest that an initial design damping ratio ζ-value of 0.8% is appropriate for CLT, but conservative considering the consistent increase observed due to an applied distributed mass on the floor.

6.3 Field CLT test results

The field tests comprised natural frequency measurements and static deflection measurements on bare CLT multi-panel floors on the second floor of a three-storey CLT building. The in-situ tests were taken over three days in December 2016, in Bishop’s Stortford, Hertfordshire, UK. The building which was under construction is illustrated in Figures 5.32 and 5.34.

The study included three rooms that varied in size and support conditions. The measurements were taken using the non-destructive test guidelines outlined in prEN 16929: 2015 [112] where output only data found the natural frequencies of the floors and a point load applied midspan provided the static deflection for measurement of the floors flexural stiffness.

The rooms shared seven 180 mm 5-ply CLT floor panels that spanned the breadth of the building north-south, which was 11767 mm in total. Rooms 1 and 3 were located either side of a stairwell on the north side of a central corridor, while the third larger room was situated on the south side of the building (Room 2), (illustrated in Figure 5.34). The panels spanned 5641 mm and 4497 mm, respectively. The rooms on the floor below were of a similar plan layout. The panels were connected in parallel with half-lap joints (Figure 2.15a), and supported on the CLT walls below with vertical washer-head screws. The upper wall panels were connected to the floor using angle brackets. Figure 6.39 shows a typical wall-to-floor junction.

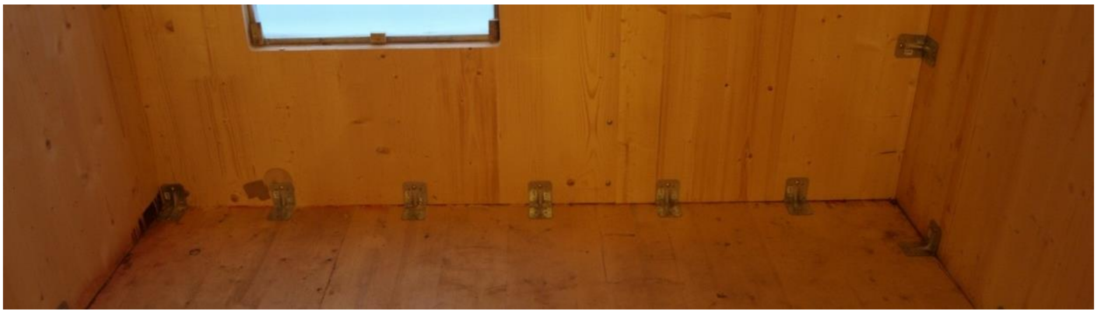

Figure 6.39 *Wall-to-floor assembly at an external wall in Bishop's Stortford, UK*

The panel widths range from 2181 mm to 2897 mm. Room 1, 2, and 3 comprised four, seven, and two 180 mm 5-ply CLT floor panels, respectively.

Point load static deflections were measured in each room, and the natural frequencies were recorded in Rooms 1 and 3.

6.3.1 Room environment

The room temperature for all tests ranged between 7.8˚C and 12.2˚C, averaging at 9.5˚C. The relative humidity of the rooms ranged between 81.0% and 98.0%, averaging 90.4% over the duration of the testing.

6.3.2 Initial theoretical frequency results

In advance of the site visit, preliminary FE models were derived to refine the scope of the frequency testing. The numerical models were developed of representative single-panel one-way spanning floors to provide estimates of the fundamental frequency values. The dimensions and characteristic properties were taken from construction drawings, which were provided by the CLT contractor and the project design engineers. Both the minimum and maximum rotational support conditions were examined for the FE analysis. The panel was assumed to be isotropic, with a modulus of elasticity of 12.000 E9 N/m^2, a Poisson's ratio of 0.203, and a mean density of 468.09 kg/m^3. Software (CLT Designer) that incorporates the specific technical data from common CLT panel manufacturers was also used to predict the fundamental frequencies of the floors. The initial estimated values are charted in Table 6.10.

Table 6.10 *Initial floor fundamental frequency estimates*

Room	*Support conditions*	*Fundamental frequency (Hz)*	
		FEM	*CLT Designer*
1	*Fully-fixed*	*34.05*	*-*
	Simply-supported	*14.88*	*14.99*
3	*Fully-fixed*	*34.05*	*-*
	Simply-supported	*14.88*	*14.99*

6.3.3 Static point load deflection results

The static deflection due to a concentrated dead load consisting ten 10 kg steel masses mounted on a 100 mm x 100 mm load pad was measured midspan in each room.

A digital level mounted outside the room measured the deflection change to an accuracy of ± 0.01 mm. Without changing the position of the load or the measurement device, the test was repeated three times, with the result averaged. The differences between successive readings of each test location was less than 5%, and the time between successive readings was greater than 1 min., in accordance with prEN 16929:2015 [112] guidelines. The applied mass was increased to 183 kg by a person standing adjacent to the steel masses and the tests were repeated. The static point load deflection measurements are presented in Table 6.11 and Figure 6.40.

Table 6.11 *In-situ static point load deflection results*

Room	*Static point load Deflection (mm)*	
	100 kg Mid-floor	*183.3 kg Mid-floor*
1	*0.20*	*0.40*
2	*0.13*	*0.20*
3	*0.13*	*0.30*

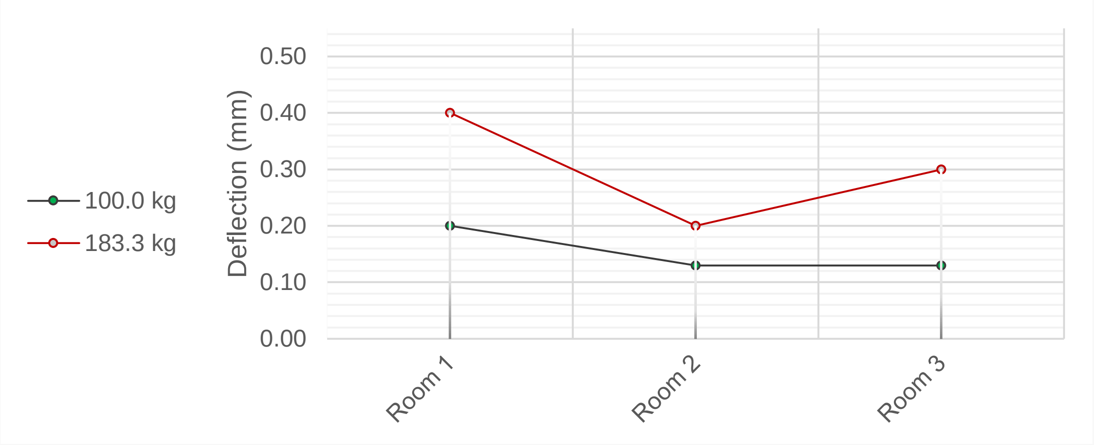

Figure 6.40 *Static point in-situ deflection results, Rooms 1, 2, and 3*

The deflections measured ranged between 0.13 mm and 0.20 mm due to the applied 100 kg mass, and up to 0.40 mm when the mass was increased to 183 kg.

As the span of Room 1 and 3 are equal, the deflection midspan might be expected to equate. However, Room 1 is twice as wide as Room 3; four, and two panels wide, respectively. Similarly, the span of Room 2 was less than the other two rooms, so the deflection may be expected to be less. However, the room was seven panels wide. It may be interpreted therefore that the flexural stiffness of a CLT floor is influenced by the number of panels connected in parallel.

Summary of deflections in-situ

The limiting deflection values across Europe range between 0.5 mm/kN and 4.0 mm/kN [121]. The maximum 1 kN point load deflection recorded in the field tests were less than 0.20 mm/kN. As the European standards currently relate to traditional timber floor construction, it may be inferred from the field CLT deflection results that the flexural stiffness of CLT floors is greater than what is expected from traditional timber floor construction.

Results suggest that a floor’s flexural stiffness is influenced by the floor width.

6.3.4 Impulse frequency results

The natural frequencies of the in-situ CLT floors in Rooms 1 and 3 were measured by applying an impulse and recording the vibration response. The impulse excitation was provided by dropping a 2 kg rubber ball from waist height, 1100 mm, onto pre-marked points on the floor. FFT converted the time domain to frequency values.

Figures 6.41 and 6.42 show a sample impulse time response and the corresponding FFT frequency domain measurement.

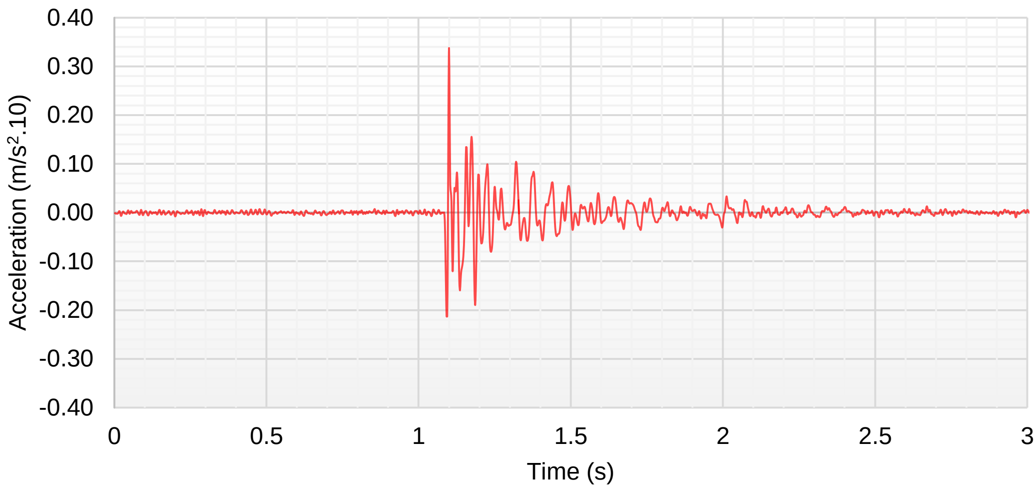

Figure 6.41 *Sample in-situ impulse measurement (time domain): Room 1*

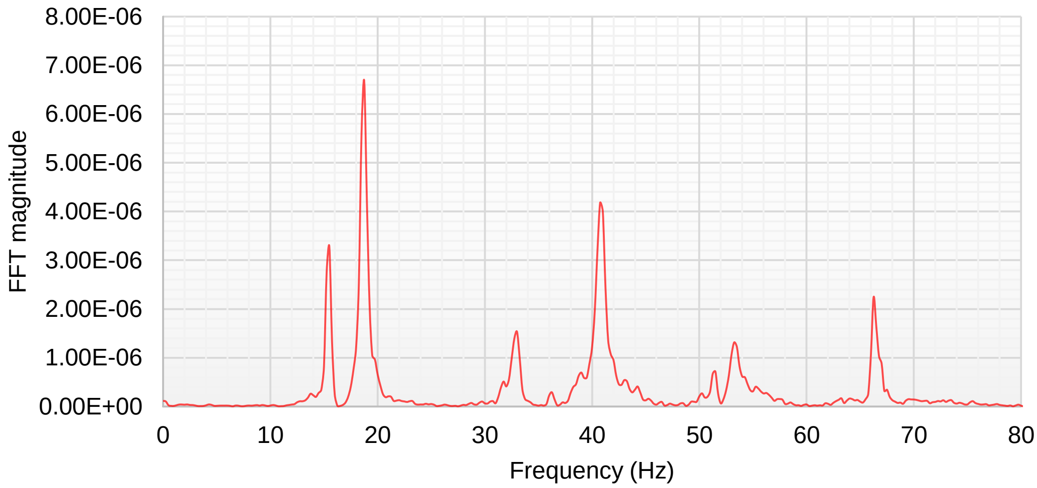

Figure 6.42 *FFT of the Room 1 impulse measurement (frequency domain): 0 to 80 Hz*

To capture all the natural frequencies, including any modes with a node at the centre of the floor panel, the impulses were provided at midspan and at quarter span, with the transducers alternating from quarter span to midspan. The Peak Amplitude method was used to compute the frequency values. Measurements were repeated, recorded four times, and the result was averaged.

The average frequency results of both Rooms 1 and 3 are given in Table 6.12, and Figure 6.43. The first ten modes are charted of the sixteen that were recorded below

80 Hz in Room 1, the four-panel floor. The seven modes recorded below 80 Hz are charted for the two-panel floor, Room 3.

Table 6.12 *Impulse test results for natural frequencies 0 to 80 Hz, Rooms 1 and 3*

Number of panels	*Natural frequencies (Hz)*									
	Mode 1	*Mode 2*	*Mode 3*	*Mode 4*	*Mode 5*	*Mode 6*	*Mode 7*	*Mode 8*	*Mode 9*	*Mode 10*
4	*14.75*	*15.50*	*18.75*	*33.00*	*36.00*	*41.00*	*42.75*	*46.25*	*48.25*	*50.25*
2	*16.50*	*19.25*	*31.50*	*33.50*	*50.75*	*57.75*	*66.75*	-	-	-

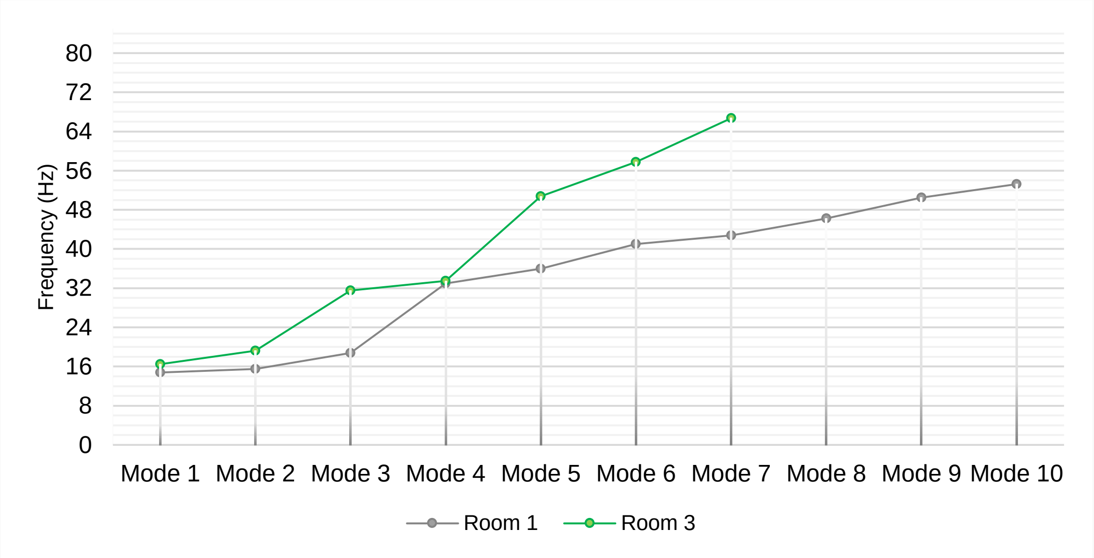

Figure 6.43 *Impulse test results for natural frequencies 0 to 80 Hz, Rooms 1 and 3*

As the floor span for both rooms was equal, the difference in the number of natural modes in the frequency range of interest indicates that additional panels connected in parallel reduce the mode separation.

However, another parameter must be noted; at the time of testing not all fixings to the west side of Room 3 were in place. The fundamental mode for Room 3 was recorded at 16.50 Hz. The increase in the fundamental frequency may be attributed to this factor also.

Summary of frequency results in-situ

The in-situ CLT floors performed well with regard to European timber design frequency criteria, the natural frequencies for both rooms spanning 5641 mm were significantly greater than the recommended 8 Hz limit set out in EC-5 [22]. However, the number of natural modes below a 40 Hz may be critical in complying with the unit input velocity criterion. Only the first-order modes below a 40 Hz frequency range are considered. There are five modes for Room 1 and four recorded in Room 3 in the 0 to 40 Hz range of interest, but their order was not determined from the impulse testing.

FE models were developed subsequently which are compared with the experimental results to examine the possible shape and order of the modes for both the two- and four-panel floors. The FE modal and displacement analysis are presented in Chapter 7 with the results charted in Chapter 8.

6.4 Conclusions

Experimental laboratory and field test programmes were developed to examine the first four research objectives to examine the influence on floor serviceability, (i) of alternative CLT support details; (ii) providing an acoustic non-structural elastomeric interlayer; and (iii) an evenly distributed mass on the floor were measured; with (iv) field tests examining multi-panel CLT floors that are integrated in a CLT building.

The maximum support rigidity was achieved in the laboratory platform assembled floor when combining angle brackets at close spacing (Assembly H, with brackets 200 mm c/c) in addition to vertical partially-threaded screw fixings (Assembly B, with vertical screws at 300 mm c/c). Results showed that additional fixings at the CLT floor supports improved the deflection results to 0.158 mm/kN from 0.178 mm/kN and the natural frequency results were improved by 6%.

There was no clear benefit in support rigidity, influencing flexural stiffness and natural frequency values by using inclined pairs of screws in preference to vertical screws (Assembly E and B, respectively). The vertical screws provided a better damping performance, but the differences were not substantial, from 0.85% to 0.98% in the case of the fundamental mode, respectively.

The variance between the different brackets types, in combination with vertical screw pairs at the same spacing (Assemblies F and G), was negligible.

Comparing the alternative balloon assemblies, using supporting angle brackets at 250 mm spacing (Assembly I) and inclined screw pairs at 250 mm spacing (Assembly J), indicates that the inclined screw pairs improved static deflection and natural frequency results, from 0.219 mm/kN to 0.201 mm and from 20.05 Hz to 20.45 Hz, respectively.

The damping ratio ζ-values were marginally improved from 0.80% to 0.91%, however, the bracket supported floor generally performed better with respect to accelerance, 0.108 $m/s^2/N$ compared to 0.116 $m/s^2/N$ for the fundamental mode and more substantially to 0.157 $m/s^2/N$ compared with 0.294 $m/s^2/N$ for the fourth mode, respectively.

Fewer floor fixings repeatedly resulted in better floor performance with regard to accelerance and the damping ratio ζ-values, but the improvement was generally not significant.

The inclusion of a resilient interlayer into a platform assembly (Assemblies B and C) provided no benefit to deflection or natural frequency results. The effect on accelerance and damping ratio ζ-values were positive, but not substantial from 0.137 $m/s^2/N$ to 0.131 $m/s^2/N$ and from 0.98% to 1.05% in the case of the fundamental mode with more substantial effect on accelerance from 0.051 $m/s^2/N$ to 0.027 $m/s^2/N$ for the third mode, respectively.

The influence of an added mass evenly distributed on the floor was negligible with respect to static deflection, but substantially reduced the frequency values of all modes. However, accelerance and damping performance results were considerably improved, from 0.93% to 2.79 % and from 0.111 $m/s^2/N$ to 0.028 $m/s^2/N$ in the case of the second mode platform construction (Assemblies B: 28.20 Hz and D: 21.45 Hz), respectively.

In-situ static and frequency testing on two floors of a student residence CLT building measured fundamental frequencies that were multiples of the minimum limit recommended in EC-5 [22]. However, a marked reduction in the natural mode separation was recorded. The more parallel panels, the greater the number of modes in the frequency range of interest which is significant with regard to compliance with EC-5 [22] velocity impulse criteria.

The experimental results indicate that the dynamic response to pedestrian traffic on all the CLT floors tested would be transient. Transient vibrations are regulated by a floors fundamental frequency and flexural stiffness, which the experimental results clearly indicate are determined by the floor geometry with marginal effect observed from the type of connection provided at the CLT floor support. While all laboratory and field floors tested were substantially compliant with the European timber design frequency criteria (EC-5 [22]), a criteria which is based on floor geometry, its mass and stiffness, and the number of parallel panels may be more appropriate to CLT design.

In the case of long spanning or timber concrete composite floors, where the fundamental frequency is reduced to below 8 Hz and therefore resonant with footfall, the damping ratio ζ and accelerance performance are critical to abating the magnitude and duration of annoying vibrations to below defined acceptable levels (ISO 10137: 2007 C.1, C.2, and C.3 [115]). The experimental results clearly indicate that an evenly distributed mass is the most efficient method to improve the damping ratio ζ and accelerance performance and should be considered initially as a solution to any disturbing resonant floor vibrations.

The following chapter outlines the numerical modelling programme that was developed to address the remaining three research questions.

7 FE ANALYSIS OF CLT FLOOR SYSTEMS

7.1 Introduction

This chapter outlines the FE programme developed to examine how common design variations of domestic, office, or school upper storey floors in mid-rise CLT construction design influence the stiffness and modal characteristics of the floor.

The numerical modelling programme included calibrating FE models of the laboratory and field tested CLT floors with experimental flexural stiffness and modal frequency results. This modelling approach was then replicated to develop a parametric study of a generic three-panel room, a standard twin-bed hotel room [195], and a classroom design taken from the Irish Primary School Design Guidelines [196].

While current timber design standards [22] set out basic serviceability limit design for single-span, simply supported rectangular floors, it has been proposed that accurate prediction of a floors dynamic response and mitigation of annoying vibration requires a more robust design approach [124][151]. An efficient and straightforward numerical modelling method is needed to represent non-rectangular floors, floor openings, and support configurations. It is asserted that an uncomplicated method to evaluate how typical objects in buildings impact on the perception of floor vibrations is needed [164].

The study aims to quantify the degree of influence of the following parameters:

- Span orientation
- Intermediate support configuration
- Floor openings to accommodate vertical circulation (large)
- Floor openings to accommodate service penetrations (small)
- Support to floor openings
- Non-structural discrete and distributed added mass replicating typical loading

The models were developed using ABAQUS 6.14 FE software.

Measuring responses for a particular dynamic loading gives limited practical information on the suitability of one floor design over another with respect to the overall comfort performance of a floor. However, establishing a floors flexural stiffness, the fundamental frequency, and natural mode separation of a floor are critically important in establishing the vibration response with respect to footfall loading and determining if the response to pedestrian traffic or other human activity is a transient or resonant response in the floor.

The numerical programme concentrates on the static deflection and modal frequency values for each layout modelled.

7.2 Overview of numerical analysis

A single-panel CLT floor FE model was initially developed to characterise one CLT floor panel. This model was calibrated with the laboratory experimental testing. Multi-panel floor models replicating the field tested floors were then developed and calibrated with the field measurements to characterise the connection between parallel panels. Using the FE modelling approach that was attuned with the experimental testing, generic and particular room layout models were developed to investigate the effect of common design variations and loadings on a CLT floor with respect to its serviceability performance.

Figures 7.1 to 7.5 chart the alternative FE investigations that were developed.

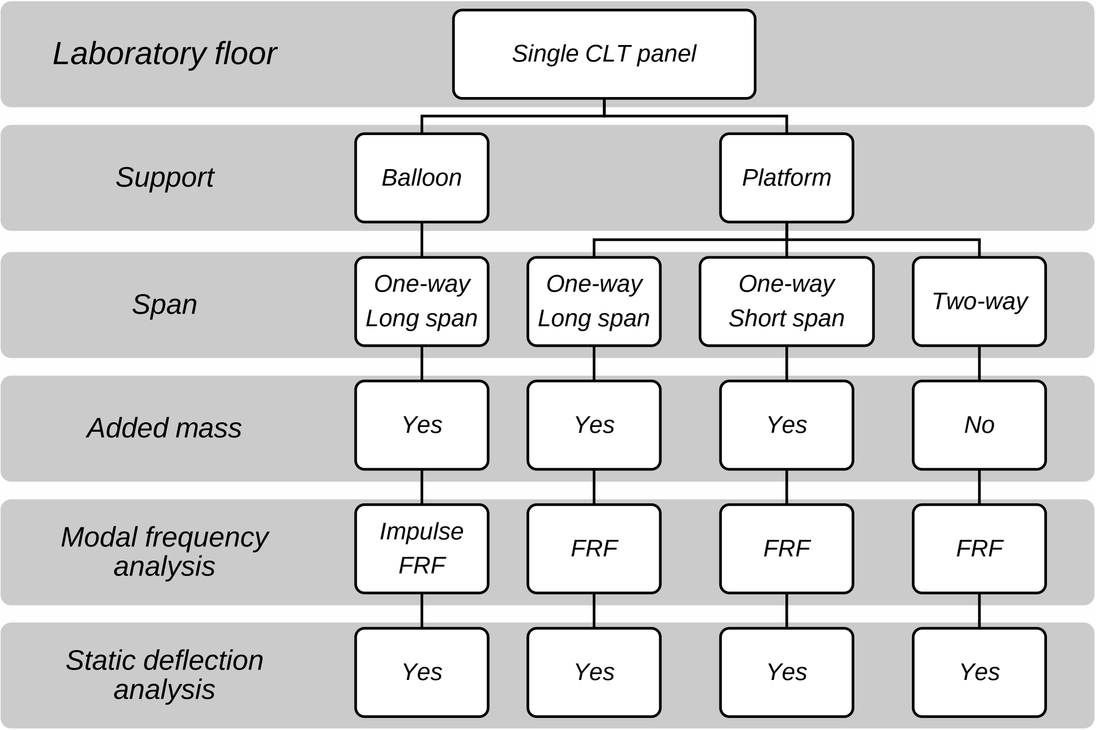
Laboratory floor
Single CLT panel
Support
Balloon
Platform
Span
One-way Long span
One-way Long span
One-way Short span
Two-way
Added mass
Yes
Yes
Yes
No
Modal frequency analysis
Impulse FRF
FRF
FRF
FRF
Static deflection analysis
Yes
Yes
Yes
Yes

Figure 7.1 *Numerical analysis of laboratory tested floor*

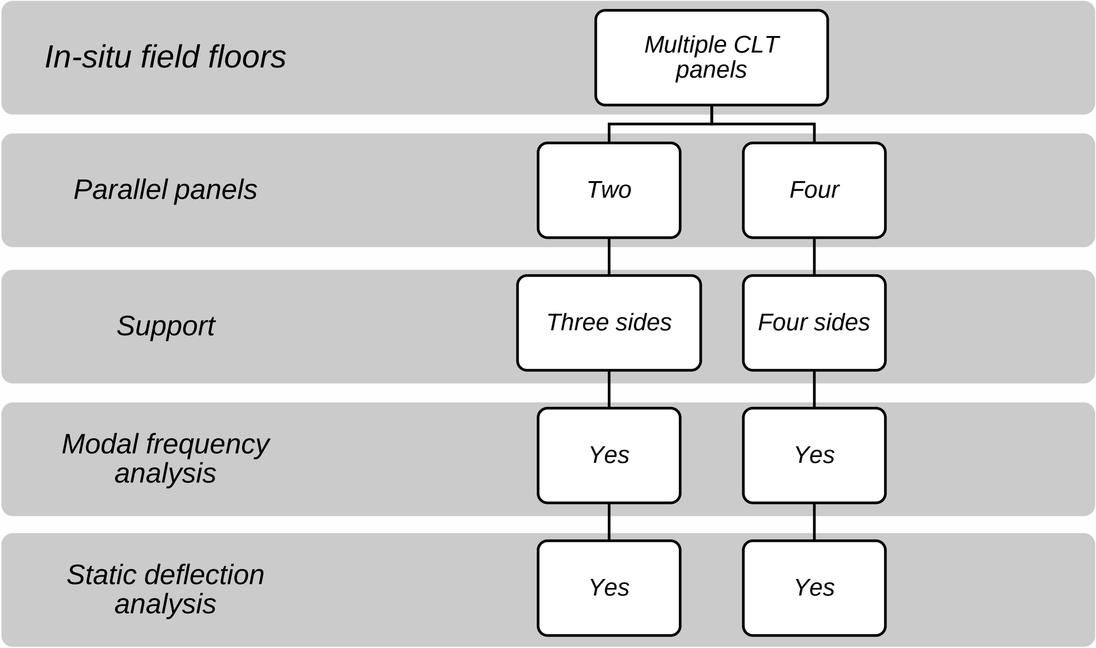
In-situ field floors
Multiple CLT panels
Parallel panels
Two
Four
Support
Three sides
Four sides
Modal frequency analysis
Yes
Yes
Static deflection analysis
Yes
Yes

Figure 7.2 *Numerical analysis of field tested CLT floors*

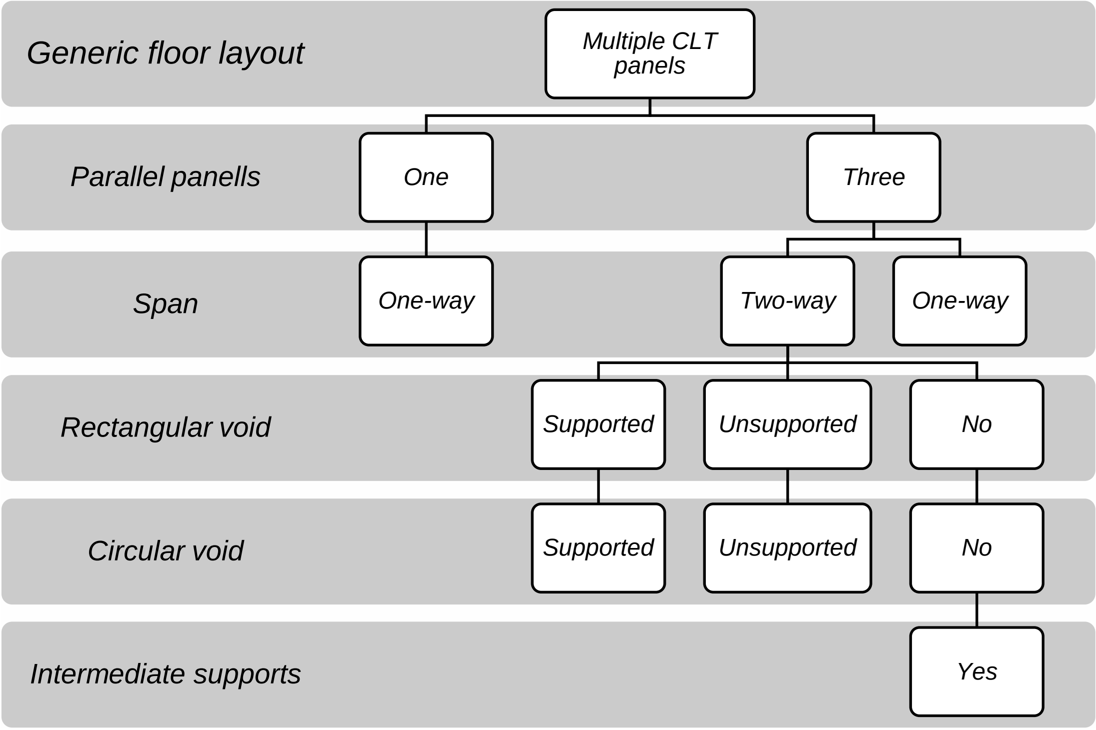
Generic floor layout
Multiple CLT panels
Parallel panells
One
Three
Span
One-way
Two-way
One-way
Rectangular void
Supported
Unsupported
No
Circular void
Supported
Unsupported
No
Intermediate supports
Yes

Figure 7.3 *Numerical analysis of generic floor layout*

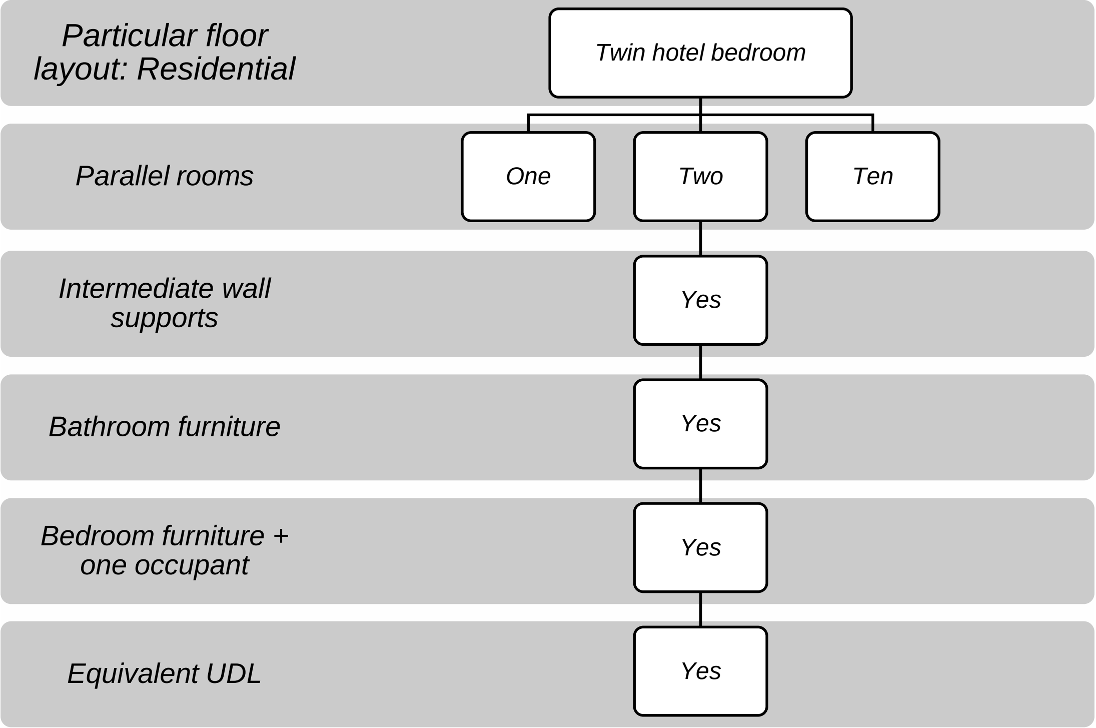
Particular floor layout: Residential
Twin hotel bedroom
Parallel rooms
One
Two
Ten
Intermediate wall supports
Yes
Bathroom furniture
Yes
Bedroom furniture + one occupant
Yes
Equivalent UDL
Yes

Figure 7.4 *Numerical analysis of twin hotel room floor layout*

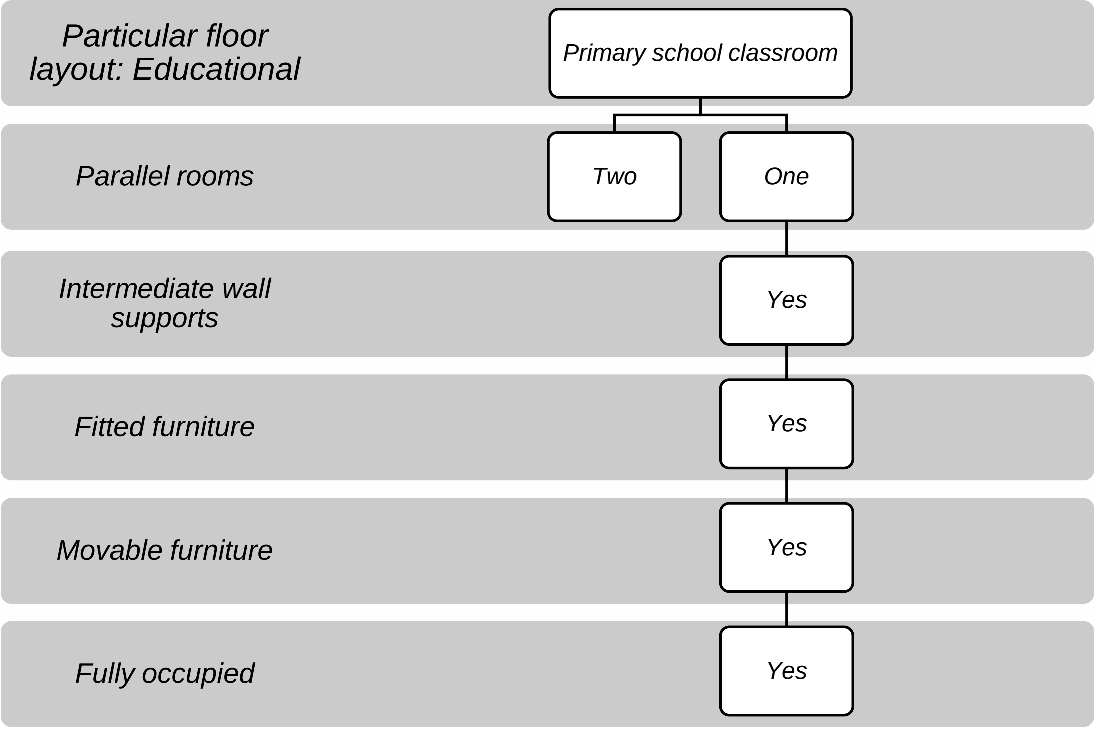
Particular floor layout: Educational
Primary school classroom
Parallel rooms
Two
One
Intermediate wall supports
Yes
Fitted furniture
Yes
Movable furniture
Yes
Fully occupied
Yes

Figure 7.5 *Numerical analysis of primary classroom floor layout*

7.2.1 Numerical background of Abaqus dynamic analysis

By means of superposition, the MDOF of the dynamics of any system may be reduced to a SDOF system [95], [98], with the governing equations of a MDOF system written in matrix form, Equation (7.1). The eigenvalue problem for the natural modes of small vibration of a FE model is available from linear perturbation of the equilibrium equation of the system, notated by Equation (7.2).

$$(\mu^2[M] \ + \mu[C] + [K]\ )\{\phi\} = 0 \tag{7.1}$$

$$(\mu^2 M^{MN} + \mu C^{\ MN} + K^{MN})\ \phi^N = 0 \tag{7.2}$$

where M^{MN} represents a symmetric and positive mass matrix, C^{MN} is the damping matrix, and K^{NM} defines the stiffness matrix, which may, or may not be positive or symmetrical. The term μ represents the eigenvalue and ϕ^N is the mode of vibration, the eigenvector. *M* and *N* represents the finite number of degrees-of freedom. Complex eigenvalues and eigenvectors are to be expected in any real system, but for eigenvalue extraction, the damping matrix C^{MN}, is omitted and the stiffness matrix K^{NM}, is assumed to be symmetric and positive. The system will then contain only real squared eigenvalues μ^2 , and real eigenvectors ϕ^N . Thus μ becomes an imaginary eigenvalue $\mu = i\omega$, where ω is the circular frequency (Eq. (3.5)) and the eigenvalue problem is represented by Equation (7.3).

$$(-\ \omega^2[M] \ + [K]\ )\{\phi\} = 0 \tag{7.3}$$

Eigenvalue extraction in Abaqus of symmetrized systems applies a Lanczos iteration approach. Hybrid elements and contact elements result in Lagrange multipliers in the system of equations, resulting in an indefinite stiffness matrix K^{MN}, but the terms of the mass matrix M^{MN}, corresponding to the Lagrange multipliers equate to zero. Therefore, Equation (7.3) still applies. The presentation of the mode shape vectors is always subjected to a normalisation procedure, depending on the particular Eigen solution but often based on making the largest element in each vector equal to unity [197].

7.3 FE modelling of laboratory tested floor

FE models were developed of the single CLT panel floor that was tested in the laboratory. The alternative span orientations of the floor and the influence of added mass was studied. Both minimum and maximum degrees of rotation was applied to the support boundaries to establish the relative rotational rigidity of the fixing configurations of the supports studied in the laboratory.

Geometry and boundary conditions

The FE analysis of the single-panel CLT floors replicate the laboratory study support orientations spanning the floor at 3812 mm (platform Assemblies B, H, and with added mass, D), 4000 mm (balloon Assemblies J, and with added mass, K), a short span of 2212 mm (platform Assembly L and Assembly O, with added mass), and a two-way span configuration spanning 2212 mm and 3812 mm (platform Assembly P). Each floor orientation is illustrated in Figures 7.6 to 7.9.

Both the minimum and maximum rotational constraint conditions were examined with a boundary line defined along the edge of the floor in the case of the balloon assembly floor (Figure 7.7). To replicate the platform assembly configurations, the boundary conditions were defined along a line 94 mm from, and parallel to the relevant edge of the floor panel, (Figures 7.6, 7.8, and 7.9). The 94 mm dimension coincides with the inner face of the three-ply CLT laboratory support walls.

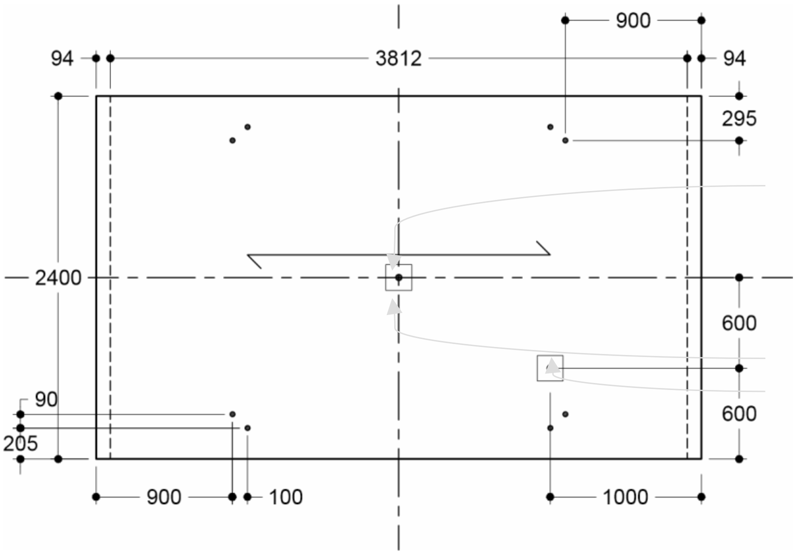

2no. Ø 30 mm lifting eyes per panel corner

100 mm x 100 mm loading pad midspan

Shaker locations:
Midspan
Quarter span
2no. Ø 20 mm perforations

Figure 7.6 *One-way long span platform construction with the shaker locations (Assemblies B, H, and D)*

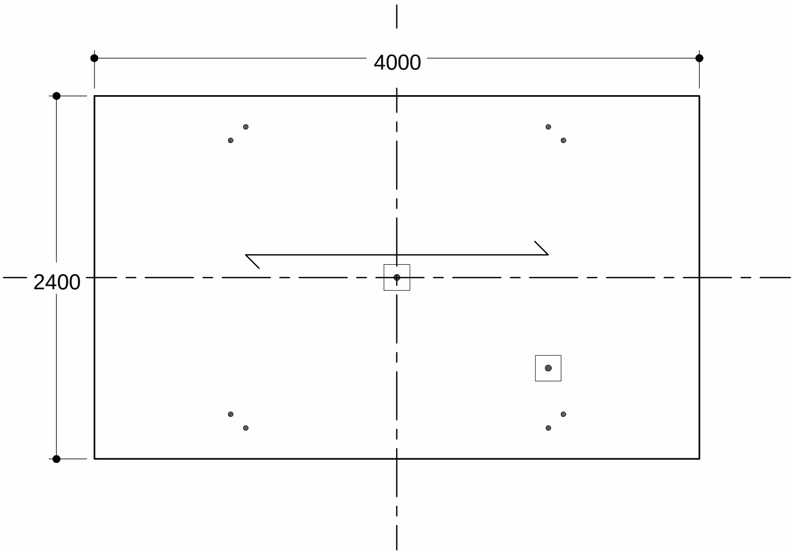

Figure 7.7 *One-way long span balloon construction (Assemblies J and K)*

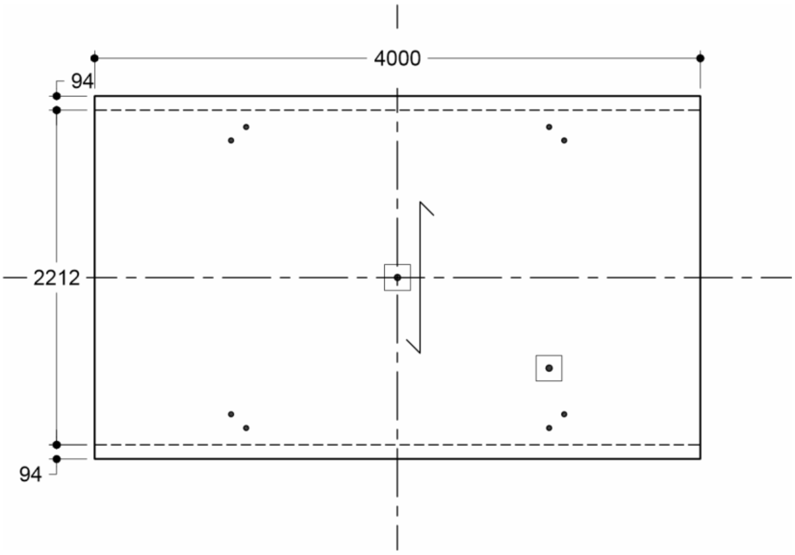
4000
94
2212
94

Figure 7.8 *One-way short span platform construction (Assemblies L and O)*

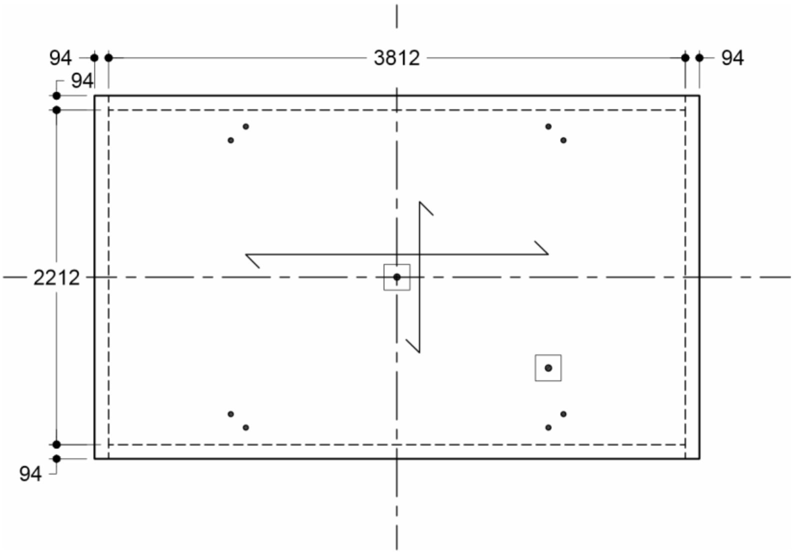

Figure 7.9 *Two-way spanning platform construction (Assembly P)*

FE Mesh

The laboratory CLT floor panel was modelled using general linear, reduced integration, shell element of type S4R, and linear triangular shell elements of type S3. The CLT floor panel was represented by a 5-ply orthotropic composite layup with the orientation of each successive ply rotated 90° to simulate cross-laminated characteristics of CLT. A thickness was applied to each ply, 34 mm and 30 mm alternately, representing the 162 mm lamella build-up of the floor. Following a mesh convergence study a global element size 25 mm was found to be suitable. The models comprised a total of 19,461 elements, 18,231 S4R and 1,230 S3 elements. For completeness all penetrations in the laboratory floor was replicated in the numerical analysis. The geometry of the circular added masses were incorporated in the global mesh. The added non-structural mass was then applied by increasing the density of the top ply of the floor locally. Figure 7.10 shows the mesh applied to the model representing the 162 mm x 2400 mm x 4000 mm plan of the CLT floor tested in the laboratory.

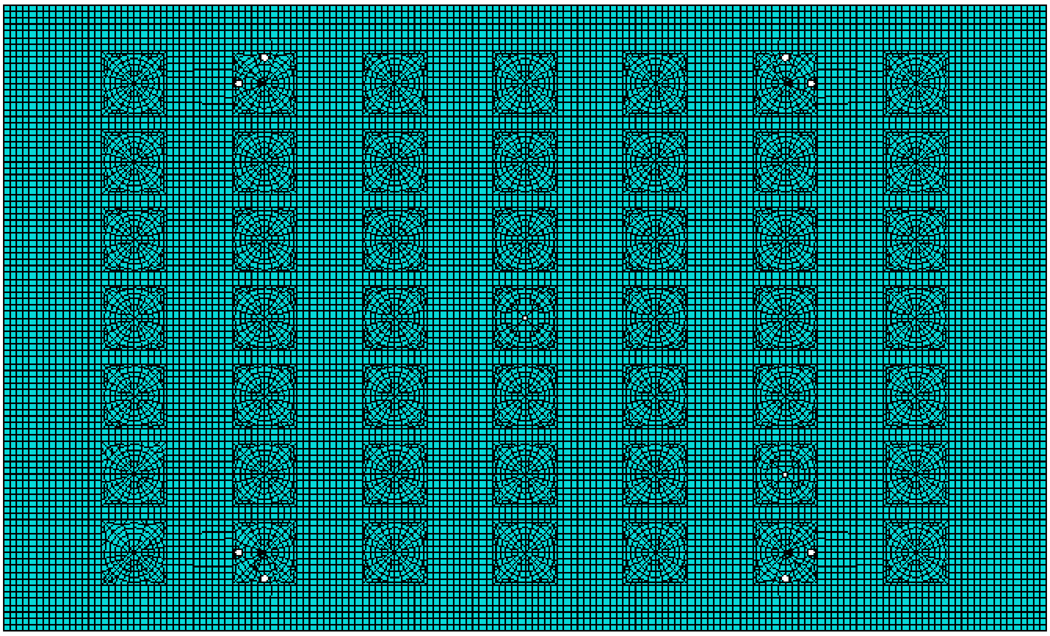

Figure 7.10 *Single-panel CLT floor panel mesh, generally 25 mm element size*

The floor panel dimensions are outlined in Figure 7.6. The mass distribution is illustrated in Figure 7.11.

Material properties

The material properties of the base timber for the CLT panel was orthotropic and linear elastic. A consistent orthotropic set previously applied by Bejtka and Blaβ [198] in numerical modelling of Grade C24 spruce formed the basis of the timber base material characteristics of the model. The modulus of elasticity, shear modulus, and rolling shear modulus were amended to that outlined in the CLT manufacturer's technical data sheets (ETA KLH.UK 2016 [199]). The bulk density is representative of the measured size and mass of the actual floor panel. Table 7.1 lists the material properties that were applied.

Table 7.1 *Material properties for CLT finite element model of laboratory 162 mm five-ply floor*

Property	*Symbol*	*Value*	*Units*
Modulus of elasticity: Longitudinal direction	*E1*	*12.000 E +9*	N/m^2
Modulus of elasticity: Rotational direction	*E2*	*0.370 E +9*	N/m^2
Modulus of elasticity: Tangential direction	*E3*	*0.370 E +9*	N/m^2
Shear modulus	*G12*	*0.690 E +9*	N/m^2
Shear modulus	*G13*	*0.690 E +9*	N/m^2
Rolling shear modulus	*G23*	*0.050 E +9*	N/m^2
Poisson's ratio	*v 12*	*0.511*	
Poisson's ratio	*v 13*	*0.511*	
Poisson's ratio	*v 23*	*0.203*	
Bulk density	$\rho_{CLT,}$	*468*	kg/m^3

Types of analysis

For each floor configuration, a static displacement analysis was carried out to determine the maximum displacement due to the application of a load of 1 kN applied pressure load over an area of 100 mm x 100 mm which corresponds to the experimental testing arrangement.

A mode-frequency analysis was then performed to determine the floor's natural frequencies and mode shapes. The analysis used the linear perturbation Lanczos iteration procedure.

The initial FE model was compared with the diagnostic impulse test of Assembly I (Section 5.3.6: Figure 5.14, Table 5.3, and Figure 7.7). This assembly was selected as the impulse was applied from a separately supported scaffold. Neither the added mass of the mechanical exciter nor a person standing was included, therefore the scope for error in the model was minimum.

To correlate with the modal analysis of the other laboratory floor assemblies, it was necessary to characterise the mass of the mechanical exciter in the model. To avoid changing the stiffness of the floor panel, its original thickness was maintained, with the mass of the exciter distributed over a finite area of the 34 mm top ply of the model. At the exciter location the density over an area of 100 mm x 100 mm was increased to

49,660 kg/m^3. This value included the 15.5 kg mass of the exciter and the mass of the 100 mm x 100 mm top ply of the floor panel combined.

Equating with the experimental test procedure, separate models were generated with the exciter located at midspan for measurement of the first and fourth modes and moved to the quarter span for the second, third, and fifth mode measurement. The exciter locations are illustrated in Figure 7.6 and 7.11.

Added mass

Modelling of the added mass was carried out in the same manner as that described above for the exciter mass. The distributed added masses used in the testing of (Assemblies D, K, and O, (Section 5.3.6: Figures 5.9 to 5.17, Tables 5.1 to 5.4) were characterised by locally altering the density of discrete areas of the top ply of the floor panel at 49 locations distributed across the floor on a 500 mm x 300 mm grid. The density of a circular area of diameter 150 mm by the 34 mm thick top ply was increased to 21,190 kg/m^3 consistent with the experimentally tested floor. Figure 7.11 illustrates the added mass positions.

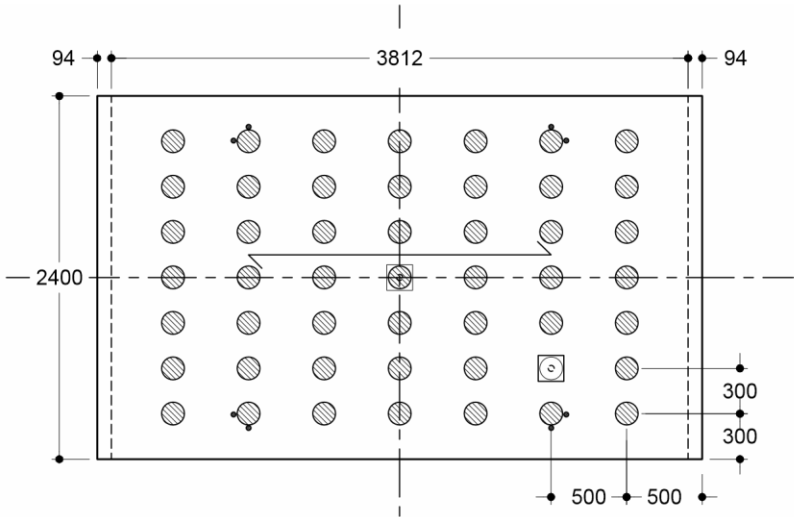

49 no added mass positions on a 500 mm x 300 mm grid

48 no. 12.5 kg masses over a Ø 150 mm area per mass

1 no. 15.5 kg exciter represented by a 100 mm x 100 mm area alternating from midspan to quarter span

Figure 7.11 *Distribution of added mass on a 500 mm x 300 mm grid (Assembly D)*

In keeping with the procedure adopted in the laboratory, the density corresponding to the added mass was exchanged with that of the exciter depending on the exciter position. The number of elements, their type, and size remained constant for each FE analysis of the laboratory floor.

7.4 FE modelling of field tested floors

As standard CLT panel dimensions range between 2400 mm and 3000 mm wide, it can be assumed that many floor layouts in practice will comprise more than one CLT panel connected in parallel. The rooms investigated in the three-storey CLT building in Bishop’s Stortford, UK, comprised multiple CLT panel floors (Figure 5.32 and 5.34). The two main aims for developing the FE models of the field tested floors was to: (i) define an appropriate floor support boundary conditions for floors integrated into a building, and (ii) to develop a suitable characterisation of the transverse connections between the panels running in parallel.

Geometry

FE models were developed to represent two of the bare CLT multi-panel floors in the field (Rooms 1 and 3). Room 1 comprised four 180 mm five-ply CLT floor panels connected with a half-lap joint and vertical partially threaded screws at 250 mm spacing. The room measured 5641 mm x 10080 mm in total.

Room 3 was approximately half the width of Room 1, measuring 5641 mm and 5178 mm wide. It comprised two 180 mm five-ply CLT floor panels again connected in parallel with a half-lap joint and partially threaded screws at 250 mm spacing.

The floor panels of the field-tested floors spanned the full breadth of the building north-south, 11767 mm in total. This accommodated two rooms either side of a central corridor. The floor plan is illustrated in Figure 5.34. The FE analysis included the total span of the CLT panels, including the corridor and opposite south room (Room 2).

Mesh and material properties

The field tested CLT floors were modelled using the general linear, reduced integration, shell element S4R. The CLT floor panels were represented by a 5-ply orthotropic composite layup with the orientation of each successive ply rotated 90° to simulate cross-laminated characteristics of CLT. A thickness was applied to each ply, 40 mm and 30 mm alternately, representing the 180 mm lamella build-up of the floor. Following a mesh convergence study, a global element size 40 mm was found to be suitable. The FE models of Rooms 1 and 3 comprised 74,962 and 37,256 elements, respectively.

The orthotropic material properties set used to model the laboratory tested floor, outlined in Table 7.1 was applied to the multi-panel field tested floor models.

Boundary conditions and analysis

The boundary conditions were defined as pinned. To replicate the platform construction in the field, the boundary conditions were defined along the inner edge of the supporting walls and at each edge of the corridor walls. In the case of Room 1, the floor was supported in the same way for the transverse span. In the case of Room 3, one floor edge parallel to the main span was not restricted, to replicate on site fixing conditions at the time of testing.

In order to model the half-lap connection between adjacent panels, the mesh was designed to ensure that the nodes were located at screw positions corresponding to the screw locations in each panel. Multi-point constraints (MPC) connected the parallel adjacent points at 250 mm spacing. Rotation was permitted along the span axis of the panels, while the other five degrees of freedom were tied.

The modal analysis procedure applied to the laboratory floor was replicated in the field floor analysis.

7.5 Generic FE room design

Geometry

A model of a generic 7000 mm by 7000 mm CLT floor was developed to investigate the relative influence of floor penetrations, support to the floor penetrations, and non-loadbearing partition walls on the modal response of the floor. The floor comprised three 5-ply CLT panels connected in parallel. The panel dimensions were each 180 mm x 2330 mm x 7000 mm.

Some initial modelling was undertaken to establish the baseline model of the floor. This included modelling the response of a single one-way spanning simply-supported floor panel, then a three-panel floor spanning one-way, and finally a three-panel floor spanning in both directions.

Mesh and material properties

The floor was modelled using the general linear, reduced integration, shell element of type S4R, and linear triangular shell elements of type S3. The CLT floor panel was represented by a 5-ply orthotropic composite layup with the orientation of each successive ply rotated 90°, as before. A thickness was applied to each ply, 40 mm and 30 mm alternately, representing the 180 mm lamella build-up of the floor. A global element size 40 mm was found to provide an appropriate mesh density.

The orthotropic material properties used to model the laboratory and field tested floors that are outlined in Table 7.1 were applied.

Boundary conditions and analysis

The boundary conditions were defined as pinned. Parallel panels were connected with MPC at 250 mm spacing. Rotation in the MPC was permitted along the span axis of the panels, while the other five degrees of freedom were tied.

The modal analysis procedure applied in the laboratory floor was replicated.

7.5.1 Floor voids

The influence of floor penetrations on the dynamic performance of the generic 7000 mm x 7000 mm CLT floor was investigated.

There are many reasons why a void is introduced in a floor plan. Most commonly this is to facilitate services, with electrical or drainage voids through walls and floors generally measuring no more than 100 mm in diameter. Larger openings of up to 1200 mm are necessary in buildings to provide mechanical ventilation. It is common to carry ventilation shafts through the walls on each storey, rising or dropping to the next floor by means of a vertical, walled duct. However, for the purposes of an aesthetic, light or space, a void of any shape or size may be incorporated into a design, but the largest void that will always occur in the floor of a multi-storey building is that for a stairway. Most stairwells will measure at least 1800 mm x 2700 mm.

To simulate the impact of different void sizes and shapes, the following void arrangements for the two-way spanning seven meter square floor were modelled: (i) a 1800 mm x 2700 mm rectangular void, (ii) a 1800 mm diameter circular opening, and (iii) a number of small 100 mm diameter service penetrations adjacent to the floor supports. For the large rectangular voids, the impact of void location was also investigated. Figures 7.12 to 7.17 show the floor geometry of the voids that were examined.

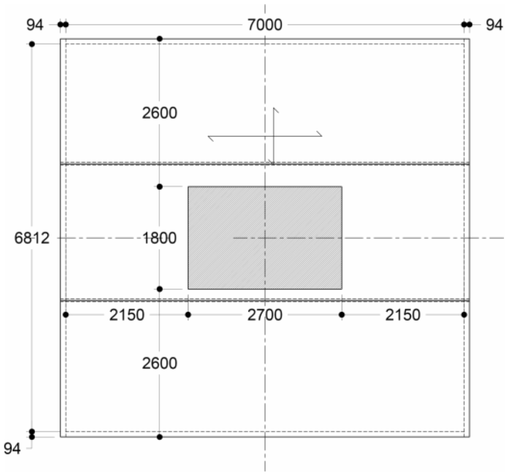
94
7000
94
2600
6812
1800
2150
2700
2150
2600
94

Figure 7.12 *2700 x 1800 mm rectangular stairwell midspan*

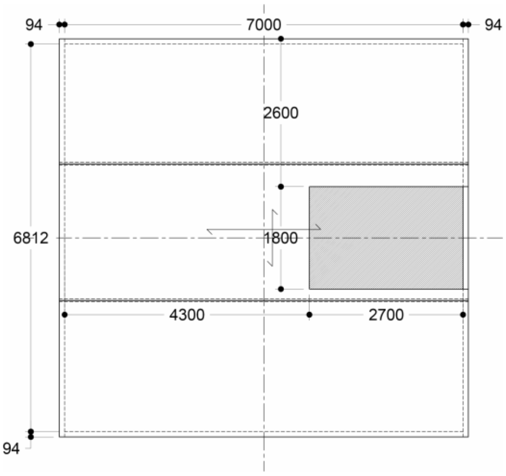
94
7000
94
2600
6812
1800
4300
2700
94

Figure 7.13 *2700 x 1800 mm rectangular stairwell midspan adjacent a support*

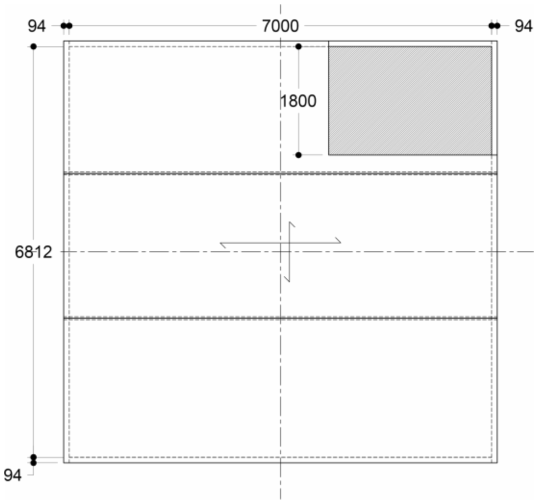
94
7000
94
1800
6812
94

Figure 7.14 *2700 x 1800 mm rectangular stairwell adjacent two supporting walls*

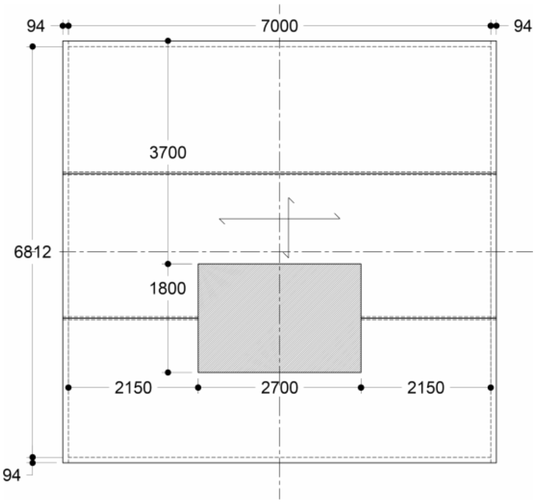
94
7000
94
3700
6812
1800
2150
2700
2150
94

Figure 7.15 *2700 x 1800 mm rectangular stairwell straddling two panels*

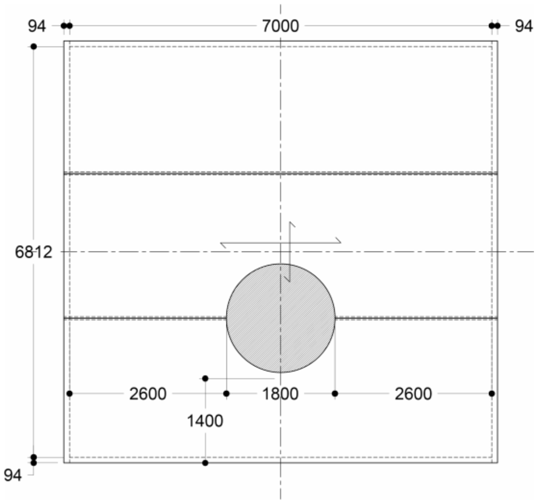
94
7000
94
6812
2600
1800
2600
1400
94

Figure 7.16 *Ø 1800 mm stairwell between two panels*

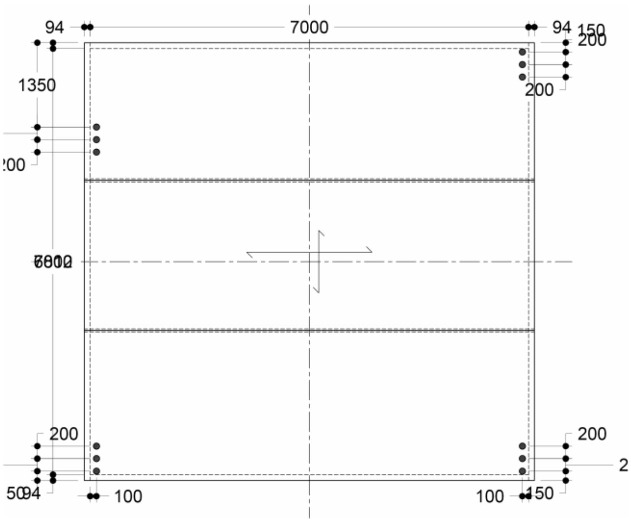
94
7000
94
150
200
1350
200
200
6812
200
200
2
50
94
100
100
150

Figure 7.17 *Ø 100 mm service penetrations adjacent the floor support*

In the case of a rectangular void positioned midspan (Figure 7.12), analysis of the void with unsupported edges, simply supported along both 2700 mm long edges, and simply-supported at two perpendicular edges to the opening were compared. For the alternative rectangular void locations, the effect of the void unsupported and supported on all sides was studied. Similarly, modal analysis of the circular void (Figure 7.16) unsupported and supported were compared.

7.5.2 Internal partition walls

The impact of non-loadbearing partition walls on the modal response was investigated numerically. Three alternative configurations were compared: (i) An intermediate support at quarter span as shown in Figure 7.18, (ii) cross supports at midspan (Figure 7.19), and (iii) diagonal cross supports were examined (Figure 7.20). The natural frequencies and mode shapes were determined in each case.

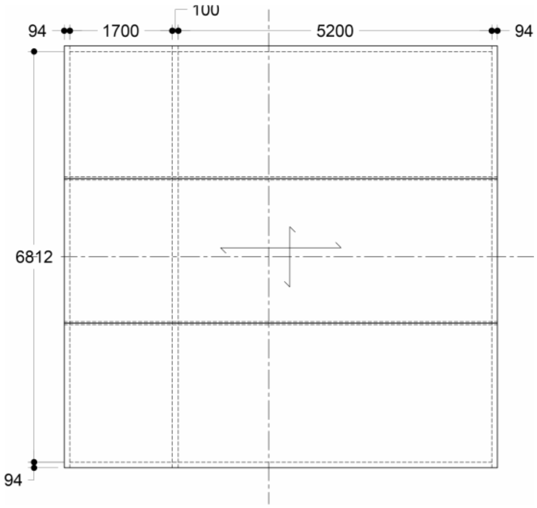

Figure 7.18 *Quarter-span support*

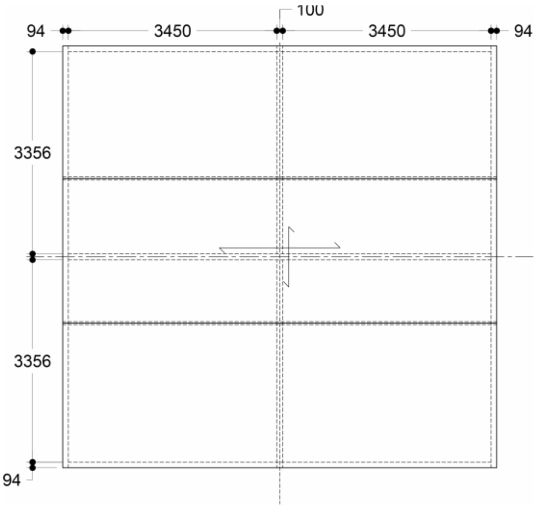

Figure 7.19 *Cross midspan support*

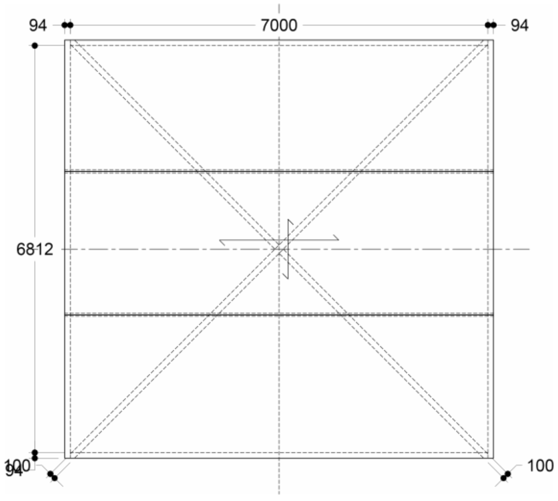

Figure 7.20 *Cross diagonal supports*

7.6 Specific standard room design

Two standard room designs were modelled to examine the influence of floor geometry, intermediate support, and loading distributions that occur commonly, but are not accommodated within the current serviceability design standards.

It is often the case in modern design, where multiple iterations of the same building for the same purpose is intended, that whole buildings or a substantial number of the room layouts follow a universal standardised design template. Multinational developers, most notably global hotel and restaurant franchises, frequently use this design approach as is very time and cost efficient. It is the preferred building and refurbishment design strategy used by financial institutions. The template plans and specifications often include specific guidelines on internal furnishings and room fit-outs. This derivative design method is very suited to public school building and has been adopted by the Irish Department of Education and Science.

In this study, the serviceability performance of two commonly replicated room design layouts is examined: (i) A standard twin hotel room [195] and (ii) a classroom design taken from the Irish Generic Primary School Design Guidelines [196]. The principal research questions investigated are the influence on the floors flexural stiffness and modal frequency values of:

- Intermediate non-structural partition walls
- Non-structural discrete masses replicating typical furniture
- Non-structural discrete masses replicating the expected human loading
- Equivalent evenly distributed added mass representing the discrete masses

7.6.1 Residential: Twin hotel room model

A common example of a widely-adopted standardised room layout is a hotel bedroom. High-density, single-occupancy, residential development, including student accommodation follow a similar template. Back-to-back rooms are provided either side of a central circulation corridor to maximise the access to the external façade, thereby optimising the use of light and ventilation.

The space and furniture requirements for each modern hotel room are set-out by quality standards with regard to the star-rating of the hotel and other tourism boards.

Although the style of the furniture may be updated from time to time, each item is usually required. The location of doors and windows make any remodelling of the rooms and furniture layout quite difficult. Only in the case of a complete overhaul of the building, or a change of the star-rating would the furniture layout change to any significant degree.

Geometry

A standard hotel twin room with standard furniture layout is illustrated in Figure 7.21 [195].

A typical service void in the floor within a walled duct is shown. The void is supported on all sides, therefore it can be argued that the void may be neglected in the model, that only the support boundary conditions of the duct walls are influential. The void and support replicating the duct walls were included in the FE model of the floor for completeness.

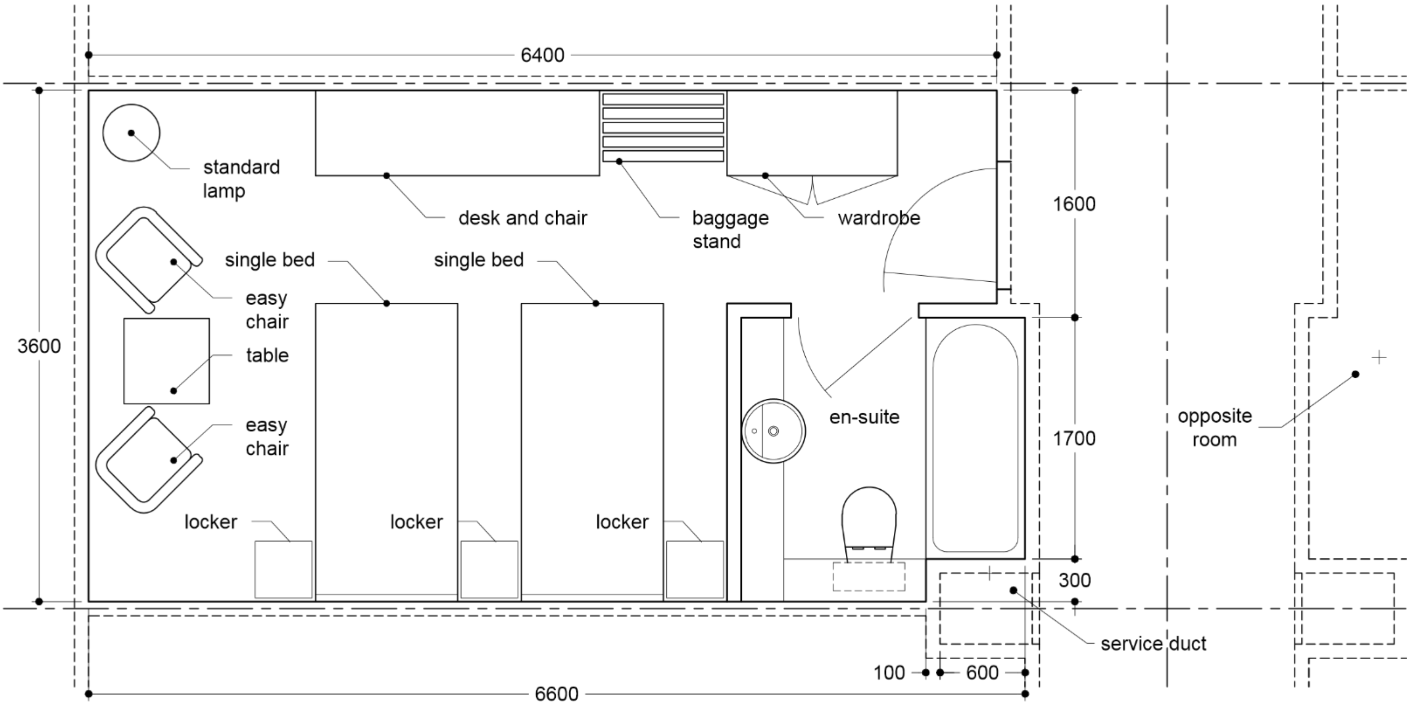
6400
standard lamp
desk and chair
baggage stand
wardrobe
1600
single bed
single bed
easy chair
3600
table
en-suite
easy chair
1700
opposite room
locker
locker
locker
300
service duct
100
600
6600

Figure 7.21 *Standard modern twin-bed hotel room with en-suite and furniture fit-out [195]*

A hotel/student residential building floor design including minimum fire escape route distances may comprise up to twenty rooms between the protected vertical circulation routes. Ten rooms similar to that shown in Figure 7.21 would be placed in parallel each side of a central corridor. To investigate the serviceability of a single room, an

FE model of two rooms comprising one and a half panels spanning either side of the 1800 mm central corridor was developed. The panels were supported by the structural external and corridor walls.

All non-load bearing partitions and furniture were omitted in this initial analysis. The room and corridor model geometry is illustrated in Figure 7. 22.

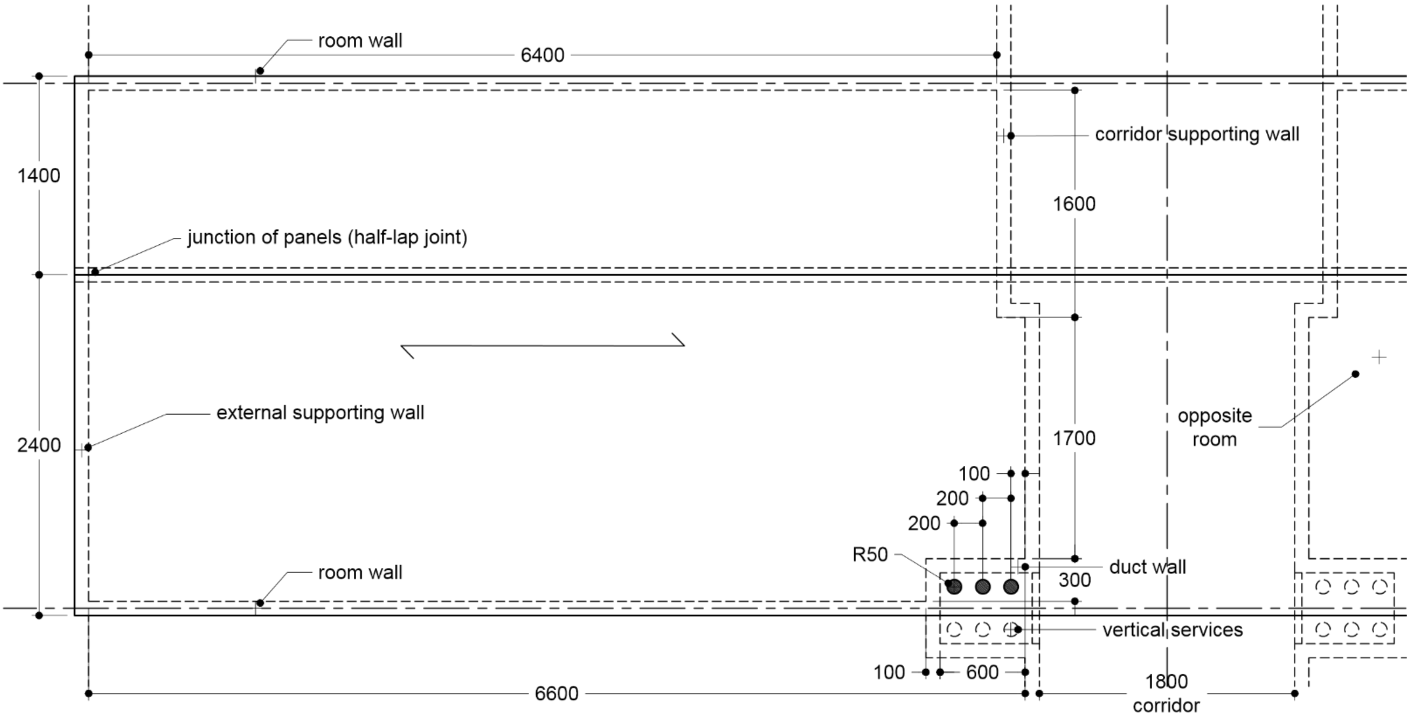
room wall
6400
1400
corridor supporting wall
1600
junction of panels (half-lap joint)
external supporting wall
2400
1700
opposite
room
100
200
200
R50
duct wall
room wall
300
vertical services
100
600
6600
1800
corridor

Figure 7.22 *Standard modern twin-bedded hotel room without internal walls or furniture*

Three additional models were developed; (i) a model of twenty rooms, ten rooms in series either side of the central corridor, (ii) a six-roomed model, and (iii) a four-roomed model were developed. It was found that a four-roomed model (two-rooms adjacent) sufficiently represented the natural modes that were predicted in the twenty room representation.

For this reason, the four-roomed model was taken as the baseline model to compare the influence of the intermediate partition walls, furniture, and the analysis of the distributed added mass.

Mesh and material properties

The models were developed using the general linear, reduced integration, shell element of type S4R, and linear triangular shell elements of type S3. The CLT floor panel was represented by a 5-ply orthotropic composite layup with the orientation of each successive ply rotated 90° to simulate cross-laminated characteristics of CLT. A thickness was applied to each ply, 40 mm and 30 mm alternately, representing the 180 mm lamella build-up of the floor. Following a mesh convergence study a global element size 40 mm was found to be suitable. The models comprised a total of 72,994 elements, 72,622 S4R and 372 of type S3.

The orthotropic material properties used to model the laboratory and field tested floors that are outlined in Table 7.1 were applied.

Boundary conditions and analysis

The boundary conditions were defined by setting the out-of-plane displacement component to zero for all nodes along the lines corresponding to the inner edge of the supporting walls and at each edge of the corridor walls. The half-lap joint between panels was modelled using the same MPC approach used in the field and generic room models. The static and modal analysis procedures applied in the laboratory, field, and parametric floor studies was repeated for the hotel room analysis.

Internal partition walls

In order to investigate the influence of non-loadbearing partition walls on the response of the floor, the baseline four-roomed models was adapted to include the internal partition walls that enclose the room’s en-suite, shown in Figure 7.23.

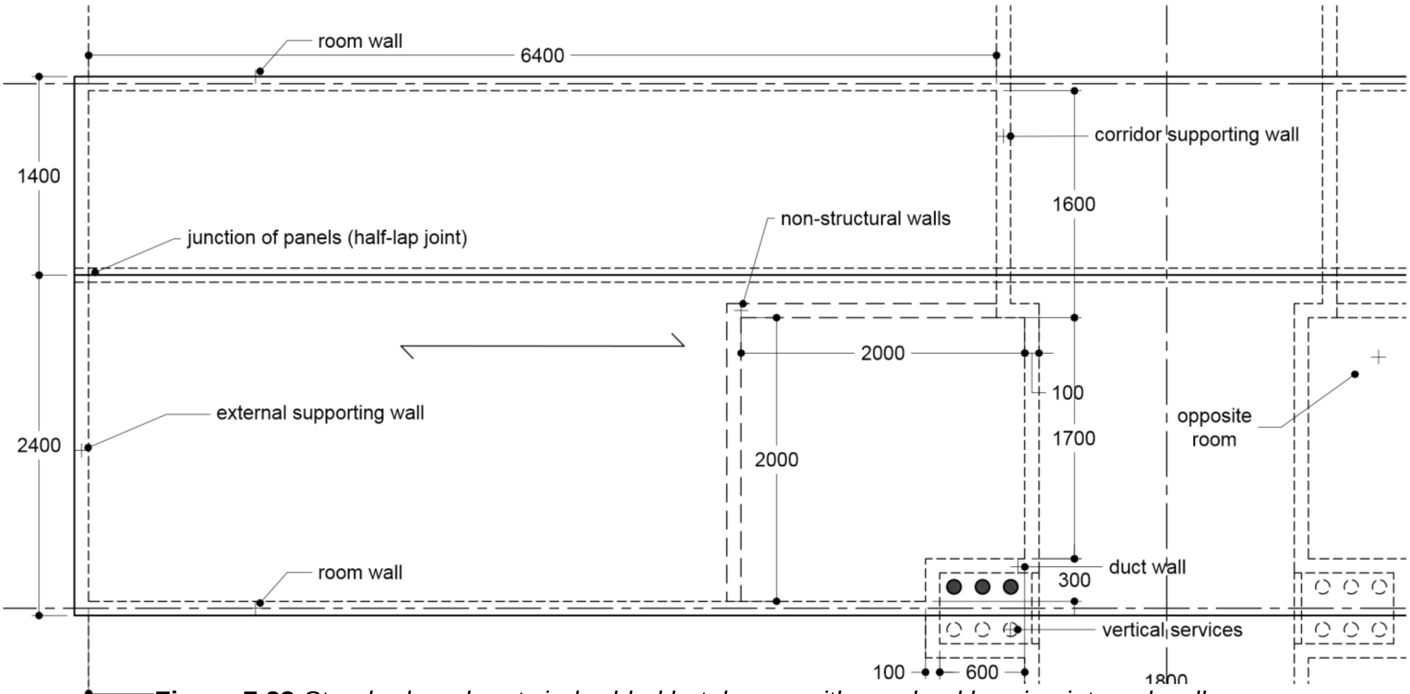
room wall
6400
1400
corridor supporting wall
1600
junction of panels (half-lap joint)
non-structural walls
2000
100
external supporting wall
2400
1700
opposite room
2000
room wall
duct wall
300
vertical services
100
600
1800

Figure 7.23 *Standard modern twin-bedded hotel room with non-load bearing internal walls*

This involved setting the out-of-plane displacement component to zero for all nodes along the lines corresponding to the edge of the walls.

Added discrete and distributed mass

The model was adapted to include the mass of the en-suite furniture and then the bedroom furniture (Figure 7.21). Analysis determined the influence of added mass due to furniture and occupancy of the room. Only one occupant was included in the analysis of the furnished room. The person was assumed to have a mass of 70 kg and was positioned sitting at the writing desk. The individual masses of the bathroom and bedroom furniture are outlined in Table 7.2.

Table 7.2 *Standard hotel furniture*

Furniture item	*Mass per unit*	*Units*
Single wooden bed	*52*	*kg*
Bedside locker	*15*	*kg*
Chair	*15*	*kg*
Table	*15*	*kg*
Standard floor lamp	*5*	*kg*
Writing desk and chair	*27*	*kg*
Baggage stand	*4*	*kg*
Wardrobe	*55*	*kg*
Bath (non-metal)	*25*	*kg*
Toilet	*30*	*kg*
Ceramic sink	*20*	*kg*

Evenly distributed equivalent mass

An additional analysis applied the equivalent mass of the furniture and one occupant evenly distributed across the whole floor area, with, and without non-structural partition walls.

7.6.2 Standard schoolroom design

There are numerous examples of schools and other educational facilities constructed using CLT [43][44][45][46][47].

The offsite manufacturing and sequenced assembly make CLT construction very suited to school development. CLT is an appropriate floor material choice where traditional timber-joisted floors are not generally suitable due to floor span. Structural timber in school design is often left exposed, with designers claiming an additional health benefit from the exposed timber and improved acoustic performance [48].

An FE model was developed to examine the influence of: (i) the serviceability performance of the floor, (ii) non-structural discrete masses replicating standard specified fixed furniture [196], and (iii) the distributed mass due to the rooms occupancy.

Geometry

The room measurement of the modelled classroom, were in accordance with the Irish Department of Education and Sciences requirements.

The room comprised more than four CLT panels spanning two classrooms, separated by a central 1800 mm wide corridor. The overall room size was 10423 mm x 7600 mm. The corridor widens by 885 mm at the classroom entrance. A separate room measuring over 3000 mm x 2000 mm positioned opposite the door within the classroom provides sanitary and w.c. facilities.

In the FE analysis of the standard hotel room, discussed in Section 7.6.1, it was found that added mass adjacent supporting walls did not significantly influence the flexural stiffness and modal frequency of the floor. Therefore the mass of wash hand basins, w.c.s, and cubicles were not considered in the model. The internal partitions separating the sanitary accommodation from the classroom were included only.

The standard classroom layout is illustrated in Figure 7.24., while Figure 7.25 shows the CLT panel configuration that was modelled.

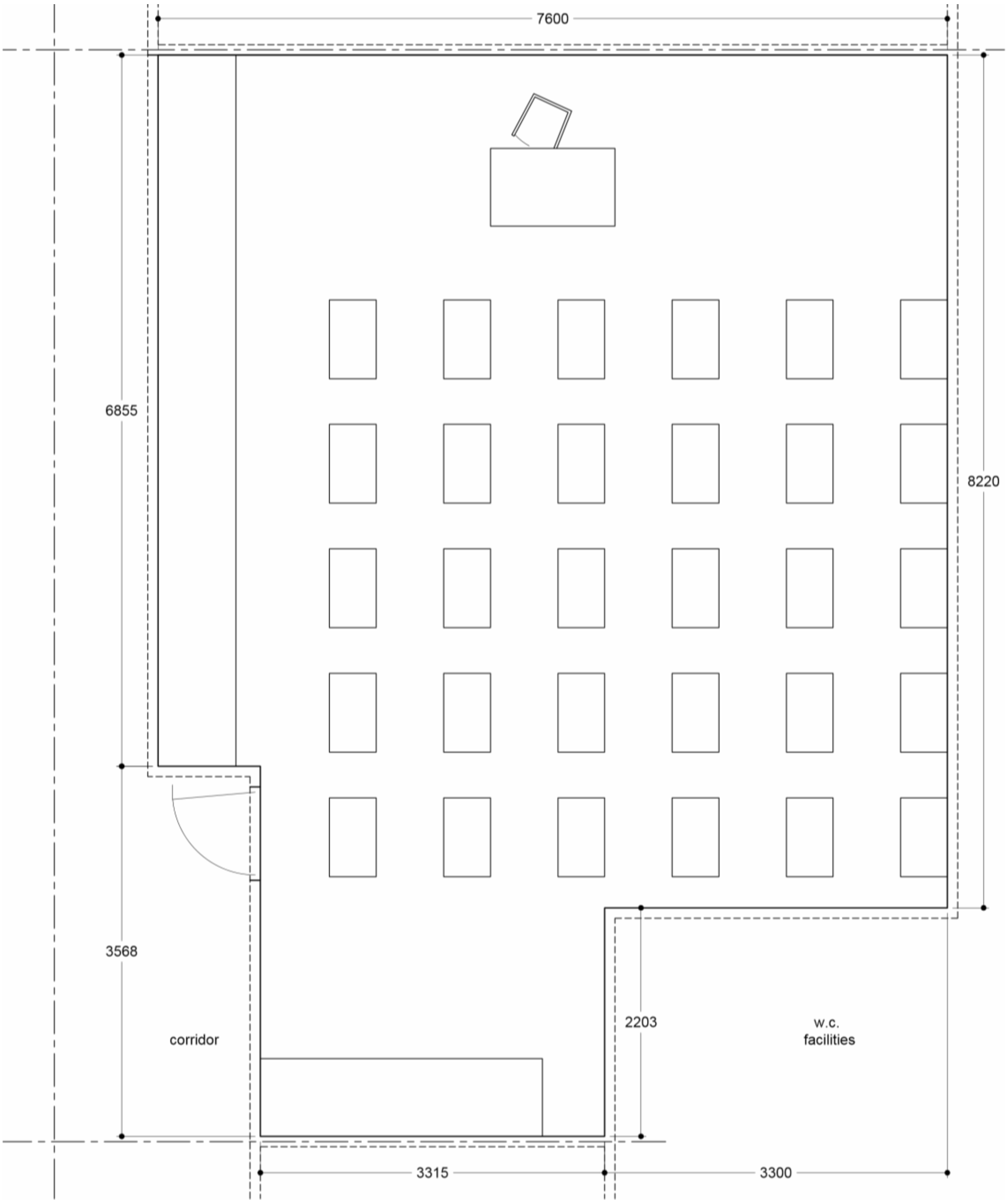
7600
6855
8220
3568
2203
corridor
w.c.
facilities
3315
3300

Figure 7.24 *Irish Department of Education and Sciences generic classroom design for primary schools [196].*

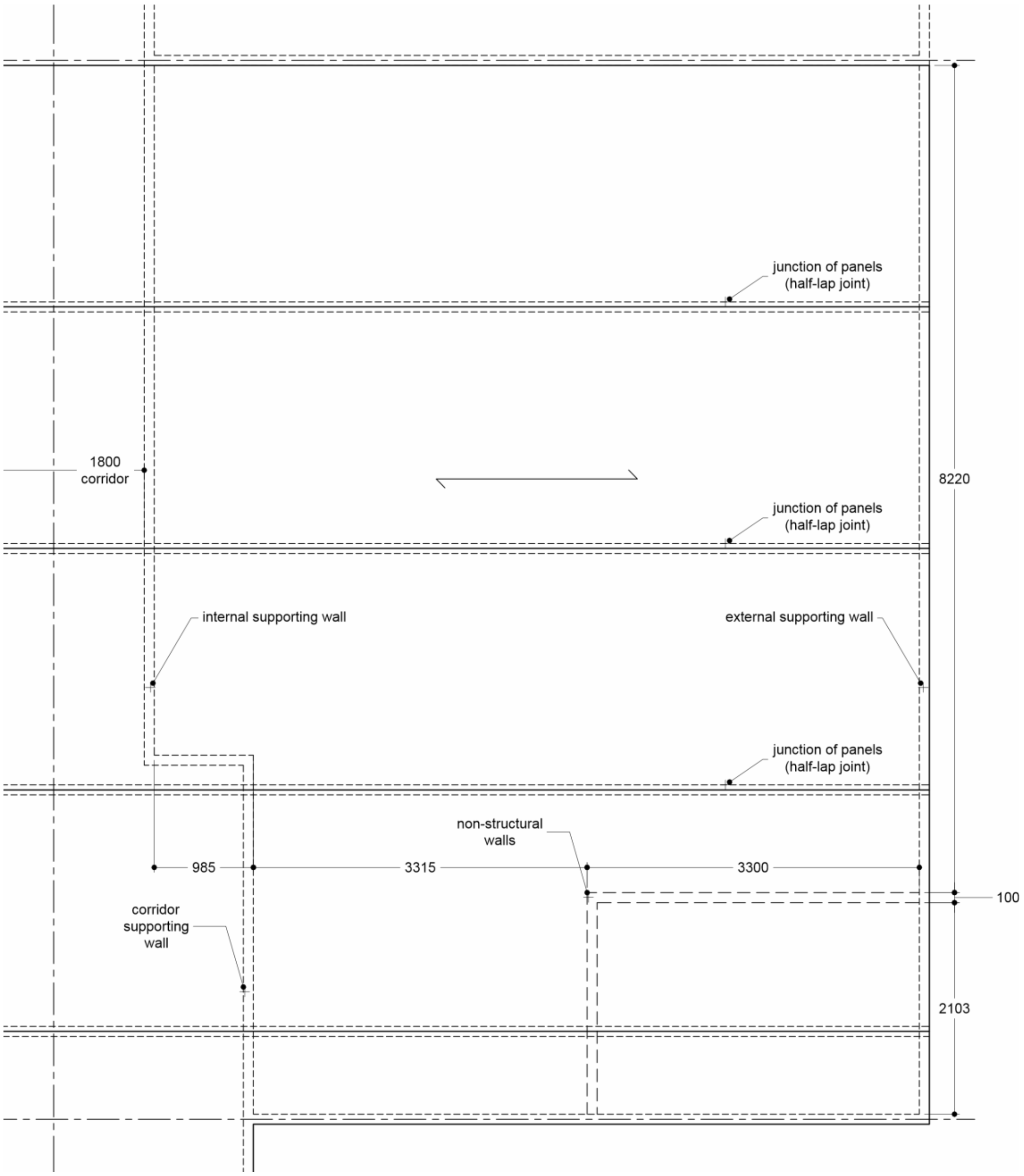
junction of panels
(half-lap joint)
1800
corridor
8220
junction of panels
(half-lap joint)
internal supporting wall
external supporting wall
junction of panels
(half-lap joint)
non-structural
walls
985
3315
3300
100
corridor
supporting
wall
2103

Figure 7.25 *Classroom CLT panel layout*

Mesh and material properties

The classroom models were developed using the general linear, reduced integration, shell element of type S4R, and linear triangular shell elements of type S3. The CLT floor panel was represented by a 5-ply orthotropic composite layup with the orientation of each successive ply rotated 90° to simulate cross-laminated characteristics of CLT. A thickness was applied to each ply, 40 mm and 30 mm alternately, representing the 180 mm lamella build-up of the floor.

Following a mesh convergence study a global element size 40 mm was found to be suitable. The models comprised 61,422 elements, in total.

Boundary conditions and analysis

The boundary conditions were defined by setting the out-of-plane displacement component to zero for all nodes along the lines corresponding to the inner edges of the external supporting walls and at each edge of the corridor walls. The half-lap joint between panels was modelled using the same MPC approach used in the field and generic room models.

The static and modal analysis procedures applied in the laboratory, field, and parametric floor studies was repeated for the hotel room analysis.

Analysis of the classroom layout comprising two rooms and the adjoining corridor was carried out. All furniture was omitted, but the non-load bearing partition walls were included. The external walls, classroom party walls, and corridor walls were regarded as supporting and structural and, therefore, included in the initial analysis. An additional exploratory model was developed to investigate the benefit of including a possible room adjacent (four classrooms) in the analysis. A comparison of the two-roomed and four roomed FE model results indicated that the two-roomed classroom FE representation was deemed to be appropriate. Therefore, the remaining analysis was carried out using the two-roomed model.

Added non-structural fixed mass

The model was adapted to include the mass of the fitted furniture that comprised wall cabinets measuring 6855 mm between the room entrance and the top of the class and also computer stations at the bottom of the room outside the w.c. facilities (Figure 7.24). The fixed furniture dimensions and positions in the room are in accordance with the specific requirements set out by the Irish Department of Education and Science. The mass was added to the floor by increasing the density of the top 40 mm ply of the CLT floor locally. The individual masses of the furniture are outlined in Table 7.3.

Added non-structural non-fixed mass

The model was then further adapted to include the mass of furniture that was not fixed but necessary in a classroom, namely the student and teacher desks and chairs. The maximum loading was assumed to be thirty students with one teacher at the head of the class. The applied masses of the unfixed furniture are also included in Table 7.3.

Table 7.3 *Standard classroom furniture masses*

Item	*Mass*	*Units*
Cabinets	*70*	*kg*
Computer station	*210*	*kg*
Teachers desk	*98*	*Kg*
Teachers chair	*21.75*	*kg*
Students desk	*16*	*kg*
Students chair	*21.75*	*kg*

Human loading

The model was finally amended to investigate the influence of the room occupancy on the modal response of the room. The mass of one teacher and all the students seated at their desks was added to the FE model. All people were assumed to have a mass of 70 kg.

7.7 Conclusions

A numerical modelling programme was developed and implemented to achieve the following objectives: (i) to develop an appropriate, efficient, and straightforward modelling approach to predict the dynamic response of a CLT floor, (ii) including multiple panel floors, (iii) non-rectangular floors, (iv) floor openings, (v) support configurations, and (vi) an uncomplicated method to evaluate how typical objects in buildings impact on a floor’s vibration response.

The FE modelling programme included models of the experimentally tested floors including the single-panel laboratory floor and multi-panel field CLT floors. The numerical models were compared with the experimental results with respect to the floor’s flexural stiffness and natural frequency values. A parametric FE study was then developed to specifically focus on the influence on the floors flexural stiffness and modal frequency values with respect to:

- Floor openings to accommodate vertical circulation
- Floor openings to accommodate service penetrations

- Support to floor openings
- Intermediate supports

Subsequently FE models representing an industry standard hotel twin bedroom and a primary school classroom. The models were developed to examine the serviceability performance of the floor and to examine the influence on the floors flexural stiffness and modal frequency values with respect to:

- Non-loadbearing internal partition walls
- Non-structural discrete masses replicating typical fixed furniture
- Non-structural discrete added mass due to movable distributed furniture

The comparative influence of discrete masses represented as an equivalent evenly distributed mass over the floor area and the benefit of modelling adjacent rooms in a building plan when examining the static and dynamic response of a particular room was also explored.

The FE modal and displacement results are presented in Chapter 8.

8 FE CLT FLOOR RESULTS

8.1 Introduction

This chapter outlines the results of the FE programme developed to examine how common design variations influence the serviceability performance of upper storey floors in mid-rise CLT construction. The FE modelling programme included calibrating FE models of the laboratory and field tested CLT floors with experimental flexural stiffness and modal frequency results. A parametric study of a generic three-panel room, a standard twin-bed hotel room [195], and a classroom design taken from the Irish Primary School Design Guidelines [196] were also investigated.

8.2 FE model of laboratory tested floor

FE models were developed of the single CLT panel floor that was tested in the laboratory. The alternative span orientations of the floor and the influence of added mass was studied. Both minimum and maximum degrees of rotation was applied to the support boundaries. The support orientations spanning the floor at 3812 mm (platform Assemblies B, H, and with added mass, D), 4000 mm (balloon Assemblies J, and with added mass, K), a short span of 2212 mm (platform Assembly L and Assembly O, with added mass), and a two-way span configuration spanning 2212 mm and 3812 mm (platform Assembly P) were examined. Each floor orientation is illustrated in Figures 7.6 to 7.9.

8.2.1 Static point load FE deflection results

For each floor configuration, a static displacement analysis was carried out to determine the maximum displacement due to the application of a load of 1 kN pressure load over an area of 100 mm x 100 mm corresponding to the experimental testing arrangement. Table 8.1 outlines the FE results of the displacement analysis for both the minimum and maximum degrees of rotation of the support boundaries. The comparative experimental results (Assemblies B, H, D, J, K, L, O, and P) are included in the table. Figure 8.1 charts the FE and experimental results and the minimum EC-5 [22] static deflection limit. Figure 8.2 charts the FE and experimental results with the minimum and maximum static 1 kN deflection EC-5 [22] limits and the Irish NA limit for floors spanning less than 4000 mm of 1.8 mm/kN [111] marked for reference.

Table 8.1 *FE displacement analysis due to a 1kN load applied midspan, with experimental results for Assemblies B, H, D, J, K, L, O, and P*

Floor to wall Assembly	*Load added*	*Deflection (mm)*
		1kN Static point load applied midspan
	One-way long span: Platform construction	
B		*0.18*
H		*0.16*
FEM	*Simply-supported*	*0.24*
FEM	*Fully-fixed*	*0.13*
D	●	*0.18*
FEM	*Simply-supported*	*0.23*
FEM	*Fully-fixed*	*0.13*
	One-way long span: Balloon construction	
J		*0.20*
FEM	*Simply-supported*	*0.26*
FEM	*Fully-fixed*	*0.14*
K	●	*0.20*
FEM	*Simply-supported*	*0.26*
FEM	*Fully-fixed*	*0.13*
	One-way short span: Platform construction	
L		*0.11*
FEM	*Simply-supported*	*0.16*
FEM	*Fully-fixed*	*0.10*
O	●	*0.10*
FEM	*Simply-supported*	*0.15*
FEM	*Fully-fixed*	*0.10*
	Two-way span: Platform construction	
P		*0.10*
FEM	*Simply-supported*	*0.15*
FEM	*Fully-fixed*	*0.10*

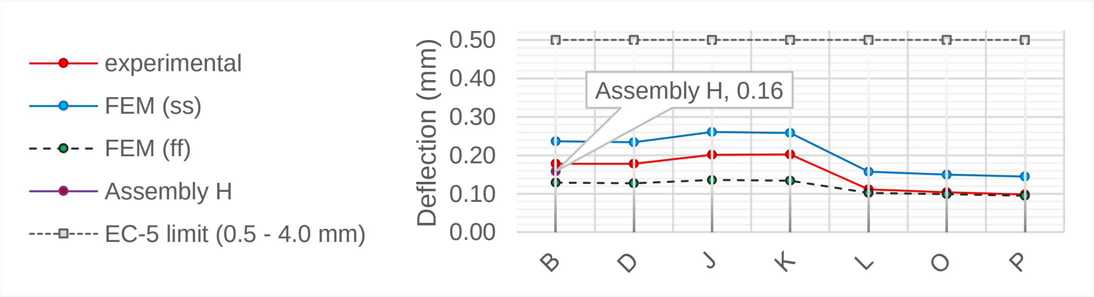

Figure 8.1 *Static deflection results, Assemblies B, H, and D; J and K; L and O; and P with EC-5 [22] minimum deflection limits 0.5 mm/kN*

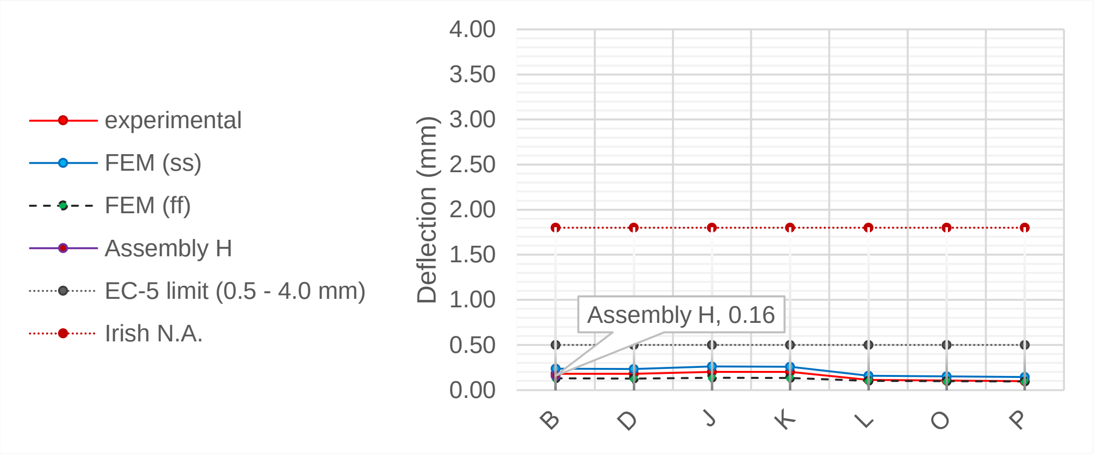

Figure 8.2 *Static deflection results, Assemblies B, H, and D; J and K; L and O; and P with EC-5 [22] 0.5 to 4.0 mm/kN limits and Irish NA: 1.8 mm/kN for spans ≤ 4000 mm [111].*

Summary of FE deflection results *(laboratory tested floor)*

The FE displacement analysis for the model with minimum restriction on rotational stiffness at the supports (simply-supported / pinned) spanning 3812 mm (platform Assemblies B, H, and with added mass, D), ranged between 0.23 and 0.24 mm. Applying a maximum rotational stiffness at the boundaries, where all six degrees of freedom are fixed, resulted in a deflection midspan of 0.13 mm for both models with, and without added mass. The equivalent experimental results with, and without added mass, were 0.18 mm in both cases. The experimental test assembly with the maximum rotational stiffness at the supports of the assemblies tested was that of Assembly H, where a 0.16 mm/kN deflection was recorded experimentally.

The FE displacement results of the floor model spanning 4000 mm (balloon Assemblies J, and with added mass, K), were 0.26 mm and 0.14 mm for the floor panel without mass for minimum and maximum restriction on the degrees of rotation, respectively. The difference in the deflection results for the floor with mass was negligible. The equivalent experimental results with, and without added mass were 0.20 mm in both cases, again midway between the results of the results from the FE models with maximum and minimum rotation at the supports.

In the case of the FE analysis of the floor spanning in the alternative short span 2212 mm (platform Assembly L and Assembly O, with added mass), results ranged between 0.16 mm and 0.10 mm for the floor panel without mass. The difference due to an evenly distributed added mass was again negligible. The equivalent experimental results with, and without added mass were 0.11 mm and 0.10 mm, respectively.

The FE displacement results of the floor model spanning in two-ways (platform Assembly P), were 0.15 mm and 0.10 mm for minimum and maximum restriction on the degrees of rotation at the supports, respectively. The equivalent experimental results was 0.10 mm.

Comparing FE results with maximum and minimum rotational stiffness at the supports with the experimental test results found that the experimental results for the long-spanning floor were generally midway between both FE limits. Where the floor was supported in the short span, the maximum rotational stiffness generally coincided with the experimental results.

The FE deflection results of the floor with, and without added mass, coincided with the observation from the experimental testing that non-structural added mass has negligible influence on flexural stiffness of the CLT floor. The experimental deflection results found that the alternative fixing configurations do not notably affect the flexural stiffness of the floor (Section 6.2.2). Comparing the FE analysis of minimum and maximum rotational stiffness and the experimental testing results imply that assuming the floor fixing to be simply-supported in all instances is conservative, but appropriate considering the variance between both results was less than a fifth of a millimetre (between 0.05 mm and 0.16 mm) in all instances.

Comparing the deflection results with the current deflection limits set in the European standard and the Irish NAs to the standard [22][111], all FE and experimental results were significantly less that the limit provided for a floor of the same span of 0.50 mm and 1.80 mm, respectively [121].

8.2.2 Modal frequency FE results

Theoretical frequency estimates

Table 8.2 outlines the FE results of the initial modal frequency analysis for the floor model spanning 4000 mm, without added mass. The mass of the electromagnetic shaker was also omitted (comparable to the balloon Assembly I, impulse test). Five modes were predicted by the FE modal analysis in the 0 to 80 Hz range for both the minimum and maximum degrees of rotation of the support boundaries.

Table 8.2 *Initial FE frequency mode shape estimates for Assembly I: 0 to 80 Hz*

Fully-fixed	*Simply-supported*
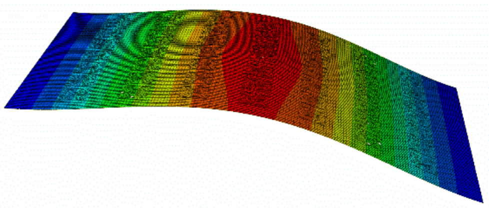	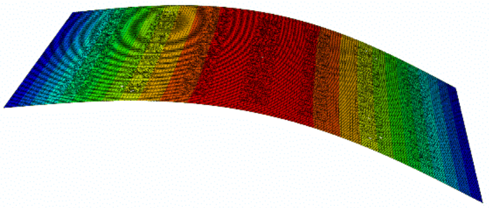
Mode 1: 35.60 Hz	*Mode 1: 19.58 Hz*
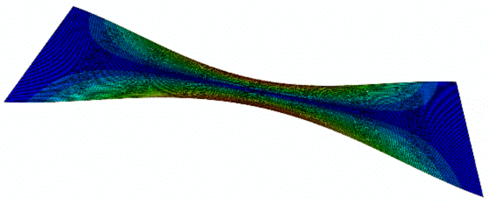	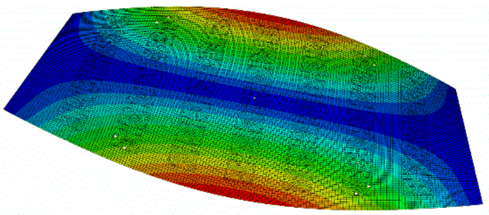
Mode 2: 38.79 Hz	*Mode 2: 25.32 Hz*
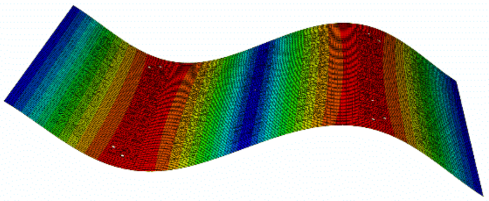	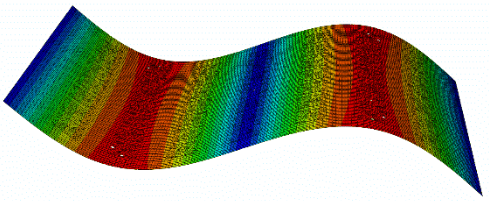
Mode 3: 79.27 Hz	*Mode 3: 65.84 Hz*
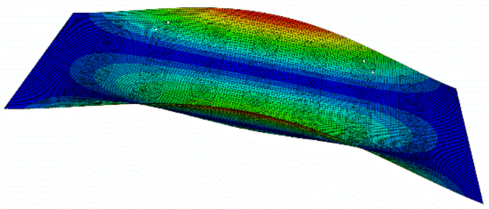	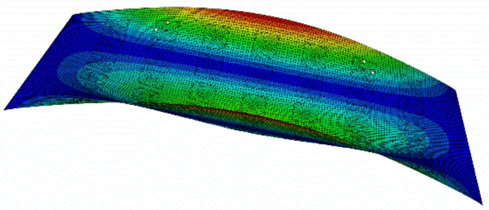
Mode 4: 74.19 Hz	*Mode 4: 68.80 Hz*
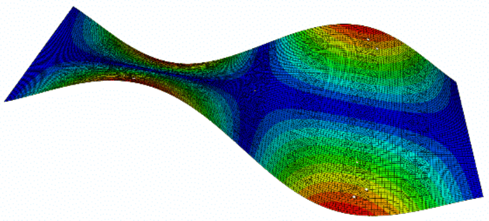	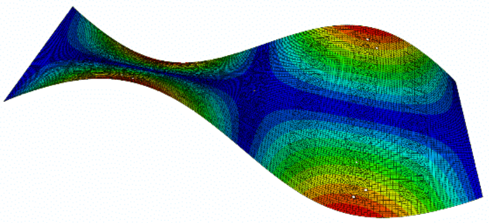
Mode 5: 83.72 Hz	*Mode 5: 71.13 Hz*

One-way long-span platform construction *(Assemblies B, H, and D)*

To correlate with the experimental FRF modal testing in the laboratory, it was necessary to include the mass of the mechanical exciter in the FE model. In keeping with the experimental test procedure, separate FE models were generated with the exciter located at midspan to determine the first and fourth modes and at the quarter span for the second, third, and fifth mode measurement. The exciter locations are illustrated in Figures 7.6 and 7.11.

The FE modal analysis of the floor spanning 3812 mm (platform Assembly B to H) including the mass of the electromagnetic shaker, generated five modes within the frequency range of interest 0 to 80 Hz.

Added mass

Additionally, alternative FE models were developed to include the distributed added masses, representing the added mass in the experimental laboratory testing (Assemblies D, K, and O). The mass was incorporated into the floor model by locally altering the density of the top ply of the floor panel locally at 49 locations distributed across the floor. Figure 7.11 illustrates the added mass positions.

Table 8.3 shows the modal frequency results for both the minimum and maximum degrees of rotation of the support boundaries for the floor spanning 3812 mm with, and without non-structural added mass. The comparative experimental results (platform Assemblies B, H, and with added mass, D) are included.

Table 8.3 *FE frequency results compared for platform Assemblies B, H, and D*

Floor to wall Assembly	*Load added*	*Natural frequencies (Hz)*				
		Mode 1	*Mode 2*	*Mode 3*	*Mode 4*	*Mode 5*
	One-way long span: Platform construction					
B		*21.90*	*28.20*	*72.65*	*78.05*	*-*
H		*23.40*	*29.70*	*74.10*	*78.90*	*-*
FEM	*Simply-supported*	*20.92*	*27.47*	*68.97*	*67.84*	*75.65*
FEM	*Fully-fixed*	*37.29*	*41.21*	*81.70*	*72.81*	*87.90*
D	●	*16.35*	*21.45*	*53.95*	*69.25*	*65.35*
FEM	*Simply-supported*	*15.30*	*21.34*	*50.43*	*55.85*	*57.75*
FEM	*Fully-fixed*	*27.31*	*31.64*	*59.79*	*59.93*	*66.65*

The mode shapes for the floor without added mass for both the minimum and maximum degrees of rotation of the support boundaries are illustrated in Table 8.4.

Table 8.4 *FE modal results 0 to 80 Hz, for Assemblies B and H*

Fully-fixed	*Simply-supported*
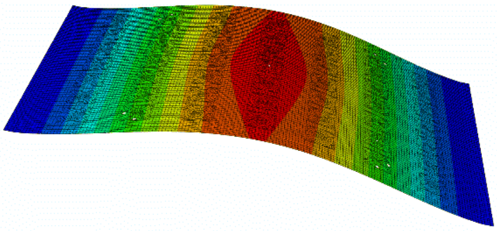	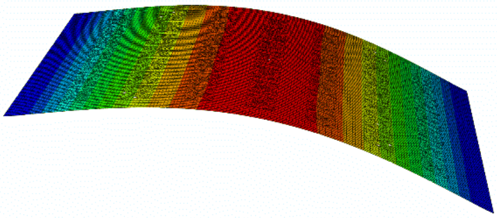
Mode 1: 37.29 Hz	*Mode 1: 20.92 Hz*
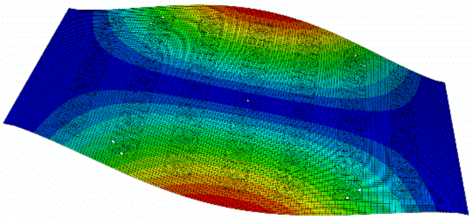	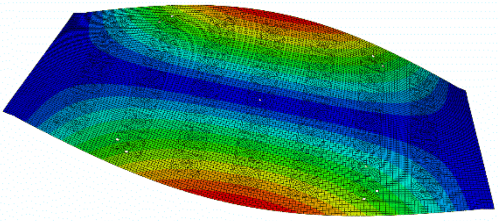
Mode 2: 41.21 Hz	*Mode 2: 27.47 Hz*
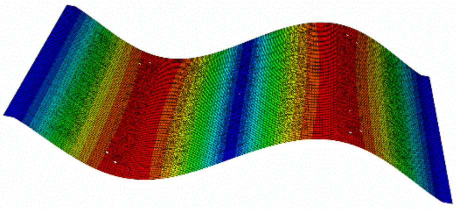	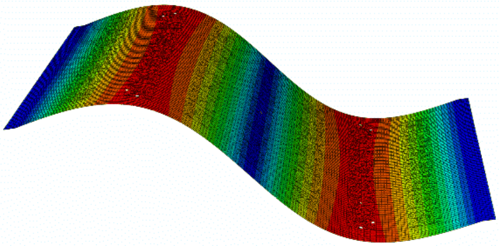
Mode 3: 81.70 Hz	*Mode 3: 68.97 Hz*
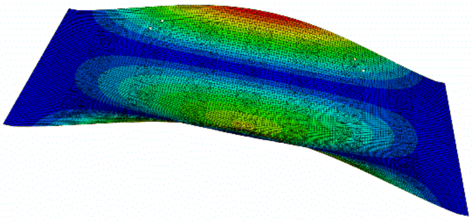	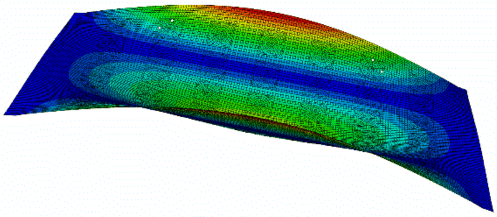
Mode 4: 72.81 Hz	*Mode 4: 67.84 Hz*
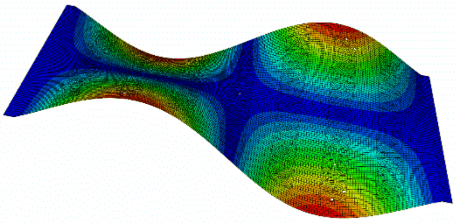	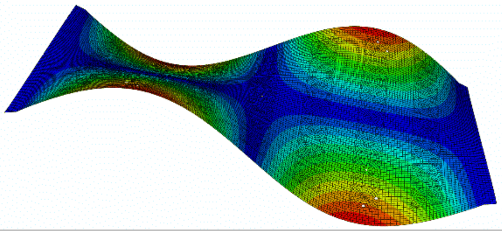
Mode 5: 87.90 Hz	*Mode 5: 75.65 Hz*

Figure 8.3 charts the modal frequency results for both the minimum and maximum degrees of rotation of the support boundaries for the floor spanning 3812 mm without added mass. The comparative experimental results (platform Assemblies B and H) are included.

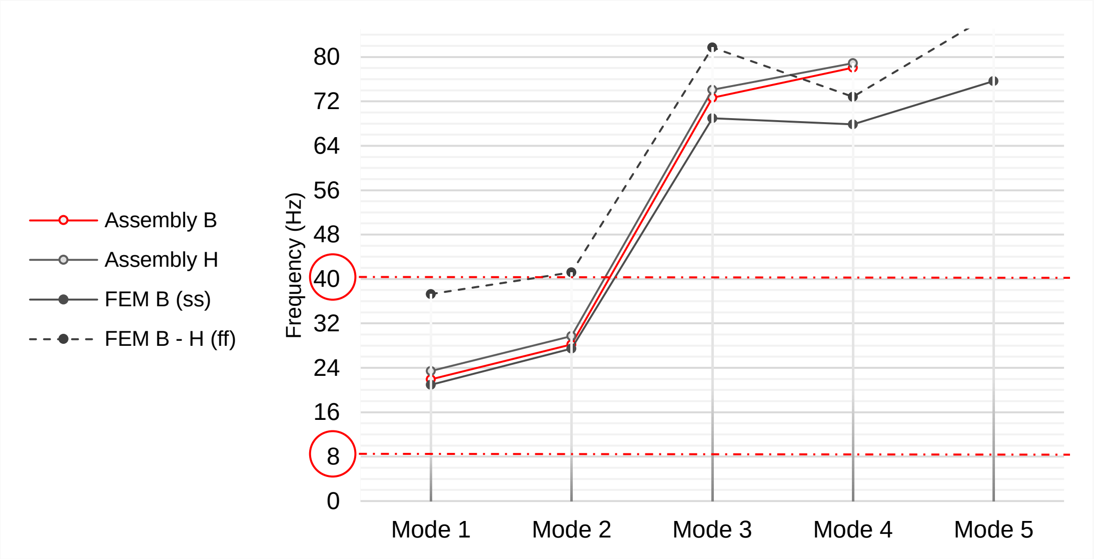

Figure 8.3 *FE and experimental frequency results for platform Assemblies B and H*

The FE modal analysis of the floor model with minimum restriction on rotational stiffness at the supports (simply-supported / pinned) spanning 3812 mm (platform Assemblies B and H) showed good correlation with the experimental test results for the first two modes. The variance was less than 1 Hz and 2.5 Hz compared with the experimental test Assemblies B and H, respectively. The laboratory example with the maximum rotational stiffness at the supports, of that tested, was Assembly H. Compared with the FE model where all six degrees of freedom are fixed, the variance in frequency results was over 11 Hz, which implies that the support rigidity was not significantly increased in the laboratory assembly (H).

The first two modes of all the FE modal analysis and experimental results were below 40 Hz. A reduced number of first-order modes below 40 Hz is important to ensure compliance with the current European timber frequency and unit impulse velocity criteria in EC-5 [22]. Therefore, a good characterisation of all modes below 40 Hz is particularly import in predicting the serviceability performance of a floor. Characterising the FE support as simply-supported provided close correlation with the experimental results in the case of the modes below 40 Hz.

The correlation at the third mode was not as close at 3.7 Hz and 5.1 Hz for Assemblies B and H, respectively and was more conservative for the higher modes.

Added mass

Figure 8.4 charts the modal frequency results for both the minimum and maximum degrees of rotation of the support boundaries for the floor spanning 3812 mm with non-structural added mass. The comparative experimental results (platform Assembly D) are included.

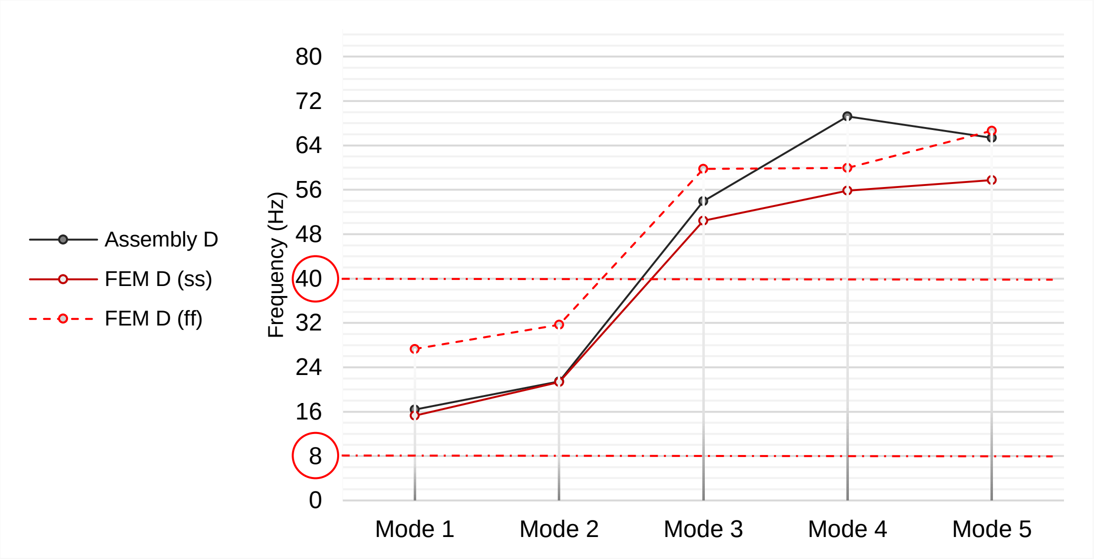

Figure 8.4 *FE and experimental frequency results for platform Assembly D*

The correlation between FE and experimental results was similar in the case of the floor assembly with added mass. The variance between the simply-supported FE modal analysis and the experimental results for the first two modes was negligible (less than 1 Hz), while the FE results for the model with maximum rotational stiffness boundary conditions were greater than the experimental results by over 10 Hz.

Comparing the third mode frequency values showed a variance of 3.5 Hz, characterising the boundary conditions as simply-supported and were significantly more conservative for the higher modes below 80 Hz.

One-way long-span balloon construction *(Assemblies J and K)*

Table 8.5 shows the modal frequency results for both the minimum and maximum degrees of rotation of the support boundaries for the floor spanning 4000 mm with, and without non-structural added mass. The comparative experimental results (balloon Assemblies J and with added mass, K) are included.

Table 8.5 *FE frequency results compared for platform Assemblies J and K*

Floor to wall Assembly	*Load added*	*Natural frequencies (Hz)*				
		Mode 1	*Mode 2*	*Mode 3*	*Mode 4*	*Mode 5*
	One-way long span: Balloon construction					
J		*20.45*	*25.65*	*68.20*	*77.20*	*77.50*
FEM	*Simply-supported*	*19.16*	*25.12*	*64.04*	*66.45*	*70.16*
FEM	*Fully-fixed*	*34.68*	*38.52*	*76.74*	*71.38*	*82.64*
K	●	*14.90*	*19.20*	*50.85*	*67.45*	*63.80*
FEM	*Simply-supported*	*14.00*	*19.52*	*46.82*	*54.70*	*53.71*
FEM	*Fully-fixed*	*25.38*	*29.61*	*56.11*	*58.65*	*62.83*

Figure 8.5 charts the modal frequency results for both the minimum and maximum degrees of rotation of the support boundaries for the floor spanning 4000 mm without added mass. The comparative experimental results (balloon Assembly I) are included.

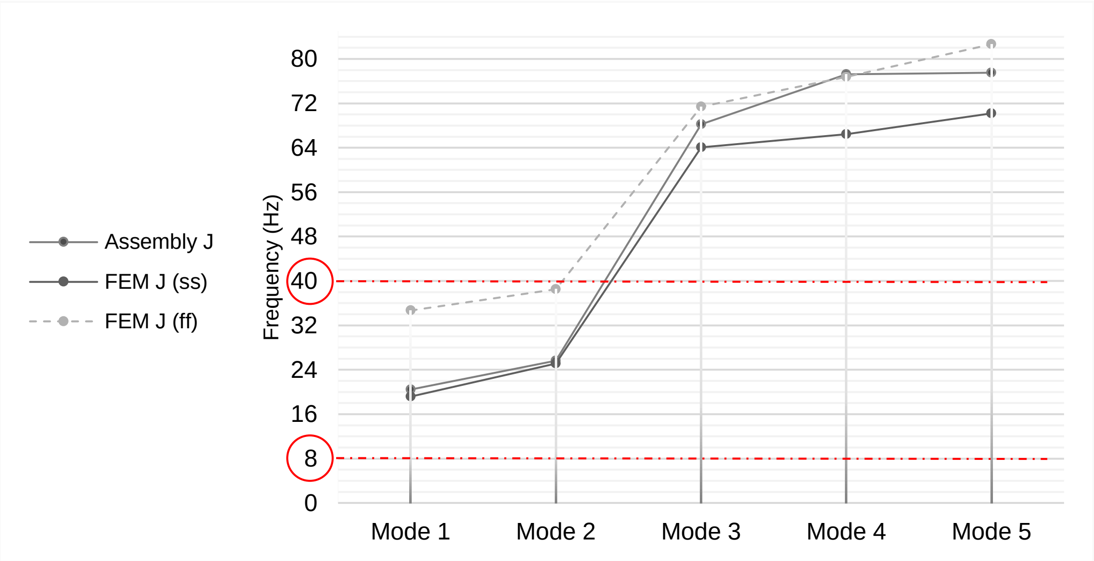

Figure 8.5 *FE and experimental frequency results for balloon Assemblies I and J*

The FE modal analysis of the floor model with minimum restriction on rotational stiffness at the supports spanning 4000 mm (balloon Assembly J) showed good correlation with the experimental test results for the first two modes. The variance was negligible between the FE and experimental frequency values. The variance with the FE model with maximum rotational stiffness at the boundaries, was greater than 12

Hz. Characterising the boundary conditions as simply-supported was generally conservative for the higher modes.

Added mass

Figure 8.6 charts the modal frequency results for both the minimum and maximum degrees of rotation of the support boundaries for the floor spanning 4000 mm with non-structural added mass. The comparative experimental results (balloon Assembly K) are included.

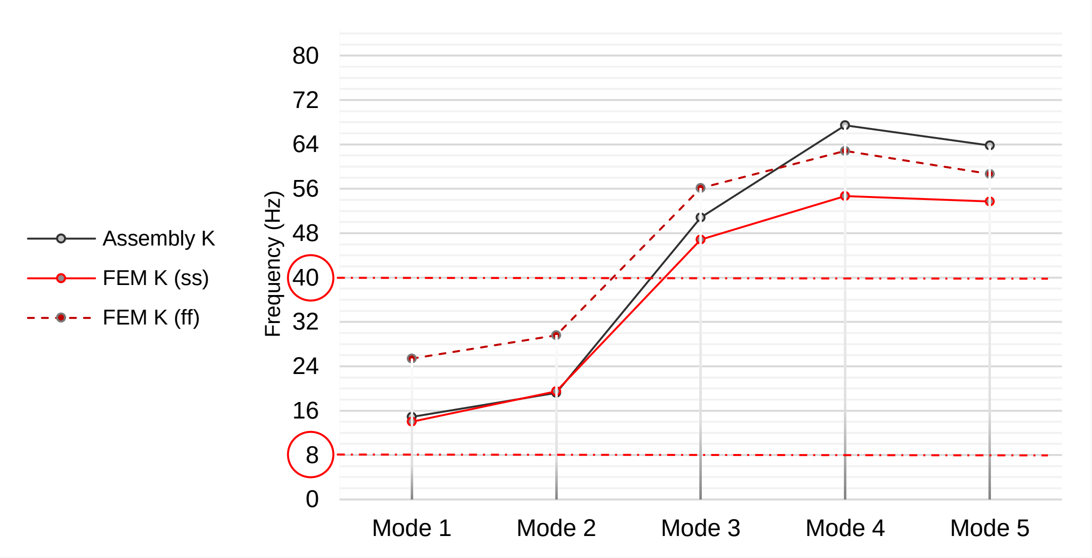

Figure 8.6 *FE and experimental frequency results for balloon Assembly K*

The variance between the simply-supported FE modal analysis and the experimental results for the first two modes was negligible (less than 1 Hz), while the FE models that had boundary conditions of maximum rotational stiffness were greater than the experimental results by over 10 Hz.

Comparing the third mode frequency values showed a variance of 3.5 Hz, characterising the boundary conditions as simply-supported and were significantly conservative for the higher modes below 80 Hz.

One-way short-span platform construction *(Assemblies L and O)*

In the case of the FE analysis of the floor spanning in the alternative short span of 2212 mm (platform Assembly L and Assembly O, with added mass), four modes were estimated by the FE modal analysis in the 0 to 80 Hz range. The mode shapes for the floor without added mass for both the minimum and maximum degrees of rotation of the support boundaries are illustrated in Table 8.6.

Table 8.6 *FE modal results 0 to 80 Hz, for Assembly L*

Fully-fixed	*Simply-supported*
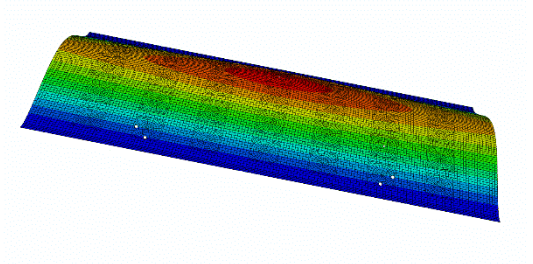	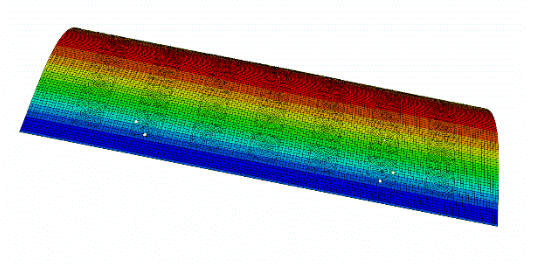
Mode 1: 51.16 Hz	*Mode 1: 30.58 Hz*
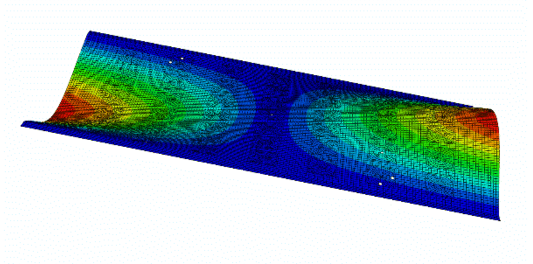	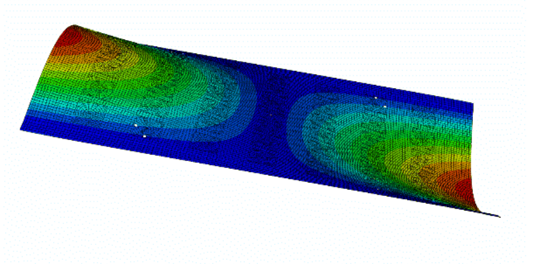
Mode 2: 54.60 Hz	*Mode 2: 35.77 Hz*
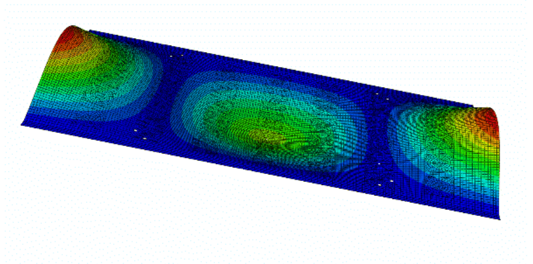	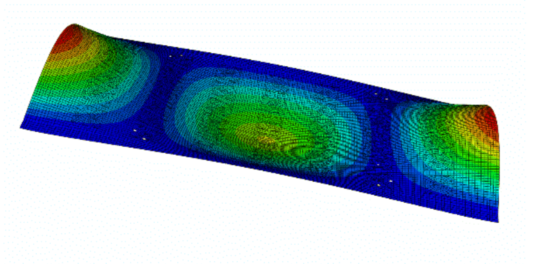
Mode 3: 70.69 Hz	*Mode 3: 60.28 Hz*
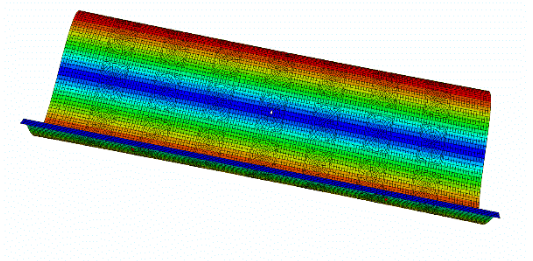	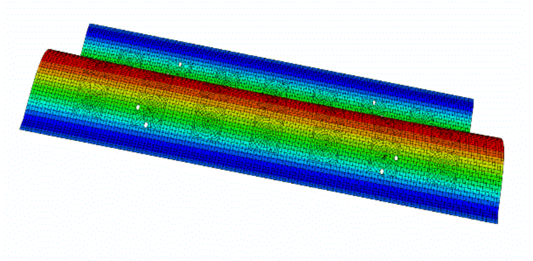
Mode 4: 106.60 Hz	*Mode 4: 94.67 Hz*

Table 8.7 shows the modal frequency results for both the minimum and maximum degrees of rotation of the support boundaries for the floor spanning 2212 mm with, and without non-structural added mass. The comparative experimental results (platform Assemblies L and with added mass, O) are included.

Table 8.7 *FE frequency results compared for platform Assemblies L and O*

Floor to wall Assembly	*Load added*	*Natural frequencies (Hz)*				
		Mode 1	*Mode 2*	*Mode 3*	*Mode 4*	*Mode 5*
	One-way short span: Platform construction					
L		*29.50*	*38.25*	*66.40*	*-*	*-*
FEM	*Simply-supported*	*30.58*	*35.77*	*60.28*	*94.67*	*-*
FEM	*Fully-fixed*	*51.16*	*54.60*	*70.69*	*106.60*	*-*
O	●	*23.95*	*29.95*	*54.95*	*68.60*	*-*
FEM	*Simply-supported*	*23.20*	*28.14*	*48.81*	*71.93*	*-*
FEM	*Fully-fixed*	*38.40*	*42.36*	*57.42*	*81.25*	*-*

Figure 8.7 charts the modal frequency results for both the minimum and maximum degrees of rotation of the support boundaries for the floor spanning 2212 mm without added mass. The comparative experimental results (platform Assembly L) are included.

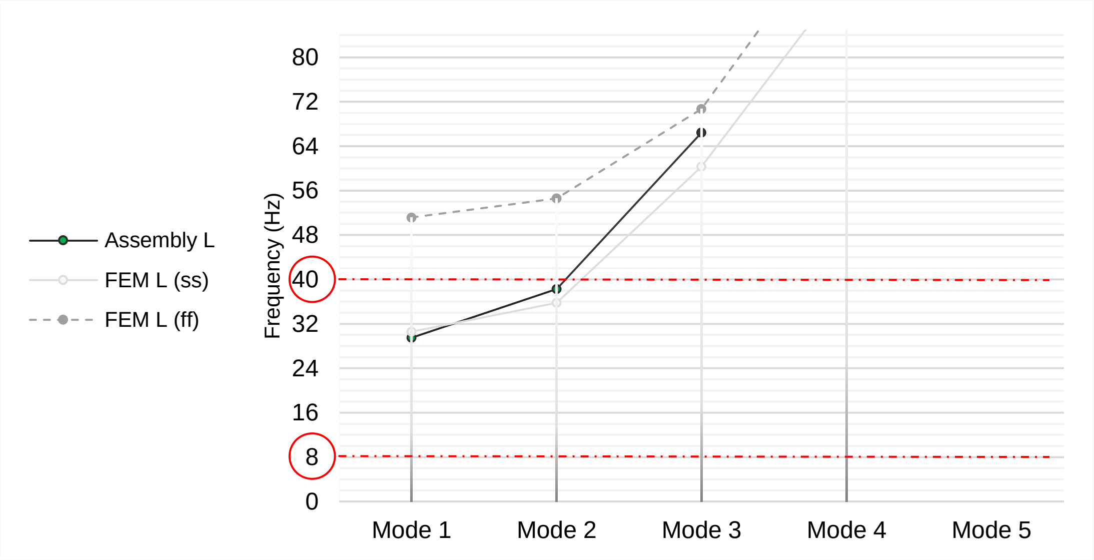

Figure 8.7 *FE and experimental frequency results for platform Assembly L*

The FE modal analysis of the floor model with minimum restriction on rotational stiffness at the supports spanning 2212 mm (platform Assembly L) showed good correlation with the experimental test results for the first two modes. The variance was less than 3 Hz compared with Assembly L experimental results. However, the first mode was underestimated by 1 Hz. The fourth mode was not recorded in the experimental tests of Assembly L.

The frequency value difference with the FE model with maximum rotational stiffness at the boundaries were 21 Hz and 16 Hz for the modes 1 and 2, respectively. Comparing the FE analysis of minimum and maximum rotational stiffness and the experimental testing results again suggest that assuming the floor fixing to be simply-supported in all instances is conservative but appropriate.

Added mass

Figure 8.8 charts the modal frequency results for both the minimum and maximum degrees of rotation of the support boundaries for the floor spanning 2212 mm with non-structural added mass. The comparative experimental results (platform Assembly O) are included.

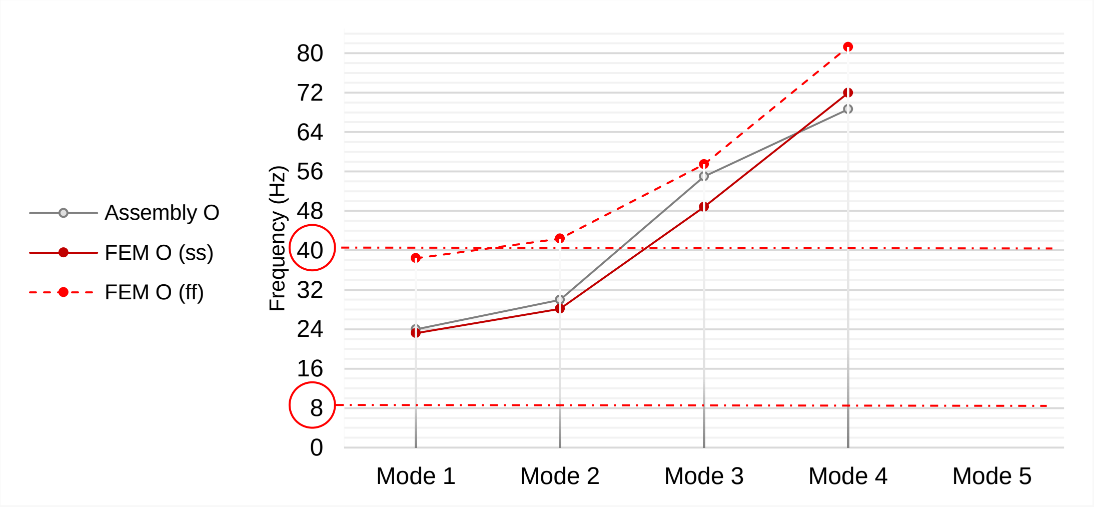

Figure 8.8 *FE and experimental frequency results for platform Assembly O*

The correlation between FE with minimum rotational stiffness and the experimental results was similar in the case of the floor assembly with added mass. The variance between both results for the first two modes was negligible (less than 2 Hz), while the FE models that had boundary conditions of maximum rotational stiffness were greater than the experimental results by over 12 Hz.

The variance between the FE modal analysis and experimental frequency results was greater than 6 Hz for the higher modes below 80 Hz. Note: characterising the boundary conditions as simply-supported for the shorter spanning floor was not always conservative.

Two-way platform construction *(Assembly P)*

In the case of the FE analysis of the floor spanning in two directions (platform Assembly P), only one mode was estimated by the FE modal analysis and only one mode was recorded in the experimental laboratory testing. The mode shapes for the floor for both the minimum and maximum degrees of rotation of the support boundaries are illustrated in Table 8.8.

Table 8.8 *FE modal results 0 to 80 Hz, for Assembly P*

Fully-fixed	*Simply-supported*
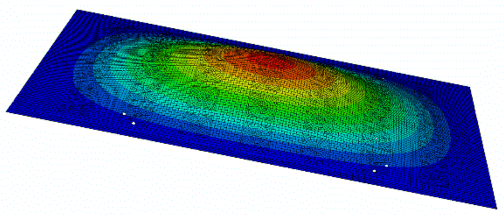	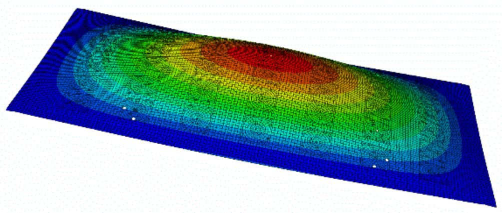
Mode 1: 62.02 Hz	*Mode 1: 39.60 Hz*

Table 8.9 and Figure 8.9 show the frequency values of the mode for both the minimum and maximum degrees of rotation of the support boundaries with the comparative experimental result (platform Assembly P) included.

Table 8.9 *FE frequency results compared for platform Assembly P*

Floor to wall Assembly	*Load added*	*Natural frequencies (Hz)*				
		Mode 1	*Mode 2*	*Mode 3*	*Mode 4*	*Mode 5*
	Two-way span: Platform construction					
P		*41.75*	-	-	-	-
FEM	*Simply-supported*	*39.60*	-	-	-	-
FEM	*Fully-fixed*	*62.02*	-	-	-	-

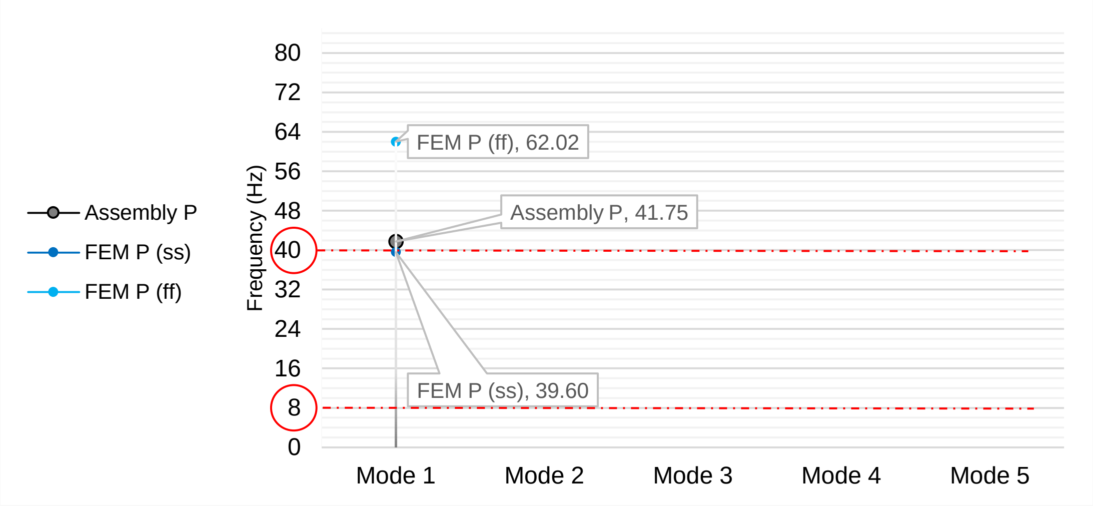

Figure 8.9 *FE and experimental frequency results for platform Assembly P*

The FE model with simply-supported boundary conditions was marginally conservative but estimated the experimental result with a significantly greater degree of accuracy, 1 Hz, compared with 20 Hz predicted with boundary conditions characterised as fixed.

Summary FE frequency results *(laboratory tested floor)*

The FE modal analysis of the floor model with a minimum restriction on rotational stiffness at the supports provided the best correlation to the experimental test results for the first two modes, for all the floor orientations examined: (i) Platform 3812 mm span Assemblies B, H, and with added mass, D, (ii) balloon 4000 mm span Assemblies J, and with added mass, K, (iii) platform short span 2212 mm Assembly L and Assembly O, with added mass, and (iv) the platform two-way span floor Assembly P. The variance between the FE simply-supported models and the experimental frequency values was generally less than 1 Hz to 2 Hz. However, a poor correlation was recorded for the higher modes, greater than 6 Hz generally.

In the case of the frequency values below 40 Hz (Modes 1 and 2) the FE modal analysis with maximum rotational stiffness at the boundaries, where all six degrees of freedom were fixed, the variance in frequency results were greater than 11 Hz in all instances.

As a good characterisation of modes below 40 Hz is particularly import in predicting the serviceability performance of a floor with respect to human activity and pedestrian excitation (EC-5 [22]), it may be reasoned from the FE modal analysis that the support conditions of CLT floors be characterised as simply-supported regardless of the type of fixing used.

Characterising the boundary conditions as simply-supported was not always conservative for the shorter spanning floor (Assemblies L and O). However, the variance between the results were less than 2 Hz.

8.3 FE models of the field tested floors

FE models were developed of two of the three rooms investigated experimentally in-situ in a three-storey CLT building in Bishop’s Stortford, UK. The rooms comprised multiple CLT panel floors (Figures 5.32 and 5.34).

The two main aims for developing the FE models of the field tested floors was to establish: (i) if defining the floor support as simply-supported holds true for floors integrated into a building, and (ii) to develop a suitable characterisation of the transverse connections between the panels running in parallel.

The first three mode shapes of the floors of Rooms 1 and 3 are illustrated in Table 8.10. The support boundaries were defined with the minimum degrees of rotation (simply-supported) for both room models. Parallel panels were connected with MPC at 250 mm spacing, with rotation permitted along the span axis of the panels, while the other five degrees of freedom were tied.

Table 8.11 and Figure 8.10 show the first ten modes of the FE results for Room 1. The comparative experimental field result for the first ten modes are also included. The FE model predicted 16 modes below 83 Hz, while the experimental testing recorded 16 natural modes in the 0 to 80 Hz range.

The CLT panels that were tested in-situ comprised three spans, Room 1 and 3, the central corridor and Room 2. Only the natural modes that occur in the tested rooms (Rooms 1 and 3) are illustrated. Any natural modes predicted in FE for Room 2 are ignored as there are no experimental measurements to validate their value. Some exploratory tests were taken along the central corridor on site, however no modes in the 0 to 80 Hz range were recorded. The subsequent FE analysis also did not predict natural modes below 80 Hz along the central corridor.

Table 8.10 *FE mode shape results for Room 1 and 3: Modes 1 to 3*

Room 1	*Room 3*
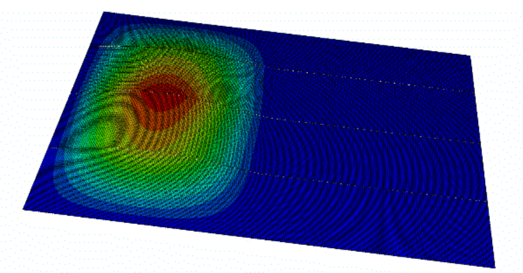	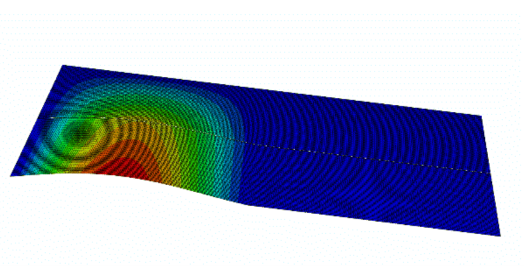
Mode 1: 15.43 Hz	*Mode 1: 15.43 Hz*
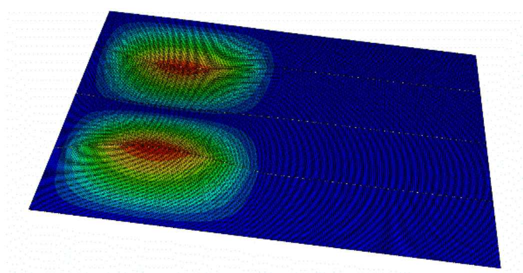	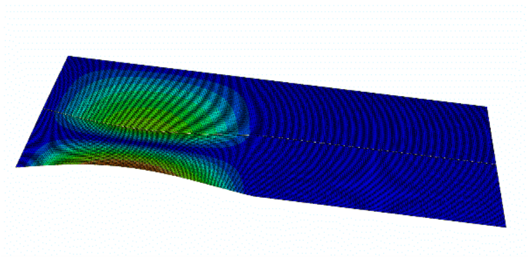
Mode 2: 16.57 Hz	*Mode 2: 18.55 Hz*
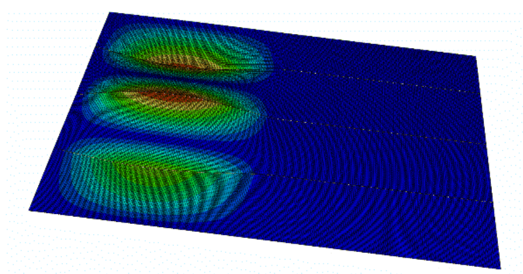	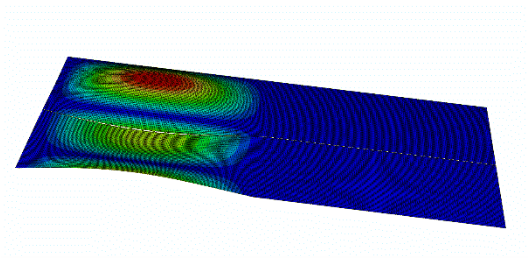
Mode 3: 18.50 Hz	*Mode 3: 35.54 Hz*

Table 8.11 *Experimental Impulse and FE results compared for Room 1: Modes 1 to 10*

Room	*Natural frequencies (Hz)*									
	Mode 1	*Mode 2*	*Mode 3*	*Mode 4*	*Mode 5*	*Mode 6*	*Mode 7*	*Mode 8*	*Mode 9*	*Mode 10*
Room 1	*14.75*	*15.50*	*18.75*	*33.00*	*36.00*	*41.00*	*42.75*	*46.25*	*50.25*	*53.25*
FEM	*15.43*	*16.57*	*18.50*	*31.55*	*38.46*	*44.76*	*45.92*	*48.00*	*48.74*	*54.80*

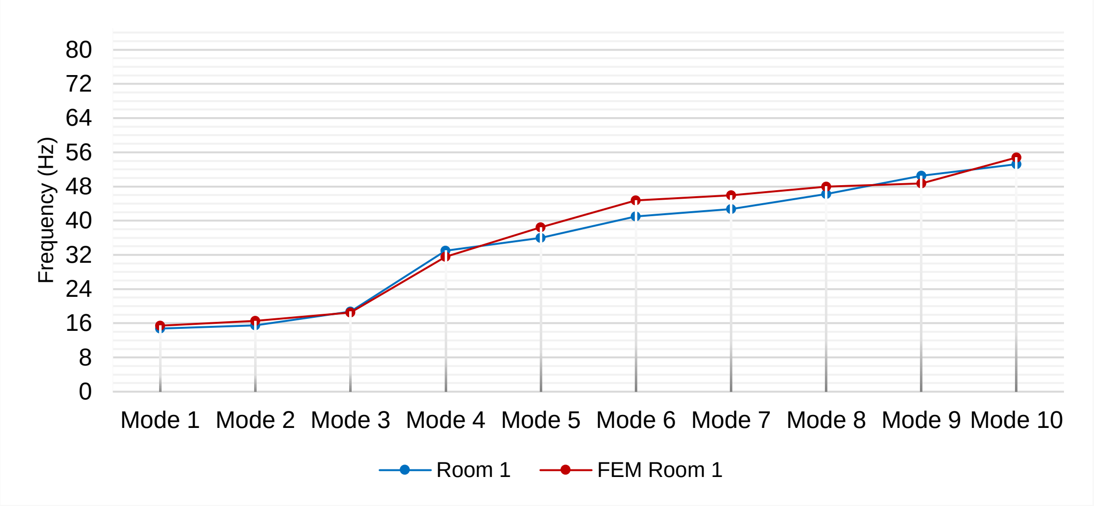

Figure 8.10 *Experimental Impulse and FE results compared for Room 1: Modes 1 to 10*

Table 8.12 and Figure 8.11 show the seven natural modes predicted by the FE analysis of Room 3. The support boundary conditions were again defined with the minimum degree of rotation (simply-supported) and the comparative experimental field result of seven natural modes in the 0 to 80 Hz range are also included.

Table 8.12 *Experimental Impulse and FE results compared for Room 3. Modes 1 to 7*

Room	*Natural frequencies (Hz)*						
	Mode 1	*Mode 2*	*Mode 3*	*Mode 4*	*Mode 5*	*Mode 6*	*Mode 7*
Room 3	*16.50*	*19.25*	*31.50*	*33.50*	*50.75*	*57.75*	*66.75*
FEM	*15.43*	*18.55*	*35.54*	*44.76*	*47.98*	*58.49*	*58.51*

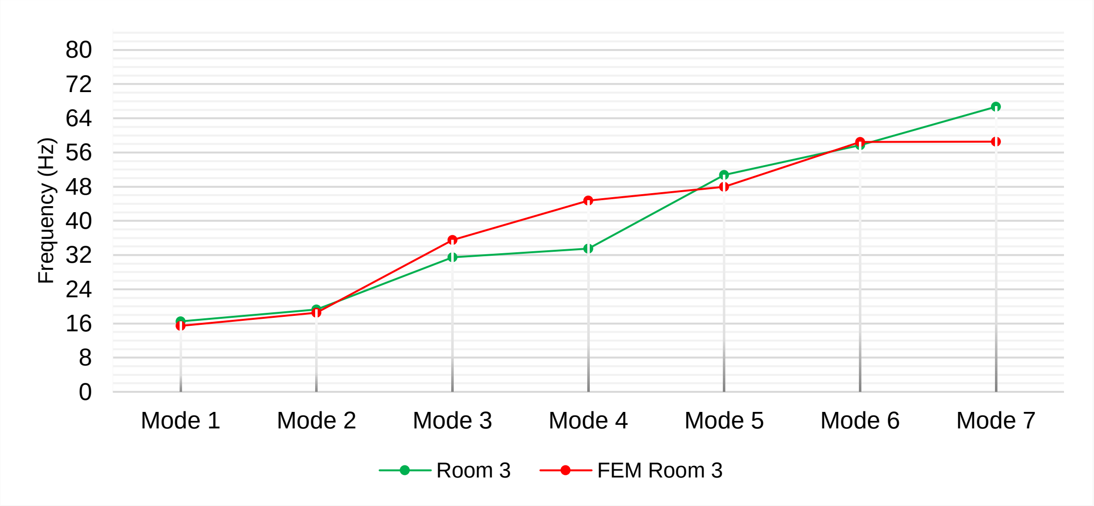

Figure 8.11 *Experimental Impulse and FE results compared for Room 3. Modes 1 to 7*

Summary FE frequency results *(field tested floor)*

The FE modal analysis of the floors with the minimum restriction on rotational stiffness at the supports (simply-supported / pinned) showed good correlation with the experimental field test results. The variance was less than 1 Hz for the first four modes for Room 1 and the first two modes for Room 3. A greater disparity between FE analysis and experimental results was found in the higher modes.

Both the FE analysis and the field tests identified five natural modes that were less than 40 Hz for Room 1. Three modes below 40 Hz were predicted in the FE analysis for Room 3, while four modes were measured experimentally.

A reduced number of first-order modes below 40 Hz is important to ensure compliance with the current European timber frequency and unit impulse velocity criteria in EC-5 [22]. Therefore, a good characterisation of all modes below 40 Hz is particularly import in predicting the serviceability performance of a floor. The variance between the FE analysis and the experimental field test results for the natural frequency values below 40 Hz was less than 2.5 Hz and less than 4 Hz for the higher modes in Room 1.

The correlation was better between the FE analysis and field test results for Room 1 compared with Room 3. The variance between the FE analysis and the experimental field test results for the natural frequency values ranged between 1 Hz and were less than 11.5 Hz for the natural mode values in Room 3.

An explanation for a lower correlation in higher modes in Room 3 may be attributed to the support to one side of the floor along the axis normal to the span. At the time of testing not all fixings to the west side of the room were in place, therefore no boundary restriction was defined along this edge of the floor in the FE model. This is an idealised representation of the in-situ conditions, as a degree of rotational stiffness due to friction from the supporting wall would be expected in the floor.

It must also be noted that the mass and characteristic properties that were used to develop the FE models of the in-situ floors were estimated, based on Bejtka and Blaβ's [198] orthotropic set for Grade C24 spruce (Table 7.1) amended in accordance with the CLT manufacturer's technical data sheets (ETA KLH.UK 2016 [199]).

The generally good correlation to be observed between the experimental field results and the numerical results show that characterising the junction of parallel panels by permitting rotation along the span axis of the panels, while the other five degrees of freedom were tied was appropriate.

8.4 Parametric study of a multi-panel CLT floor

A model of a generic 7000 mm by 7000 mm CLT floor was developed to investigate the relative influence of: (i) alternative floor penetrations, (ii) intermediate support conditions. The floor comprised three five-ply CLT panels connected in parallel. The panels each measured 180 mm x 2330 mm x 7000 mm.

An initial investigation was made to establish the variation in modal properties between an FE model of a single panel spanning one-way (SP), a three-panel floor spanning one-way (MP), and finally a three-panel floor spanning in both directions (MP-TS), which ultimately was taken as the baseline model of the floor. The first three mode shapes of each analysis are illustrated in Table 8.13.

Table 8.13 *FE mode shape results of one CLT panel spanning 7000 mm (SP), a 7000 mm x 7000 mm three-panel floor spanning one direction (MP), and spanning in two directions (MP-TS). Modes 1 to 3*

Single-panel model: SP	*Multi-panel model: MP*	*Two-way supported: MP-TS*
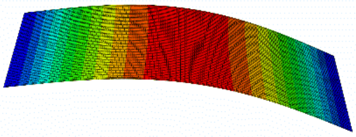	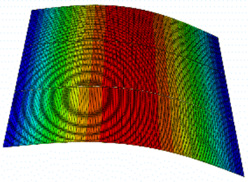	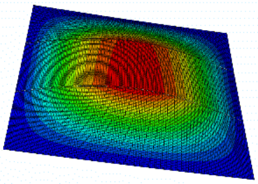
Mode 1: 8.18 Hz	*Mode 1: 8.18 Hz*	*Mode 1: 9.19 Hz*
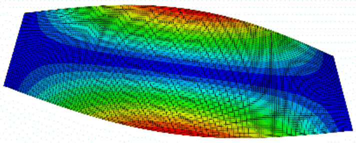	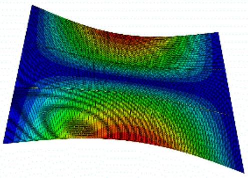	*No corresponding mode*
Mode 2: 14.56 Hz	*Mode 2: 9.13 Hz*	
	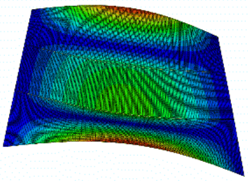	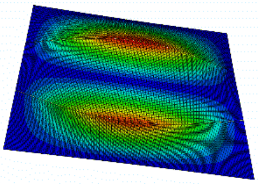
	Mode 3: 12.02 Hz	*Mode 2: 12.11 Hz*

The support boundaries were defined with the minimum degrees of rotation (simply-supported) for all cases. Parallel panels were connected with MPC at 250 mm spacing, with rotation permitted along the span axis of the panels, while the other five degrees of freedom were tied. Table 8.14 and Figure 8.12 show the first ten modes of the FE results for , a three-panel floor spanning one-way (MP), with the corresponding modes of the single span, one-panel (SP), and the three-panel floor spanning in both directions (MP-TS) shown.

Table 8.14 *FE frequency results of one CLT panel spanning 7000 mm (SP), a 7000 mm x 7000 mm three-panel floor spanning one direction (MP), and spanning in two directions (MP-TS). Modes 1 to 10*

Model	*5-ply CLT panel spanning 7000 mm Natural frequencies (Hz)*									
	Mode 1	*Mode 2*	*Mode 3*	*Mode 4*	*Mode 5*	*Mode 6*	*Mode 7*	*Mode 8*	*Mode 9*	*Mode 10*
SP	*8.18*	-	-	*14.56*	*29.81*	-	-	*36.92*	-	-
MP	*8.18*	*9.13*	*12.02*	*14.86*	*29.81*	*30.67*	*33.64*	*37.30*	*41.19*	*54.44*
MP-TS	*9.19*	-	*12.11*	-	*30.75*	*33.81*	*34.55*	*46.09*	*47.64*	*58.40*

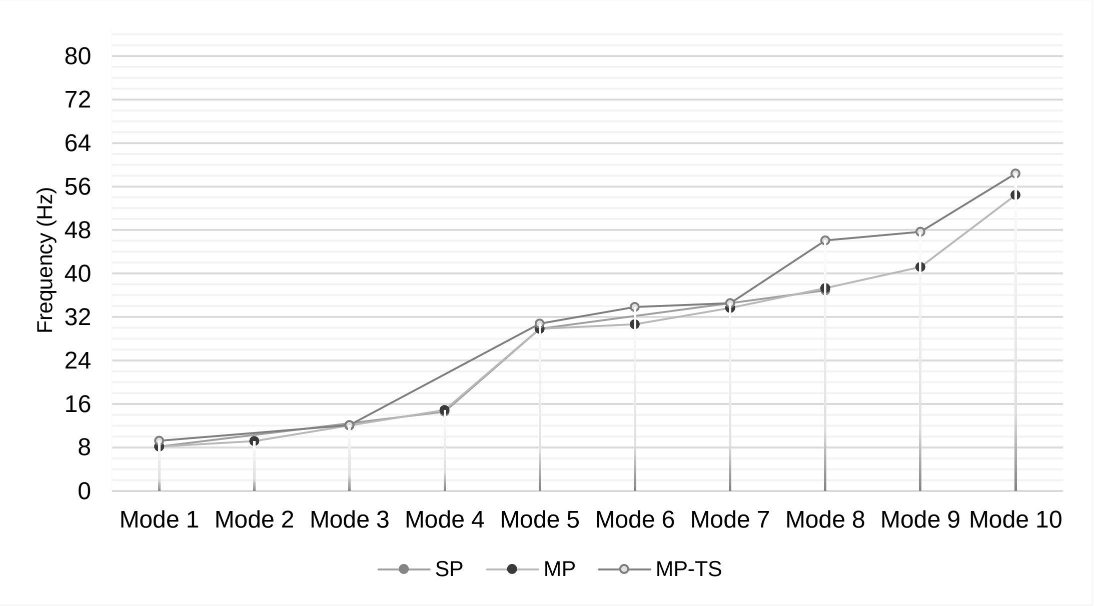

Figure 8.12 *FE frequency results of one CLT panel spanning 7000 mm (SP), a 7000 mm x 7000 mm three-panel floor spanning one direction (MP), and spanning in two directions (MP-TS). Modes 1 to 10*

The FE modal analysis of the floor represented as a single CLT panel (SP) predicted seven modes with frequency values less than 80 Hz. The FE analysis of the three-panel floor spanning in one direction only (MP) predicted 18 modes of interest, while the two-way spanning floor model (MP-TS) predicted 13 natural modes within the 0 to 80 Hz frequency range.

The variation in fundamental frequency results were relatively small for each analysis, but the mode separation was significantly reduced in the two-way spanning floor. The single-panel model (SP) did not predict transverse modes present in the multi-panel models (MP and MP-TS). This suggests that although a single-panel numerical model is useful in predicting fundamental frequencies, it will not anticipate the range of natural modes that are likely in a floor comprising multiple panels.

Comparing the alternative support conditions applied to the multi-panel floor models it may be seen that that the one-way spanning floor (MP) predicted additional transverse modes that were not expected in a floor with secondary supports along the edge parallel to the main span (MP-TS). The results of this study imply that modelling of all the panels and any transverse support condition present is necessary to reliably predict the number of modes to be expected in a multi-panel CLT floor.

Rectangular floor void

Taking the two-way spanning floor model (MP-TS) as the baseline model of the floor, the influence of introducing a rectangular void measuring 1800 mm x 2700 mm to replicate a stairwell was introduced midspan. The modal results of the floor with the void unsupported (A), simply-supporting the void along each 2700 mm parallel edge (B), and along two adjacent edges (C) were compared. The first three mode shapes are illustrated in Table 8.15. Table 8.16 and Figure 8.13 show the first ten modes of the FE results in each case.

8.15 *FE mode shape results of a three-panel floor spanning in two directions with a 1800 mm x 2700 mm void, unsupported (A), supported along two parallel sides (B), and along two adjacent sides (C). Modes 1 to 3*

Void unsupported: A	*Void simply-supported on two long sides: B*	*Void supported on two adjacent sides: C*
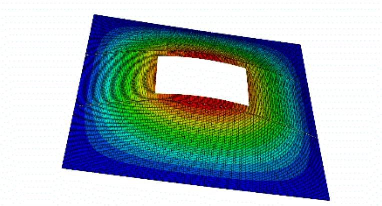	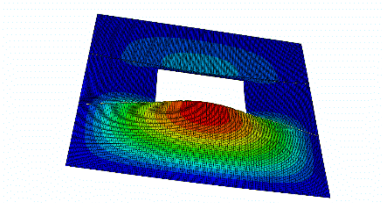	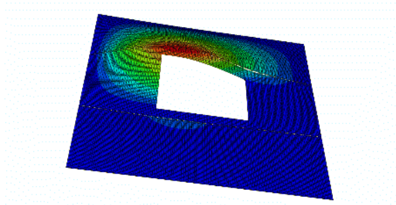
Mode 1: 9.01 Hz	*Mode 1: 23.31 Hz*	*Mode 1: 16.67 Hz*
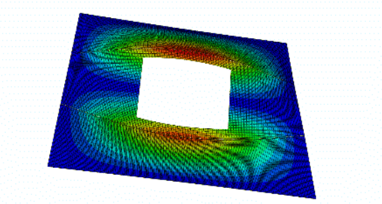	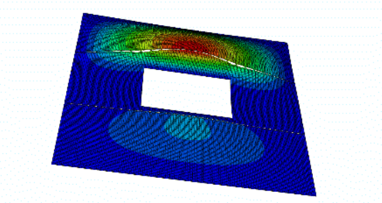	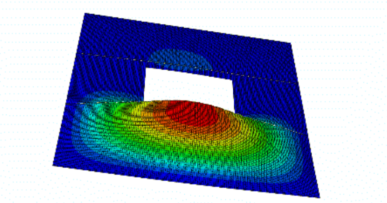
Mode 2: 12.06 Hz	*Mode 2: 24.96 Hz*	*Mode 2: 23.63 Hz*
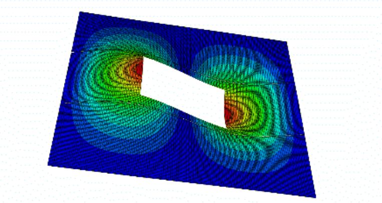	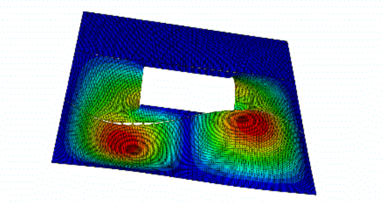	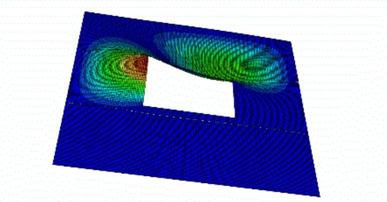
Mode 3: 24.33 Hz	*Mode 3: 39.74 Hz*	*Mode 3: 33.66 Hz*

Table 8.16 *FE frequency results of a three-panel floor spanning in two directions with a 1800 mm x 2700 mm void, unsupported (A), supported along two parallel sides (B), and along two adjacent sides (C). Modes 1 to 10*

Model	*Generic three-panel, 5-ply CLT 7000 x 7000 mm floor with 1800 X 2700 mm void Natural frequencies (Hz)*									
	Mode 1	*Mode 2*	*Mode 3*	*Mode 4*	*Mode 5*	*Mode 6*	*Mode 7*	*Mode 8*	*Mode 9*	*Mode 10*
A	*9.01*	*12.06*	*24.33*	*31.95*	*33.39*	*43.96*	*46.12*	*53.65*	*57.68*	*60.54*
B	*23.31*	*24.96*	*39.74*	*40.80*	*42.59*	*44.74*	*54.67*	*60.98*	*63.49*	*65.77*
C	*16.67*	*23.63*	*33.66*	*40.28*	*43.61*	*54.49*	*55.58*	*62.05*	*64.99*	*66.63*
	Extract from Table 8.14 (MP-TS)									
No void	*9.19*	*12.11*	*30.75*	*33.81*	*34.55*	*46.09*	*47.64*	*58.40*	*60.03*	*61.86*

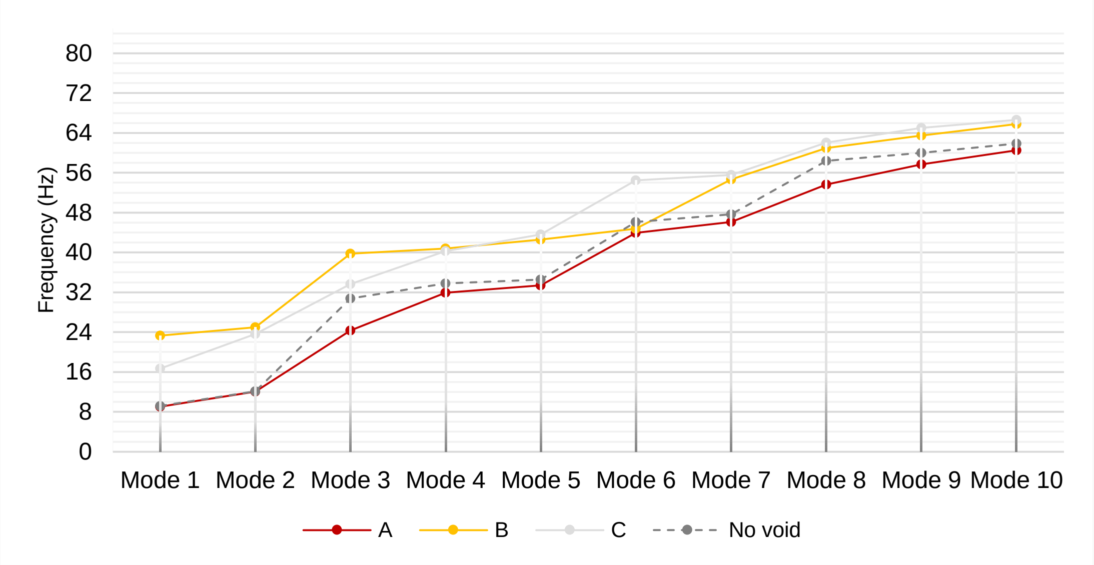

Figure 8.13 *FE frequency results of a three-panel floor spanning in two directions with a 1800 mm x 2700 mm void, unsupported (A), supported along two parallel sides (B), and along two adjacent sides (C), with (MP-TS) is represented by a broken line. Modes 1 to 10*

The FE model where the rectangular void was unsupported (A), predicted 14 modes within the range of interest, compared with 13 modes for the floor without a void (MP-TS). The difference due to the void unsupported for the fundamental and second natural mode was negligible. However, the higher natural frequency values were reduced due to the void. Supporting the floor void along the two longer edges (B), increased the frequency values significantly and reduced the number of modes in the range of interest to 12 natural modes. Characterising the floor and void supported along two adjacent sides (C) also increased the natural frequency values, with 13 modes predicted in the frequency range of interest. The floor void simply-supported along the parallel 2700 mm edges (B) generally provided the optimum modal results compared with the other examples (MP-TS, A, and C).

Alternative rectangular void locations

FE models to investigate the influence of introducing the 1800 mm x 2700 mm rectangular void at alternative positions on the floor were then developed.

The modal results of the floor with the void unsupported adjacent the main floor support (D), adjacent the corner of the floor (E), and midspan over two panels (F) were compared. The first three mode shapes are illustrated in Table 8.17. Table 8.18 and Figure 8.14 show the first ten modes of the FE results in each case.

Table 8.17 *FE mode shape results of the 1800 mm x 2700 mm void unsupported adjacent the main floor support (D), adjacent the corner of the floor (E), and midspan over two panels (F). Modes 1 to 3.*

Adjacent main support: D	*Corner of the floor: E*	*Midspan over two panels: F*
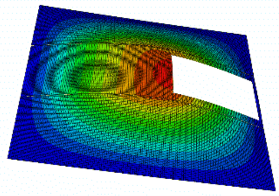	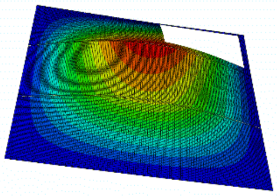	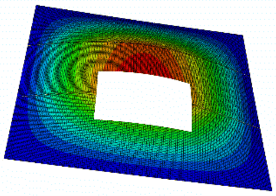
Mode 1: 8.51 Hz	*Mode 1: 8.76 Hz*	*Mode 1: 9.06 Hz*
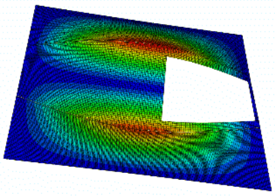	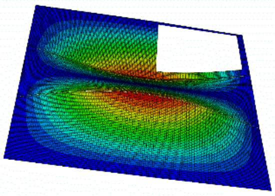	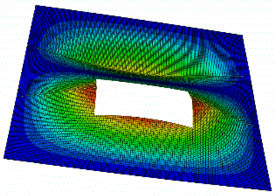
Mode 2: 11.10 Hz	*Mode 2: 11.81 Hz*	*Mode 2: 13.28 Hz*
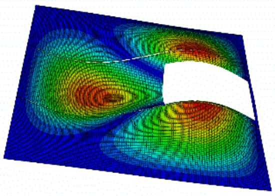	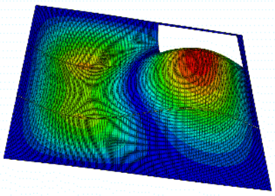	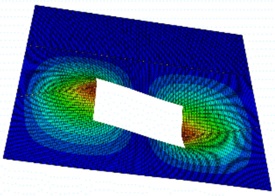
Mode 3: 29.78 Hz	*Mode 3: 30.36 Hz*	*Mode 3: 22.09 Hz*

Table 8.18 *FE frequency results of 1800 mm x 2700 mm void unsupported adjacent the main floor support (D), adjacent the corner of the floor (E), and midspan over two panels (F). Modes 1 to 10.*

Model	*Generic three-panel, 5-ply CLT 7000 x 7000 mm floor with 1800 X 2700 mm void unsupported Natural frequencies (Hz)*									
	Mode 1	*Mode 2*	*Mode 3*	*Mode 4*	*Mode 5*	*Mode 6*	*Mode 7*	*Mode 8*	*Mode 9*	*Mode 10*
D	*8.51*	*11.10*	*29.78*	*33.12*	*35.22*	*45.95*	*48.17*	*55.72*	*58.83*	*61.03*
E	*8.76*	*11.81*	*30.36*	*33.06*	*35.67*	*44.65*	*49.25*	*55.89*	*60.17*	*60.85*
F	*9.06*	*13.28*	*22.09*	*26.04*	*32.05*	*40.86*	*44.58*	*52.46*	*55.45*	*66.63*
	Extract from Table 8.14 (MP-TS) and 8.16 (A)									
No void	*9.19*	*12.11*	*30.75*	*33.81*	*34.55*	*46.09*	*47.64*	*58.40*	*60.03*	*61.86*
A	*9.01*	*12.06*	*24.33*	*31.95*	*33.39*	*43.96*	*46.12*	*53.65*	*57.68*	*60.54*

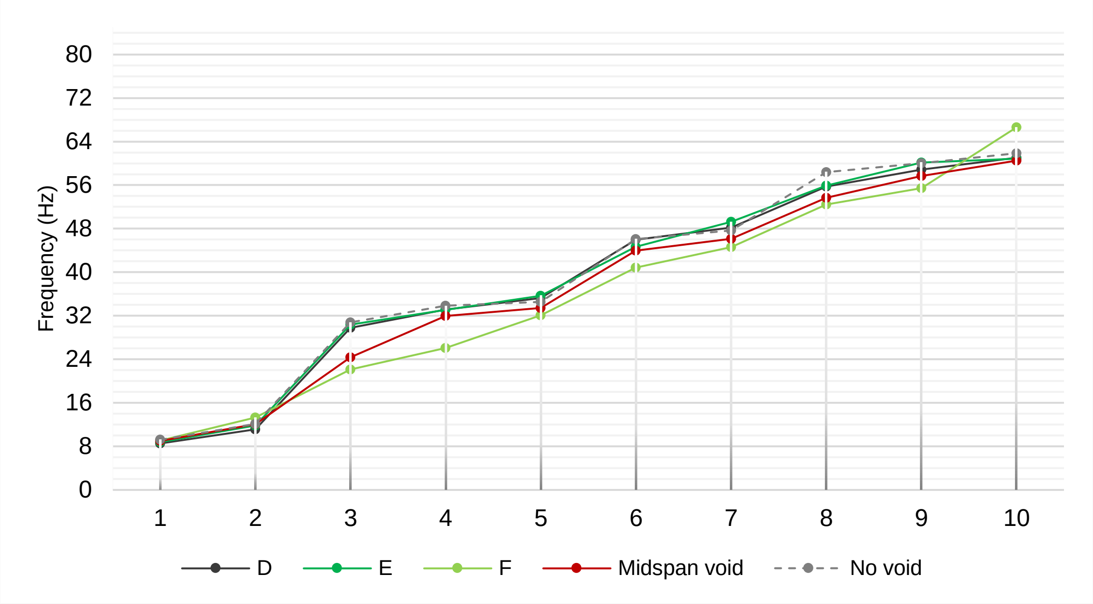

Figure 8.14 *FE frequency results of the 1800 mm x 2700 mm void unsupported adjacent the main floor support (D), adjacent the corner of the floor (E), and midspan over two panels (F). Modes 1 to 10. (MP-TS) is represented by a broken grey line, the void unsupported mid-floor is shown in red (A).*

The FE modal results of the 1800 mm x 2700 mm void unsupported at different locations on the floor (D, E, and F) are very similar regardless of the position of the void in the floor. The difference for the fundamental and second natural mode was negligible. A void positioned completely within one floor panel performed better than if positioned between two adjacent panels (F).

Alternative rectangular void locations simply-supported

The FE models were then modified to investigate the influence of simply-supporting the 1800 mm x 2700 mm rectangular void at the alternative positions on the floor.

The first three mode shapes with the void adjacent the main floor support (D’), adjacent the corner of the floor (E’), and midspan over two panels (F’) are illustrated in Table 8.19. Table 8.20 and Figure 8.15 show the first ten modes of the FE results in each case.

Table 8.19 *FE mode shape results of the 1800 mm x 2700 mm void simply-supported adjacent the main floor support (D'), adjacent the corner of the floor (E'), and midspan over two panels (F'). Modes 1 to 3.*

Supported on all sides: D'	*Supported on all sides: E'*	*Supported on all sides: F'*
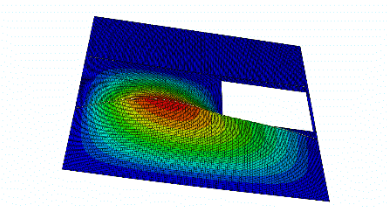	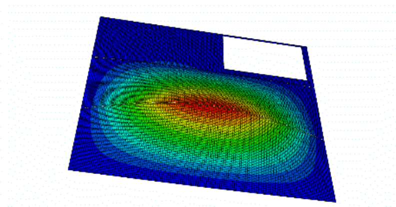	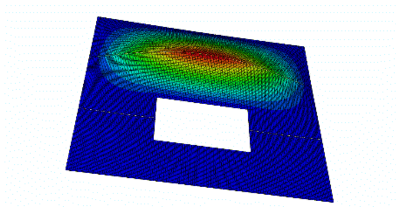
Mode 1: 19.88 Hz	*Mode 1: 10.16 Hz*	*Mode 1: 12.75 Hz*
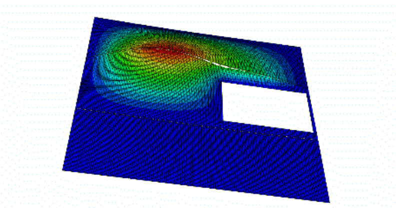	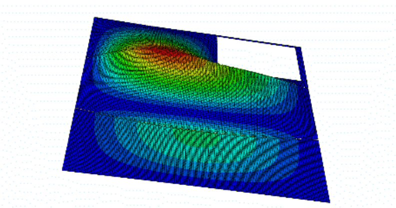	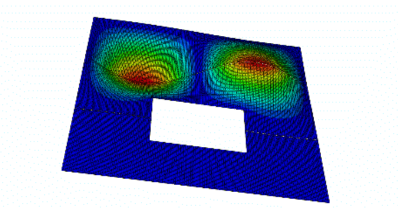
Mode 2: 20.58 Hz	*Mode 2: 12.22 Hz*	*Mode 2: 33.66 Hz*
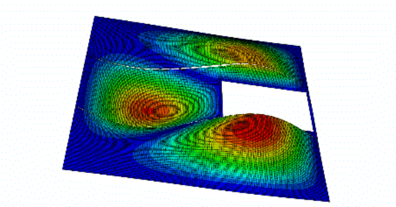	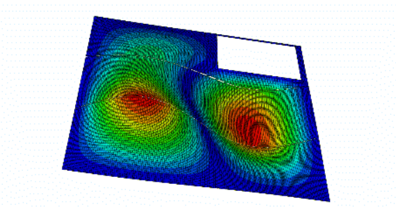	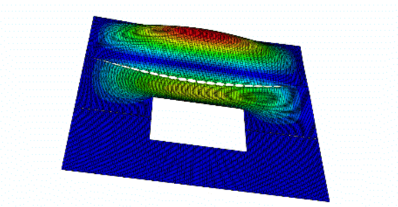
Mode 3: 32.21 Hz	*Mode 3: 31.22 Hz*	*Mode 3: 46.23 Hz*

Table 8.20 *FE frequency results of the 1800 mm x 2700 mm void simply-supported adjacent the main floor support (D'), adjacent the corner of the floor (E'), and midspan over two panels (F'). Modes 1 to 10*

Model	*Generic three-panel, 5-ply CLT 7000 x 7000 mm floor with 1800 X 2700 mm void supported on all sides Natural frequencies (Hz)*									
	Mode 1	*Mode 2*	*Mode 3*	*Mode 4*	*Mode 5*	*Mode 6*	*Mode 7*	*Mode 8*	*Mode 9*	*Mode 10*
D'	*19.88*	*20.58*	*32.21*	*36.14*	*43.14*	*50.78*	*60.74*	*64.43*	*65.07*	*65.93*
E'	*10.61*	*12.22*	*31.22*	*34.91*	*40.61*	*47.30*	*55.23*	*60.64*	*63.51*	*66.25*
F'	*12.75*	*33.66*	*46.23*	*56.35*	*61.75*	*65.88*	*66.37*	*70.93*	*73.77*	*78.78*
	Extract from Table 8.14 (MP-TS)									
No void	*9.19*	*12.11*	*30.75*	*33.81*	*34.55*	*46.09*	*47.64*	*58.40*	*60.03*	*61.86*

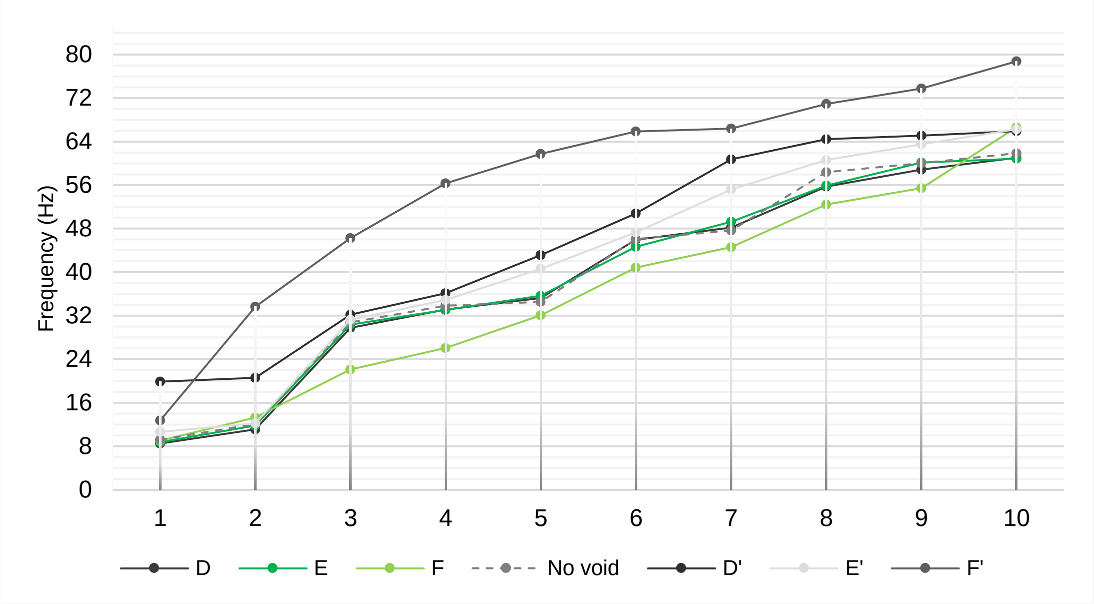

Figure 8.15 *FE frequency results of the 1800 mm x 2700 mm void simply-supported adjacent the main floor support (D'), adjacent the corner of the floor (E'), and midspan over two panels (F'). Modes 1 to 10. (MP-TS) is represented by a broken grey line*

Introducing a simple-support to the floor void increased the natural frequency values in all cases. The FE model predicted 12 modes in the range of interest for Case D', while Cases E' an F' were found to have 13 and 10 modes below 80 Hz, respectively. Providing support for the void positioned adjacent to the main floor support (D and D') gave the optimum fundamental frequency results, with the value increased from 8.51 Hz to 19.88 Hz. The higher natural mode results were most improved in the case of the void spanning two panels (F and F'), for both the frequency values and the mode separation. The void positioned in the corner of the floor (E and E') was least impacted by providing additional support to the edge of the void.

Curved floor void

To examine the effect of a curved penetration in a CLT floor an 1800 mm diameter circular void was introduced in the generic floor (MP-TS), unsupported (G), and supported (G') continuously along the edge of the void. The impact of introducing twelve small 100 mm diameter service penetrations adjacent the floor supports were also examined (H). The first three modes are illustrated in Table 8.21. Table 8.22 and Figure 8.16 show the first ten modes of the FE results in each case.

Table 8.21 *FE mode shape results due to an Ø 1800 mm void unsupported (G), supported (G'), and small service penetrations (H). Modes 1 to 3.*

Unsupported: G	*Supported: G'*	*Small service penetrations H*
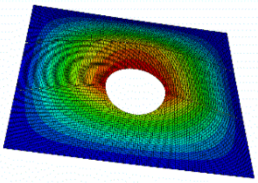	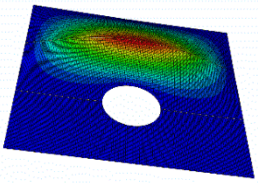	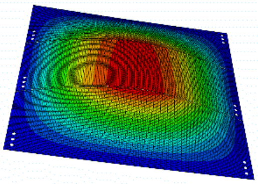
Mode 1: 8.75Hz	*Mode 1: 12.79 Hz*	*Mode 1: 9.18 Hz*
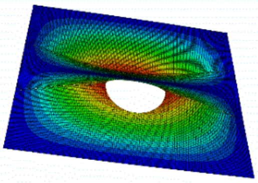	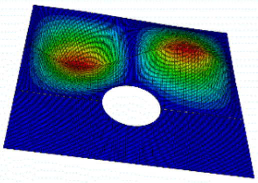	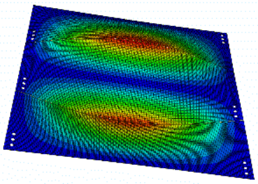
Mode 2: 12.49 Hz	*Mode 2: 32.47 Hz*	*Mode 2: 12.09 Hz*
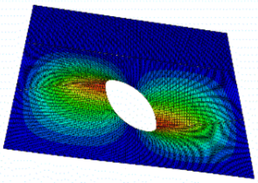	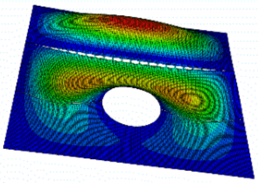	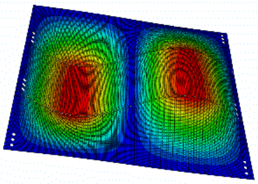
Mode 3: 23.78 Hz	*Mode 3: 42.86 Hz*	*Mode 3: 30.71 Hz*

Table 8.22 *FE frequency results due to an Ø 1800 mm void unsupported (G), supported (G'), and small service penetrations (H). Modes 1 to 10*

Model	*Generic three-panel, 5-ply CLT 7000 x 7000 mm floor with Ø 1800 mm void compared with Ø 100 mm service penetrations Natural frequencies (Hz)*									
	Mode 1	*Mode 2*	*Mode 3*	*Mode 4*	*Mode 5*	*Mode 6*	*Mode 7*	*Mode 8*	*Mode 9*	*Mode 10*
G	*8.75*	*12.49*	*23.78*	*31.20*	*32.19*	*45.89*	*46.01*	*56.56*	*58.18*	*61.22*
G'	*12.79*	*32.47*	*42.86*	*45.99*	*47.86*	*50.98*	*56.52*	*62.45*	*62.60*	*71.12*
H	*9.18*	*12.09*	*30.71*	*33.74*	*34.53*	*46.07*	*47.59*	*58.33*	*59.89*	*61.83*
	Extract from Table 8.14									
No void	*9.19*	*12.11*	*30.75*	*33.81*	*34.55*	*46.09*	*47.64*	*58.40*	*60.03*	*61.86*

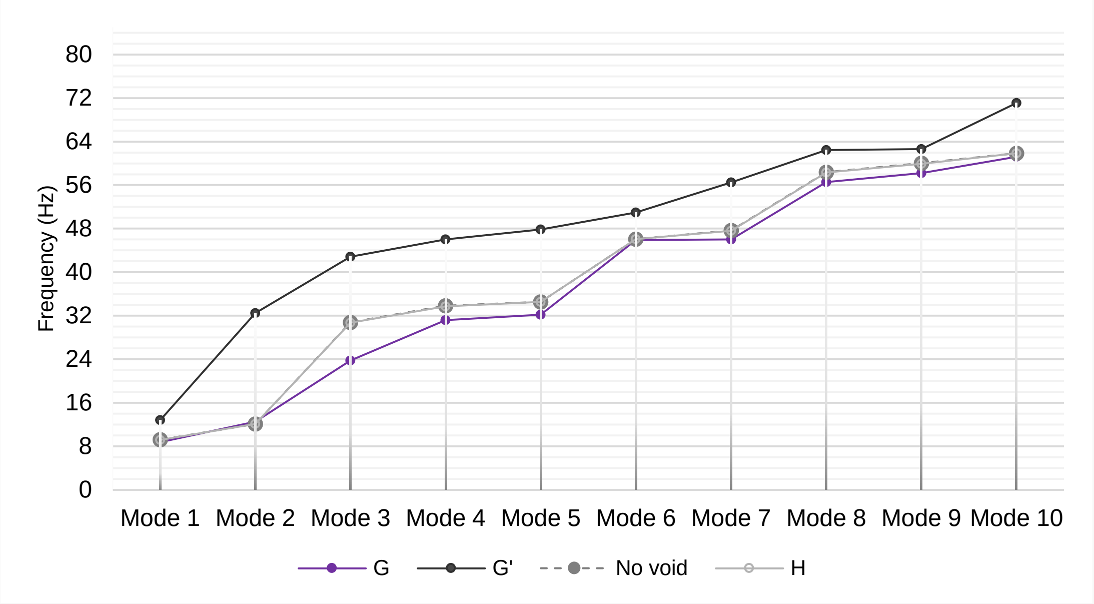

Figure 8.16 *FE frequency results due to an Ø 1800 mm void unsupported (G), supported (G'), and small service penetrations (H). Modes 1 to 10. (MP-TS) is represented by a broken grey line.*

The FE modal analysis introducing an 1800 mm diameter circular void unsupported (G), had a negligible influence on the fundamental and second natural mode, but generally reduced the higher natural mode values compared with the modal analysis of the generic floor (MP-TS). In all 13 modes within the range of interest were predicted. Simply-supporting the floor void (G') improved the frequency values and reduced the number of modes to 12. Introducing small 100 mm diameter service penetrations adjacent the floor supports (H), did not significantly impact on the frequency values of the natural modes of the floor.

Summary of FE frequency results *(floor voids)*

Taking an overview of the results of the alternative floor penetrations in the same generic floor suggest that it is the support, rather than the void, or the location of the void that most influence modal frequency values. However, it can be observed from Tables 8.13, 8.15, 8.17, 8.19 and 8.21 that the shape of the natural modes were notably altered in most instances. Where the floor void was unsupported, the rectangular void straddling two panels was predicted to be the optimum position, with a fundamental frequency predicted at 9.06 Hz from 8.51 Hz compared with positioning the void midspan adjacent a floor edge support (Models F and D, respectively). The highest fundamental frequency value when the floor void is supported was recorded for Model

D’ at 19.88 Hz, but the mode separation was most improved in the case of the supported rectangular void straddling two panels (Model F’). Similar results were recorded for the circular void. Small 100 mm diameter service penetrations within 100 mm of the floor edge (Model H) did not impact natural modal values to any significant extent.

Internal partition walls

The FE model of the generic 7000 mm by 7000 mm CLT floor (MP-TS) was then amended to investigate the relative influence of non-loadbearing partition walls on the modal characteristics of the floor. Three alternative support orientations were compared: (i) An intermediate support at quarter span (I), (ii) cross supports at midspan (J), and (iii) diagonal cross supports (K), (illustrated in Figures 7.18, 7.19, and 7.20, respectively). The first three modes of each intermediate support case are shown in Table 8.23. Table 8.24 and Figure 8.17 chart the first ten modes of the FE modal frequency results in each case.

Table 8.23 *FE mode shape results of the three-panel floor spanning in two directions with an intermediate support at quarter-span (I), cross intermediate supports midspan (J), and diagonal cross support (K). Modes 1 to 3*

Quarter-span support:I	*Cross supports: J*	*Diagonal supports: K*
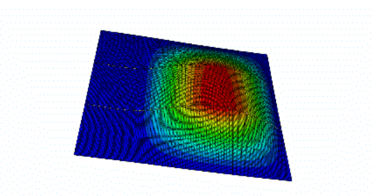	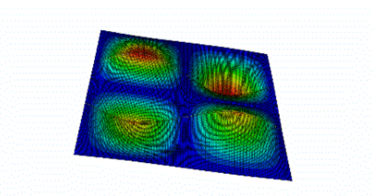	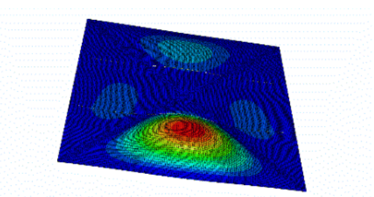
Mode 1: 18.72 Hz	*Mode 1: 36.13 Hz*	*Mode 1: 47.89 Hz*
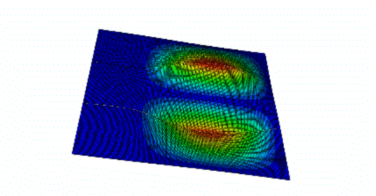	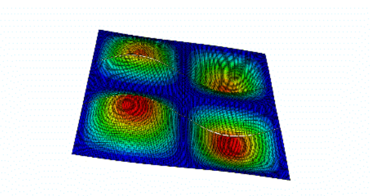	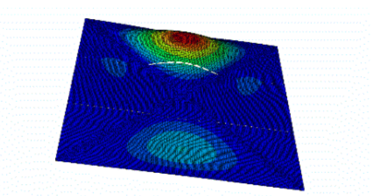
Mode 2: 21.25 Hz	*Mode 2: 39.74 Hz*	*Mode 2: 48.16 Hz*
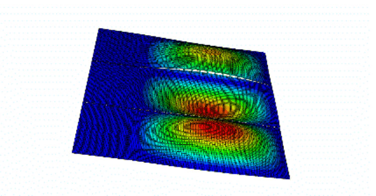	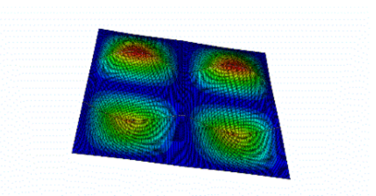	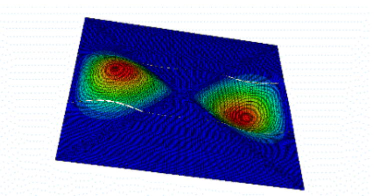
Mode 3: 38.98 Hz	*Mode 3: 42.95 Hz*	*Mode 3: 55.72 Hz*

Table 8.24 *FE frequency results of the three-panel floor spanning in two directions with an intermediate support at quarter-span (I), cross intermediate supports midspan (J), and diagonal cross support (K). Modes 1 to 10*

Model	*Generic three-panel, 5-ply CLT 7000 x 7000 mm floor with intermediate internal supports Natural frequencies (Hz)*									
	Mode 1	*Mode 2*	*Mode 3*	*Mode 4*	*Mode 5*	*Mode 6*	*Mode 7*	*Mode 8*	*Mode 9*	*Mode 10*
I	*18.72*	*21.25*	*38.98*	*50.06*	*52.96*	*55.57*	*65.57*	*65.42*		
J	*36.13*	*39.74*	*42.95*	*46.12*	*59.93*	*63.65*	*64.33*	*67.85*	-	-
K	*47.89*	*48.16*	*55.72*	*56.78*	*79.28*	*79.54*	-	-	-	-
	Extract from Table 8.14									
MP-TS	*9.19*	*12.11*	*30.75*	*33.81*	*34.55*	*46.09*	*47.64*	*58.40*	*60.03*	*61.86*

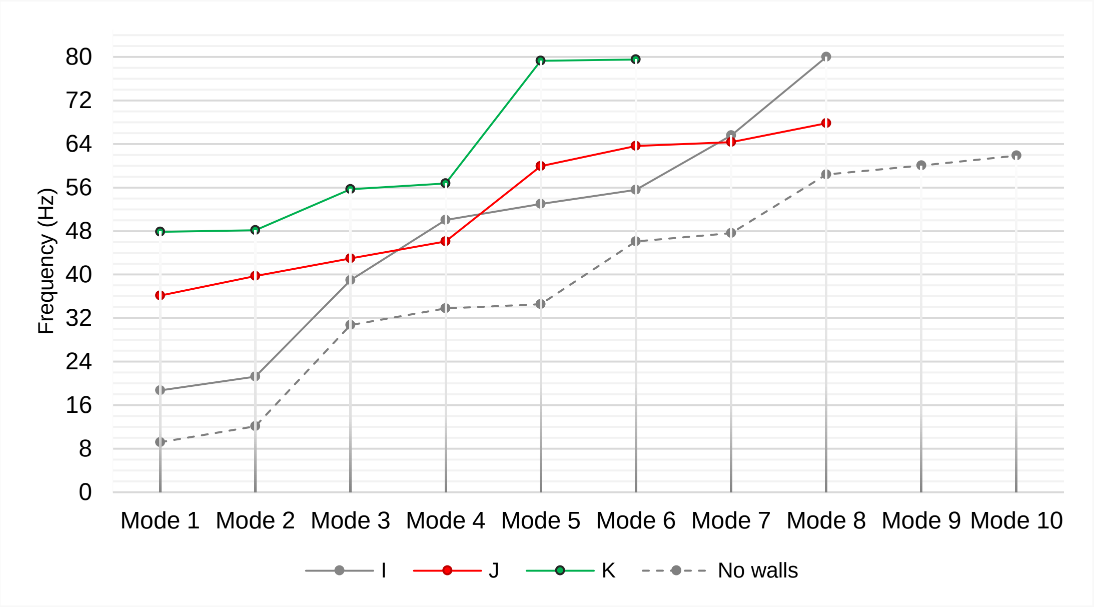

Figure 8.17 *FE frequency results of the three-panel floor spanning in two directions with an intermediate support at quarter-span (I), cross intermediate supports midspan (J), and diagonal cross support (K). Modes 1 to 10. (MP-TS) is represented by a broken grey line.*

The introduction of an intermediate simple-support increased the natural frequency values in all cases. Representing a partition wall at quarter-span (I) improved the fundamental frequency by over 9 H, from 9.2 Hz to 18.7 Hz. Simulating a simple-support in two directions through the floor’s midspan (J) further improved the fundamental frequency value to 36.1 Hz. Alternatively providing cross support in the diagonal direction (K) further improving the fundamental frequency to 47.9 Hz.

The trend in frequency values generally continued for the higher modes. The FE model predicted eight modes in the range of interest for the quarter and midspan supports.

This number was reduced to six modes where diagonal cross support was introduced in the model.

Summary of FE frequency results *(internal walls)*

While the selected locations and orientations of the intermediate supports were arbitrary, the FE analysis clearly showed the significant influence that the introduction of intermediate supports and their positions can have on the dynamic performance of a floor. Providing an intermediate support on the diagonal axis of the floor increased the modal frequency values to a greater degree than the other support orientations.

8.5 Specific standard room design

In this study, the serviceability performance of two commonly replicated room design layouts is examined: (i) A standard twin hotel room [195] and (ii) a classroom design taken from the Irish Generic Primary School Design Guidelines [196].

8.5.1 Residential: Twin hotel room model

A standard twin hotel room with standard furniture layout is illustrated in Figure 7.21 [195]. A hotel or student residential building floor layout design will frequently comprise up to twenty standard rooms, ten either side of a central corridor. This floor layout optimises the floor space while complying with fire horizontal escape-route criteria [200].

To establish a baseline model of one room, an initial FE model was developed of two standard rooms comprising one and a half panels spanning either side of an 1800 mm wide central corridor. The panels were supported by the external and corridor structural walls. Three additional models were then developed; (i) a model of twenty rooms, ten rooms in series either side of the central corridor, (ii) a six-roomed model, and (iii) a four-roomed model were developed.

The first three mode shapes of the two- and four room FE model are illustrated in Table 8.25. Table 8.26 and Figure 8.18 chart the first ten modes of the FE modal frequency results in each case.

Table 8.25 *FE mode shape results of two, and four standard twin hotel rooms unfurnished (UF). Modes 1 to 3*

Two rooms	*Four rooms*
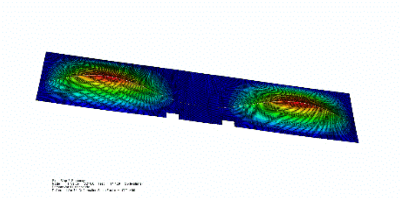	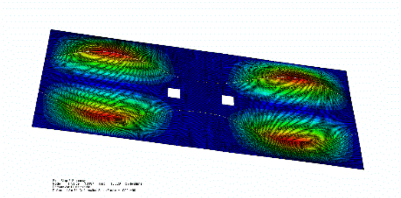
Mode 1: 14.43 Hz	*Mode 1: 16.23 Hz*
No corresponding mode	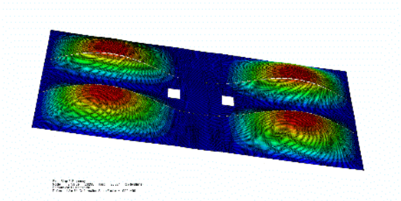
	Mode 2: 22.67 Hz
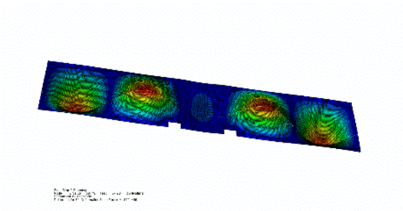	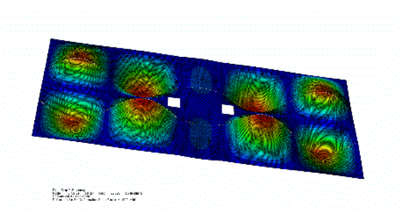
Mode 2: 37.93 Hz	*Mode 3: 38.57 Hz*

Table 8.26 *FE frequency results of the two- and four- standard twin hotel room unfurnished (UF). Modes 1 to 10*

Loading	*Typical single occupancy residential accommodation Natural frequencies (Hz)*									
	Mode 1	*Mode 2*	*Mode 3*	*Mode 4*	*Mode 5*	*Mode 6*	*Mode 7*	*Mode 8*	*Mode 9*	*Mode 10*
2-rooms (UF)	*14.43*	-	*37.93*	*41.68*	-	-	*57.28*	-	*67.86*	-
4-rooms (UF)	*16.23*	*22.67*	*38.57*	*41.16*	*42.36*	*46.86*	*57.86*	*61.06*	*68.16*	*69.34*

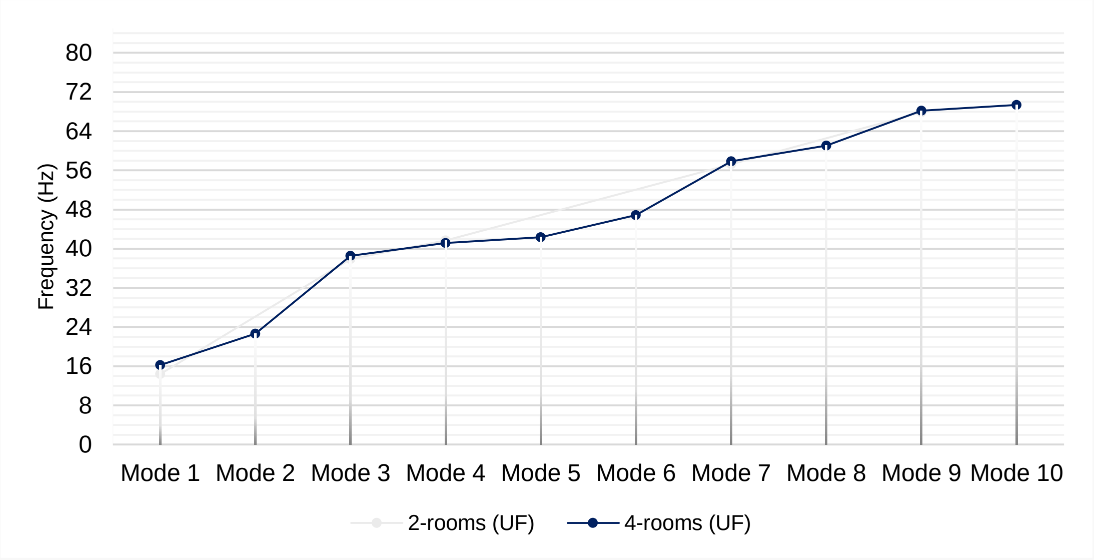

Figure 8.18 *FE frequency results of the two- and four- standard twin hotel room unfurnished (UF). Modes 1 to 10*

The FE predictions using the two-roomed model were conservative with respect to the fundamental frequency, however many of the natural modes were not predicted. It is clear from the FE predictions that to reliably predict all modes, the four-roomed representation is required. Therefore, the four-roomed FE model with only the external and corridor structural walls which were represented as simple supports, was taken as the baseline model (UF).

This model was then adapted to include simple supports to represent the non-structural en-suite partition walls (PW), and then to also include the discrete masses of the bathroom furniture (BF), (Figure 7.21).

The first three modes of each case are shown in Table 8.27.

Table 8.27 *FE mode shape results of the four standard twin hotel rooms with the addition of en-suite partitions (PW), and the bathroom fittings (BF). Modes 1 to 3.*

Internal partition walls (PW)	*Bathroom fit-out included (BF)*
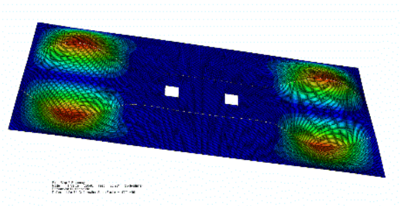	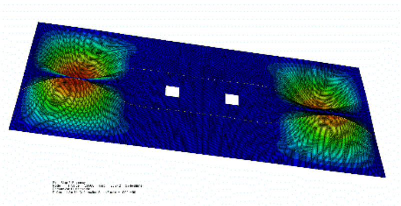
Mode 1: 25.93 Hz	*Mode 1: 25.94 Hz*
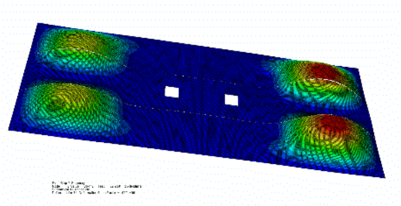	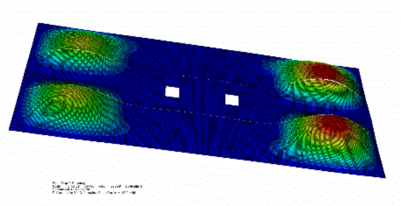
Mode 2: 29.95 Hz	*Mode 2: 29.96 Hz*
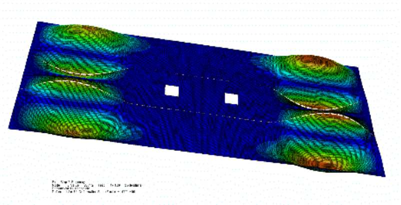	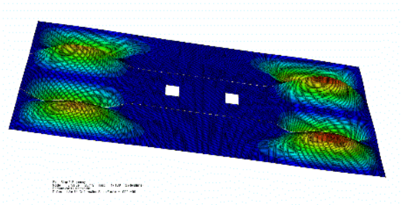
Mode 3: 47.14 Hz	*Mode 3: 41.14 Hz*

The baseline model (UF) was then further adapted to include the discrete masses of standard furniture with one occupant (FF). An alternative model combined all the discrete masses of the furniture and applied them evenly across the floor (UDL). The first three modes of the fully occupied (FF) and (UDL) modal results are shown in Table 8.28.

Table 8.28 *FE mode shape results of the four standard twin hotel rooms with the addition of the discrete loading of the rooms fully furnished (FF), and the equivalent mass evenly distributed (UDL) Modes 1 to 3.*

Discrete furniture (FF)	*Evenly distributed equivilent mass (UDL)*
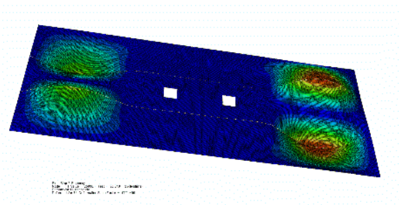	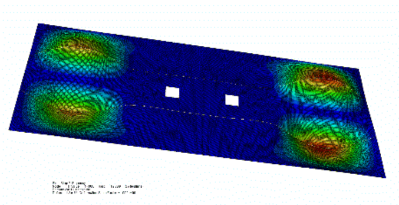
Mode 1: 25.21 Hz	*Mode 1: 19.37 Hz*
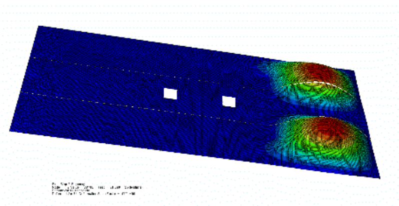	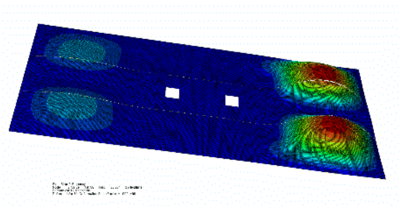
Mode 2: 31.10 Hz	*Mode 2: 22.37 Hz*
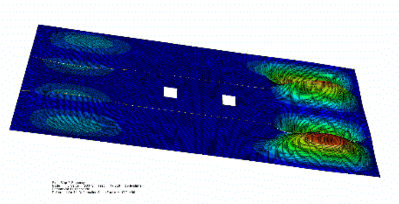	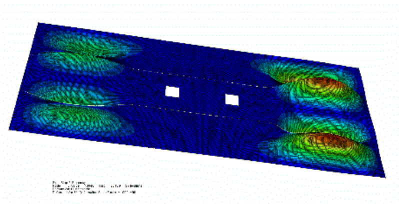
Mode 3: 47.83 Hz	*Mode 3: 35.18 Hz*

Finally the evenly distributed mass model was amended to omit any non-loadbearing walls. Table 8.29 and Figure 8.19 chart the first ten modes of the FE modal frequency results in each case.

Table 8.29 *FE results for a typical hotel four bedroom layout, comparing the unloaded floor (UF), the effect of internal non-load bearing partitions (PW), with bathroom fittings (BF), fully furnished (FF), and the equivalent loading evenly distributed across the floor (UDL). The rooms with an evenly distributed load without internal en-suite walls is also charted (UDL-W) The natural frequencies modes ranging 0 to 80 Hz are presented.*

Loading	*Typical single occupancy residential accommodation Natural frequencies (Hz)*									
	Mode 1	*Mode 2*	*Mode 3*	*Mode 4*	*Mode 5*	*Mode 6*	*Mode 7*	*Mode 8*	*Mode 9*	*Mode 10*
UF	*16.23*	*22.67*	*38.57*	*41.16*	*42.36*	*46.86*	*57.86*	*61.06*	*68.16*	*69.34*
PW	*25.93*	*29.95*	*47.14*	*51.27*	*63.86*	*64.55*	*75.06*	*77.62*	-	-
BF	*25.94*	*29.60*	*41.14*	*51.27*	*63.86*	*64.56*	*75.05*	*77.62*	-	-
FF	*25.21*	*31.10*	*47.23*	*53.17*	*61.54*	*62.92*	*73.69*	*76.35*	-	-
UDL	*19.37*	*22.37*	*35.18*	*38.26*	*47.67*	*48.21*	*56.02*	*57.93*	*67.24*	
UDL-W	*12.11*	*16.93*	*28.79*	*30.73*	*31.61*	*34.97*	*43.17*	*45.56*	*50.89*	*51.23*

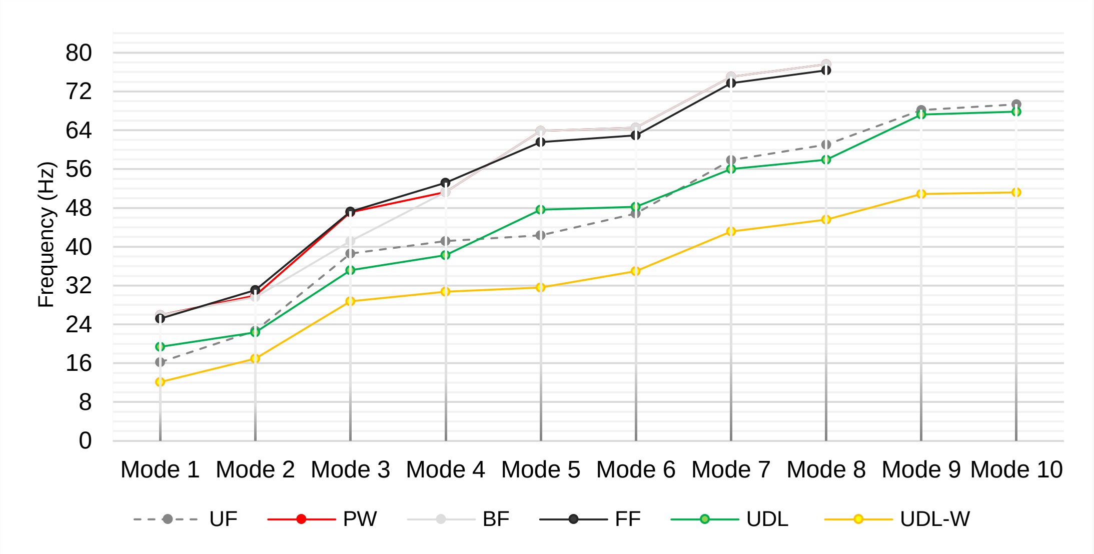

Figure 8.19 *FE results for a typical hotel bedroom layout, comparing the unloaded floor (UF), the effect of internal non-load bearing partitions (PW), including the bathroom fittings (BF), fully furnished (FF), and the equivalent loading evenly distributed across the floor (UDL). The rooms with an evenly distributed load without internal en-suite walls is also charted (UDL-W). Natural frequencies modes ranging 0 to 80 Hz*

The FE analysis of the specific room design again showed that the inclusion of intermediate supports significantly influenced the modal response of the floor, from 16.2 Hz (UF baseline value) to 25.9 Hz in the case of the fundamental frequency. The inclusion of the discrete masses representing the en-suite (BF) and room furniture (FF) had a negligible influence on the modal frequency values. The mass of the furniture and one occupant evenly distributed over the floor area (UDL) however, resulted a notable reduction in the natural frequency values predicted, from 25.9 Hz (PW) to 19.4 Hz (UDL) for the fundamental frequency result. Omitting the intermediate supports while applying the floor loading evenly over the floor (UDL-W), reduced natural modal frequency values further to 12.1 Hz.

The results of the study indicate that representing the standard hotel room without intermediate supports and applying the anticipated floor loading evenly over the floor, will predict very conservative frequency values, less than half the value predicted in a model with the intermediate supports and discrete masses more accurately represented.

Static 1 kN point load deflection analysis *(twin hotel room)*

A static displacement analysis was carried out to determine the maximum displacement due to the application of a load of 1 kN pressure load over an area of 100 mm x 100 mm centrally in the bedroom and in the corridor (FF mass distribution model). The static deflection results were 0.12 mm and 0.09 mm in the bedroom and corridor, respectively.

***Summary of FE results** (twin hotel room)*

The FE models of the standard room with, and without intermediate non-structural supports and for each mass distribution scenario predicted fundamental frequency and deflection results substantially compliant with current European timber design serviceability criteria (EC-5 [22]). The FE study shows that omitting intermediate supports and applying the anticipated floor loading evenly over the floor in FE modal analysis will predict considerably conservative modal values compared with accurately representing the fixed walls and discrete masses.

However, the most significant observation from the FE standard hotel room analysis was with regard to the central corridors, where a uniform pedestrian excitation is most likely. All FE modal analysis, including representing all ten rooms in series, and with, and without discrete or distributed added mass, measured natural modes substantially outside the range of footfall excitation, over 40 Hz in all cases.

8.5.2 Standard schoolroom design

A FE model was developed to study the serviceability performance of a standard classroom. The layout of the classroom is an extract from the complete school design proposed in the Irish Generic Primary School Design Guidelines [196].

The main objectives for developing this FE model was examine the impact of: (i) non-structural discrete masses replicating standard specified fixed furniture [196], and (ii) the distributed mass due to the rooms occupancy.

As a consequence of the observations made from the previous study (twin hotel room layout) it was assumed that the mass of the sanitary facility fit-out would not significantly impact on results, therefore, the FE model representing the classroom omitted the mass associated with the sanitary accommodation. The internal partitions were represented as simple-supports.

Table 8.30 shows the first three natural modes for the floor without added mass (UF), with standard fixed furniture (FF), and fully occupied (FO). Table 8.31 and Figure 8.20 present the first ten natural frequencies for each model.

Table 8.30 *FE modal results for a standard Classroom layout, with the room unfurnished (UF), fully furnished (FF), and fully occupied (FO). Modes 1 to 3*

Unfurnished (UF)	*Fully furnituished (FF)*	*Fully occupied (FO)*
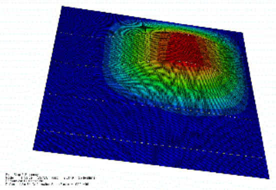	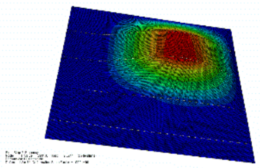	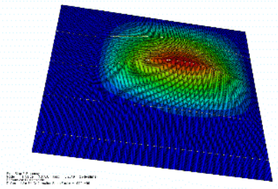
Mode 1: 9.52 Hz	*Mode 1: 9.59 Hz*	*Mode 1: 6.81 Hz*
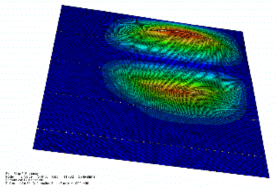	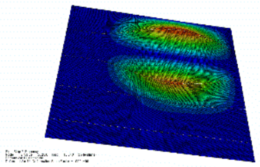	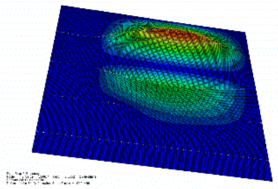
Mode 2: 11.76 Hz	*Mode 2: 12.04 Hz*	*Mode 2: 9.22 Hz*
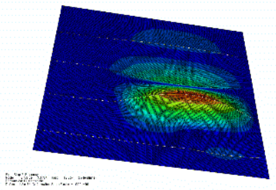	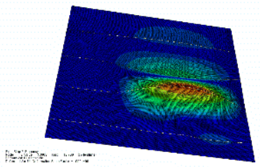	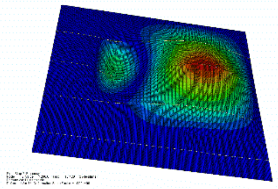
Mode 3: 18.65 Hz	*Mode 3: 18.77 Hz*	*Mode 3: 13.05 Hz*

Table 8.31 *FE frequency results for a standard Classroom layout, with the room unfurnished (UF), fully furnished (FF), and fully occupied (FO). Modes 1 to 10*

Loading	*Standard classroom in accordance with Irish generic school layout recommendations Natural frequencies (Hz)*									
	Mode 1	*Mode 2*	*Mode 3*	*Mode 4*	*Mode 5*	*Mode 6*	*Mode 7*	*Mode 8*	*Mode 9*	*Mode 10*
UF	*9.52*	*11.76*	*18.65*	*27.72*	*30.31*	*35.81*	*37.02*	*41.37*	*46.75*	*46.94*
FF	*9.59*	*12.04*	*18.77*	*24.96*	*30.59*	*35.98*	*37.28*	*41.10*	*46.85*	*47.36*
FO	*6.81*	*9.22*	*13.05*	*20.37*	*24.06*	*26.96*	*27.94*	*34.91*	*37.25*	*39.35*

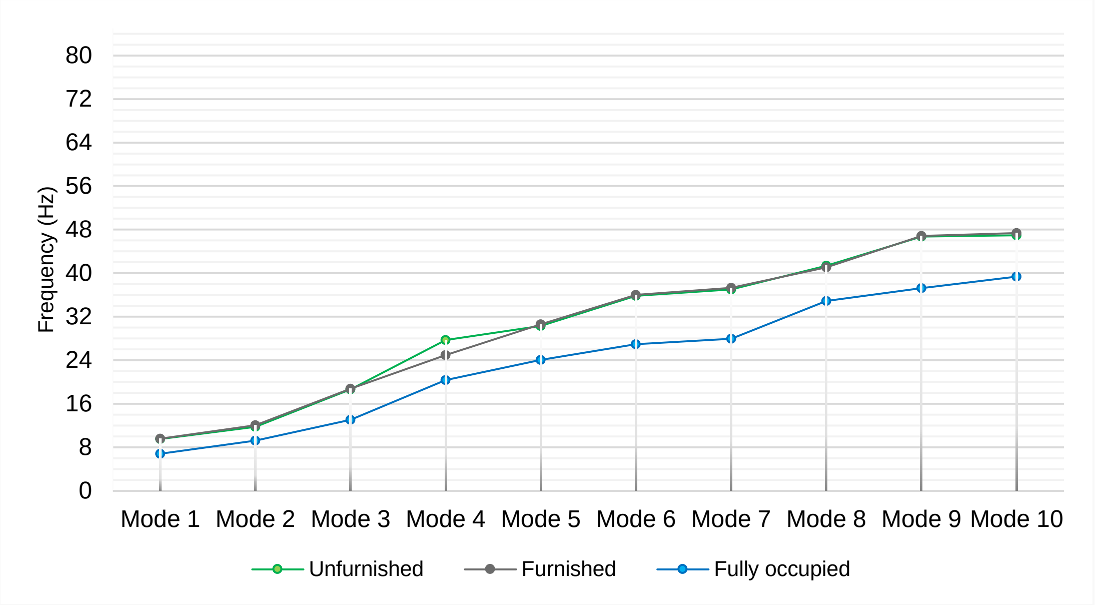

Figure 8.20 *FE frequency results for a standard Classroom layout, with the room unfurnished (UF), fully furnished (FF), and fully occupied (FO). Modes 1 to 10*

The results of the FE analysis of the classroom showed that the non-structural discrete masses replicating standard specified fixed furniture (FF) which was located adjacent the corridor wall and between the access door and the sanitary accommodation (Figure 7.24 [196]), had a negligible influence on the frequency results. Representing the distributed mass of the room occupied (FO) significantly reduced the frequency values, from 9.5 Hz (UF baseline value) to 6.8 Hz in the case of the fundamental frequency. This trend continued for the higher modes.

Static 1 kN point load deflection analysis *(schoolroom)*

A static displacement analysis was carried out to determine the maximum displacement due to the application of a load of 1 kN pressure load over an area of 100 mm x 100 mm centrally in the classroom. The static deflection result was 0.31 mm.

Summary of FE results *(schoolroom)*

The static deflection and natural frequency values predicted for the 5-ply floor unoccupied (UF and FF) was in compliance current European timber design serviceability criteria (EC-5 [22]). The deflection was greater than 0.5 mm/kN and all natural frequencies were greater than 8 Hz.

Applying the US or Canadian CLT floor serviceability criteria [70][71] incorporating the measured fundamental frequency value of 9.5 Hz (UF and FF) and midspan deflection of 0.31 mm/kN into Equations (3.62) and (3.63) is shown below.

$$f/d^{0.7} \geq 13.0: \qquad 9.5\ Hz/0.31^{0.7}\ mm = \mathbf{21.6} \qquad (3.63)$$

$$d \leq f^{1.43}/39: \qquad 0.31\ mm \leq 9.5^{1.43} Hz/39 = \mathbf{0.64\ mm} \qquad (3.64)$$

The CLT floor is in compliance with the US or Canadian CLT floor serviceability criteria. Applying the velocity response criterion proposed by Willford and Young's design guide (CCIP016 [20] will predict the vibration floor response of a single impulse at the fastest pace rms velocity (Equation 3.56).

$$R = v_{rms}/0.0001\ m/s \qquad (3.56)$$

While the floor design is in compliance with EC-5 [22], considering the serviceability of the classroom floor when the room is fully occupied, the fundamental frequency predicted is within the frequency range where resonance with footfall is possible.

If floor serviceability is of particular concern the coordination of the group using the room should also be factored (ISO 10137: 2007 Table A.2 [115]). The student footfall entering the room may be synchronised from the door to the first desk, however, it is reasonable to assume that that their coordination will dissipate as they make their way to their individual place in the room.

This coordinated movement would occur in the area of the room where the modal response is minimum (Table 8.30 (UF)). As the room is largely unoccupied at this time, the synchronised pace would coincide with a high-frequency floor and responses would be transient.

Additionally, the duration of the traffic would not be constant, with movement generally confined to well-defined time spans. applying VDV multiplying factors [117] [115] would also be applicable (Equation 3.61).

If an estimate of resonant vibration response is required, Willford and Young's (CCIP016 [20] acceleration calculations are then appropriate, Equations (3.54 and 3.61).

However, substituting the fundamental frequency value of the floor fully occupied of 6.8 Hz (FO) again with the US or Canadian CLT floor serviceability criteria gives:

$$f/_{d^{0.7}} \geq 13.0: \qquad 6.8\,Hz/_{0.31^{0.7}\,mm} = \mathbf{15.5} \tag{3.63}$$

$$d \leq f^{1.43}/_{39}: \qquad 0.31\,mm \leq 6.8^{1.43}Hz/_{39} = \mathbf{0.40\,mm} \tag{3.64}$$

The FE representation of a 5-ply CLT classroom floor is still in compliance with the US or Canadian CLT serviceability limit values when the floor is fully occupied.

The natural frequencies that were predicted in the central corridor, where a uniform pedestrian excitation is most likely, were substantially outside the range of footfall excitation, over 40 Hz.

8.6 Conclusions

An efficient and straightforward numerical modelling programme was developed to predict the static deflection and dynamic response of single- and multi-panel CLT floors. The numerical models were compared with the experimental results with respect to the floor's flexural stiffness and natural frequency values.

Comparing the FE analyses of the CLT floor assuming minimum and maximum rotational stiffness with the experimental testing deflection results showed that assuming the floor fixing to be simply-supported in all instances is conservative, but appropriate. The variance between the FE results assuming minimum rotational stiffness at the supports and the experimental results was between 0.05 mm and 0.16 mm in all instances.

The FE modal analysis with pinned support conditions provided the best correlation with the experimental test results for the first two natural frequency values, for all the floor orientations examined. The variance between the FE simply-supported models and the experimental frequency values was generally less than 1 Hz to 2 Hz.

However, correlation with the higher modes was less accurate, with a variance greater than 6 Hz. Characterising the boundary conditions as simply-supported was not always conservative for the shorter spanning floor, the FE analysis overestimated the fundamental frequency of the unloaded floor model (Assembly L), however the variance was less than 1 Hz. The next natural mode was then underestimated by the FE model by less than 2.5 Hz.

As the representation of modes below 40 Hz is particularly important in predicting the serviceability performance of a floor with respect to human activity and pedestrian excitation (EC-5 [22]), it may be concluded that defining the CLT support conditions as simply-supported regardless of the type of fixing used, is best suited to predicting floor serviceability.

The parametric FE study illustrated that modelling a multi-panel floor simply as a single panel floor provided a close estimate of the fundamental mode value. However, to reliably predict higher modes, all of the parallel panels with all transverse and intermediate supports must be included in the analysis.

Investigating the modal impact of a rectangular void consistent with that required for vertical circulation in a building showed that it reduced the modal frequency marginally. The difference in the case of the fundamental mode was less than 1 Hz. This was the case regardless of the position of the void. The optimum location to position the floor void was midspan straddling two panels (Option F).

Providing support to alternative edges of the void was found to increase the frequency values substantially. The fundamental mode of the floor with a void midspan, was increased from 9.01 Hz to 16.67 Hz when the void was supported on two adjacent edges. However, the value increased to 23.31 Hz where the void was supported along two parallel edges. Similar results were observed for a large circular void in the floor. Smaller penetrations to accommodate services were found not to impact the floors natural mode shapes nor their frequency values to any significant degree. Where additional support was not given to the rectangular void edge the optimum results coincided with positioning the void centrally in the floor.

An investigation was made of a series of single occupancy rooms suitable for residential accommodation. The room layouts replicated a standard modern hotel bedroom layout design. Investigating the modal properties of the floor while discounting intermediate non-structural partitions or any loading additional to the self-weight of the floor, a good performance with respect to the European 8 Hz limit was found in all cases (EC-5 [22]). Incorporating non-structural, but fixed internal walls improved the modal properties of the floor, from 16.23 Hz (UF) to 25.93 Hz (PW) for the fundamental frequency. Including the standard loading to be expected on the floor as discrete masses did not notably impact on the natural modes of the rooms. Distributing the equivalent load evenly across the floor significantly reduced frequency values. A fundamental frequency of 19.37 Hz was found where the internal partitions were included in the model (Model UDL). This results was reduced to 12.11 Hz modelling the floor without intermediated non-structural walls and evenly distributing the added mass over the floor (Model UDL-W).

An FE investigation of a typical primary school classroom showed that the standard furnishings of a classroom do not notably influence the modal characteristics of the floor. Its performance was found to be within the European timber design 8 Hz fundamental frequency limit.

The most significant observation from the multi-room models was with regard to the areas where people are most expected to walk at a uniform pace and in unison. The natural modes of the floors in all the corridors and main circulation areas were found to be outside the range of footfall excitation. Experimental investigations of floors in-situ confirmed this.

9 CONCLUSIONS

9.1 Conclusions

This study was undertaken to examine the serviceability of CLT floors in response to pedestrian traffic within the structural vibration frequency range of people's perception.

Seven key research objectives were addressed. Experimental testing in the laboratory was used to examine the influence on floor serviceability of (i) the floor support connection detail, the fixing type, and connection position, (ii) the use of an acoustic non-structural elastomeric interlayer and (iii) the addition of an evenly distributed mass on a CLT floor. Field tests were used to examine the influence on a floor's flexural stiffness and natural frequency values of (iv) the number of CLT panels connected in parallel and a floor's integration in the building. To satisfy the remaining research objectives a numerical modelling approach was developed, to (v) determine the influence of floor voids, the void position, and the void support, and the effect of non-structural intermediate supports on CLT floor serviceability, (vi) explore the dynamic influence of irregular mass distributions that are representative of typical objects or loading on specific standard room layouts, and finally (vii) develop an efficient numerical modelling approach to identify the optimum CLT floor design choice with respect to support choices, geometry, and mass or loading distribution.

Experimental investigations

As there may be a significant variation in the connection assembly time and per item cost of alternative CLT fixing details, the study aimed to assess the effect on serviceability of different CLT floor-to-wall connection configurations so that an informed selection may be made at the design stage. To accommodate this, a laboratory experimental programme was developed to include a comprehensive range of alternative platform and balloon connection details. A 5-ply CLT floor panel measuring 162 mm x 2400 mm x 4000 mm and 94 mm 3-ply wall panels were selected. The floor geometry and wall thicknesses chosen were representative of typical CLT floor and wall panels. Common variations of industry standard fixing details were examined, and key influential parameters were measured. The following parameters were measured for each floor system (i) the flexural stiffness, determined by measuring the static 1 kN point load deflection, (ii) the frequency category (low or high), determined by measuring the fundamental frequency value of the floor, with sample time domain footfall excitation recorded to confirm transient or resonant excitation, (iii) the natural frequencies and their mode shapes in the 0 to 80 Hz range, (iv) the accelerance values of resonant modes, (v) and their damping ratio ζ values.

The effect on serviceability due to alternate span directions was also examined in the laboratory tests, while field measurements compared static deflection and natural frequency results of two floors of equal span comprising two and four panels connected in parallel.

Test results

The laboratory results show clearly that the choice of connection detail at the supports of a CLT floor does not influence the natural mode shape nor the mode frequency values to any significant extent. The CLT floor panel's inherent mass, rigidity, and span was found to dominate its serviceability performance.

All floors tested were substantially compliant with the current European timber design frequency criteria (EC-5 [22]). The maximum static point load deflection recorded for a 4000 mm span floor was 0.219 mm/kN. The Irish NA limit for a timber floor of the same span is 1.800 mm/kN [111]. This equates to an improved flexural stiffness performance in a CLT floor of almost a factor of 10 over the limiting value of a traditional timber-joisted floor. The minimum fundamental frequency value recorded was 14.90 Hz, which increased to 20.45 Hz where the floor was unloaded (laboratory Assemblies K and J). The minimum fundamental frequency limit in EC-5 [22] is 8 Hz, unless additional investigations are made. A fundamental frequency greater than 8 Hz ensures that the dynamic response to footfall is transient, hence negating the possibility of resonant build-up of potentially annoying vibrations from footfall.

The maximum support rigidity was achieved in the laboratory when combining angle brackets at close spacing (Assembly H, with brackets 200 mm c/c) in addition to vertical partially-threaded screw fixings (Assembly B, with vertical screws at 300 mm c/c). Results showed that additional fixings at the CLT floor supports improved the deflection results to 0.158 mm/kN from 0.178 mm/kN with natural frequency results improved by up to 6%. Comparing different brackets types, in combination with vertical screw pairs at the same spacing (Assemblies F and G), showed negligible variation in results. There was no clear deflection or frequency benefit recorded using inclined pairs of screws in preference to vertical screws (Assembly E and B, respectively). Floor assemblies consisting of vertical screws generally outperformed inclined pairs of screws with regard to damping, but the variations in results were not substantial, from 0.85% to 0.98% in the case of the fundamental mode, respectively. Comparing the alternative balloon assemblies, using supporting angle brackets at 250 mm spacing (Assembly I) and inclined screw pairs at 250 mm spacing (Assembly J), showed that the inclined screw pairs improved static deflection, natural frequency, and damping ratio ζ-values results marginally, from 0.219 mm/kN to 0.201 mm, from 20.05 Hz to 20.45 Hz, and from 0.80% to 0.91%, respectively. However, the bracket supported floor generally performed better with respect to accelerance, increasing 0.108 m/s^2/N from 0.116 m/s^2/N for the fundamental mode and more substantially to 0.157 m/s^2/N compared with 0.294 m/s^2/N for the fourth mode, respectively. Spanning the single-panel laboratory floor in two directions improved flexural stiffness of the floor and increased the natural frequency values considerably, by over 40%. However, the resonant vibration magnitudes increased from 0.024 m/s^2/N to 0.158 m/s^2/N and the damping performance of the floor was reduced from 1.51% to 1.33%, respectively.

Addressing the second research objective, there was no clear deflection or frequency benefit measured due to the inclusion of a resilient interlayer (Assemblies B and C). The effect on accelerance and damping ratio ζ-values were positive, but not substantial from 0.137 m/s^2/N to 0.131 m/s^2/N and from 0.98% to 1.05% in the case of the fundamental mode with more notable effect on accelerance from 0.051 m/s^2/N to 0.027 m/s^2/N for the third mode, respectively. It should be noted however, that the load on the junction was significantly less than the design load expected on the resilient interlayer.

The influence of an added mass evenly distributed on the floor, equivalent to the mass of a non-structural floor screed, was measured using three different laboratory floor-wall junction arrangements of different spans in order to address the third research objective. The addition of the mass consistently reduced the frequency values of the natural modes. Comparing the one-way long spanning platform floor with, and without, added mass (Assemblies B and D), the fundamental frequency value reduced from 21.90 Hz to 16.35 Hz, respectively. However, the damping ratio ζ-value increased from 0.98% to 1.66 % for the same mode and significantly increased from 0.93 % to 2.79% in the case of the second natural mode. The accelerance improved from a value of 0.137 $m/s^2/N$ to 0.046 $m/s^2/N$ for vibrations in resonance with Mode 1, respectively. The point load deflection results were unchanged. The results show that while additional mass on a floor will reduce the fundamental frequency value, it may be assumed to provide a positive influence with respect magnitude and duration of any resonant vibrations.

The fourth research objective required in-situ static and frequency testing on two floors of a student residence CLT building. Fundamental frequencies that were multiples of the minimum limit recommended in EC-5 [22] (8Hz) were recorded. However, the field tests of floors comprising multiple panels connected in parallel showed a marked reduction in the natural mode separation compared to a single-panel floor. The mode separation and the number of first order modes below a defined range can prove significant with regard to compliance with EC-5 [22] velocity impulse criteria and highlights the importance of accounting for the complete floor geometry in floor vibration assessment.

The experimental results indicate that the dynamic response to pedestrian traffic on all the CLT floors tested would be transient. Transient vibrations are regulated by a floors fundamental frequency and flexural stiffness, which the experimental results clearly indicate are determined by the CLT floor geometry. Only marginal effects were observed from the type of connection provided at the CLT floor support. While the laboratory and field floors tested were substantially compliant with the European timber design frequency criteria (EC-5 [22]), a criterion, which is based on floor geometry, its mass and stiffness, and the number of parallel panels, may be more appropriate to CLT serviceability design.

In the case of long spanning or timber concrete composite floors, where the fundamental frequency is reduced to below 8 Hz and therefore resonant with footfall, the damping ratio ζ and accelerance performance are critical to abating the magnitude and duration of annoying vibrations to below defined acceptable levels (ISO 10137: 2007 C.1, C.2, and C.3 [115]). Moreover, vibrations in floors may be as a result of mechanical excitation at frequencies coincident with natural modes. The experimental results show that reducing the number of floor support fixings consistently resulted in better floor performance with regard to accelerance and damping. The inclusion of an elastomer resilient interlayer also improved accelerance and damping ratio ζ-values. However, the positive dynamic effect in both cases was marginal and therefore not recommended as a mitigating solution to resonant dynamic behaviour. In contrast, the experimental results clearly indicate that an evenly distributed mass significantly improves the damping ratio ζ and accelerance performance and should be primarily considered as a solution to any disturbing resonant floor vibrations.

Numerical analysis

To satisfy the fifth, sixth, and seventh research objectives a numerical modelling approach was developed. Initial FE models of single-panel and multi-panel CLT floors were developed and then calibrated with the experimental static deflection and modal frequency results. Defining the floor edge supports as simply supported, i.e. with a minimum restriction on rotational stiffness, best correlated to the experimentally recorded values especially for the critical modes below 40 Hz, regardless of the type of fixing used. Comparing the FE deflection predictions for the cases of minimum and maximum support rotational stiffness showed that the experimental deflection results when assuming the floor fixing was simply supported is, in all instances, conservative but appropriate. The floor panel-to-panel junctions in the multi-panel floors tested in the field were represented by permitting rotation along the span axis of the panels, while the other five degrees of freedom were tied. The numerical multi-panel floors correlated well with the field test results giving a degree of confidence that this numerical approach is suited to CLT serviceability prediction.

Comparing the experimental field-tested floors with calibrated numerical models showed that the CLT floor’s integration into the building was not significantly influential to its serviceability performance (Research objective (iv)). It should be noted however, that the floors that were examined were on the top storey of the building and further field tests are recommended to examine other situations.

A numerical parameter study on floor penetrations was developed to specifically examine the effect of rectangular and circular voids, with different combinations of supported and unsupported edges, in a multi-panel CLT floor. The floor void sizes were representative of stairwell openings. Small service penetrations and the effect of the position of the rectangular voids on the floor were also studied.

The analysis showed that it is the support, rather than the void, or the location of the void that most influences the modal frequency values, with the shape of the natural modes notably altered in all instances. With respect to the fundamental frequency value, the optimum location for the unsupported rectangular floor void was when positioned straddling two panels, with predicted values of 9.06 Hz compared to 8.51 Hz when the void is positioned at midspan adjacent a floor edge support (Models F and D, respectively). For the case of the supported rectangular floor void, the optimum void location was midspan adjacent a floor edge support (Model D') at 19.88 Hz. With respect to mode separation, the optimum location for the supported rectangular floor void supported was straddling two panels (Model F').

An 1800 mm diameter unsupported circular void (Model G) had a negligible influence on the fundamental and second natural modes of the floor, but generally reduced the higher natural mode values. Simply-supporting the circular floor void (Model G') improved the frequency values generally and reduced the number of modes in the range of interest (0 to 80 Hz). Small 100 mm diameter service penetrations within 100 mm of the floor edge (Model H) did not impact natural modal values to any significant extent.

Analysis on the effect of non-structural intermediate supports on the same floor confirmed the established consensus [158] [132][172] [138] that intermediate supports significantly affect a floors modal properties. The numerical study showed that the angle of the support relative to the main floor span, dramatically influences the dynamic performance of a floor. Including cross supports diagonal to the floor span predicted a fundamental mode value of 47.89 Hz compared with 9.19 Hz for the floor without supports.

Numerical study of standard room designs

Smith and Chui [164] proposed examining how common objects in dwellings may impact on the perception of accelerations to a human observer. Using the numerical approach that was calibrated with experimental results, specific mass distributions consistent with typical fittings and furnishings were examined. Numerical models of two standard rooms were developed, namely, a twin hotel bedroom and a standard classroom [195] [196].

The results of the FE hotel room analysis showed that non-structural, but fixed, internal walls improved the modal properties from 16.23 Hz (UF) to 25.93 Hz (PW) for the fundamental frequency. Including masses representing typical discrete floor loads did not notably impact on the natural modes of the rooms. However, distributing the equivalent mass evenly across the floor significantly reduced frequency values. A fundamental frequency of 19.37 Hz was determined where the internal partitions were included in the model (Model UDL). This was reduced to 12.11 Hz when modelling the floor without non-structural walls and evenly distributing the added mass of furniture and fittings over the floor area (Model UDL-W).

Finally, the predicted point load deflection and natural frequency results show that pedestrian excitation in the main circulation routes, the corridors where people are most expected to walk at a uniform pace and in unison, may be regarded as transient.

9.2 Contribution to knowledge

The existing European timber design standard EN 1995-1-1 (EC-5) [22] does not provide specific guidance on CLT serviceability design [23]. The following are observations made from the results of this research that are pertinent to any revision of serviceability and CLT design of the current timber design code.

- The dynamic response to pedestrian traffic on CLT floors spanning up to 6 meters can be regarded as transient.
- Transient vibrations are regulated by a floor’s fundamental frequency and its flexural stiffness. The experimental results show that the floor geometry and mass dominate the fundamental frequency and flexural stiffness properties of a CLT floor, with minimal effect observed from the type, and spacing of connections provided at the floor support.
- In the case of CLT floors where the fundamental frequency is reduced to below 8 Hz due to the floor span or mass and is therefore resonant with footfall, the provision of evenly distributed mass was identified as the most efficient method to mitigate resonant dynamic behaviour in the floor.

- The measurements in the field show that the number of panels connected in parallel do not significantly influence the fundamental frequency of a CLT floor, but substantially effect the mode separation of the other higher natural mode values.
- Spanning a single-panel CLT floor in two directions notably affects the floor’s serviceability behaviour.

While current timber design standards [22] set out basic serviceability design limits for single-span, simply supported rectangular floors, a more robust design approach [124][151] including a straightforward numerical modelling method would more accurately represent non-uniform floor geometry, floor openings, and support configurations. It is asserted that an uncomplicated method to evaluate how typical objects in buildings impact on the perception of floor vibrations is also needed [164]. It can be concluded from this research that the following analysis approach are suitable to implementation in practise for the design of CLT floor systems.

- A CLT floor may be represented accurately for modes below 40 Hz with a two-dimensional multi-ply numerical model with an orthotropic composite layup. The floor edge supports may be represented as pinned supports in FE and the CLT panel-to-panel junctions in multi-panel floors may be defined by permitting rotation along the span axis of the panels, while the other five degrees of freedom are tied.
- Floor voids, their position and support, and any intermediate supports that are fixed can significantly impact on the dynamic behaviour of a CLT floor. Therefore, it is recommended to assess the modal properties of the whole floor including voids and all fixed supports using FE at the design stage where possible.

Finally, a criterion which is based on floor geometry, its mass, and stiffness, including all alternative floor supports, and the number of panels connected in parallel is recommended to assess CLT floor serviceability at design stage.

9.3 Future work

Supplementary research from this study on CLT floors may include the following:

- Experimental dynamic analysis on the proportional influence of the magnitude and distribution of added non-structural discrete masses with regard to accelerance and damping performance of CLT floors.
- Experimental static and dynamic investigations on the influence of integrated structural toppings to CLT floors on the floor’s flexural stiffness and dynamic response.
- A laboratory experimental static and dynamic investigations on the influence on serviceability of alternative connections of parallel panels in multi-panel CLT floors.
- Development of numerical models which replicate the dynamic force of a mechanical exciter to facilitate the calibration of FE models so that the influence of different excitation forces may be examined.
- Analysis of CLT floors incorporating the mass, position, and excitation force of common household appliances to provide an informed approach to a CLT residential building design. This will potentially inform the optimum kitchen or utility room layouts or service room locations in a multi-storey CLT development.
- Assessment of the operating vibration frequencies of mechanical services that are communal to multi-occupant buildings, including air-conditioning and heat-condensing units. Results would serve to inform their optimum location. The current practice is to position appliances on external facades or on the roof, which may not be appropriate for CLT construction.

REFERENCES

[1] United Nations Department of Economic and Social Affairs/Population Division, “World Population Prospects: The 2015 Revision, Key Findings and Advance Tables,” New York, 2015.

[2] United Nations Department of Economic and Social Affairs/Population Division, “World Population 2015,” New York, 2015.

[3] C. D. Oliver, N. T. Nassar, B. R. Lippke, and J. B. McCarter, “Carbon, Fossil Fuel, and Biodiversity Mitigation With Wood and Forests,” *J. Sustain. For.*, vol. 33, no. 3, pp. 248–275, 2014.

[4] P. Kauppi *et al.*, “Climate Smart Forestry in Europe,” *European Forest Institute*, 2018. [Online]. Available: https://www.efi.int/articles/climate-smart-forestry-missing-link.

[5] Pinterest, “Ballinasloe swimming pool.” .

[6] Oifig an tSoláthair, *Building Regulations 2011 Technical Guidance Document L Fuel and Energy - Dwellings*. Ireland, 2011.

[7] CEN, *I.S. EN 1634-1:2014+A1:2018&LC:2018 - Part 1: Fire resistance test for door and shutter assemblies and openable windows*. 2018.

[8] S. M. Timber, “Grandview Heights Aquatic Centre.” [Online]. Available: https://seagatestructures.com/projects/grandview-aquatic/. [Accessed: 08-Jul-2019].

[9] HCMA Architecture, “Grandview Heights Aquatic Centre.” [Online]. Available: https://hcma.ca/project/grandviewheights/. [Accessed: 10-Oct-2018].

[10] P. Fast and D. Ratzlaff, “Design of the roof for the Grandview Heights aquatic centre, Surrey, Canada,” *the structureengineer.org*. [Online]. Available: http://www.fastepp.com/wp-content/uploads/TSE67_Project-Focus_AquaticCentre-v3.pdf. [Accessed: 10-Oct-2018].

[11] C. Risen, “Popular Science,” *Cross-laminated timber is the most advanced*

building material, Feb-2014.

[12] "Australia enters Age of Timber Buildings as first CLT plant fires up," *The Urban Developer,* 2018. [Online]. Available: https://theurbandeveloper.com/articles/australia-enters-age-of-timber-buildings-as-first-clt-plant-fires-up.

[13] S. V. Ohlsson, "Floor vibrations and human discomfort.," PhD Thesis: Chalmers University of Technology, Goteborg, Sweden, 1982.

[14] S. A. Hernández Maldonado and Y. H. Chui, "Effect of End Support Conditions on the Vibrational Performance of Cross-Laminated Timber Floors," in *World Conference on Timber Engineering*, 2014.

[15] J. Liu and F. Lam, "Experimental test of coupling effect on CLT angle bracket connections," *Eng. Struct.*, vol. 171, no. January, pp. 862–873, 2018.

[16] C. Loss, A. Hossain, and T. Tannert, "Simple cross-laminated timber shear connections with spatially arranged screws," *Eng. Struct.*, vol. 173, no. April, pp. 340–356, 2018.

[17] A. Pavic and P. Reynolds, "Vibration serviceability of long-span concrete building floors. Part 1: Review of background information," *Shock Vib. Dig.*, vol. 34, no. 3, pp. 191–211, 2002.

[18] T. M. Murray, "Building Floor Vibrations," *Eng. Journal/American Inst. Steel Constr.*, pp. 102–109, 1991.

[19] A.L. Smith, S. J. Hicks, and P. J. Devine, *Design of Floors for Vibration : A New Approach (SCI P354),* Revised Ed. Berkshire: SCI, 2009.

[20] M. R. Willford and P. Young, *A design guide for footfall induced vibration of structures (CCIP-016)*. Surrey: CCIP, 2006.

[21] T. M. Murray, D. E. Allen, and E. E. Ungar, *Steel Design Guide Series 11: Floor Vibrations due to Human Activity*. American Institute of Steel Construction, Inc., 2003.

[22] CEN, *I.S. EN 1995-1-1: 2004 & AC:2006 & A1:2008 & A2:2014. Eurocode 5:*

Design of timber structures - Part 1-1: General - Common rules and rules for buildings. NSAI, 2014.

[23] M. Jeleč, D. Varevac, and V. Rajčić, “Cross-laminated timber (CLT) – A state of the art report,” *J. Croat. Assoc. Civ. Eng.*, vol. 70, no. 02, pp. 75–95, 2018.

[24] P. Zumbrunnen and J. Fovargue, “Mid rise CLT Buildings - The UK’s experience and Potential for Australia and New Zealand,” in *World Conference on Timber Engineering*, 2012.

[25] G. Fink, J. Kohler, and R. Brandner, “Application of European design principles to cross laminated timber,” *Eng. Struct.*, vol. 171, no. December 2017, pp. 934–943, 2018.

[26] J. Mairs, “Anders Berensson proposes wooden skyscraper with decorative facade for Stockholm,” *Dezeeen*, 2018. [Online]. Available: https://www.dezeen.com/2016/04/25/anders-berensson-architects-tratoppen-wooden-skyscraper-concept-stockholm-cross-laminated-timber/. [Accessed: 12-Sep-2018].

[27] H. Ellyatt, “World’s tallest wooden skyscraper planned in Tokyo.” [Online]. Available: World’s tallest wooden skyscraper planned in Tokyo.

[28] P. Architecture, “Oakwood Timber Tower London, UK.” [Online]. Available: http://www.plparchitecture.com/oakwood-timber-tower.html. [Accessed: 12-Sep-2018].

[29] R. M. Foster, T. P. S. Reynolds, and M. H. Ramage, “What is tall timber? Towards the formal classification of timber as a material of tall building design .,” in *World Conference on Timber Engineering*, 2018.

[30] J. Mairs, “PLP Architecture proposes London’s first wooden skyscraper at the Barbican,” *Dezeen*. [Online]. Available: https://www.dezeen.com/2016/04/08/plp-architecture-cambridge-university-london-first-wooden-skyscraper-barbican/. [Accessed: 03-Jul-2019].

[31] P. Kotecki, “Stockholm might get an entire neighbohood of 31 wooden skyscrapers.” [Online]. Available: https://www.businessinsider.com/swedish-

architect-planning-to-build-31-wooden-skyscrapers-in-stockholm-2018.

[32] India Block, “Anders Berensson Architects proposes ‘wooden skyscraper city’ for Stockholm,” *Deezen*, 2018. [Online]. Available: https://www.dezeen.com/2018/09/07/anders-berensson-architects-wooden-skyscraper-city-stockholm-sweden-architecture/.

[33] “Wood Skyscrapers.” [Online]. Available: http://www.woodskyscrapers.org/projects.html. [Accessed: 12-Sep-2018].

[34] A. Thistleton, *100 Projects UK CLT*. Softwood Lumber Board & Forestry Innovation Investment, 2018.

[35] D. Architects, “Maggie’s Oldham.” [Online]. Available: http://drmm.co.uk/projects/view-maggies-oldham. [Accessed: 10-Oct-2018].

[36] A. De Rijke, P. Marsh, S. Morgan, and J. Lencer, “dRMM Architects.” [Online]. Available: http://drmm.co.uk/. [Accessed: 29-Aug-2019].

[37] T. Harley, G. White, A. Dowdall, J. Bawcombe, A. Mcrobie, and R. Steinke, “Dalston Lane - The world’s tallest CLT building,” in *World Conference on Timber Engineering*, 2016.

[38] L. Alter, “Dalston Lane: The world’s largest Cross-laminated timber building,” 2017. [Online]. Available: https://www.treehugger.com/green-architecture/dalston-lane-worlds-largest-cross-laminated-timber-building.html.

[39] N. Bergen, “Case study of UBC Brock Commons-Construction details and methods,” in *World Conference on Timber Engineering*, 2016.

[40] P. Fast, B. Gafner, R. Jackson, and J. Li, “Case Study : an 18 Storey Tall Mass Timber Hybrid Student Residence At the University of British Columbia , Vancouver,” in *World Conference on Timber Engineering*, 2016.

[41] E. Poirier, M. Moudgil, A. Fallahi, S. Staub-French, and Thomas Tannert, “Design and Construction of a 53-meter-tall Timber Building at the University of British Columbia,” in *World Conference on Timber Engineering*, 2016.

[42] "Minister Bruton announces plans to establish 42 new schools over the next 4 years," *The Department of Education and Skills-Press Release*, 13-Apr-2018.

[43] S. R. Architects, "The Open Academy, City Academy." [Online]. Available: https://www.sheppardrobson.com/architecture/view/city-academy-norwich.

[44] dRMM, "Kingsdale School, St. Abans Academy, Clapham Manor." [Online]. Available: http://drmm.co.uk/projects/kingsdale-school-transformation.

[45] Hawkins/Brown, "Bishop's Stortford, City of Londons Freemen's Swimming Pool, Ivydale School." [Online]. Available: https://www.hawkinsbrown.com/sectors/education.

[46] "KLUK: Portfolio." [Online]. Available: http://www.klhuk.com. [Accessed: 14-Sep-2018].

[47] "Eurban UK: Built Work." [Online]. Available: http://www.eurban.co.uk/built-work/. [Accessed: 14-Sep-2018].

[48] P. Pintos, "Our Lady of the Assumption Catholic Primary School / BVN," *ArchDaily*, 2019. [Online]. Available: https://www.archdaily.com/914735/our-lady-of-the-assumption-catholic-primary-school-bvn?utm_medium=email&utm_source=ArchDaily List&kth=639,333.

[49] A. Angeli, A. Polastri, E. Callegari, and M. Chiodega, "Mechanical Characterization of an Innovative Connection System for CLT Structures," in *World Conference on Timber Engineering*, 2016.

[50] A. Kraler, J. Kögl, R. Maderebner, and M. Flach, "Sherpa-Clt-Connector for Cross Laminated Timber Elements," in *World Conference on Timber Engineering*, 2014.

[51] Gb-legname.com, "Domestic CLT construction." [Online]. Available: http://www.gb-legname.com/panel-contralaminado-en.html. [Accessed: 03-Jul-2019].

[52] "X-RAD." [Online]. Available: https://www.rothoblaas.com/products/fastening/x-rad. [Accessed: 26-Jun-2018].

[53] S. Winter and J. Haas, “The Kampa Building Innovation Center - a high-rise ‘ real timber ’ building,” in *World Conference on Timber Engineering*, 2016.

[54] E. Gasparri, F. Lam, and Y. Liu, “Compression perpendicular to grain behavior for the design of a prefabricated CLT façade horizontal joint,” in *World Conference on Timber Engineering*, 2016, pp. 3–4.

[55] H. Mpidi Bita and T. Tannert, “Disproportionate collapse prevention analysis for a mid-rise flat-plate cross-laminated timber building.pdf,” *Eng. Struct.*, vol. 178, pp. 460–471, 2019.

[56] J. Schneider, T. Tannert, S. Tesfamariam, and S. F. Stiemer, “Experimental assessment of a novel steel tube connector in cross-laminated timber,” *Eng. Struct.*, vol. 177, no. March 2017, pp. 283–290, 2018.

[57] P. Dietsch and S. Winter, “Eurocode 5—Future Developments towards a More Comprehensive Code on Timber Structures,” *Struct. Eng. Int.*, vol. 22, pp. 223–231, 2012.

[58] The European Commission, “Mandate M/515 EN – Mandate for amending existing Eurocodes and extending the scope of Structural Eurocodes,” no. January 2006, pp. 1–8, 2012.

[59] CEN, *I.S. EN 16351 Timber structures - Cross laminated timber - Requirements*. NSAI, 2015.

[60] H. Bauer and G. Schickhofer, “Test configurations and analysis for determining characteristic properties of CLT,” in *World Conference on Timber Engineering*, 2016.

[61] G. Fink, J. Kohler, and R. Brandner, “Application of European design principles to cross laminated timber,” *Engineering Structures*, 2018. [Online]. Available: http://dx.doi.org/10.1016/j.engstruct.2018.02.081.

[62] M. Mohammad *et al.*, “Design approaches for CLT connections,” *Wood Fibre Sci. 50(Special Issue)*, vol. 50, no. August 2017, pp. 27–47, 2018.

[63] DIN, *1995-1-1/NA:2010-12 German National Annex – Eurocode 5: Design of timber structures*. Germany: Deutsches Institut für Normung (DIN), 2010.

[64] ON, *ÖNORM B 1995-1-1:2010 Austrian National Annex – Eurocode 5: Bemessung und Konstruktion von Holzbauten*. Austria: Austrian Standards Institute/Österreichisches Normungsinstitut (ON), 2010.

[65] G. Schickhofer, T. Bogensperger, and T. Moosbrugger, Eds., *BSP-Handbuch, Holz-Massivbauweise in Brettsperrholz,* 2nd ed. Graz: Verlag der Technischen Universität Graz, 2010.

[66] M. Wallner-Novak, J. Koppelhuber, and K. Pock, *Information Brettsperrholz Bemessung Grundlagen für Statik und Konstruktion nach Eurocode*. 2013.

[67] A. Thiel and G. Schickhofer, “CLT designer - A software tool for designing cross laminated timber elements: 1D-plate-design,” in *World Conference on Timber Engineering,* 2010.

[68] A. Thiel, “ULS and SLS design and its implementation in the CLTdesigner,” in *COST Action FP1004: Focus Solid Timber Solutions-European Conference on Cross Laminated Timber (CLT)*, 2013, pp. 77–102.

[69] M. Teibinger and I. Matzinger, *Construction with Cross-Laminated Timber in Multi-Storey Buildings: Focus on Building Physics*. Vienna, Austria, 2013.

[70] FP Innovations, *CLT Handbook: Canadian Edition*. 2011.

[71] FP Innovations and Binational Softwood Lumber Council, *CLT Handbook: US Edition*. 2013.

[72] XLam NZ Ltd., *CLT design guide V1.4 NZ*. 2013.

[73] CEN, *EN 338 Structural timber - Strength classes*. NSAI, 2009.

[74] R. Brandner, G. Flatscher, A. Ringhofer, G. Schickhofer, and A. Thiel, “Cross laminated timber (CLT): Overview and Development,” *Eur. J. Wood Wood Prod.,* vol. 74, no. 3, pp. 331–351, 2016.

[75] CEN, *I.S. EN 15497 Structural finger jointed solid timber - Performance requirements and minimum production requirements*. 2014.

[76] R. Brandner, “Production and technology of Cross Laminated Timber (CLT): A state-of-the-art report,” in *COST Action FP1004: Focus Solid Timber*

Solutions-European Conference on Cross Laminated Timber (CLT), 2013, pp. 3–36.

[77] H. Unterwieser and G. Schickhofer, "Characteristic values and test configurations of CLT with focus on selected properties," in *COST Action FP1004: Focus Solid Timber Solutions-European Conference on Cross Laminated Timber (CLT)*, 2013, pp. 53–73.

[78] APA-The Engineered Wood Association, *Standard for Performance-Rated Cross-Laminated Timber*. USA: American National Standards Institute, 2011.

[79] T. Bogensperger, G. Silly, and G. Schickhofer, "Comparison of methods of approximation verification procedures for cross laminated timber. Research Report, holz.bau forschungs gmbh," Graz, Austria, 2012.

[80] G. Jeitler, M. Augustin, and G. Schickhofer, "Birch GLT and CLT. Mechanical properties of glued laminated timber and cross laminated timber produced with the wood species birch," in *World Conference on Timber Engineering*, 2016.

[81] V. Baño, D. Godoy, D. Figueredo, and A. Vega, "Structural performance of CLT panels in bending made from Loblolly/Slash Pine of low mechanical properties," *Materials (Basel).*, 2018.

[82] M. He, X. Sun, and Z. Li, "Bending and compressive properties of cross-laminated timber (CLT) panels made from Canadian hemlock," *Constr. Build. Mater.*, vol. 185, pp. 175–183, 2018.

[83] Y. Liao *et al.*, "Feasibility of manufacturing cross-laminated timber using fast-grown small diameter eucalyptus lumbers," *Constr. Build. Mater.*, vol. 132, pp. 508–515, 2017.

[84] H. Pangh, H. Zarea, N. Kotlarewski, P. Moradpour, M. Lee, and G. Nolan, "Flexural performance of cross-laminated timber constructed from fibre-managed plantation eucalyptus," *Constr. Build. Mater.*, vol. 208, pp. 535–542, 2019.

[85] R. Cherry, A. Manalo, W. Karunasena, and G. Stringer, "Out-of-grade sawn pine_ A state-of-the-art review on challenges and new opportunities in cross

laminated timber (CLT) _ Elsevier Enhanced Reader.pdf,” *Constr. Build. Mater.*, pp. 858–868, 2019.

[86] G. M. Raftery and A. M. Harte, “Material characterisation of fast-grown plantation spruce,” *Struct. Build.*, vol. 167, 2013.

[87] G. Raftery, A. Harte, and P. Rodd, “Qualification of Wood Adhesives for Structural Softwood Glulam with Large Juvenile Wood Content,” *J. Inst. Wood Sci.*, vol. 18, no. 1, pp. 24–34, Jun. 2008.

[88] D. Crawford, R. Hairstans, and R. E. Smith, “Feasibility of cross-laminated timber production from UK Sitka spruce,” in *COST Action FP1004: Focus Solid Timber Solutions-European Conference on Cross Laminated Timber (CLT)*, 2013, pp. 37–52.

[89] K. S. Sikora, D. O. McPolin, and A. M. Harte, “Effects of the thickness of cross-laminated timber (CLT) panels made from Irish Sitka spruce on mechanical performance in bending and shear,” *Constr. Build. Mater.*, vol. 116, pp. 141–150, 2016.

[90] C. O’Ceallaigh, K. Sikora, and A. Harte, “The Influence of Panel Lay-Up on the Characteristic Bending and Rolling Shear Strength of CLT,” *Buildings*, vol. 8, no. 9, p. 114, 2018.

[91] A. Polastri, I. Giongo, S. Pacchioli, and M. Piazza, “Structural analysis of CLT multi-storey buildings assembled with the innovative X-RAD connection system,” in *World Conference on Timber Engineering*, 2016.

[92] F. Pérez and T. Wallwork, “Connections between CLT elements and future challanges for CLT in practice,” in *Proceedings of the Joint Conference of COST Actions FP1402 & FP1404*, 2016, pp. 137–153.

[93] “COST Action FP1402 ‘Basis of Structural Timber Design’ - from research to standards.” [Online]. Available: https://www.costfp1402.tum.de/home/. [Accessed: 19-Jun-2018].

[94] M. Stepinac, J. M. Cabrero, K. Ranasinghe, and M. Kleiber, “Proposal for reorganization of the connections chapter of Eurocode 5,” *Eng. Struct.*, vol.

170, no. May, pp. 135–145, 2018.

[95] D. J. Ewins, *Modal Testing: Theory, Practice, and Application*, 2nd ed. John Wiley & Sons, 2000.

[96] C. M. Harris, *Shock and Vibration Handbook*, Fourth. McGraw-Hill, 1996.

[97] H. J. Pain, *The physics of vibrations and waves*. John Wiley & Sons Ltd., 2008.

[98] N. M. M. Maia and J. M. M. Silva, Eds., *Theoretical and Experimental Modal Analysis*. Research Studies Press, 1997.

[99] E. Kausel, “Single Degree of Freedom Systems,” in *Advanced Structural Dynamics*, Cambridge University Press, 2017, pp. 55–130.

[100] P.-E. Eriksson, “Vibration of low-frequency floors. Dynamic forces and response predictions,” PhD Thesis: Chalmers University of Technology, Goteborg, Sweden, 1994.

[101] G. Garber, *Design and Construction of Concrete Floors*, 2nd ed. 2005.

[102] J. M. W. Brownjohn and A. Pavic, “Vibration control of ultra-sensitive facilities,” *ICE Proc. Struct. Build.*, vol. 159, no. SB5, pp. 295–306, 2006.

[103] M. J. Hudson and P. Reynolds, “Implementation considerations for active vibration control in the design of floor structures,” *Eng. Struct.*, vol. 44, pp. 334–358, 2012.

[104] J. E. C. Carmona, S. M. Avila, and G. Doz, “Proposal of a tuned mass damper with friction damping to control excessive floor vibrations,” *Eng. Struct.*, vol. 148, pp. 81–100, 2017.

[105] ISO, *ISO 2631-2 Mechanical Vibration and Shock-Evaluation of Human Exposure to Whole Body Vibration Part 2: Vibration in buildings (1Hz to 80 Hz)*. ISO, 1989.

[106] ISO, *ISO 7626-1 Mechanical vibration and shock — Experimental determination of mechanical mobility — Part 1: Basic terms and definitions, and transducer specifications*. Ireland: ISO, 2011.

[107] BSI, *BS 7385-1 Evaluation and measurement for vibration in buildings - Part*

1: Guide for measurement of vibrations and evaluation of their effects on buildings. BSI, 1990.

[108] ISO, *ISO 2631-4 Mechanical vibration and shock — Evaluation of human exposure to whole-body vibration Part 4: Guidelines for the evaluation of the effects of vibration and rotational motion on passenger and crew comfort in fixed-guideway transport systems*. ISO, 2010.

[109] CEN, *I.S. EN ISO 8041 Human response to vibration - Measuring instrumentation*. NSAI, 2005.

[110] BSI, *BS 7385-2 Evaluation and measurement for vibration in buildings Part 2: Guide to damage levels from groundborne vibration*. BSI, 1993.

[111] NSAI, *1995-1-1/NA+A1:2005 Irish National Annex – Eurocode 5: Design of timber structures*. Ireland: National Standards Authority of Ireland (NSAI), 2013.

[112] CEN/124 TC, *prEN 16929 Test Methods - Timber flooring systems - Determination of vibration properties*. 124 TC, 2015.

[113] ISO, *ISO 2631-2 Mechanical Vibration and Shock-Evaluation of Human Exposure to Whole Body Vibration Part 2: Vibration in buildings (1Hz to 80 Hz)*. ISO, 2003.

[114] ISO, *ISO 2631-1 Mechanical Vibration and Shock-Evaluation of Human Exposure to Whole-body Vibration: Part 1: General Requirements*. ISO, 2010.

[115] ISO, *ISO 10137 Bases for Design of Structures - Serviceability of buildings and walkways against vibrations*. ISO, 2007.

[116] ISO, *IS0 2631-1 Mechanical vibration and shock - Evaluation of human exposure to whole-body vibration Part 1: General requirements*. ISO, 1997.

[117] BSI, *BS 6472-1 Guide to evaluation of human exposure to vibration in buildings Part 1: Vibration sources other than blasting*. BSI, 2008.

[118] M. J. Griffin, *Handbook of human vibration*. Academic Press Inc., 1990.

[119] S. Ohlsson, *Springiness and human induced floor vibrations: A Design Guide*.

Stockholm, Sweden: Swedish Council for Building Research, 1988.

[120] CEN, *I.S. EN 1990: 2002 + NA 2005 Eurocode - Basis of structural design*. CEN, 2010.

[121] B. Zhang, B. Rasmussen, A. Jorissen, and A. Harte, “Comparison of vibrational comfort assessment criteria for design of timber floors among the European countries,” *Eng. Struct.*, vol. 52, no. 52, pp. 592–607, 2013.

[122] E. Shahabpoor, A. Pavic, V. Racic, and S. Zivanovic, “Effect of group walking traffic on dynamic properties of pedestrian structures,” *J. Sound Vib.*, vol. 387, pp. 207–225, 2017.

[123] S. C. Kerr, “Human Induced Loading on Staircases,” PhD Thesis: University College London, 1998.

[124] L. Hu and S. Gagnon, “Controlling cross-laminated timber (CLT) floor vibrations: Fundamentals and method,” in *World Conference on Timber Engineering*, 2012.

[125] D. M. Onysko, “Serviceability criterion for residential floors based on a field study of consumer response.,” 1985.

[126] L. J. Hu, Y. H. Chui, and D. M. Onysko, “Vibration serviceability of timber floors in residential construction,” *Prog. Struct. Eng. Mater.*, vol. 3, no. 3, pp. 228–237, 2001.

[127] A. Homb and S. T. Kolstad, “Evaluation of floor vibration properties using measurements and calculations,” *Eng. Struct.*, vol. 175, pp. 168–176, 2018.

[128] L. J. Hu, “Serviceability design criteria for commercial and multi-family floors.,” 2000.

[129] Aamir Muhammad Khokhar, “Influence of lateral element stiffness on performance of wooden floors,” The University of New Brunswick, 2004.

[130] J. Weckendorf, “Dynamic Response of Structural Timber Flooring Systems,” PhD Thesis: Edinburgh Napier University, 2009.

[131] M. M. Ebadi, G. Doudak, and I. Smith, “Vibration responses of glulam beam-

and-deck floors," *Eng. Struct.*, vol. 156, no. November 2017, pp. 235–242, 2018.

[132] D. Casagrande, I. Giongo, F. Pederzolli, A. Franciosi, and M. Piazza, "Analytical, numerical and experimental assessment of vibration performance in timber floors," *Eng. Struct.*, vol. 168, no. May, pp. 748–758, 2018.

[133] A. Homb, "Floor vibrations and low frequency sound pressure levels using a rubber ball impact method," in *InterNoise - International Congress and Exhibition on Noise Control Engineering*, 2000, no. 29th.

[134] N. W. M. Bishop, M. R. Willford, and R. Pumphrey, "Human induced loading on flexible staircases," *Saf. Sci.*, vol. 18, no. 94, pp. 261–276, 1995.

[135] P. Andrade, J. Santos, and P. Escorcio, "Application of the effective impulse approach to stairs," in *Procedia Structural Integrity*, 2017.

[136] A. Homb, "Low frequency sound and vibrations from impacts on timber floor constructions," Norwegian University of Science and Technology, 2005.

[137] P. Hamm, A. Richter, and S. Winter, "Floor vibrations – new results," in *World Conference on Timber Engineering*, 2010.

[138] S. E. Zimmer and M. Augustin, "Vibrational Behaviour of Cross Laminated Timber Floors in Residental Buildings," in *World Conference on Timber Engineering*, 2016.

[139] J. Fernández Martínez, L. Hermanns, A. Fraile de Lerma, and E. Alarcón Álvarez, "Jumping load models applied on a gymnasium floor," *Eng. Struct.*, vol. 125, pp. 26–38, 2016.

[140] V. Racic and J. M. W. Brownjohn, "Stochastic model of near-periodic vertical loads due to humans walking," *Adv. Eng. Informatics*, vol. 25, no. 2, pp. 259–275, 2011.

[141] A. S. Mohammed, A. Pavic, and V. Racic, "Improved model for human induced vibrations of high-frequency floors," *Eng. Struct.*, vol. 168, no. May, pp. 950–966, 2018.

[142] E. Bassoli, K. Van Nimmen, L. Vincenzi, and P. Van den Broeck, “A spectral load model for pedestrian excitation including vertical human-structure interaction,” *Eng. Struct.*, vol. 156, no. December 2016, pp. 537–547, 2018.

[143] E. Shahabpoor, A. Pavic, and V. Racic, “Structural vibration serviceability: New design framework featuring human-structure interaction,” *Eng. Struct.*, vol. 136, pp. 295–311, 2017.

[144] J. Chen, R. Xu, and M. Zhang, “Acceleration response spectrum for predicting floor vibration due to occupants walking,” *J. Sound Vib.*, pp. 3564–3579, 2014.

[145] T. Ji, B. R. Ellis, and A. J. Bell, “Horizontal movements of frame structures induced by vertical loads,” *Proc. ICE - Struct. Build.*, vol. 156, no. 2, pp. 141–150, 2003.

[146] G. Li, T. Ji, and J. Chen, “Determination of the dynamic load factors for crowd jumping using motion capture technique,” *Eng. Struct.*, vol. 174, no. July, pp. 1–9, 2018.

[147] K. Van Nimmen, G. Lombaert, G. De Roeck, and P. Van Den Broeck, “The impact of vertical human-structure interaction on the response of footbridges to pedestrian excitation,” *J. Sound Vib.*, vol. 402, pp. 104–121, 2017.

[148] Z. Muhammad, P. Reynolds, O. Avci, and M. Hussein, “Review of Pedestrian Load Models for Vibration Serviceability Assessment of Floor Structures,” *Vibration*, vol. 2, no. 1, pp. 1–24, 2018.

[149] A. Rönnquist, L. Wollebæk, and K. Bell, “Dynamic behavior and analysis of a slender timber footbridge,” in *World Conference on Timber Engineering*, 2006.

[150] B. Zhang, A. Kermani, and T. Fillingham, “Vibrational performance of timber floors constructed with metal web joists,” *Eng. Struct.*, vol. 56, pp. 1321–1334, 2013.

[151] N. Labonnote, A. Rønnquist, and K. A. Malo, “Prediction of material damping in timber floors, and subsequent evaluation of structural damping,” *Mater. Struct.*, vol. 48, no. 6, pp. 1965–1975, 2015.

[152] N. Labonnote, “Damping in timber structures,” PhD Thesis: Norwegian

University of Science and Technology, 2012.

[153] B. J. Schwarz and M. H. Richardson, “Experimental Modal Analysis,” in *CSI Reliability Week*, 1999, pp. 1–12.

[154] M. Popovski, Z. Chen, and B. Gafner, “Structural Behaviour of Point-Supported CLT Floor Systems,” in *World Conference on Timber Engineering*, 2016, pp. 5463–5470.

[155] K. Jarnerö, A. Brandt, and A. Olsson, “Vibration properties of a timber floor assessed in laboratory and during building construction,” in *Inter Noise 2010*, 2010, pp. 1–10.

[156] K. Jarnero, Å. Bolmsvik, A. Brandt, and A. Olsson, “Effect of flexible supports on vibration performance of timber floors,” in *Euronoise*, 2012, pp. 214–219.

[157] K. Jarnerö, “Vibrations in timber floors-Dynamic properties and human perception,” PhD Thesis: Linnéuniversitetet, 2014.

[158] K. Jarnerö, A. Brandt, and A. Olsson, “Vibration properties of a timber floor assessed in laboratory and during construction,” *Eng. Struct.*, vol. 82, pp. 44–54, Jan. 2015.

[159] A. Campbell, B. Gill, and R. Harrison, “Design and detailing of timber structures for fitness and gymnasia buildings : Experience from Sky health & fitness centre,” in *World Conference on Timber Engineering*, 2016.

[160] P. Reynolds and A. Pavic, “Impulse hammer versus shaker excitation for the modal testing of building floors,” *Exp. Tech.*, vol. 24, no. 3, pp. 39–44, 2000.

[161] G. A. Papagiannopoulos and G. D. Hatzigeorgiou, “On the use of the half-power bandwidth method to estimate damping in building structures,” *Soil Dyn. Earthq. Eng.*, vol. 31, no. 7, pp. 1075–1079, 2011.

[162] CEN, *I.S. EN 13183-2 Moisture content of a piece of sawn timber Part 2: Estimation by electrical resistance method*. NSAI, 2002.

[163] CEN, *I.S. EN 322 Wood-based panels Determination of moisture content*. NSAI, 1993.

[164] I. Smith and Y. H. Chui, “Design of lightweight wooden floors to avoid human discomfort,” *Can. J. Civ. Eng.*, vol. 15/502/51, no. 254–262, 1988.

[165] B. Zhang, A. Kermani, and T. Fillingham, “Vibrations of metal web joist timber floors with strongbacks,” *ICE Proc. Struct. Build.*, 2015.

[166] H. Xiong, J. Kang, and X. Lu, “Field testing and investigation of the dynamic performance and comfort of timber floors,” *Jounal Asian Archit. Build. Eng.*, no. November, pp. 407–412, 2011.

[167] J. Weckendorf and I. Smith, “Dynamic characteristics of shallow floors with Cross-Laminated-Timber Spines,” in *World Conference on Timber Engineering*, 2012.

[168] A. Cappellini, S. Manzoni, M. Vanali, and A. Cigada, “Evaluation of the dynamic behaviour of steel staircases damped by the presence of people,” *Eng. Struct.*, vol. 115, pp. 165–178, 2016.

[169] S. A. Hernández Maldonado and Y. H. Chui, “Vibrational performance of cross laminated timber floors,” in *World Conference on Timber Engineering*, 2012.

[170] C. Uí Chúláin, K. Sikora, and A. M. Harte, “Influence of Connection Systems on Serviceability Response of Clt Timber Flooring,” in *World Conference on Timber Engineering*, 2016.

[171] T. Reynolds, D. Casagrande, and R. Tomasi, “Comparison of multi-storey cross-laminated timber and timber frame buildings by in situ modal analysis,” *Constr. Build. Mater.*, vol. 102, pp. 1009–1017, 2016.

[172] D. Casagrande, M. Piazza, A. Franciosi, and F. Pederzolli, “Assessment of Timber Floor Vibration Performance : a Case Study in Italy,” in *World Conference on Timber Engineering*, 2014.

[173] E. M. Meghlat, M. Oudjene, H. Ait-Aider, and J. L. Batoz, “A new approach to model nailed and screwed timber joints using the finite element method,” *Constr. Build. Mater.*, vol. 41, pp. 263–269, 2013.

[174] P. Sejkot and S. Ormarsson, “Numerical modelling of connection of timber beams using angle brackets with a rib,” in *Short Term Scientific Mission: COST*

FP 1004, 2015.

[175] K. Jarnerö, A. Brandt, and A. Olsson, “In situ testing of timber floor vibration properties,” in *World Conference on Timber Engineering*, 2010.

[176] I. Glisovic and B. Stevanovic, “Vibrational Behaviour of Timber Floors,” in *World Conference on Timber Engineering*, 2010.

[177] M. Izzi, A. Polastri, and M. Fragiacomo, “Modelling the mechanical behaviour of typical wall-to-floor connection systems for cross-laminated timber structures,” *Eng. Struct.*, vol. 162, no. January, pp. 270–282, 2018.

[178] I. Gavric, G. Rinaldin, C. Amadio, M. Fragiacomo, and A. Ceccotti, “Experimental-numerical analyses of the seismic behaviour of cross-laminated wall systems,” *15th World Conf. Earthq. Eng. WCEE*, 2012.

[179] G. Rinaldin, C. Amadio, and M. Fragiacomo, “A component approach for the hysteretic behaviour of connections in cross-laminated wooden structures,” *Earthq. Eng. Struct. Dyn.*, vol. 42, pp. 2023–2042, 2013.

[180] CEN, *EN 1194 Timber structures- Glued laminated timber - Strength classes and determination of characteristic values*. 1999.

[181] J. Xu and J. D. Dolan, “Development of nailed wood joint element in ABAQUS,” *J. Struct. Eng.*, vol. 135, 2009.

[182] I. Gavric, M. Fragiacomo, and A. Ceccotti, “Cyclic behaviour of typical metal connectors for cross-laminated (CLT) structures,” *Mater. Struct. Constr.*, vol. 48, no. 6, pp. 1841–1857, 2015.

[183] E. Ussher, M. Sadeghi, J. Weckendorf, and I. Smith, “Vibration Serviceability Design Analysis of Cross-Laminated-Timber Floor Systems,” in *World Conference on Timber Engineering*, 2014.

[184] K. Lewis, B. Basaglia, R. Shrestha, and K. Crews, “The use of cross-laminated timber for long span flooring in commercial buildings,” in *World Conference on Timber Engineering*, 2016.

[185] R. Szilard, *Theories and Applications of Plate Analysis: Classical Numerical*

and Engineering Methods. John Wiley & Sons; Har/Cdr edition (17 Feb. 2004), 2014.

[186] J. Weckendorf, T. Toratti, I. Smith, and T. Tannert, “Vibration serviceability performance of timber floors. European Journal of Wood and Wood Products.,” *Eur. J. Wood Wood Prod.*, vol. 74, no. 3, pp. 353–367, 2016.

[187] S. Zhang, J. Zhou, J. Niederwestberg, and Y. H. Chui, “Effect of end support restraints on vibration performance of cross laminated timber floors: An analytical approach,” *Eng. Struct.*, vol. 189, no. January, pp. 186–194, 2019.

[188] CEN, *I.S. EN 1991-1-1 Eurocode 1: Actions on structures Part 1-1: General actions*. NSAI, 2005.

[189] A. Speranza, L. Barbaresi, and F. Morandi, “Experimental analysis of flanking transmission of different connection systems for CLT panels,” in *World Conference on Timber Engineering*, 2016.

[190] “Rothoblaas srl.” [Online]. Available: https://www.rothoblaas.com/. [Accessed: 16-May-2019].

[191] KLH Massivholz GmbH, *KLH-CLT Structural Pre-analysis tables*. KLH Massivholz GmbH, 2017.

[192] Hanlon Concrete, “Ultraflo Floor screed.” [Online]. Available: http://www.hanlonconcrete.ie/products/floor-screed. [Accessed: 23-Jul-2019].

[193] Health and Safety Authority, *Guide to the Safety, Health and Welfare at Work (General Application) Regulations 2007. Part 4: Work at Height*. Ireland, 2007.

[194] Health & Safety Authority, *Code of Practice for Access and Working Scaffolds*. Ireland, 2008.

[195] D. Adler, *Metric Handbook: Planning and Design Data*, 2nd ed. Architectural Press, 1999.

[196] The Department of Education and Science, *Generic repeat design for primary schools. Issue 2*. Republic of Ireland, 2004.

[197] Dassault Systemes, “Abaqus/CAE v6.7.” .

[198] H. J. Blaß and I. Bejtka, “Numerische Berechnung der Tragfähigkeit und der Steifigkeit von querzugverstärkten Verbindungen mit stiftförmigen Verbindungsmitteln. Karlsruher,” Karlsruhe, Germany, 2008.

[199] European Organisation for Technical Approvals, “ETA-06/0138: KLH Massivholz GmbH. Solid wood slab element to be used as structural elements in buildings,” ETA-06/0138 with validity from 01.07.2011 to 30.06.2016, 2017.

[200] Oifig an tSoláthair, *Building Regulations 2006 Technical Guidance Document B - Fire Safety*, vol. 1. 2006.

APPENDIX A

The NI LabVIEW 2014 software programmes developed to record and process the experimental dynamic data are illustrated in Figures A.1 and A.2.

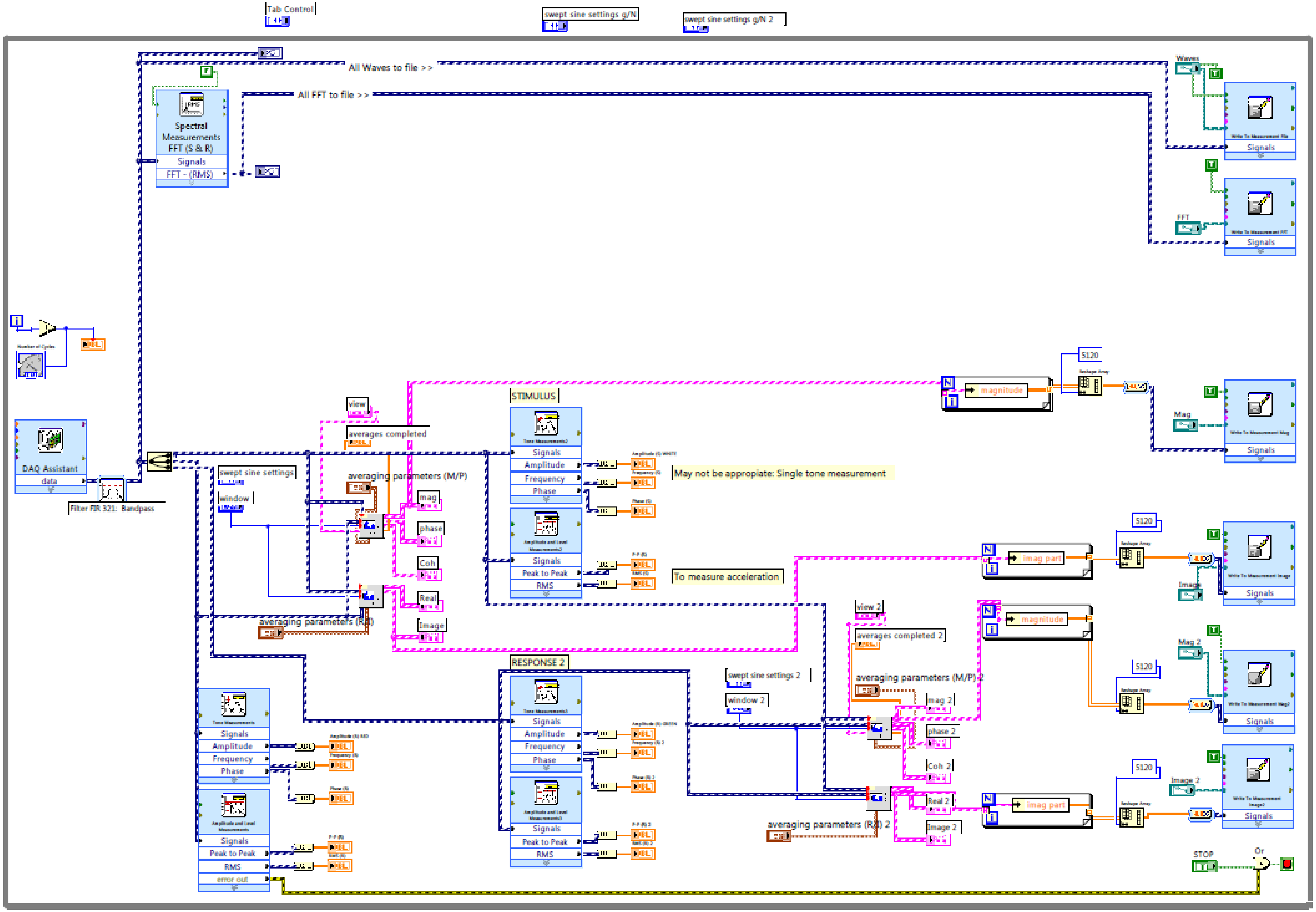
Tab Control
swept sine settings g/N
swept sine settings g/N 2
All Waves to file >>
All FFT to file >>
Spectral Measurements FFT (S & R)
Signals
FFT - (RMS)
Waves
Write To Measurement File
Signals
FFT
Number of Cycles
DAQ Assistant
data
Filter FIR 321 Bandpass
view
averages completed
swept sine settings
window
averaging parameters (M/P)
mag
phase
Coh
Real
Image
averaging parameters (RMS)
STIMULUS
Tone Measurements2
Signals
Amplitude
Frequency
Phase
Amplitude and Level Measurements2
Peak to Peak
RMS
May not be appropiate: Single tone measurement
To measure acceleration
magnitude
5120
Reshape Array
Mag
imag part
Image
view 2
averages completed 2
averaging parameters (M/P) 2
mag 2
phase 2
Coh 2
Real 2
Image 2
swept sine settings 2
window 2
averaging parameters (RMS) 2
Mag 2
Image 2
RESPONSE 2
Tone Measurements3
Amplitude and Level Measurements3
Tone Measurements
Amplitude and Level Measurements
error out
STOP
Or

Figure A.1 *LabVIEW program developed to convert the force and response signals to FRF*

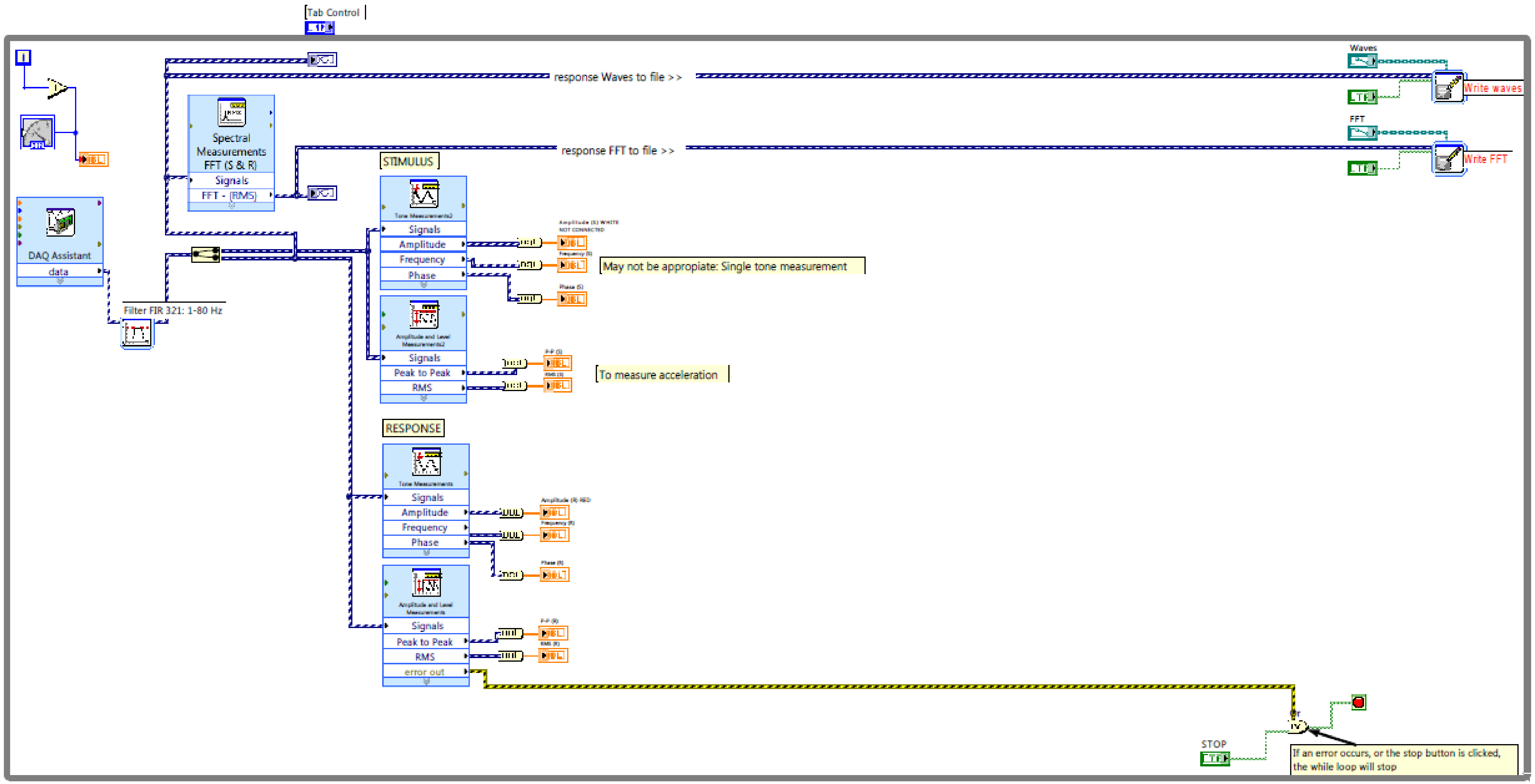

Tab Control
response Waves to file >>
response FFT to file >>
Waves
Write waves
FFT
Write FFT
Spectral Measurements FFT (S & R)
Signals
FFT - (RMS)
DAQ Assistant
data
Filter FIR 321: 1-80 Hz
STIMULUS
Tone Measurements2
Signals
Amplitude
Frequency
Phase
Amplitude (S) WHITE NOT CONNECTED
Frequency (S)
Phase (S)
Amplitude and Level Measurements2
Signals
Peak to Peak
RMS
P-P (S)
RMS (S)
RESPONSE
Tone Measurements
Signals
Amplitude
Frequency
Phase
Amplitude (R) RED
Frequency (R)
Phase (R)
Amplitude and Level Measurements
Signals
Peak to Peak
RMS
error out
P-P (R)
RMS (R)
STOP

May not be appropiate: Single tone measurement

To measure acceleration

If an error occurs, or the stop button is clicked, the while loop will stop

Figure A.2 *LabVIEW program developed to measure diagnostic impulse impact excitation*

APPENDIX B

The results of each laboratory test, Assemblies A to P, including the environmental conditions of the room and the floor at the time of each test.

ASSEMBLY A

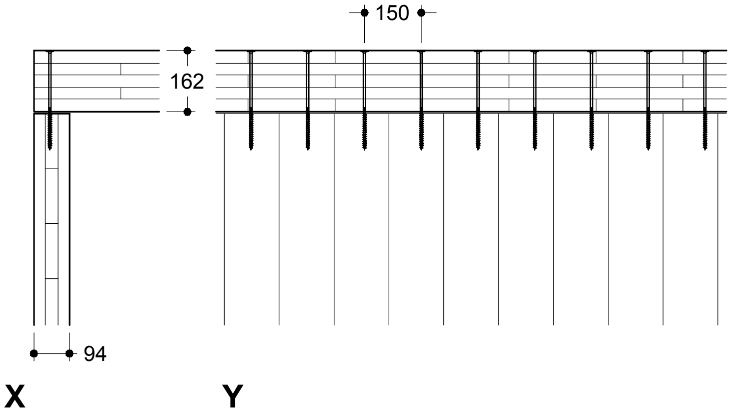
150
162
94
X
Y

SUPPORT DETAILS

One-way spanning
Platform construction
Long span

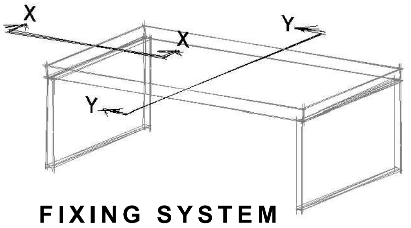

FIXING SYSTEM

Ø 8 x 260 mm partially threaded washer-head vertical screws @ 150mm c/c

RESILIENT INTERLAYER

No

LOAD ADDED

No

ENVIRONMENTAL CONDITIONS

Room temperature (°C):	20.4
Relative humidity (%):	47.7
Moisture content of panel (%):	13.0

Deflection (mm)	Static 1kN point-load applied mid-span	0.179

Mode shape	Mode	Frequency (Hz)	Damping ζ (%)	Acceleration ($m/s^2/N$)
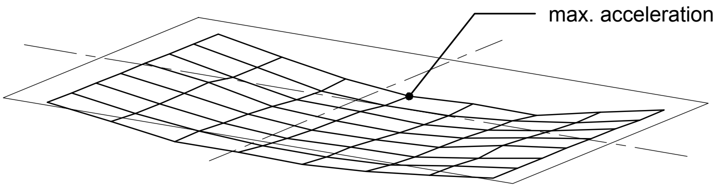 max. acceleration	1	22.35	0.94	0.134
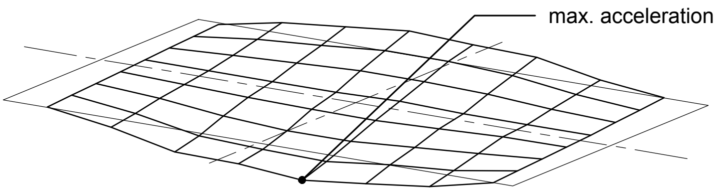 max. acceleration	2	28.75	0.90	0.127
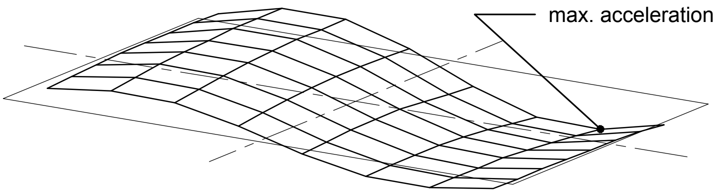 max. acceleration	3	73.10	1.32	0.058
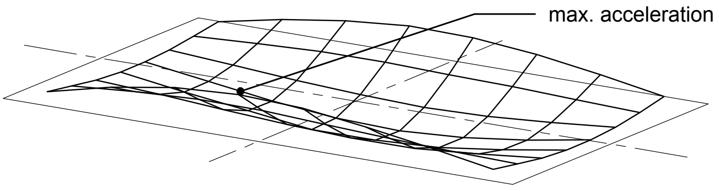 max. acceleration	4	78.35	0.61	0.303

ASSEMBLY B

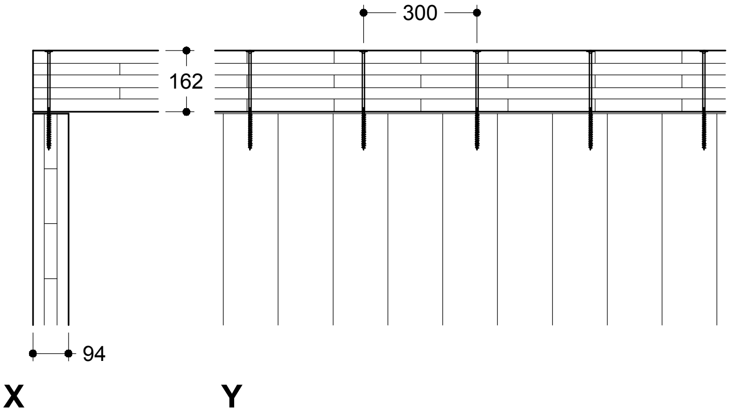
300
162
94
X
Y

SUPPORT DETAILS

One-way spanning
Platform construction
Long span

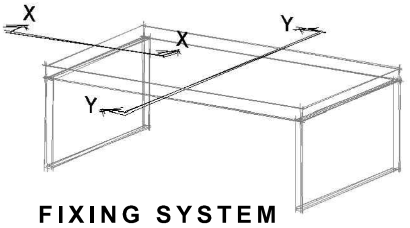

FIXING SYSTEM

Ø 8 x 260 mm partially threaded washer-head vertical screws @ 300mm c/c

RESILIENT INTERLAYER

No

LOAD ADDED

No

ENVIRONMENTAL CONDITIONS

Room temperature (°C):	20.5
Relative humidity (%):	60.2
Moisture content of panel (%):	13.7

Deflection (mm)	Static 1kN point-load applied mid-span			0.178
Mode shape	Mode	Frequency (Hz)	Damping ζ (%)	Acceleration ($m/s^2/N$)
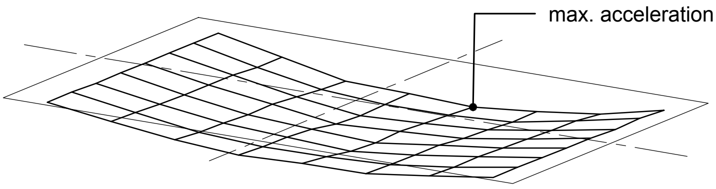 max. acceleration	1	21.90	0.98	0.137
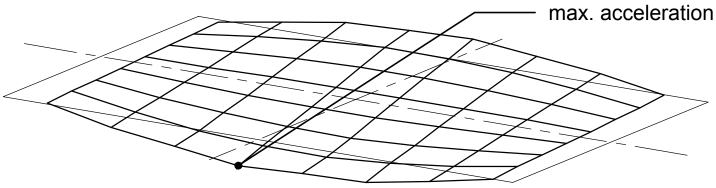 max. acceleration	2	28.20	0.93	0.111
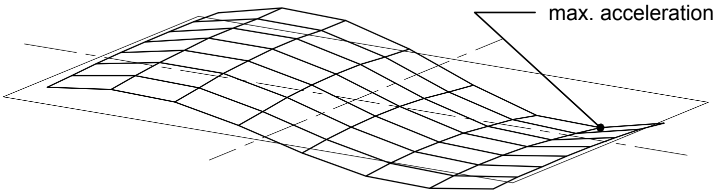 max. acceleration	3	72.65	1.54	0.051
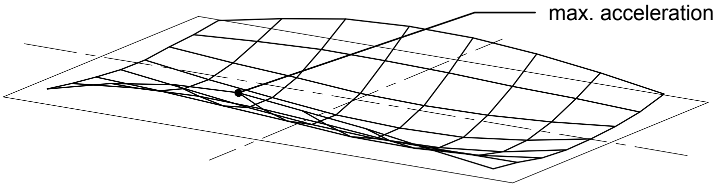 max. acceleration	4	78.05	0.68	0.289

ASSEMBLY C

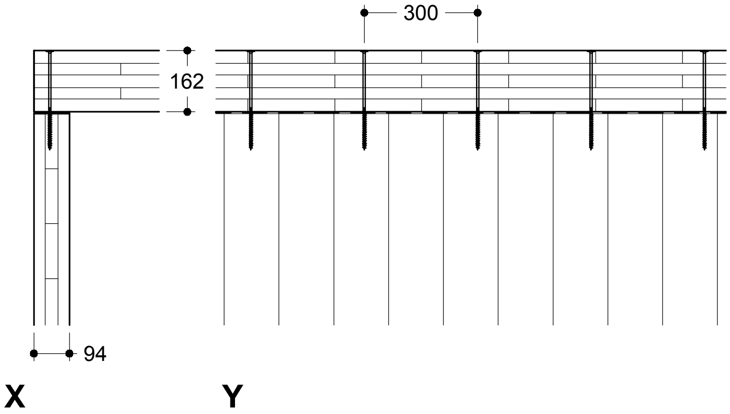
300
162
94
X
Y

SUPPORT DETAILS

One-way spanning
Platform construction
Long span

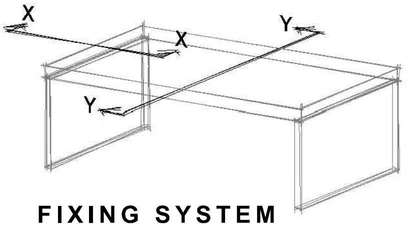

FIXING SYSTEM

Ø 8 x 260 mm partially threaded washer-head vertical screws @ 300mm c/c

RESILIENT INTERLAYER

Yes

LOAD ADDED

No

ENVIRONMENTAL CONDITIONS

Room temperature (°C):	19.6
Relative humidity (%):	38.4
Moisture content of panel (%):	11.2

Deflection (mm)	Static 1kN point-load applied mid-span	0.185

Mode shape	Mode	Frequency (Hz)	Damping ζ (%)	Acceleration (m/s^2/N)
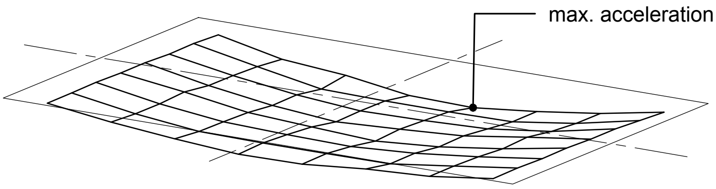 max. acceleration	1	21.50	1.05	0.131
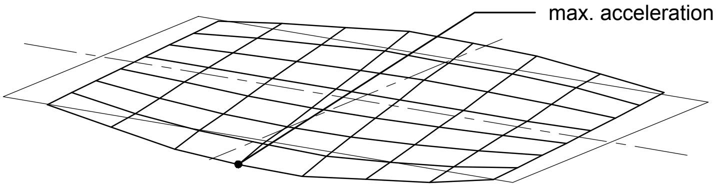 max. acceleration	2	27.30	1.28	0.074
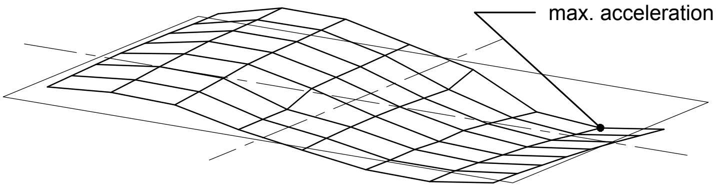 max. acceleration	3	70.35	1.52	0.027
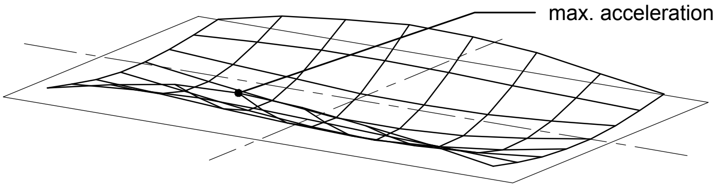 max. acceleration	4	78.25	0.82	0.232

ASSEMBLY D

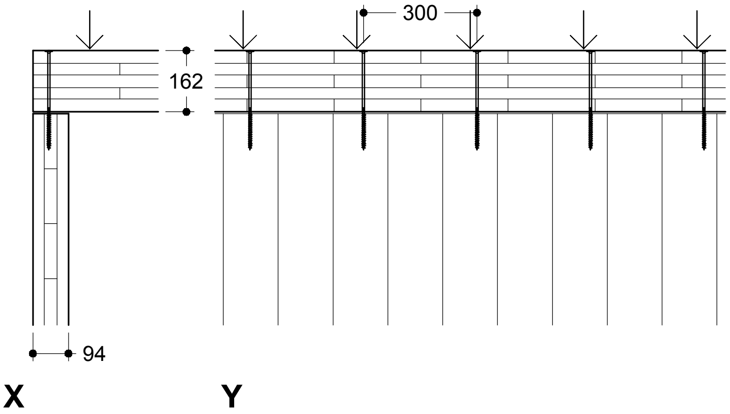

SUPPORT DETAILS

One-way spanning
Platform construction
Long span

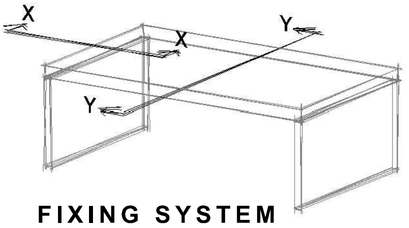

FIXING SYSTEM

Ø 8 x 260 mm partially threaded washer-head vertical screws @ 300mm c/c

RESILIENT INTERLAYER

No

LOAD ADDED

Yes

ENVIRONMENTAL CONDITIONS

Room temperature (°C):	19.6
Relative humidity (%):	38.5
Moisture content of panel (%):	11.1

Deflection (mm)	Static 1kN point-load applied mid-span			0.178
Mode shape	Mode	Frequency (Hz)	Damping ζ (%)	Acceleration ($m/s^2/N$)
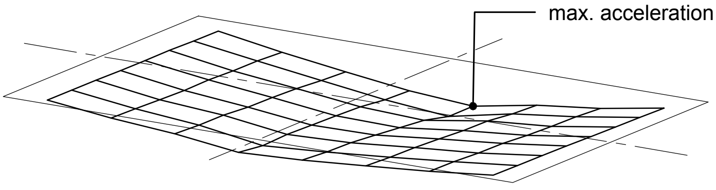 max. acceleration	1	16.35	1.66	0.046
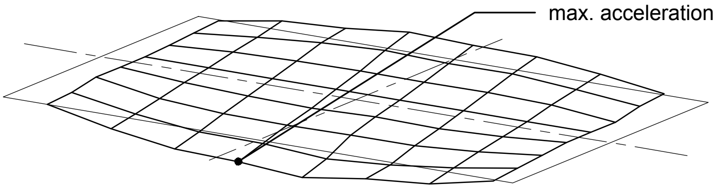 max. acceleration	2	21.45	2.79	0.028
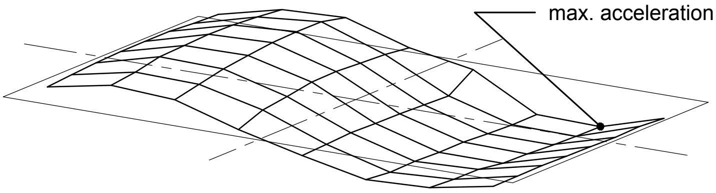 max. acceleration	3	53.95	1.56	0.026
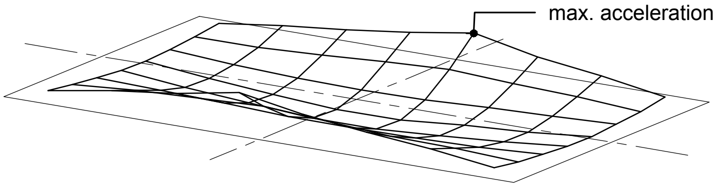 max. acceleration	4	69.25	1.74	0.031
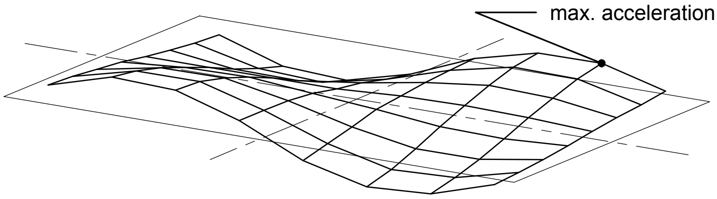 max. acceleration	5	65.35	1.17	0.061

ASSEMBLY E

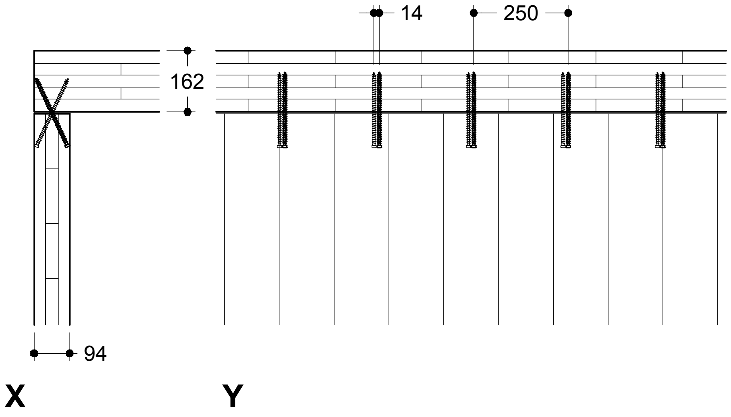
14
250
162
94
X
Y

SUPPORT DETAILS

One-way spanning
Platform construction
Long span

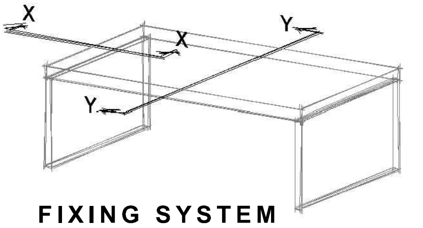

FIXING SYSTEM

Ø 9 x 200 mm fully threaded cylindrical-head inclined screws @ 250mm c/c

RESILIENT INTERLAYER

No

LOAD ADDED

No

ENVIRONMENTAL CONDITIONS

Room temperature (°C):	19.8
Relative humidity (%):	58.5
Moisture content of panel (%):	11.2

Deflection (mm)	Static 1kN point-load applied mid-span	0.176

Mode shape	Mode	Frequency (Hz)	Damping ζ (%)	Acceleration (m/s^2/N)
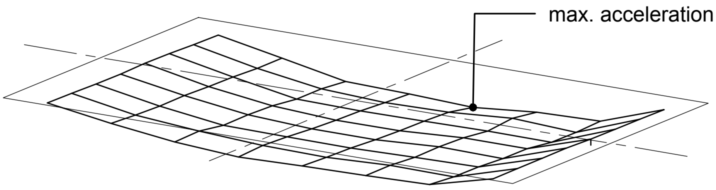 max. acceleration	1	22.05	0.85	0.172
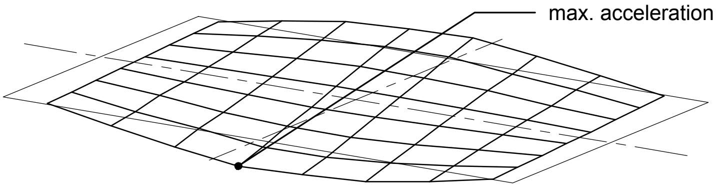 max. acceleration	2	28.55	0.82	0.145
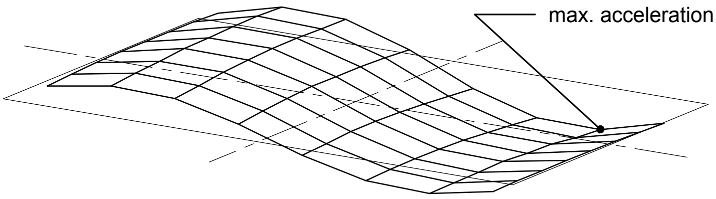 max. acceleration	3	73.10	1.18	0.062
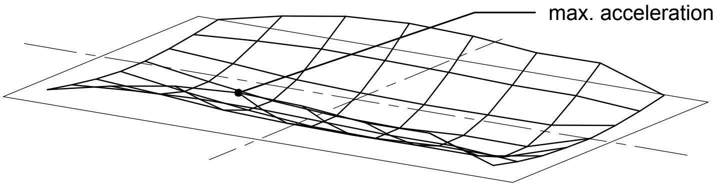 max. acceleration	4	78.35	0.66	0.277

ASSEMBLY F

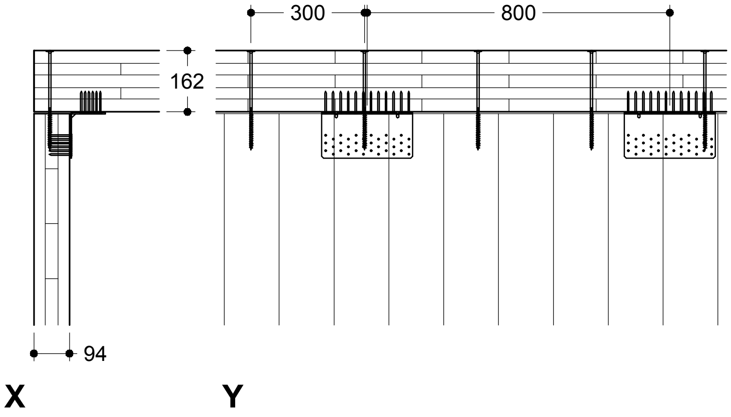
300
800
162
94
X
Y

SUPPORT DETAILS

One-way spanning
Platform construction
Long span

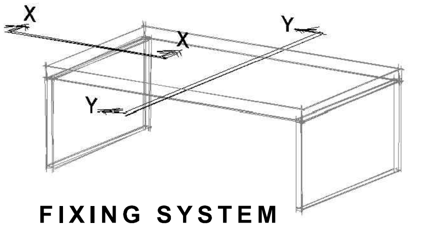

FIXING SYSTEM

Ø 8 x 260 mm partially threaded washer-head vertical screws @ 300mm c/c
240 x 93 x 120 angle shear-stress brackets@ 800 mm c/c

RESILIENT INTERLAYER

No

LOAD ADDED

No

ENVIRONMENTAL CONDITIONS

Room temperature (°C):	20.6
Relative humidity (%):	59.6
Moisture content of panel (%):	11.8

Deflection (mm)	Static 1kN point-load applied mid-span			0.172
Mode shape	Mode	Frequency (Hz)	Damping ζ (%)	Acceleration ($m/s^2/N$)
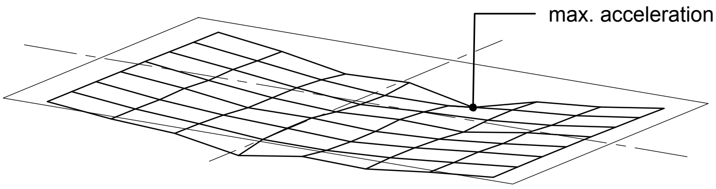 max. acceleration	1	22.30	0.92	0.148
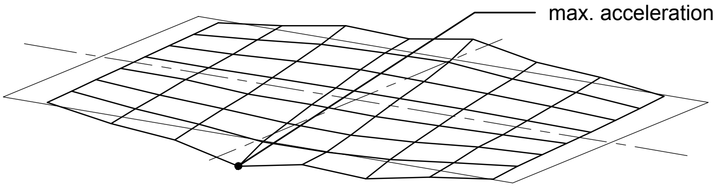 max. acceleration	2	28.35	0.88	0.132
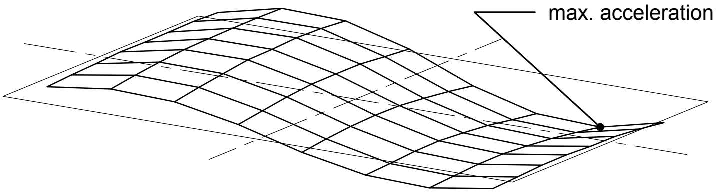 max. acceleration	3	72.95	1.30	0.063
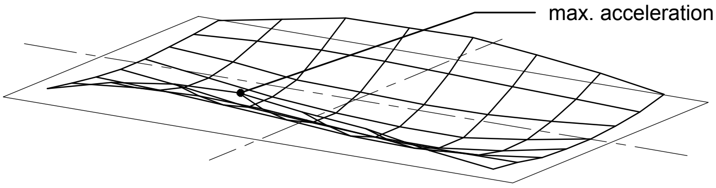 max. acceleration	4	78.20	0.65	0.311

ASSEMBLY G

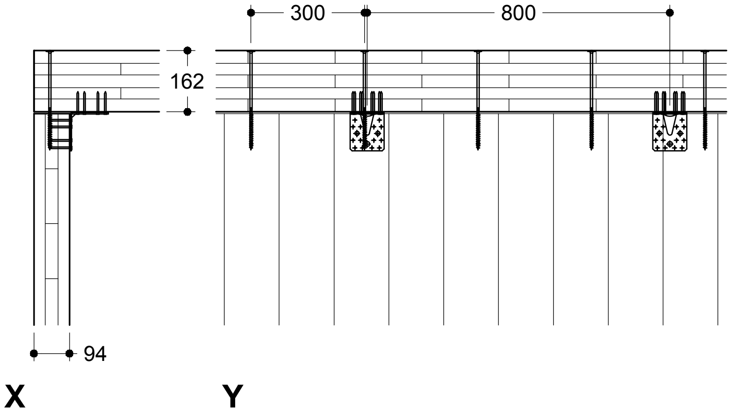
300
800
162
94
X
Y

SUPPORT DETAILS

One-way spanning
Platform construction
Long span

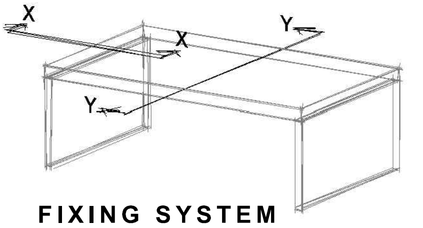

FIXING SYSTEM

Ø 8 x 260 mm partially threaded washer-head vertical screws @ 300mm c/c
100 x 100 x 90 reinforced angle brackets@ 800 mm c/c

RESILIENT INTERLAYER

No

LOAD ADDED

No

ENVIRONMENTAL CONDITIONS

Room temperature (°C):	19.9
Relative humidity (%):	52.0
Moisture content of panel (%):	11.5

Deflection (mm)	Static 1kN point-load applied mid-span	0.177

Mode shape	Mode	Frequency (Hz)	Damping ζ (%)	Acceleration ($m/s^2/N$)
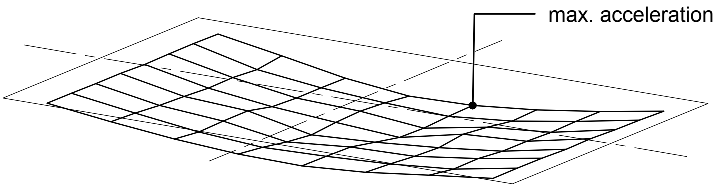 max. acceleration	1	22.00	0.96	0.148
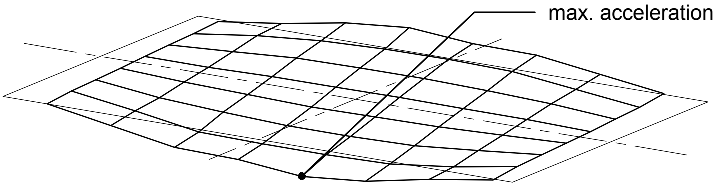 max. acceleration	2	28.25	0.91	0.107
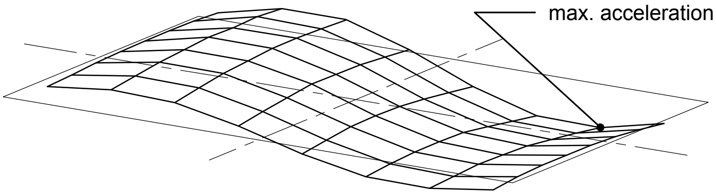 max. acceleration	3	72.75	1.36	0.063
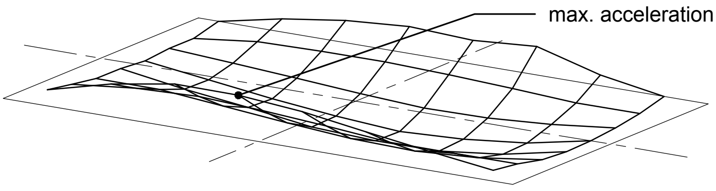 max. acceleration	4	78.15	0.63	0.279

ASSEMBLY H

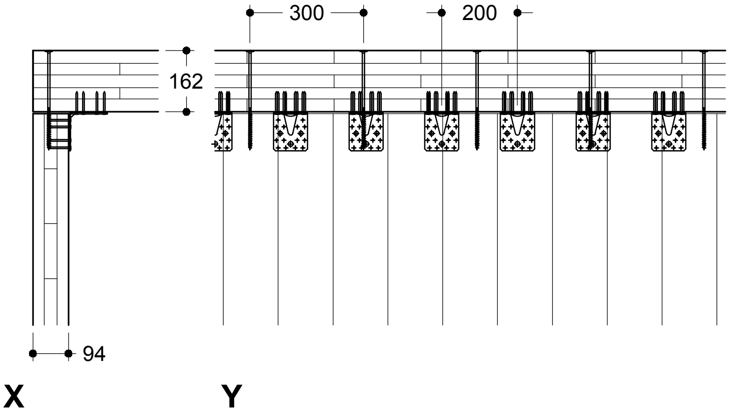
300
200
162
94
X
Y

SUPPORT DETAILS

One-way spanning
Platform construction
Long span

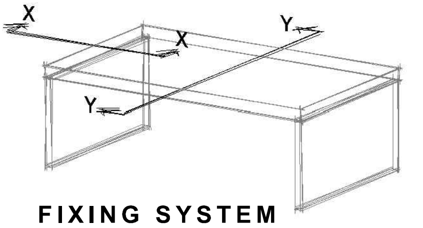

FIXING SYSTEM

Ø 8 x 260 mm partially threaded washer-head vertical screws @ 300mm c/c
100 x 100 x 90 reinforced angle brackets@ 200 mm c/c

RESILIENT INTERLAYER

No

LOAD ADDED

No

ENVIRONMENTAL CONDITIONS

Room temperature (°C):	19.5
Relative humidity (%):	53.0
Moisture content of panel (%):	11.6

Deflection (mm)	Static 1kN point-load applied mid-span	0.158

Mode shape	Mode	Frequency (Hz)	Damping ζ (%)	Acceleration ($m/s^2/N$)
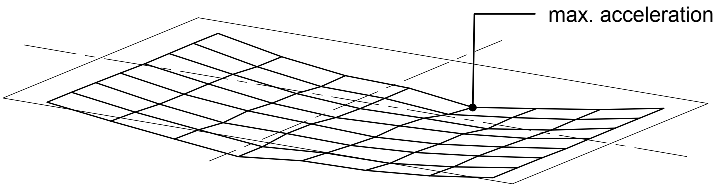 max. acceleration	1	23.40	0.87	0.147
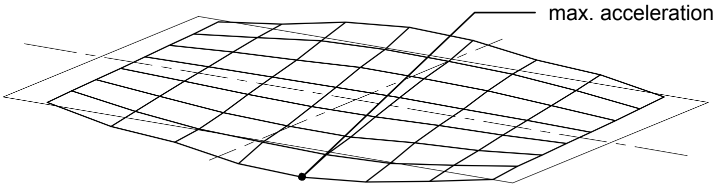 max. acceleration	2	29.70	0.84	0.137
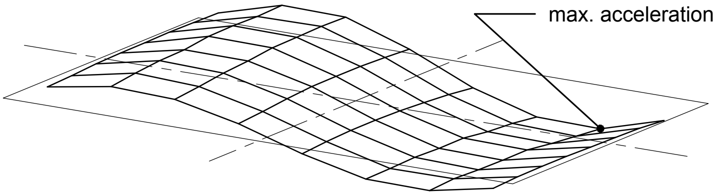 max. acceleration	3	74.10	1.20	0.050
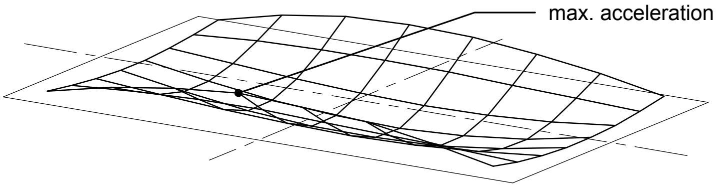 max. acceleration	4	78.90	0.63	0.301

ASSEMBLY I

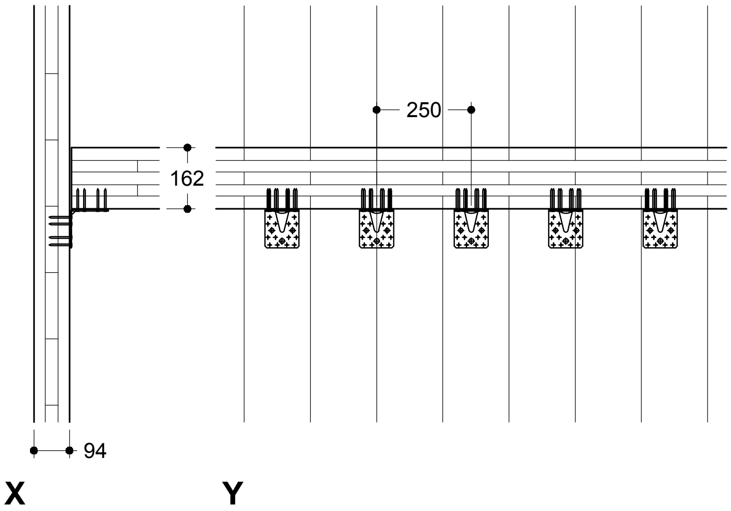
250
162
94
X
Y

SUPPORT DETAILS

One-way spanning
Balloon construction
Long span

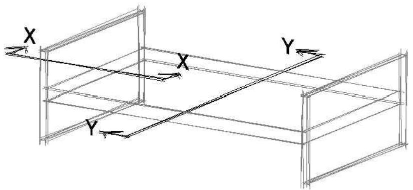

FIXING SYSTEM

100 x 100 x 90 mm reinforced angle bracket (ref. Rothoblaas WBR-100) @ 250mm c/c Ø5 x 50 mm LBS screws, 2 x 7no. per bracket.

RESILIENT INTERLAYER

No

LOAD ADDED

No

ENVIRONMENTAL CONDITIONS

Room temperature (°C):	20.1
Relative humidity (%):	65.0
Moisture content of panel (%):	11.4

Deflection (mm)	Static 1kN point-load applied mid-span	0.219

Mode shape	Mode	Frequency (Hz)	Damping ζ (%)	Acceleration ($m/s^2/N$)
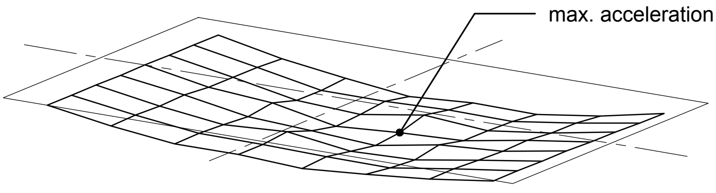 max. acceleration	1	20.05	0.80	0.108
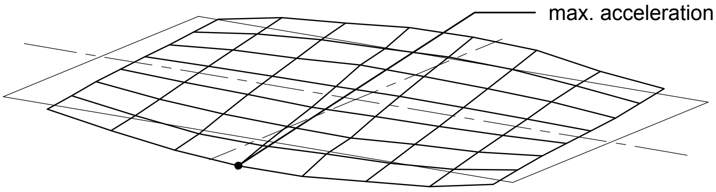 max. acceleration	2	25.05	0.83	0.117
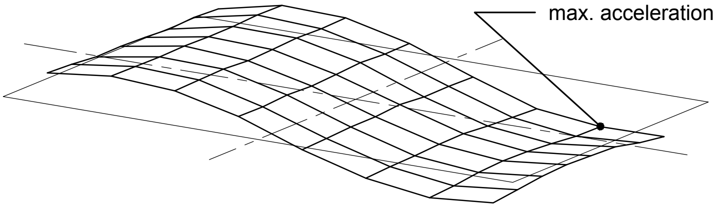 max. acceleration	3	61.05	0.94	0.051
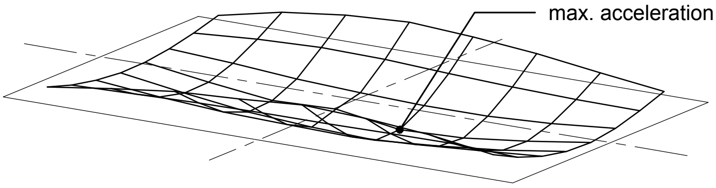 max. acceleration	4	76.05	0.70	0.157
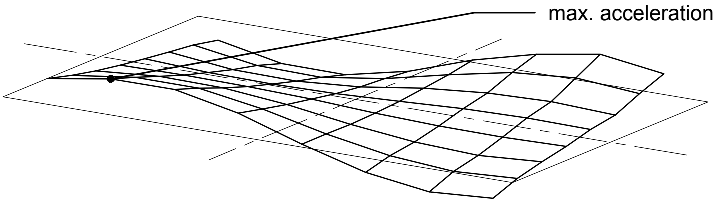 max. acceleration	5	69.85	0.94	0.057

ASSEMBLY J

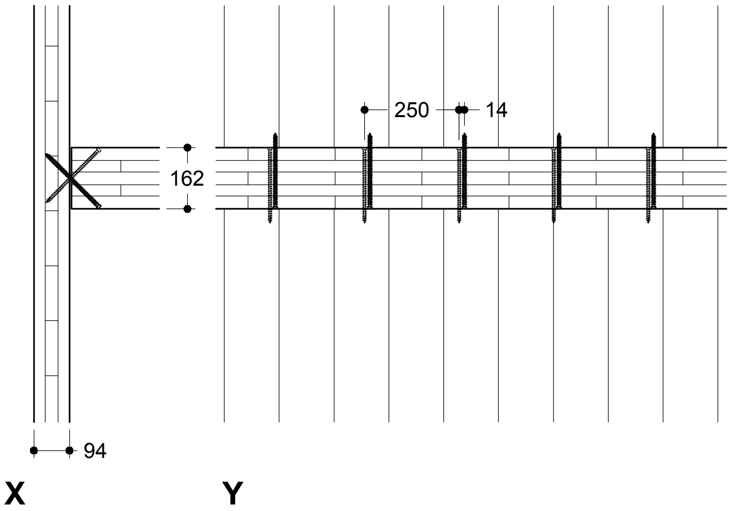
250
14
162
94
X
Y

SUPPORT DETAILS

One-way spanning
Balloon construction
Long span

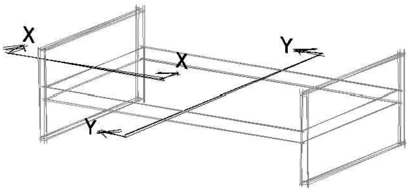

FIXING SYSTEM

Ø 9 x 200 mm fully threaded cylindrical-head screws inclined pairs @ 250mm c/c

RESILIENT INTERLAYER

No

LOAD ADDED

No

ENVIRONMENTAL CONDITIONS

Room temperature (°C): 19.8
Relative humidity (%): 47.8
Moisture content of panel (%): 11.1

Deflection (mm)	Static 1kN point-load applied mid-span			0.201
Mode shape	Mode	Frequency (Hz)	Damping ζ (%)	Acceleration ($m/s^2/N$)
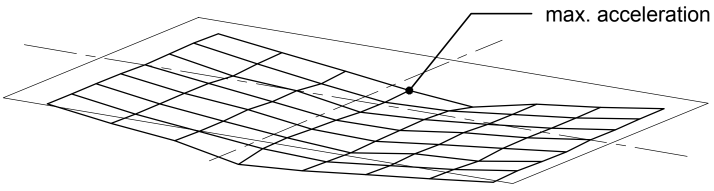 max. acceleration	1	20.45	0.91	0.116
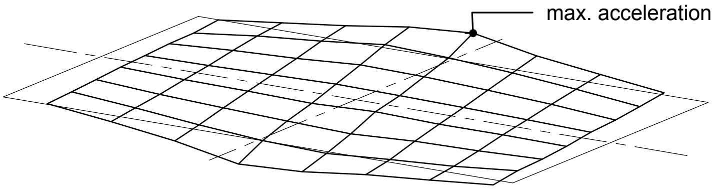 max. acceleration	2	25.65	0.90	0.099
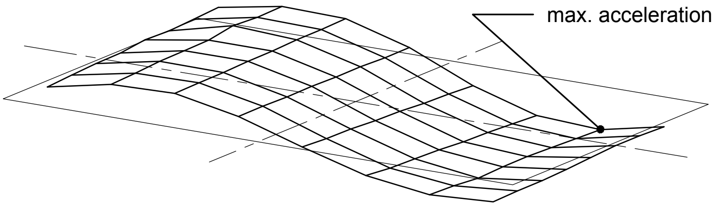 max. acceleration	3	68.20	1.01	0.055
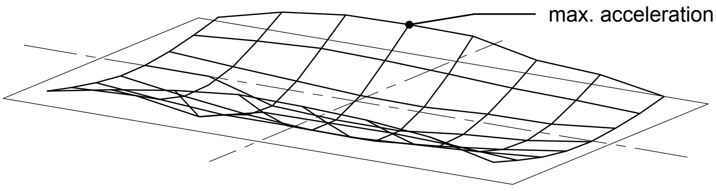 max. acceleration	4	77.20	0.58	0.294
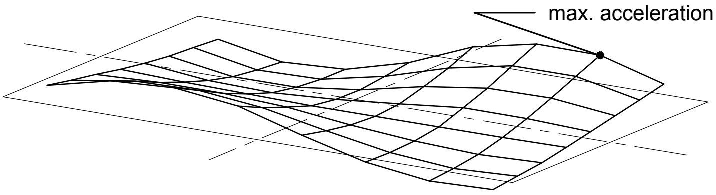 max. acceleration	5	77.50	0.76	0.125

ASSEMBLY K

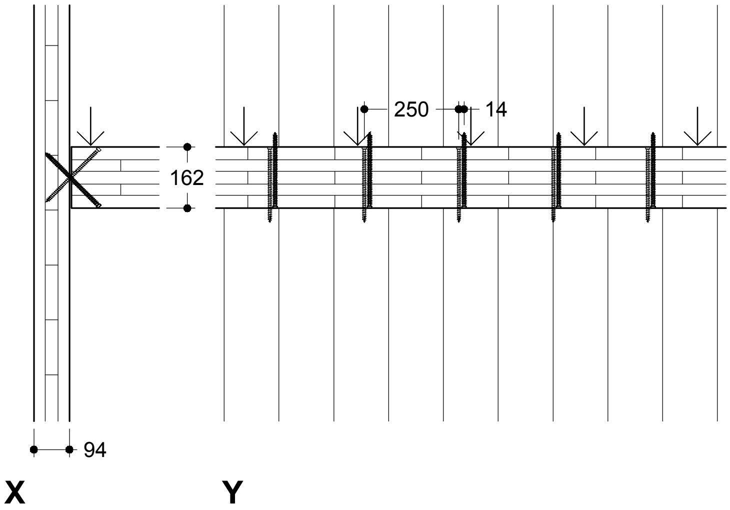
250
14
162
94
X
Y

SUPPORT DETAILS

One-way spanning
Balloon construction
Long span

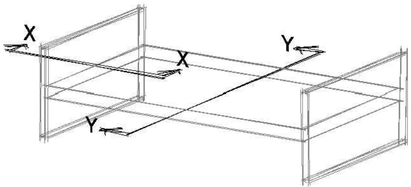

FIXING SYSTEM

Ø 9 x 200 mm fully threaded cylindrical-head screws inclined pairs @ 250mm c/c

RESILIENT INTERLAYER

No

LOAD ADDED

Yes

ENVIRONMENTAL CONDITIONS

Room temperature (°C):	20.1
Relative humidity (%):	39.7
Moisture content of panel (%):	11.0

Deflection (mm)	Static 1kN point-load applied mid-span	0.202

Mode shape	Mode	Frequency (Hz)	Damping ζ (%)	Acceleration (m/s^2/N)
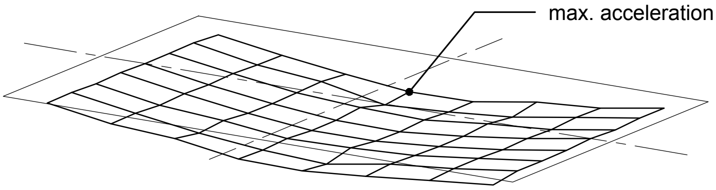 max. acceleration	1	14.90	1.95	0.038
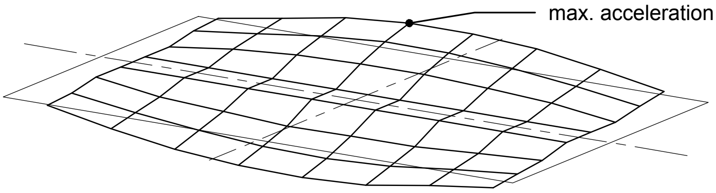 max. acceleration	2	19.20	3.40	0.018
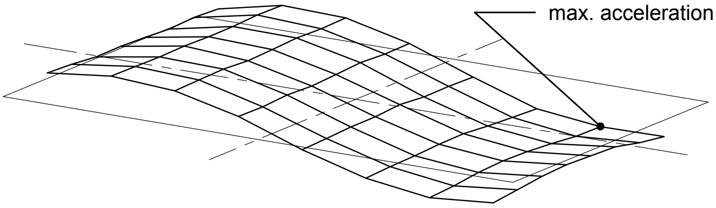 max. acceleration	3	50.85	3.32	0.011
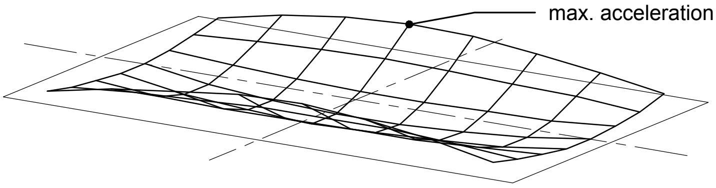 max. acceleration	4	67.45	1.79	0.027
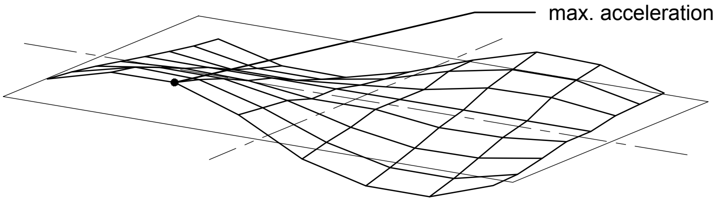 max. acceleration	5	63.80	2.09	0.019

ASSEMBLY L

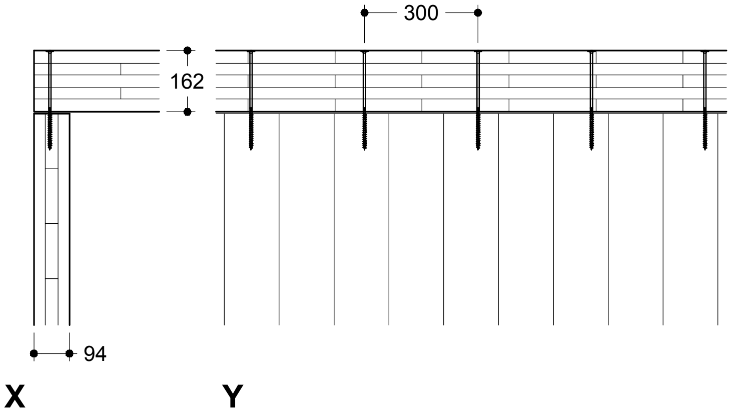
300
162
94
X
Y

SUPPORT DETAILS

One-way spanning
Platform construction
Short span

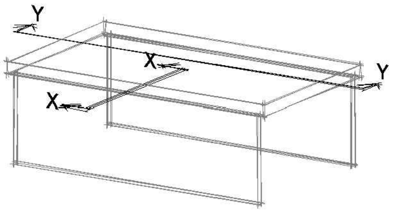

FIXING SYSTEM

Ø 8 x 260 mm partially threaded washer-head vertical screws @ 300mm c/c

RESILIENT INTERLAYER

No

LOAD ADDED

No

ENVIRONMENTAL CONDITIONS

Room temperature (°C):	18.7
Relative humidity (%):	46.5
Moisture content of panel (%):	11.2

Deflection (mm)	Static 1kN point-load applied mid-span			0.111
Mode shape	Mode	Frequency (Hz)	Damping ζ (%)	Acceleration ($m/s^2/N$)
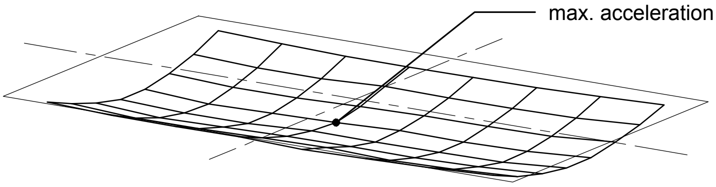 max. acceleration	1	29.50	1.51	0.024
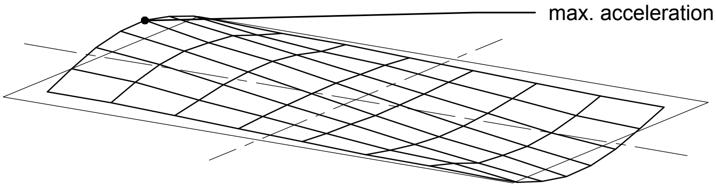 max. acceleration	2	38.25	0.82	0.101
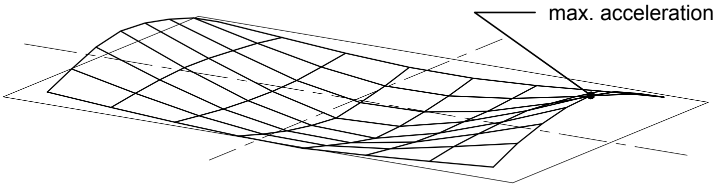 max. acceleration	3	66.40	0.76	0.215

ASSEMBLY M

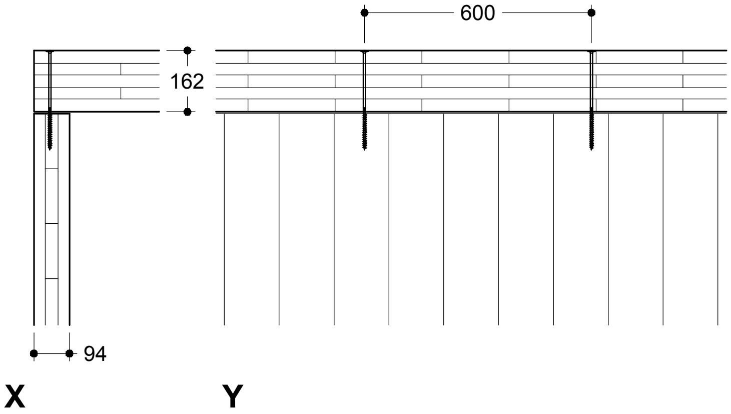
600
162
94
X
Y

SUPPORT DETAILS

One-way spanning
Platform construction
Short span

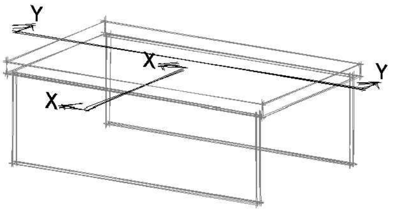

FIXING SYSTEM

Ø 8 x 260 mm partially threaded washer-head vertical screws @ 600mm c/c

RESILIENT INTERLAYER

No

LOAD ADDED

No

ENVIRONMENTAL CONDITIONS

Room temperature (°C):	18.5
Relative humidity (%):	48.5
Moisture content of panel (%):	11.2

Deflection (mm)	Static 1kN point-load applied mid-span	0.113

Mode shape	Mode	Frequency (Hz)	Damping ζ (%)	Acceleration $(m/s^2/N)$
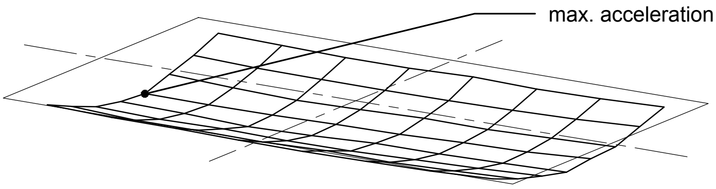 max. acceleration	1	29.05	1.60	0.026
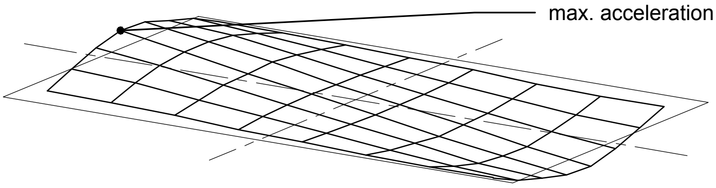 max. acceleration	2	37.55	0.79	0.108
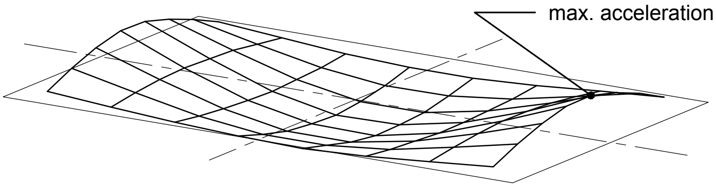 max. acceleration	3	65.75	0.97	0.197
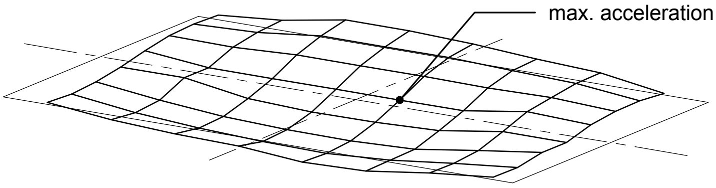 max. acceleration	4	78.50	0.94	0.015

ASSEMBLY N

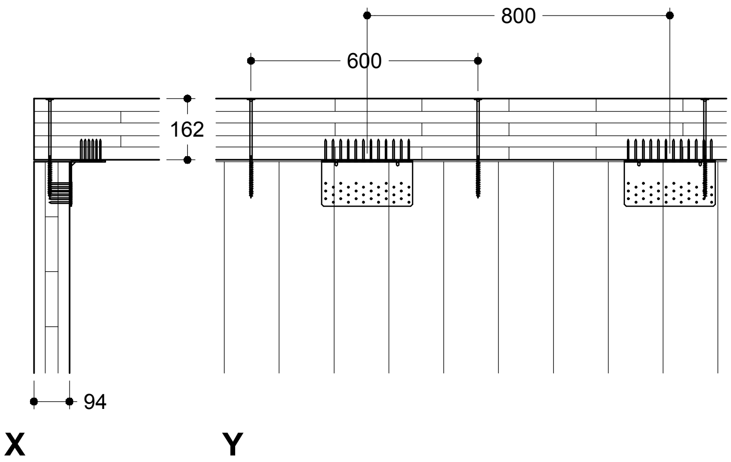
800
600
162
94
X
Y

SUPPORT DETAILS

One-way spanning
Platform construction
Short span

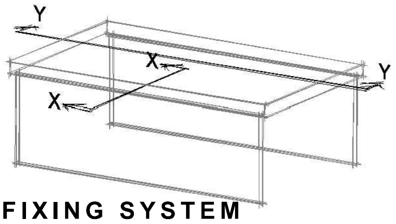

FIXING SYSTEM

Ø 8 x 260 mm partially threaded washer-head vertical screws @ 600mm c/c
240 x 93 x 120 angle shear-stress brackets@ 800 mm c/c

RESILIENT INTERLAYER

No

LOAD ADDED

No

ENVIRONMENTAL CONDITIONS

Room temperature (°C):	17.5
Relative humidity (%):	47.8
Moisture content of panel (%):	11.0

Deflection (mm)	Static 1kN point-load applied mid-span	0.103

Mode shape	Mode	Frequency (Hz)	Damping ζ (%)	Acceleration (m/s^2/N)
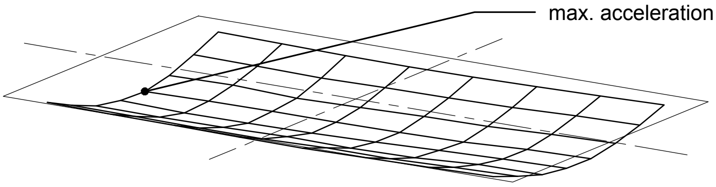 max. acceleration	1	29.70	1.52	0.013
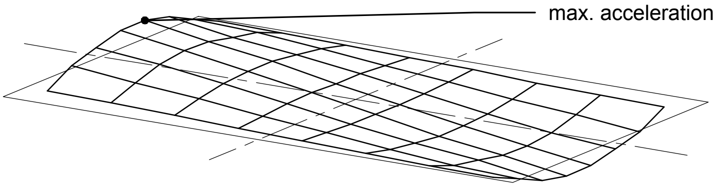 max. acceleration	2	39.20	0.81	0.105
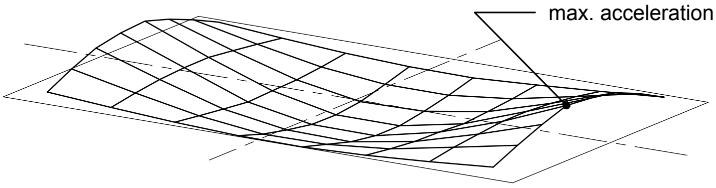 max. acceleration	3	67.45	0.68	0.225

ASSEMBLY O

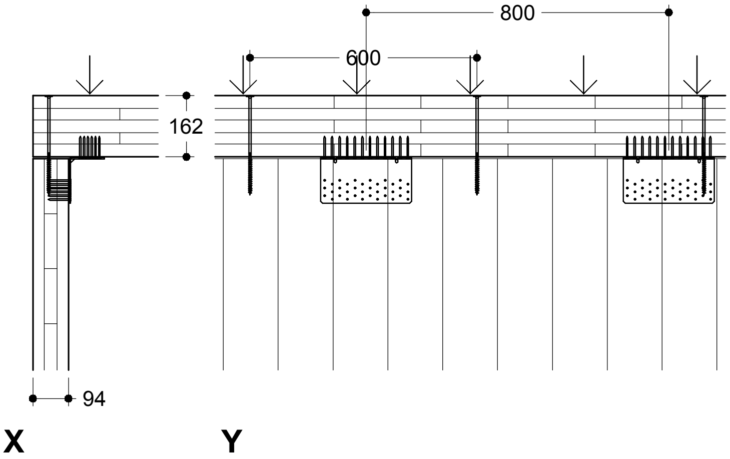
800
600
162
94
X
Y

SUPPORT DETAILS

One-way spanning
Platform construction
Short span

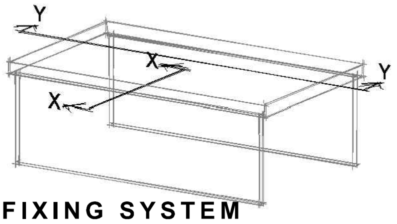

FIXING SYSTEM

Ø 8 x 260 mm partially threaded washer-head vertical screws @ 600mm c/c
240 x 93 x 120 angle shear-stress brackets@ 800 mm c/c

RESILIENT INTERLAYER

No

LOAD ADDED

Yes

ENVIRONMENTAL CONDITIONS

Room temperature (°C):	17.5
Relative humidity (%):	50.0
Moisture content of panel (%):	10.9

Deflection (mm)	Static 1kN point-load applied mid-span			0.104
Mode shape	Mode	Frequency (Hz)	Damping ζ (%)	Acceleration ($m/s^2/N$)
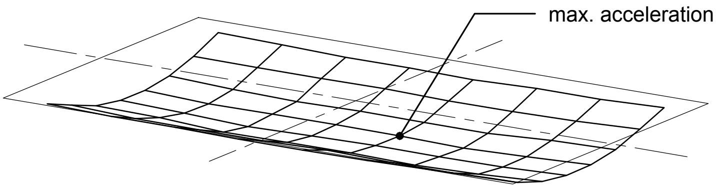 max. acceleration	1	23.95	2.17	0.035
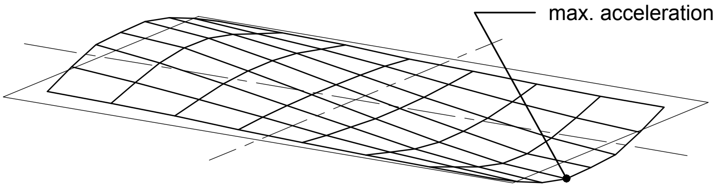 max. acceleration	2	29.95	1.83	0.027
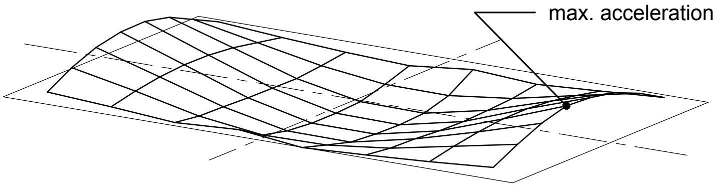 max. acceleration	3	54.95	1.88	0.040
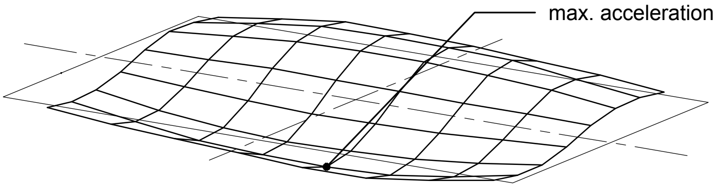 max. acceleration	4	68.60	1.29	0.026

ASSEMBLY P

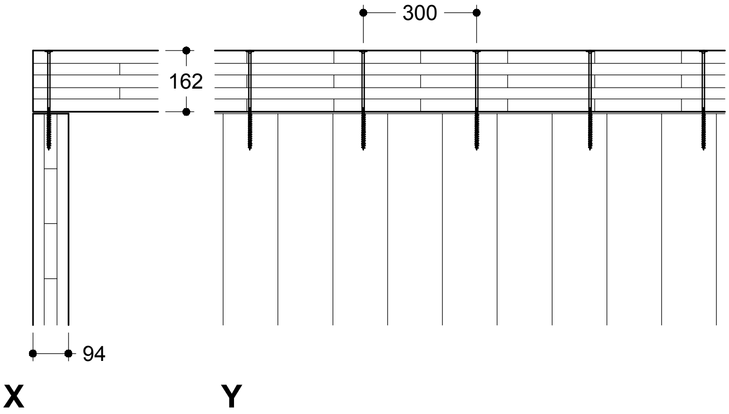

SUPPORT DETAILS

Two-way spanning
Platform construction

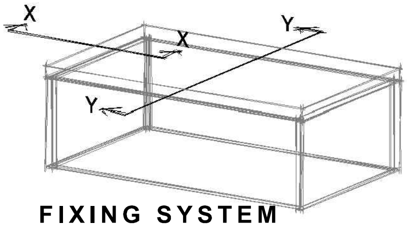

FIXING SYSTEM

Ø 8 x 260 mm partially threaded washer-head vertical screws @ 300mm c/c

RESILIENT INTERLAYER

No

LOAD ADDED

No

ENVIRONMENTAL CONDITIONS

Room temperature (°C):	18.7
Relative humidity (%):	46.3
Moisture content of panel (%):	11.4

Deflection (mm)	Static 1kN point-load applied mid-span			0.098
Mode shape	Mode	Frequency (Hz)	Damping ζ (%)	Acceleration $(m/s^2/N)$
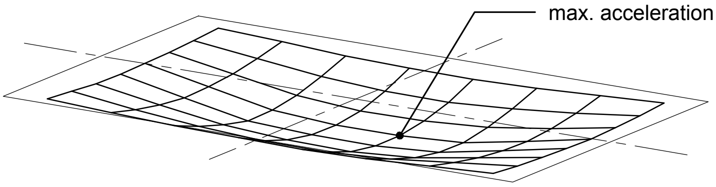 max. acceleration	1	41.75	1.33	0.158